

Study on DNA Amplification and Improvement of Detection Sensitivity by Fluorophores

(DNA増幅と蛍光色素による検出感度向上に関する研究)

KATO Tomohiro

加藤 智博

2013

Table of Contents

CHAPTER 1. GENERAL INTRODUCTION	1
1-1 Properties, structure and function of DNA	1
1-2 DNA amplification; mechanism and applications	3
1-3 DNA detection by fluorophores	5
1-4 Problems on DNA amplification and detection by fluorophores	7
1-5 Purpose of this study	7
1-6 References	8
CHAPTER 2. CLARIFICATION OF THE MECHANISM OF UNEXPECTED DNA AMPLIFICATION	10
2-1 Abstract	10
2-2 Introduction	11
2-3 Results and Discussions	13
2-3-1 Temperature dependence of <i>de novo</i> DNA synthesis	13
2-3-2 Analyses of the products of <i>de novo</i> DNA synthesis	17
2-3-3 Temperature dependence on elongation of Short ssDNA	21
2-3-4 The unusual elongation mechanism of short single strand DNA	29
2-3-5 Elongation of short DNA containing hairpins at each end	39
2-3-6 Proposed mechanism of unexpected DNA amplification	55
2-4 Conclusions	57
2-5 Experimental section	59

2-6	References	63
2-7	Appendixes	66
CHAPTER 3. LIGHTING-UP OF FLUOROPHORE BY “INSULATOR” BASE-SURROGATES		70
3-1	Abstract	70
3-2	Introduction	71
3-3	Results and Discussions	72
3-3-1	Structural analysis and thermo dynamic stability of duplex containing insulator basepairs	72
3-3-2	Shielding efficiency of cyclohexyl base pairs as insulators	77
3-3-3	The molecular design of insulator 1; requirement of cyclohexyl ring	80
3-3-4	The molecular design of insulator 2; necessity of forming pairs	83
3-3-5	Shielding dye-dye interactions	86
3-3-6	Protection of various dyes	90
3-4	Conclusions	98
3-5	Experimental section	98
3-5-1	Materials	98
3-5-2	Synthesis of the DNA modified with fluorophores and insulators	98
3-5-3	Spectroscopic measurements	100
3-5-4	Measurement of the melting temperature	100
3-5-5	NMR measurements	101
3-5-6	Computer modeling	101
3-5-7	Synthesis of phosphoramidite monomers tethering insulators and dyes	102
3-6	References	117
3-7	Appendixes	120
3-7-1	Other miscellaneous insulators	120

3-7-2	Restriction of AT hopping hole transfer	132
3-7-3	Molecular orbital calculation of dyes and nucleobases	134

CHAPTER 4. DEVELOPMENT OF A NEW ROBUST DNA-BASED FRET SYSTEM WITH STRICT CONTROL OF DYE MOBILITY WITHIN DNA DUPLEX **136**

4-1	Abstract	136
4-2	Introduction	137
4-3	Results and Discussions	140
4-3-1	Strategy and design of the FRET system.	140
4-3-2	Spectroscopic behavior of ODN-dye conjugates.	141
4-3-3	Static measurement of fluorescence spectra.	142
4-3-4	Time-resolved fluorescence measurement.	144
4-3-5	Comparison of experimental data with cylinder model.	148
4-3-6	Generality of the FRET system with tethering dyes in DNA duplex	153
4-4	Conclusions	159
4-5	Experimental section	159
4-5-1	Synthesis of pyrene (P), perylene (E) and Cy3 (Y) moiety	160
4-5-2	DNA synthesis containing pyrene (P), perylene (E) and Cy3 (Y)	164
4-5-3	Spectroscopic measurements:	166
4-5-4	Measurement of the melting temperature (T_m):	166
4-5-4	Analysis of time-resolved fluorescence using a streak camera:	167
4-5-5	Curve fitting calculation:	168
4-5-5	Calculation of transition dipole moment and molecular modeling	168
4-5-6	Calculation of FRET efficiency:	169
4-6	References	170
4-7	Appendixes	173

4-7-1 Symbols, abbreviations and their definition.	173
4-7-2 Sequence dependence of fluorophores	175
4-7-3 Fluorescence spectra (static) of all FRET pairs	176
4-7-4 Fitting data of time-resolved fluorescence spectroscopy	177
4-7-5 Exciton coupling between dyes located in close proximity	181
4-7-6 T_m analysis of all modified and native DNA duplex	181
4-7-7 Multiple incorporation of donors; light-harvesting FRET system	182
4-7-8 Theoretical calculation of Förster radii between various dyes	185
LIST OF PUBLICATIONS	188
LIST OF PRESENTATIONS	190
LIST OF AWARD	192
ACKNOWLEDGMENT	193

CHAPTER 1. GENERAL INTRODUCTION

1-1 Properties, structure and function of DNA

Deoxyribonucleic acid, DNA, is a well-known biological molecule for storing genetic information in living cells. It is consisted of four types of nucleotides; Adenine (A), Thymine (T), Guanine (G) and Cytosine (C), genetic information is encoded in a vast amount of DNA sequences written in these 4 letters (Figure 1-1). DNA forms double-stranded helical structure (duplex) by hydrophobic interaction and forming stable hydrogen bonding pair of A-T or G-C. Two strands in DNA duplex run opposite directions to each other (anti-parallel), the direction of the strand is usually defined by the bonding direction from 5' to 3' of deoxyribose backbone. Hence a sequence of DNA strand can discriminate its corresponding sequence by forming duplex (hybridization) e.g. a sequence of DNA 5'-ATGCATGC-3' hybridizes 5'-GCATGCAT-3'. This molecular recognition ability called complementary provides precise duplication of DNA sequence to preserve biological information in living cells.

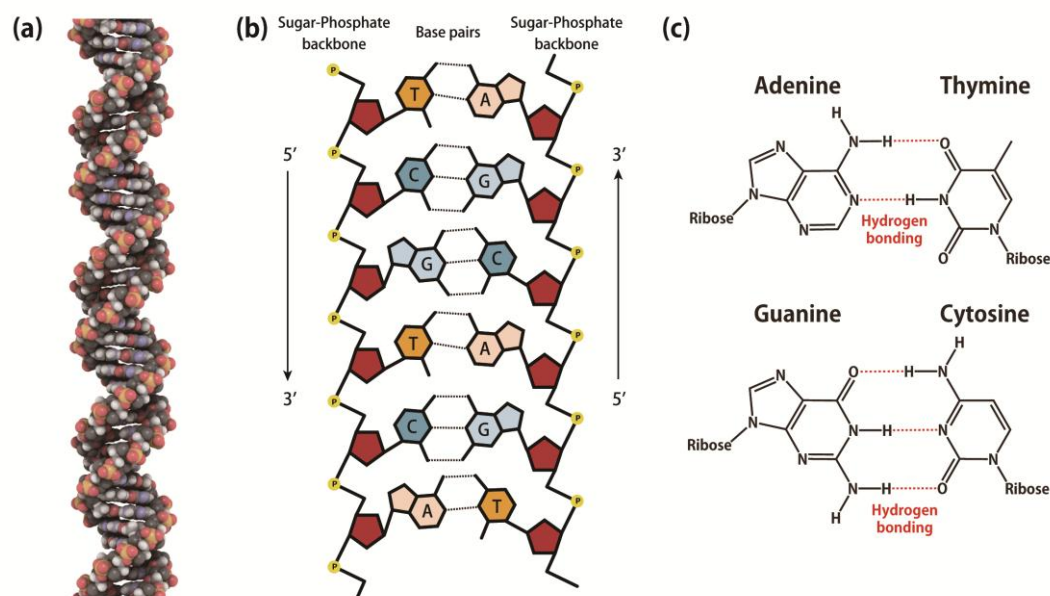


Figure 1-1. The structure of DNA. (a) Molecular model of right-handed turn of DNA helix. (b) Schematic illustration of DNA duplex. Two strands are hybridized in antiparallel manner. The direction of 5'→3' is defined by the sugar backbone. (c) Hydrogen bonding between A and T, G and C base pairs. These hydrogen bonds provide accurate molecular recognition.

Duplication of DNA is conducted by an enzyme called DNA polymerase and is highly regulated by DNA replication protein complex machineries in living cells. This enzyme is now utilized to amplify desired sequences for biological research in laboratory. PCR, Polymerase Chain Reaction is the most famous method of DNA amplification.¹ This technic is used for not only making copy of DNA but also virus detection, reading DNA sequences (DNA sequencing), identifying biological species, gene diagnosis etc. After the Human Genome Project, investigations on the connection between DNA sequence and biological function became more and more important because DNA sequence is no more than “code”, namely to know how the encoded information in DNA works in living cell is necessary.

Today, DNA analyses such as DNA microarray are important technologies to investigate how DNA works in cells because they can analyze huge quantities of expressed genes at one time.² In general, DNA samples extracted from cells are amplified by PCR and hybridized with probes on array, subsequently detected by using fluorophores (Figure 1-2). Hence the quality (e.g. sensitivity or reliability) of DNA analysis depends on accuracy of amplification and sensitivity of fluorophores labeled on DNA. Especially, the sensitivity of DNA detection is greatly important factor since it can cut down the amount of samples and find only a small amount of expressed gene. To enhance sensitivity of DNA detection should be essential for progress on biological researches based on DNA analysis.

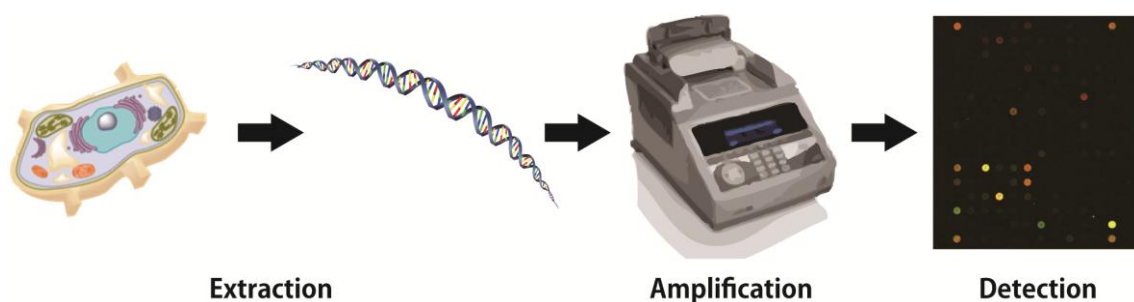


Figure 1-2. An illustration of general procedure of DNA analysis.

1-2 DNA amplification: mechanism and applications

DNA amplification is now widely utilized in biological research for obtaining copies of gene, virus detection, gene diagnosis etc. PCR, Polymerase Chain Reaction, is the most famous and widely accepted method. In PCR, a thermostable enzyme of DNA replication, thermophilic DNA polymerase plays a very important role. As shown in Figure 1-3, DNA strands containing target sequence called “Template”, chemically synthesized known sequence of short single stranded DNAs (approximately 20 bp in general) called “Primer”, thermophilic DNA polymerase and materials of DNA, dNTPs (mix solution of dATP, dTTP, dGTP and dCTP.) were mixed into the solution of reaction buffer. Usually, a pair of primer is designed to hybridize at the start and the end of target sequence. Firstly, the reaction solution is heated (around 95°C) to unhybridize template strands (denaturation). Secondly, the solution is rapidly cooled down to around 60°C and primers are hybridized with templates (annealing). After that, solution is heated again at around 70°C to activate DNA polymerase. DNA polymerase can elongate the primer replicating along with the template (primer extension). The direction of elongation is limited only 5'→3', however, some polymerase can eliminate improperly incorporated bases moving backward by using 3'→5' exonuclease activity, just like “Back Space” on typing. This proof reading activity ensures the accuracy of DNA replication. Repetition of the cycle of denaturing, annealing and primer extension multiplies the number of copied DNA at an exponential rate.

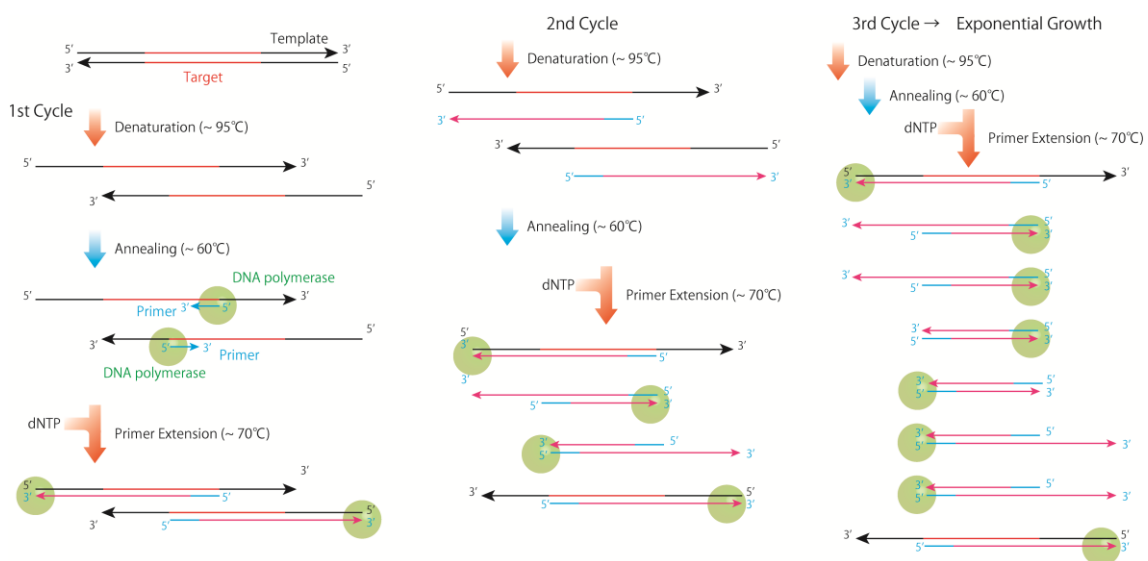


Figure 1-3. The mechanism of exponential amplification in Polymerase Chain Reaction.

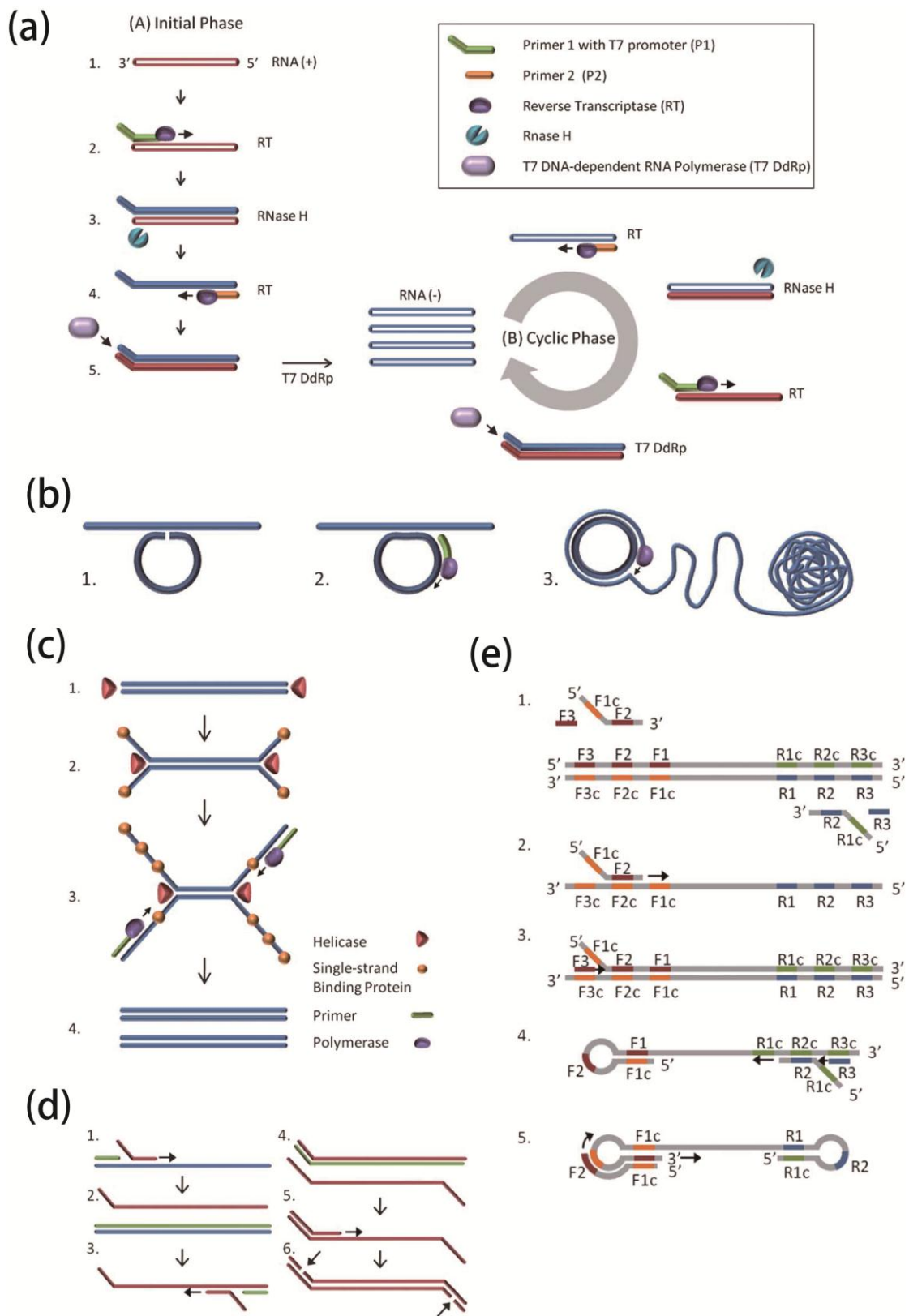


Figure 1-4. Schematic illustrations of mechanism of isothermal amplification methods.³ (a) NASBA (b)RCA (c) HDA (d)SDA (e) LAMP

As described above, the reaction solution will be heated as high as 95°C, therefore thermo stable enzyme derived from thermophilic bacteria or archea is necessary because many enzymes tend to be denatured and lose their activity at higher temperature. It is also considerable that the reaction temperature should be precisely regulated and a dedicated hardware such as thermal cycler is required. This would be a drawback for general application and practical use. Therefore isothermal DNA amplification technologies, DNA amplification methods without special temperature control system, have been developed (e.g. nucleic acid sequence-based amplification (NASBA)⁴, rolling circle amplification (RCA)⁵, strand displacement amplification (SDA)⁶, helicase dependent amplification (HDA)⁷, loop-mediated isothermal amplification (LAMP⁸), and so on⁹) (Figure 1-4). These isothermal DNA amplification methods are often integrated with detection system on a microchip for rapid diagnosis.³ Such batch system of amplification and detection would facilitate the practical applications in not only laboratory but also hospital.

1-3 DNA detection by fluorophores

Fluorophore conjugated DNA is often used for detection of nucleic acids. Presence or absence of the target sequence can be readily examined by hybridization with the fluorescent-labeled probe DNA containing the known sequence of interest. Using fluorophore as a reporter has several merits as follows.

- 1) Easy handling: Once nucleic acids used to be labeled by radio-isotope, however, handling of radio-isotope needs attentions in limited space and has a problem of their lifetime. By contrast, fluorescent dyes are relatively stable and do not require special attentions.
- 2) Highly sensitive: Today, we can use a wide variety of high-quantum yield fluorophores. Excitation by laser enables detection only single molecule in aqueous solution. The progress in optical system brought highly sensitive detection. It is also useful that population of target can be quantitatively analyzed by measuring fluorescence intensity.
- 3) Multi-color imaging available: In recent biological research, components in cells are often stained by several dyes. Fluorophores with different excitation wavelengths

enable detection of individual molecules. Such multi-color imaging provides informative results like co-localization of macromolecules. DNAs labeled with different dyes are also used in comparative study of gene expression using DNA microarray. Förster Resonance Energy Transfer (FRET) is also powerful technic using multiple fluorescent dyes. This topic is described in detail in Chapter 4.

4) A high degree of freedom for molecular design: Fluorescent dyes are chemically synthesized and can be conjugated with any desired targets. Researchers can freely design the molecular probes to improve their selectivity, sensitivity and so on.

5) Non-destructive detection: Although short wavelength like UV is harmful for biological molecules, longer wavelength such as visible light is not. Light can go through the cell membrane and many biological molecules. Hence fluorescent probes in living cell are observable by using microscope. For example, *in situ* hybridization probe technology is an excellent way to obtain live image of living cells. Such detection technologies without killing cells are highly beneficial for molecular cell biology.

Molecular Beacon (MB) is a great example of DNA detection technology using fluorophore (Figure 1-5).¹⁰ At first, MB is closed by hybridization of the stem region and the fluorophore is quenched by the closely located quencher. Once target sequence which is complementary with the loop region was added, MB will open and fluorescence is recovered from quenching owing to dissociation of the quencher. This turn-on type mechanism is popular for DNA detection. Sensitivity of MB depends on S/N ratio, namely efficient quenching to suppress background in OFF state and highly intense fluorescence emission in ON state are important. Recently many novel designs of MB have been vigorously developed to improve S/N ratio. MB is also used in quantitative Real Time PCR, which can analyze the amount of mRNA containing specific sequence.

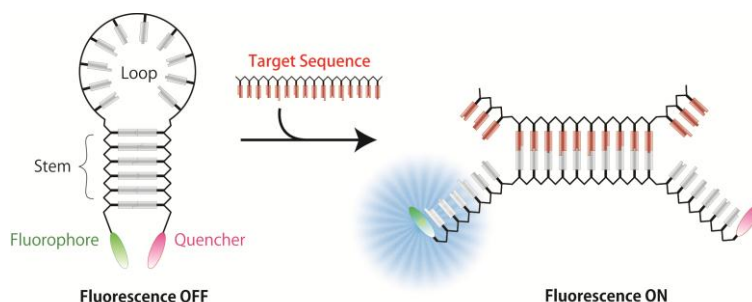


Figure 1-5. The typical design of molecular beacon.

1-4 Problems on DNA amplification and detection by fluorophores

There are several reasons why the sensitivity of DNA amplification and its detection was decreased. For DNA amplification, unexpected amplification occasionally occurs under both PCR and isothermal conditions, especially if the region to be amplified contains repetitive sequences. This unexpected amplification is a serious problem because it decreases sensitivity and what is worse, it brings a false result. For the stage of detection, fluorescence quenching by natural base pair should be avoided because the quantum yield of the fluorescent dye is the dominant factor that determines its sensitivity. In addition, small Stokes' shift is also responsible for low sensitivity. Stokes' shift is the difference between λ_{\max} of absorption and that of fluorescence emission. If Stokes' shift was too small, the scattered excitation light will intrude on the detection wavelength region and increase background. For example, Cy3, which is often used for labeling of probes in DNA microarray technology, however, Cy3 is efficiently quenched by a particular sequence of DNA and has only a small Stokes' shift of 15 nm.¹¹

1-5 Purpose of this study

To improve the sensitivity of DNA amplification and its detection, following investigations were performed.

1) Clarifying the mechanism of unexpected DNA amplification under isothermal conditions: Several elongation mechanisms under isothermal conditions have been proposed previously, however, they cannot explain highly efficient amplification of repetitive sequence. Here, we focused on *de novo* DNA synthesis, which is still obscure unexpected DNA amplification. This reaction produces very long repetitive DNA and the reaction efficiency highly depended upon the reaction temperature. Hence the products of *de novo* DNA synthesis were closely analyzed. Discussion of the mechanism and its verification were also performed.

2) Enhancement of quantum yield of fluorophores: Electron transfer between dyes and neighboring nucleobases is a primary cause of quenching. Here, we aimed at development of a new base-surrogate which can suppress electron transfer to restrict quenching by natural base pairs neighboring fluorophores. In this study, we

investigated the stability, structure, and shielding ability of artificial base pairs that contains cyclohexyl rings and their analogs.

3) Improvement of Stokes shift: One promising strategy for improvement of Stokes' shift is the utilization of Förster Resonance Electron Transfer (FRET). Several studies on the application of DNA-based FRET system have reported an increase in the "apparent" Stokes' shift.¹²⁻¹⁸ However, investigation of a FRET system *within* DNA duplex is still insufficient because fluorophores are usually introduced into outside of DNA duplex. In such case, the effect of orientation has been neglected since dyes are freely mobile and their position and orientation are not controlled sufficiently due to its difficulty. Actually, efficiency of FRET depends on distance and orientation between dyes. Therefore, we aimed at a development of a novel FRET system tethering dyes with DNA duplex to demonstrate the orientation effect based upon FRET theory.

1-6 References

- (1) a) Saiki, R. K.; Scharf, S., Faloona, F.; Mullis, K. B.; Horn, G. T.; Erlich, H. A.; Arnheim, N. *Science* **1985**, *230*, 1350–1354.
b) Saiki, R. K.; Gelfand, D. H.; Stoffel, S.; Scharf, S. J.; Higuchi, R.; Horn, G. T.; Mullis, K. B.; and Erlich, H. A. *Science* **1988**, *239*, 487–491.
- (2) Miller, M.B.; Tang, Y.-W. *Clin. Microbiol. Rev.* **2009**, *22*, 611-633.
- (3) Asiello, P. J.; Baeumner, A. J. *Lab Chip*, **2011**, *11*, 1420-1430.
- (4) Compton, J. *Nature* **1991**, *350*, 91–92.
- (5) Fire, A.; Xu, S. Q. *Proc. Natl. Acad. Sci. U.S.A.* **1995**, *92*, 4641–4645.
- (6) a) Walker, G. T.; Fraiser, M. S.; Schram, J. L.; Little, M. C.; Nadeau, J. G.; Malinowski, D. P. *Nucleic Acids Res.* **1992**, *20*, 1691–1696. B) Walker, G. T.; Little, M. C.; Nadeau, J. G.; Shank, D. D. *Proc. Natl. Acad. Sci. U.S.A.* **1992**, *89*, 392–396.
- (7) An, L.; Tang, W.; Ranalli, T.A.; Kim, H.J.; Wytiaz, J.; Kong, H. *J. Biol. Chem.* **2005**, *280*, 28952– 28958.
- (8) Notomi, T.; Okayama, H.; Masubuchi, H.; Yonekawa, T.; Watanabe, K.; Amino, N.; Hase, T; *Nucleic Acids Res.* **2000**, *28*, e63.

- (9) Van Ness, J.; Van Ness, L. K.; Galas, D. J. *Proc. Natl. Acad. Sci. U.S.A.* **2003**, *100*, 4504–4509.
- (10) a) Juskowiak, B. *Anal. Bioanal. Chem.* **2011**, *399*, 3157–3176.
- b) Tan, W.; Wang, K.; Drake, T. J. *Curr. Opin. Chem. Biol.* **2004**, *8*, 547–553.
- c) Kashida, H.; Takatsu, T.; Fujii, T.; Sekiguchi, K.; Liang, X. G.; Niwa, K.; Takase, T.; Yoshida, Y.; Asanuma, H. *Angew. Chem.* **2009**, *121*, 7178–7181; *Angew. Chem. Int. Ed.* **2009**, *48*, 7044–7047;
- b) Hara, Y.; Fujii, T.; Kashida, H.; Sekiguchi, K.; Liang, X. G.; Niwa, K.; Takase, T.; Yoshida, Y.; Asanuma, H. *Angew. Chem.* **2010**, *122*, 5634–5638; *Angew. Chem. Int. Ed.* **2010**, *49*, 5502–5506.
- c) Johansson, M. K.; Fidder, H.; Dick, D.; Cook, R. M. *J. Am. Chem. Soc.* **2002**, *124*, 6950–6956.
- d) Johansson, M. K.; Cook, R. M. *Chem. Eur. J.* **2003**, *9*, 3466–3471.
- (11) Mujumdar, R. B.; Ernst, L. A.; Mujumdar, S. R.; Lewis, C. J.; Waggoner, A. S. *Bioconjugate Chem.* **1993**, *4*, 105–111.
- (12) Selvin, P. R.; Kenneth, S. *Methods Enzymol.* **1995**, *246*, 300–334.
- (13) Hung, S.-C.; Mathies, R. A.; Glazer, A. N. *Anal. Biochem.* **1998**, *255*, 32–38.
- (14) Kawahara, S.; Uchimaru, T.; Shigeo, M. *Chem. Commun.* **1999**, 563–564.
- (15) Tong, A. K.; Jockusch, S.; Li, Z.; Zhu, H.-R.; Akins, D. L.; Turro, N. J.; Ju, J. *J. Am. Chem. Soc.* **2001**, *123*, 12923–12924.
- (16) Ohya, Y.; Yabuki, K.; Hashimoto, M.; Nakajima, A.; Ouchi, T. *Bioconjugate Chem.* **2003**, *14*, 1057–1066.
- (17) Lewis, F. D.; Zhang, L.; Zuo, X. *J. Am. Chem. Soc.* **2005**, *127*, 10002–10003.
- (18) Iqbal, A.; Arslan, S.; Okumus, B.; Wilson, T. J.; Giraud, G.; Norman, D. G.; Ha, T.; Lilley, D. M. J. *Proc. Natl. Acad. Sci. U.S.A.* **2008**, *105*, 11176–11181.

CHAPTER 2. CLARIFICATION OF THE MECHANISM OF UNEXPECTED DNA AMPLIFICATION

2-1 Abstract

Unexpected DNA amplification is a considerable problem in DNA amplification technology such as gene diagnosis since it would bring undesired results like pseudo-positives. In this chapter, *de novo* DNA synthesis, which is assumed to be a cause of unexpected DNA amplification but its mechanism is still obscure, was focused on. First, the mechanism of *de novo* DNA synthesis, temperature dependence and properties of the products were investigated in detail. *De novo* DNA synthesis was carried out in a wide range of temperature (25-80°C). For **Vent** and **Vent(exo-)**, the synthesis efficiency varied with reaction temperature in the order of 50°C > 70°C. In addition, the reaction efficiency of **Vent(exo-)** was much slower than that of **Vent** owing to lack of exonuclease activity involving the binding with short DNA. Moreover, product DNAs contained highly repetitive sequence of palindrome and they had much higher T_m than the reaction temperature indicating that the products were forming stable duplex during reaction. Then for clarifying the mechanism of *de novo* DNA synthesis, unexpected elongation of short single stranded DNA (ssDNA) was also studied. Surprisingly, **Vent** could elongate short ssDNA such as (AC)₉, (AG)₉, (TC)₉, (TG)₉ which can NEVER form base pair. The optimal reaction temperature was correlated with GC% of short ssDNA, similar to *de novo* DNA synthesis. The mechanism of elongation of short ssDNA was investigated using dT₁₂ and radio-isotope labeled dATP. Interestingly, dT₁₂ could be elongated without its complementary strand, poly dA chain was synthesized from 3'-end of dT₁₂ suggesting that hairpin formation is important for elongation of short ssDNA. Furthermore, to explain efficient elongation in *de novo* DNA synthesis, a new reasonable elongation model called terminal hairpin formation and self-priming extension (THSP) model was proposed. In this model, only termini should be dissociated and primer extension from 3'-end of conserved hairpin sequence enables successive elongation. The validity of THSP model was also verified by using short DNA containing two hairpins at each end.

2-2 Introduction

Non-specific DNA amplification brings considerable errors in DNA analyses such as gene diagnosis since it reduces detection sensitivity and accuracy. Especially, when the amount of the template is very small, non-specific DNA amplification product would be dominant and supersede the analytes. In general, the sequence of primer is carefully designed to avoid non-specific amplification caused by mis-priming, however, non-specific amplification is occasionally carried out even if primers were appropriately designed. On the other hand, isothermal DNA amplification technologies were now widely utilized for practical applications.¹⁻³ Non-specific amplification affects not only PCR but also isothermal amplification. In many cases, the mechanisms of isothermal amplification are complicated. Therefore specifying causes of non-specific amplification under isothermal condition is difficult. Namely, clarification of the mechanism of non-specific amplification is required to prevent it. Here, *de novo* DNA synthesis, which is assumed to be a cause of undesired amplification but its mechanism is still obscure, was focused on and the mechanism was investigated to find solution for avoiding non-specific amplification.

De novo DNA synthesis is defined as the synthesis of DNA from dNTPs directly by DNA polymerase. This surprising finding had been firstly reported in as early as 1960s by Kornberg *et al.*⁴⁻⁸ They described that *E. coli* polymerase I could synthesize double strand DNA such as poly (dA-dT) or poly (dG-dC) from only dNTPs without adding any DNA or RNA as template/primer under isothermal condition. Same phenomena by *M.luteus* DNA polymerase and calf thymus DNA polymerase α were also reported by several groups.^{9,10} In 1979, however, Nazarenko *et al.* showed that *de novo* DNA synthesis by *E. coli* DNA polymerase I needed short oligonucleotides which were synthesized by contaminated dNDP-transferase.^{11,12} It had been a controversy for a long time because it was hard to eliminate completely contaminant such as DNA, RNA or other proteins.

In 1997, Ogata and Miura confirmed that highly-purified *E. coli* DNA polymerase I could NOT carry out *de novo* DNA synthesis.¹³ They also reported several highly-purified thermophilic DNA polymerase (*Tli* (Vent) and *Tth* DNA polymerase) could carry out *de novo* DNA synthesis, and the products were highly repetitive

palindromic sequence.^{14,15} For Vent DNA polymerase, the product sequence varied depending on the reaction temperature and the GC content increased upon the increase of the reaction temperature e.g. (TAAT)_n at 69°C, (TATCTAGA)_n at 74°C, (TATCCGGA)_n at 84°C, (GATCGC)_n at 94°C. In 2004, Liang *et al.* reported extreme acceleration of *de novo* DNA synthesis by adding restriction enzyme (RE-pol reaction), and proposed an exponential amplification model involving digestion-elongation cycles (Cut-grow mechanism).^{16,17} In the presence of restriction enzyme, the obtained product was consisted of the recognition sequence of the restriction enzyme. Same acceleration by using nicking endonuclease is also reported.¹⁸ Furthermore, there are some reports of *de novo* DNA synthesis by thermophilic DNA polymerases¹⁹⁻²¹ and by mesophilic DNA polymerases.²²

However, the mechanism of *de novo* DNA synthesis is still little known. Several reports described that *de novo* DNA synthesis has two steps; initiation and elongation.¹⁹ In the initiation step, short oligo nucleotide (“Short Seeds”) which should become the origin of the tandem repeat sequence may be somehow synthesized from dNTP. In the elongation step, the Short Seeds will be elongated efficiently under isothermal conditions. Some groups have proposed elongation mechanism of short repetitive sequence under isothermal conditions²³⁻²⁷, however, they are not so likely to explain the mechanism during *de novo* DNA synthesis well.

In this study, for clarifying the mechanism, *de novo* DNA synthesis by Vent DNA polymerase and Vent(exo-) DNA polymerase (hereafter abbreviated as **Vent** and **Vent(exo-)** respectively) was studied in detail. Recently, it was found that *de novo* DNA synthesis could be carried out in a wide range of temperature and the synthesis efficiency varied greatly depending on the reaction temperature.²⁸ Especially, **Vent(exo-)** was reported that it cannot carry out *de novo* DNA synthesis,^{14,20} however, *de novo* synthesized DNA was detected after long incubation time under relatively lower temperatures. Here the mechanism of *de novo* DNA synthesis was discussed and a reasonable elongation mechanism (THSP model: Terminal Hairpin formation and Self Priming elongation model) was proposed according to the results of analysis of *de novo* synthesized products. Verification of THSP model was also performed.

2-3 Results and Discussions

2-3-1 Temperature dependence of *de novo* DNA synthesis

First, the reaction conditions involving the efficiency of *de novo* DNA synthesis were investigated. It has been already reported that *de novo* DNA synthesis depends on the reaction temperature, however, only higher temperature > 64 °C was reported.^{14,15} A wide range of reaction temperature should be examined considering the conditions of PCR and isothermal amplification.

De novo DNA synthesis was carried out at various temperatures (25, 37, 50, and 70°C) by **Vent** in the presence of only dNTPs in 1× Thermopol buffer without adding any oligo nucleotides (Figure 2-1). Aliquots of the reaction mixture were taken after a certain time interval. The reaction was quenched by dilution with 0.5× TAE buffer (60~6000 times), then each samples was stained with 2× SYBR Green I. The amount of DNA was quantitatively analyzed by fluorescence measurement.

As expected, the efficiency of *de novo* DNA synthesis highly depended on the reaction temperature. **Vent** could *de novo* synthesize DNA not only under higher temperature but also relatively lower temperature (25-50°C), indicating that *de novo* DNA synthesis could be carried out in a large range of temperature (25-94°C). Moreover, the synthesis efficiency was varied with the reaction temperature in the order of 50 > 70 > 37 > 25 °C. The efficiency of *de novo* DNA synthesis at 25 °C is quite slow, however, a certain amount of DNA was detected after long time incubation of 120 h. Interestingly, the reaction speed of the *de novo* DNA synthesis at 50°C was faster than the optimal temperature for thermophilic DNA polymerase (around 70°C). The amount of synthesized DNA within 48 h was almost doubled as compared with that at 70°C (See inset in Figure 2-1). The growth in the amount of DNA at 50°C was saturated within 48h owing to exhaustion of dNTP. Although the concentration of dNTP was relatively higher (0.5 mM) than typical condition of PCR, it was exhausted only within 48 h, demonstrating that the efficiency of *de novo* DNA synthesis was considerably high.

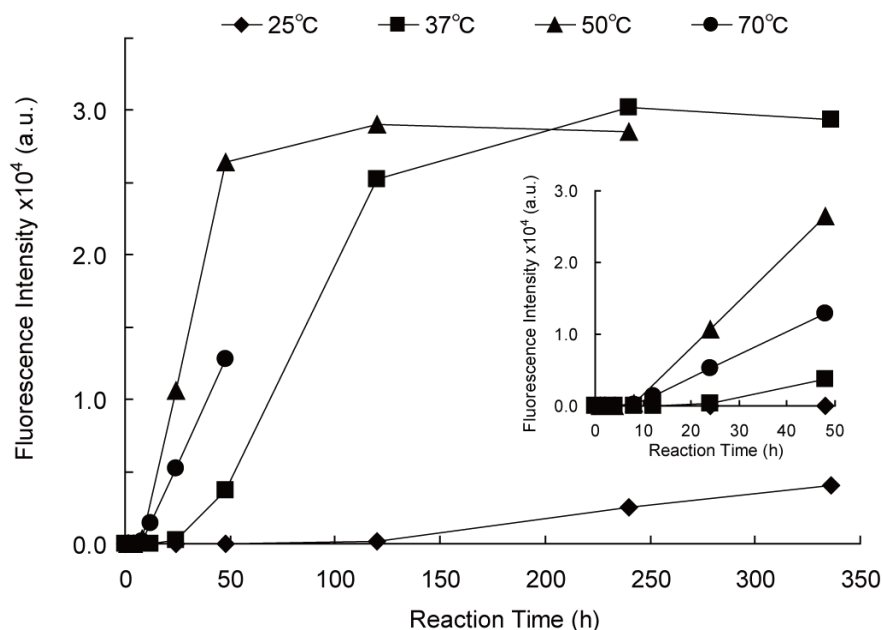


Figure 2-1 Time course of *de novo* DNA synthesis by **Vent** at various temperatures. (At 25°C (diamonds), 37°C (squares), 50°C (triangles), 70°C (circles)) Except for the concentration of DNA polymerase (20 U/mL), other reaction conditions were as same as described standard reaction conditions. The inset shows the results in the first 48 h. Fluorescence intensity was measured on FP-6500 (Jasco) after stained by 2x SYBR Green I.

Next, comparison of temperature dependence between **Vent** and **Vent(exo-)** was performed (Figure 2-2) to confirm whether **Vent(exo-)** could carry out *de novo* DNA synthesis or not. **Vent** has two distinguishable activities: polymerization and 3'→5' exonuclease activity. **Vent(exo-)** is 3'→5' exonuclease deficient mutant of **Vent**. Interestingly, despite of the previous reports of several groups, **Vent(exo-)** could also *de novo* synthesize DNA, however, its efficiency was extremely lower than that of **Vent** in any temperature. The products synthesized by **Vent** could be detected only within 20 h, whereas that of **Vent(exo-)** could be observed after incubation of > 20 h. Especially, the reaction speed by **Vent(exo-)** was very slow at 70°C and synthesized DNA could not be detected after incubation for 60 h. On the other hand, **Vent(exo-)** could also *de novo* synthesize DNA most efficiently at around 50°C. Since the difference between **Vent** and **Vent(exo-)** is only two amino residues in 3'→5' exonuclease active site D141A and E143A,²⁹ these results suggest that 3'→5' exonuclease activity would play an important role in the efficiency at early step of *de novo* DNA synthesis.

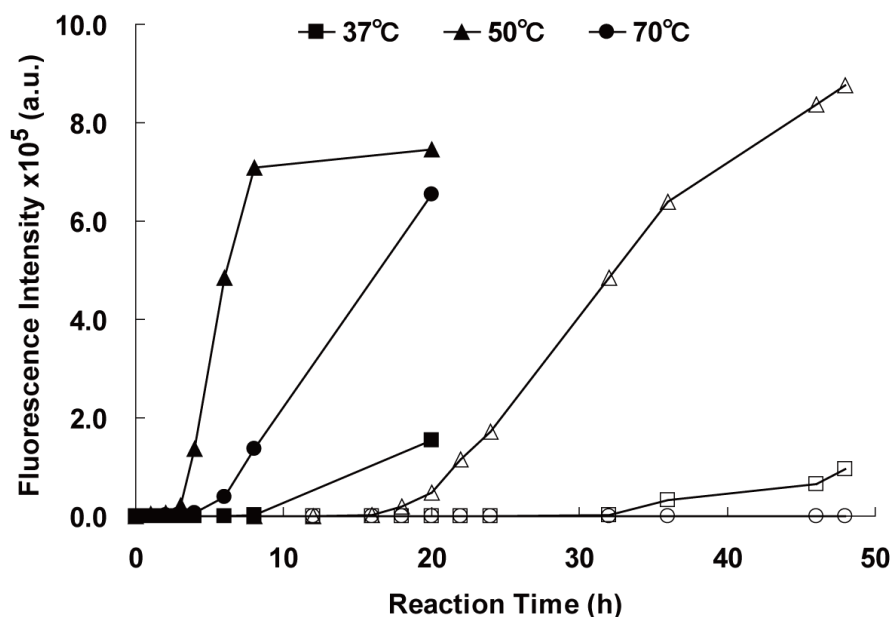


Figure 2-2 Time course of *de novo* DNA synthesis by **Vent** (filled symbols) or **Vent(exo-)** (open symbols) at 37°C (squares), 50°C (triangles), 70 °C (circles). Fluorescence was measured on FLA-3000 (Fujifilm) after stained by 2x SYBR Green I.

For investigating more detail on the temperature dependence, *de novo* DNA synthesis was carried out at 37, 45, 50, 55, 60, 70, 80°C. (Figure 2-3) Since long reaction time would bring out exhaustion of dNTPs and product DNA degradation by exonuclease activity of **Vent**, the reaction was stopped within 20 h. *De novo* DNA synthesis by **Vent(exo-)** was also performed and stopped within 60 h. Again, for both **Vent** and **Vent(exo-)**, the *de novo* synthesis efficiency was highest in a temperature range of 45-55°C. Unexpectedly, the efficiency of **Vent** was slowed down at 60°C but recovered at higher temperatures. For **Vent(exo-)**, the efficiency was extremely low at a higher temperature above 60 °C and the product DNA could not be detected.

Ogata and Miura previously reported *de novo* DNA synthesis by **Vent** at relatively higher temperature (69-94°C).¹⁵ Their report also mentioned that **Vent** could not carry out *de novo* DNA synthesis at 64°C within 3 h, however, in this study, synthesized product by **Vent** at 60°C was detected after incubation of 6 h.

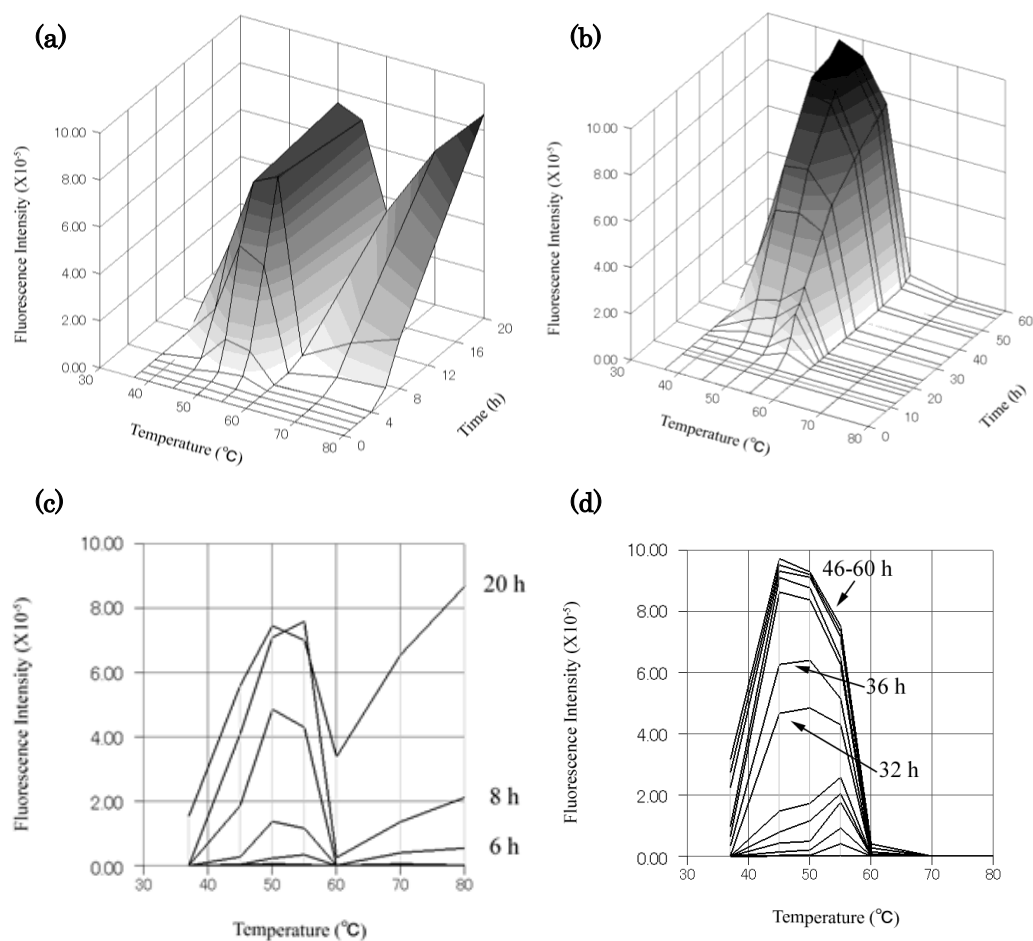


Figure 2-3. Temperature dependence on the efficiency of *de novo* DNA synthesis by **Vent** and **Vent(exo-)**. Fluorescence intensity was measured on the imaging analyzer FLA-3000 (Fujifilm) with 96-well micro plate. (a) Three dimensional view of the time course of *de novo* DNA synthesis by **Vent** at various temperatures. (b) Three dimensional view of the time course of *de novo* DNA synthesis by **Vent(exo-)** at various temperatures. (c) Cross-section view of the panel a. (d) Cross-section view of the panel b.

Vent could carry out *de novo* DNA synthesis more efficiently than **Vent(exo-)** in a large range of temperature (25-94 $^{\circ}\text{C}$), whereas **Vent(exo-)** was only at lower temperatures (25-60 $^{\circ}\text{C}$) and the reaction speed was also significantly dropped. As described, the difference between **Vent** and **Vent(exo-)** was only two substituted residues. A lacking of exonuclease activity possessed striking difference in the temperature dependence. This result suggests that exonuclease activity affects with binding of short DNA and DNA polymerase. **Vent** could catch DNA more efficiently by using binding pocket of exonuclease activity.

2-3-2 Analyses of the products of *de novo* DNA synthesis

Next, to clarify the mechanism of *de novo* DNA synthesis by **Vent** and **Vent(exo⁻)**, the products were analyzed in detail. *De novo* synthesized products were analyzed on 1% agarose gel. The products were collected from reaction tube after sufficient reaction time: around plateau of DNA synthesis (For **Vent**, 20 h, for **Vent(exo⁻)**, 60 h, respectively). As expected, the products were much longer than 10 kbp and broadly smeared (Figure 4a and b) indicating that many DNA molecules of various lengths were synthesized. In the case of **Vent** at 37°C and **Vent(exo⁻)** above 60°C, only narrow bands were observed, this may reflect that the synthesis efficiency was slow and only less number of DNA chains were elongated efficiently. Moreover, higher concentration of DNA polymerase exhibited shorter length of products. This would be because higher concentration of polymerase allows elongation of many molecules and dNTPs were exhausted in short time and it inhibited further elongation. When concentration of DNA polymerase was 20 U/mL, the products were remarkably long and difficult to be electrophoresed from the well. Since the products would contain higher order structures owing to tandem repetitive sequence, alkaline denatured agarose gel electrophoresis was also performed, however, broadly smeared long DNA products were observed. (Figure 4c) Hence, it was confirmed that very long DNA was synthesized by *de novo* DNA synthesis.

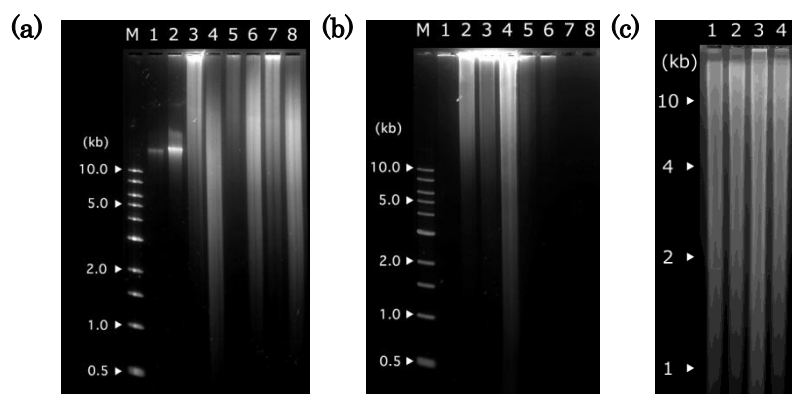


Figure 2-4. Gel patterns of the synthesized DNA under various conditions. (1% agarose gel) Odd numbered lanes are the results when 20 U/mL DNA polymerase was used and even numbered lanes are 100 U/mL. Reaction temperatures were at 37°C for Lane 1 and 2, 50 °C for Lane3 and4, 60 °C for Lane 5 and 6, 70 °C for Lane 7,8, respectively. (a) *De novo* synthesized DNA products by **Vent** (b) *De novo* synthesized DNA products by **Vent(exo⁻)**. (c) *De novo* synthesized products by **Vent** were electrophoresed on 1% alkaline denature agarose gel. Reaction temperature was 37°C for Lane 1, 50°C for Lane 2, 60°C for Lane3, 70°C for Lane 4.

In addition, T_m measurement of the product was performed. The reaction solution after sufficient time was purified by PCI/CIA treatment and ethanol precipitation, then a certain amount of purified products were resolved in 1× Thermopol Detergent Free buffer to avoid opaqueness of TritonX-100. At lower reaction temperature (37 and 50°C), T_m s of the products were almost the same (around 63 °C, Figure 2-5). These results suggested that those products have same GC content. At higher temperature than 60°C, T_m was trending higher according to the reaction temperature indicating that the sequence of the products varied with the reaction temperature. It is noteworthy that GC content increased at higher reaction temperature. These results were consistent with the reports of Ogata *et al.*¹⁵ Interestingly, in all cases, T_m s of the products were much higher than the reaction temperatures. Therefore the most part of the products was forming duplex during *de novo* DNA synthesis. Usually, DNA polymerase requires Template/Primer structure to initiate primer extension from 3'-end of the primer with 5'-overhanged template, however, such stable duplex would not be elongated in usual way. Hence another mechanism which can elongate stable duplex should be proposed.

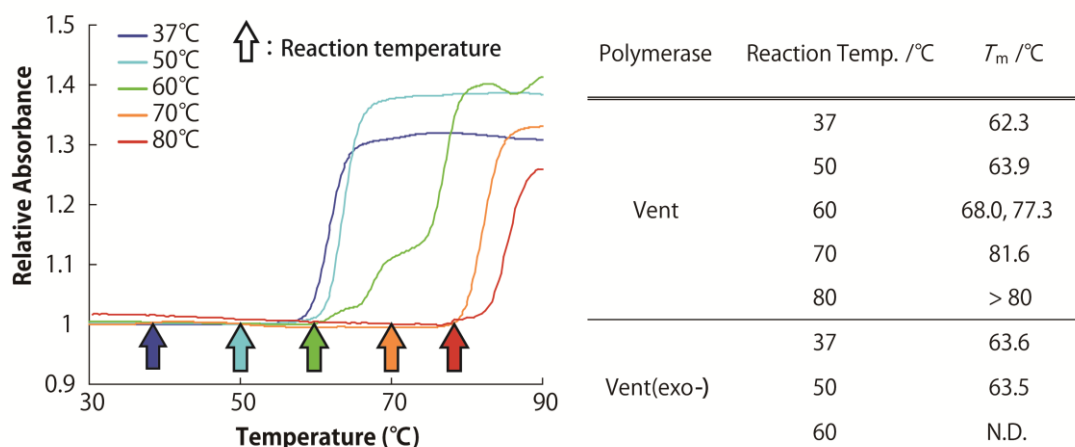


Figure 2-5. T_m values and melting curves of the products of *de novo* DNA synthesis at various temperatures. Measurement conditions: Purified products of *de novo* DNA synthesis was dissolved into 1× Thermopol Detergent Free buffer (20 mM Tris-HCl, 10 mM $(\text{NH}_4)_2\text{SO}_4$, 10 mM KCl, 2.0 mM MgSO_4 , pH 8.8). Absorbance at 260 nm was standardized at approximately 1.0. Temperature ramp was $0.5^\circ\text{C}/\text{min}^{-1}$.

Moreover, sequencing analysis of the products was performed. Purified products were digested by a slight amount of DNaseI in the presence of Mn^{2+} ion so as to obtain blunt-ended fragments. Then digested DNA was inserted into *Sma*I site in multi cloning site (MCS) of pUC19 plasmid vector. Inserted vectors were cloned and used for sequencing analysis according to standard biological methods.³⁰ The results from sequence analysis were summarized in Table 2-1. The products by **Vent** at < 60 °C and by **Vent(exo-)** at 37, 50 and 60 °C were poly (dA-dT). This coincidence was consistent with the result of T_m measurement. Again, poly (dA-dT) was synthesized at relatively lower temperatures (< 60°C) by both **Vent** and **Vent(exo-)**. The efficiency of *de novo* DNA synthesis by both **Vent** and **Vent(exo-)** was highest at around 50°C. This is because the polymerases can extend poly (dA-dT) most efficiently at around 50°C within short time. Actually, low concentration of (dA-dT)₆ was elongated efficiently by **Vent(exo-)** under isothermal condition at 50°C. (data not shown) On the other hand, poly (dA-dT) would be unstable at 60°C to form a structure which could be elongated. Thus reaction efficiency at 60°C was slowed down relative to that of 50°C. For relatively higher temperatures (> 60 °C) of **Vent**, the products were (CGTATA)_n at 70°C and (TGCA)_n at 80°C, respectively. It was confirmed that higher T_m s of the products at 70 or 80 °C arose from the increase of GC%.

Table 2-1. Sequences of the products of *de novo* synthesis at various temperatures.

Polymerase	Temperature (°C)	Sequence	GC%
Vent	37	(ATAT) _n	0
	50	(ATAT) _n	0
	60	(ATAT) _n	0
	70	(CGTATA) _n	33
	80	(TGCA) _n	50
Vent(exo-)	37	(ATAT) _n	0
	50	(ATAT) _n	0
	60	(ATAT) _n	0

As shown in Figure 2-6, the mechanism of *de novo* DNA synthesis is assumed to be separated into 2 steps. In earlier stage, “initiation step” involves the synthesis of short DNA fragment from dNTP. The short DNA fragment which can be efficiently elongated was called “Short Seeds” here. In second stage of the elongation step, synthesized Short Seeds will be elongated by DNA polymerase iteratively and long repetitious DNA will be synthesized.

Note that the products of *de novo* DNA synthesis contained highly repetitious palindromic sequences with period of 2-6 mer. This was strongly suggested that short sequences which have particular sequences (Short Seeds e.g. poly dA-dT oligomer) were somehow synthesized in the initiation step of *de novo* DNA synthesis, and then such “Short Seeds” were efficiently elongated under isothermal conditions. Taken together, questions to be solved were as follows: 1) How “Short Seeds” were synthesized in the early step? 2) How the long stable duplexes with highly repetitive sequences were efficiently elongated under isothermal conditions nevertheless the reaction temperature was much lower than T_m . For question 1, direct observation of synthesis of Short Seeds is impossible due to lower concentration of DNA fragment and detection sensitivity. Therefore, question 1 should be discussed by investigating how short sequence can be elongated. Question 2 will be discussed below, in section 2-3-5.

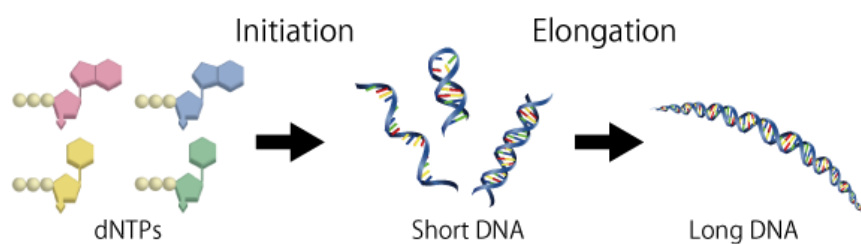


Figure 2-6 *De novo* synthesis involves 2 steps: initiation step and elongation step. In the initiation step, short DNAs as “Short Seeds” for elongation are synthesized from dNTP. In the elongation step, the “Short Seeds” are elongated to long DNA by DNA polymerase.

2-3-3 Temperature dependence on elongation of Short ssDNA

To answer the questions described above, elongation of short repetitive sequence was investigated. Poly (dA-dT) is known to be readily elongated under isothermal conditions especially at lower temperatures around 50°C. Here, to check how many molecules are required for efficient elongation, various concentrations of poly (dA-dT), (AT)₉ was added to the reaction solution. The time course of DNA amount was compared with that of *de novo* DNA synthesis (Figure 2-6) Reaction was conducted at 50°C, in which poly (dA-dT) can be efficiently elongated. As shown in Figure 2-6a, 1 nM-1 pM of (AT)₉ could be elongated within short time and a large amount of DNA was synthesized. On the other hand, less than 1 fM (48,000 molecules) of (AT)₉ exhibit no obvious effect on elongation comparing with the control (without any added DNA, equals *de novo* DNA synthesis) (Figure 2-6b). Therefore in the initiation step of *de novo* DNA synthesis, a certain amount of Short Seeds, which is comparable to 48,000 molecules of (AT)₉, would be synthesized within 8-20 h. After that, Short Seeds could be elongated efficiently and the longer products allow detection by fluorescence measurement.

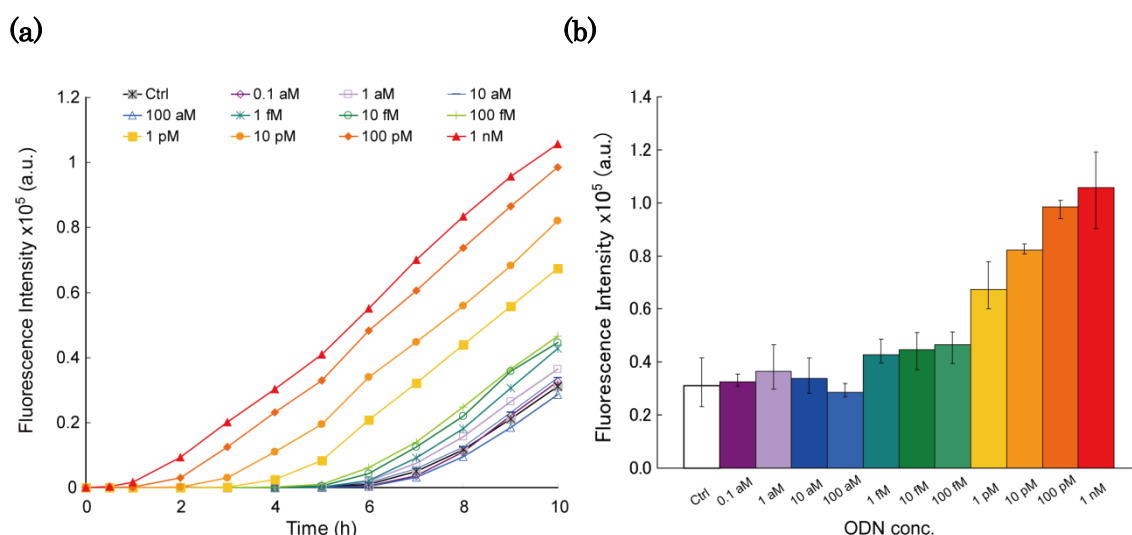


Figure 2-7. Comparison of elongation efficiency of various concentrations of (AT)₉. (a) Time course of the elongation of (AT)₉. (b) Comparison of the amounts of elongated DNA after 10 hours. Fluorescence was measured on FLA-3000 after stained by 2x SYBR Green I.

Next, short single strand DNA (short ssDNA) mimicking DNA fragment in the initiation step was reacted at various temperatures. Unlike poly (dA-dT), these short ssDNAs are seemed not to be elongated because they cannot form duplex by themselves. To know what sequence is suitable for efficient elongation will provide important information about synthesis of Short Seeds in the initiation step. In addition, the elongation of short ssDNA will be beneficial since it is similar to the non-specific amplification of primers in PCR. Temperature dependence and polymerase dependence of elongation by **Vent(exo-)** using 10 types of various sequence of ssDNA was systematically investigated here. The analysis of products was performed and its elongation mechanism was also discussed.

Here, various short ssDNAs described in Table 2-2 were reacted with **Vent(exo-)** under isothermal conditions (37, 50, 60, 70, 80°C) and the temperature dependence was investigated systematically. Reaction conditions were as follows: 20 U/mL Vent(exo-) DNA polymerase, 0.5 mM each dNTP, 100 nM DNA, in 1x Thermopol buffer for 4 hours.

Table 2-2. Names and sequences used in this section.

Name	Sequence
(AA) ₉	5' - AAAAAAAAAAAAAAAAAA - 3'
(AT) ₉	5' - ATATATATATATATATAT - 3'
(AC) ₉	5' - ACACACACACACACACAC - 3'
(AG) ₉	5' - AGAGAGAGAGAGAGAGAG - 3'
(TT) ₉	5' - TTTTTTTTTTTTTTTTTT - 3'
(TC) ₉	5' - TCTCTCTCTCTCTCTCTC - 3'
(TG) ₉	5' - TGTGTGTGTGTGTGTGTG - 3'
(CC) ₉	5' - CCCCCCCCCCCCCCCCCC - 3'
(CG) ₉	5' - CGCGCGCGCGCGCGCGCG - 3'
(GG) ₉	5' - GGGGGGGGGGGGGGGGGG - 3'

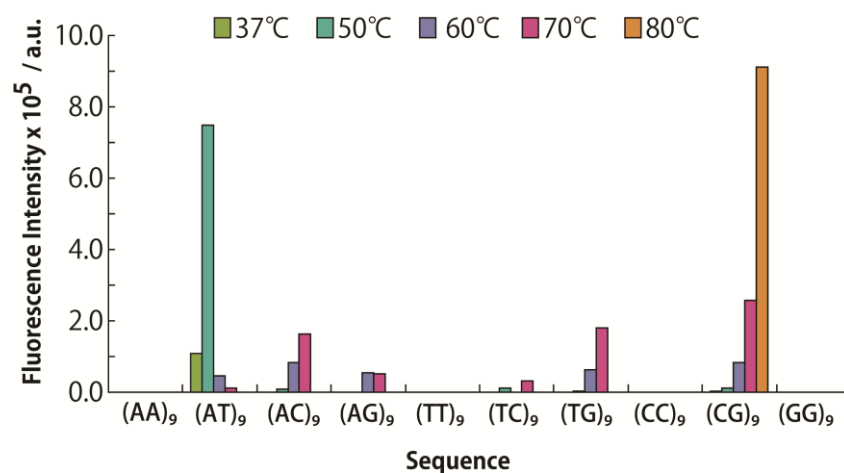


Figure 2-8. Comparison of the amount of elongated various sequence ODNs at 37, 50, 60, 70, 80°C. Reaction conditions: 20 U/mL Vent(exo⁻) DNA polymerase, 0.5 mM each dNTP, 100 nM ODNs in 1x Thermopol buffer. Fluorescent measurement was performed after staining 2x SYBR Green I on 96-well microplate.

Figure 2-8 shows quantitatively analyzed DNA amount after 4 hours of elongation reaction of various sequences. These various short ssDNA depended greatly on the reaction temperatures. (AT)₉ and (CG)₉ which were self-complementary could be efficiently elongated at 50°C and 80 °C, respectively. It was known that such self-complementary repetitious sequences tend to be elongated by slippage mechanism.^{8,23} However, the efficiency of elongation was unexpectedly high since the elongation by slippage would be slow (See below for further detail). Surprisingly, (AC)₉, (AG)₉, (TC)₉ and (TG)₉ were elongated efficiently around 70°C even though they were not self-complementary, indicating that this increase of DNA amount was caused by unusual way. The homopolymers (AA)₉, (TT)₉, (CC)₉ and (GG)₉ seemed not to be elongated, however, only (TT)₉ was elongated after long time enough (data not shown). These results clearly suggested that GC% of the ssDNA was responsible for the temperature dependence of elongation efficiency. For example, the optimal temperature for elongation of (AT)₉, GC% = 0 was 50°C. The optimal temperature for ODNs which contain GC% = 50 such as (AC)₉, (AG)₉, (TC)₉ and (TG)₉ was at 70 °C. (CG)₉, GC% =100 was at 80°C. The relation between the optimal elongation temperature and GC% of the short ssDNA suggested that the thermal stability of DNA duplex during elongation is a key factor.

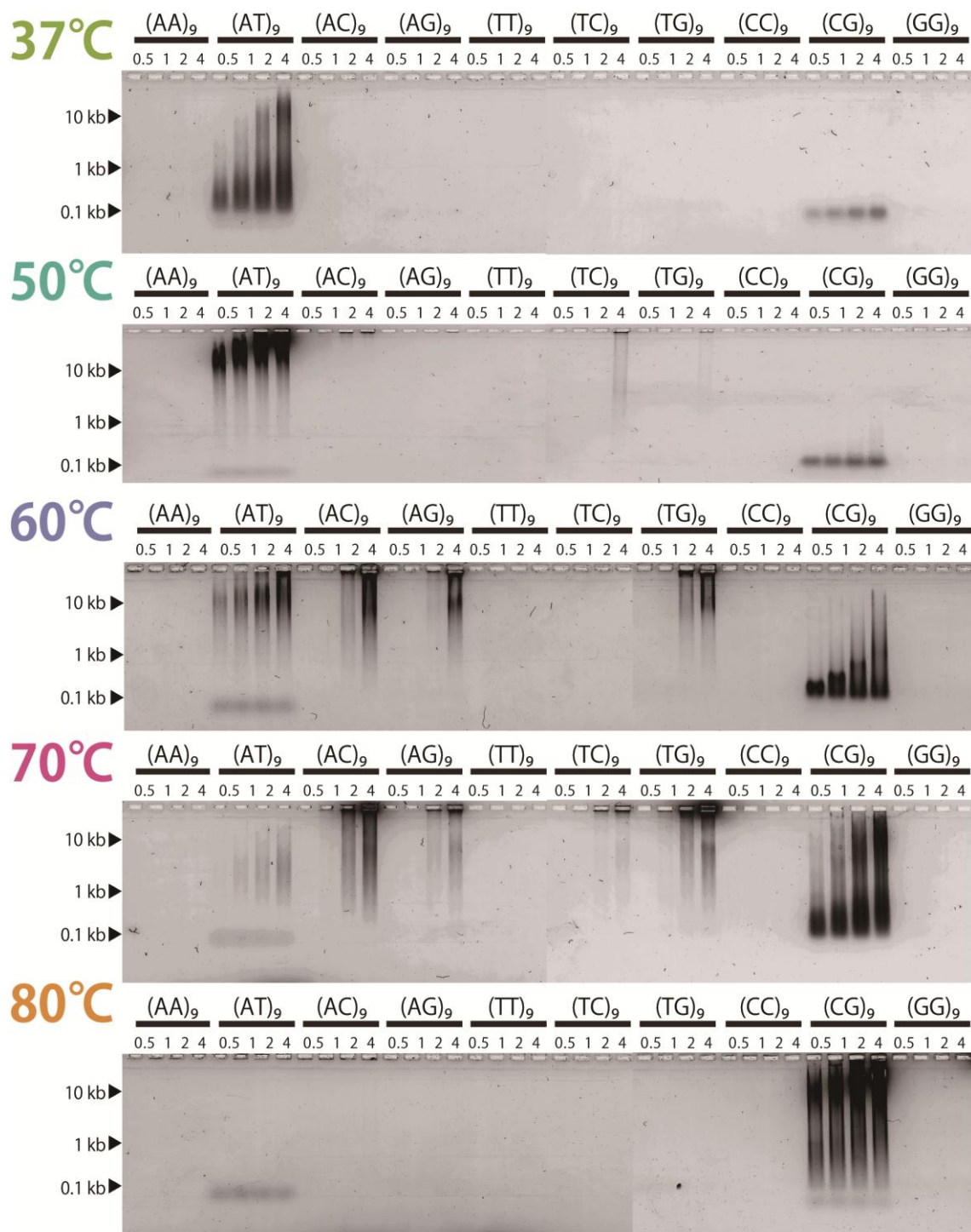


Figure 2-9. Gel patterns of elongated various sequence at 37, 50, 60, 70, 80°C. Reaction conditions: 20 U/mL DNA polymerase, 0.5 mM each dNTP, 100 nM ODNs in 1x Thermopol buffer. 1% agarose gel was stained by SYBR Green I.

For further analysis, Reaction products were also analyzed on 1% agarose gel. Aliquots of the reaction solution was collected after 0.5, 1, 2, 4 hours and mixed with an equal volume of 2x Loading dye. Agarose gel was stained by 1x SYBR Green I (Fig. 2-9). Smear gel patterns of elongated products indicated that the products have wide distribution of chain length. The highest efficiency of elongation at 70°C was (CG)₉, followed by (TG)₉, and (AC)₉. At 37 °C, only (AT)₉ was elongated and so was only (CG)₉ at 80°C. Elongation of (AC)₉, (AG)₉, (TC)₉ and (TG)₉ were observable at around 50-70°C. These results were consistent with quantitative analysis as shown in Figure 2-8, obviously demonstrating that various short ssDNA could be elongated nevertheless they cannot form any secondary structures by itself. Elongation of these ODNs is likely to progress in unusual way.

Interestingly, the results of the temperature dependence in elongation of ssDNA were very similar to that of *de novo* DNA synthesis. For example, (AT)₉ was elongated most efficiently at 50°C while *de novo* synthesized product of 50°C was poly d(AT). At 70°C, (CG)₉, (TG)₉ and (AC)₉ were elongated efficiently in this order and *de novo* synthesized product of 70°C was consisted of (TACGTA)_n. Namely, sequence composition of *de novo* synthesized product of 70°C was consisted of the sequences which can be elongated efficiently at 70°C. Hence, it is likely that the sequences of *de novo* synthesized products would be selected by favorability for elongation under reaction temperature.

Next, the elongated products of various short ssDNA were analyzed by sequencing. The results were summarized in Table 2-3. The elongated products were certainly originated from added ODN sequences (e.g. elongated (AC)₉ contained poly d(TG), which is complementary with (AC)₉.) An example of sequencing result of (TG)₉ was also shown in Figure 2-10. The product obviously contained original sequence of (TG)₉ and its complementary sequence of poly (AC), however, the lengths of them were not unified. This mixture of sequences is quite similar to palindrome sequence as observed in the products of *de novo* DNA synthesis. Appearance of complementary sequence with various length also suggested elongation by self-priming via hairpin formation of short ssDNA, however, those sequence cannot be self-primed by themselves since (AC)₉, (AG)₉, (TC)₉ and (TG)₉ do not contain pairs which can form base pairs.

Table 2-3. Sequences of elongated products from various short ssDNA

Substrate sequence	Reaction Temp. / °C	Product sequence
(AA) ₉	50	Poly dT
(AT) ₉	50	Poly d(AT)
(AC) ₉	50	Poly d(TG)
(AG) ₉	70	(TC) _n (AG) _m
(TT) ₉	70	Poly dA
(TC) ₉	70	(AG) _n (CT) _m
(TG) ₉	70	(AC) _n (TG) _m
(CC) ₉	80	Not defined
(CG) ₉	80	Poly d(CG)
(GG) ₉	80	Poly d(CG)

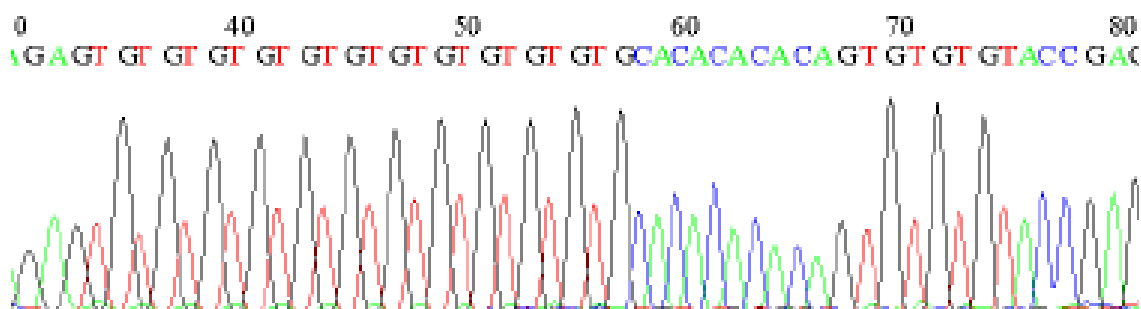


Figure 2-10. An example of the result of sequence analysis. This figure shows the sequencing result of elongated (TG)₉.

Again, short ssDNA could be elongated by abnormal mechanism involving self-priming. The clarification of the mechanism was described in the next section. This abnormal elongation will happen in DNA amplification technologies like PCR or isothermal amplification methods. Usually, primers used in those technologies are carefully designed so as not to form self-priming structure, however, the results of

elongation of short ssDNA demonstrated that well-designed primers even without formation of back-priming also would be elongated unexpectedly and cause non-specific amplifications. As shown in Figure 2-11, short ssDNA were efficiently elongated under PCR conditions. (AT)₉, (AC)₉, (TG)₉ and (CG)₉ were greatly amplified only within 15 cycles. Although target amplicons would be dominant in the presence of a certain amount of template, however, lower concentration of template would cause non-specific amplification of primer and it would be observed as considerable background which reduces the detection sensitivity.

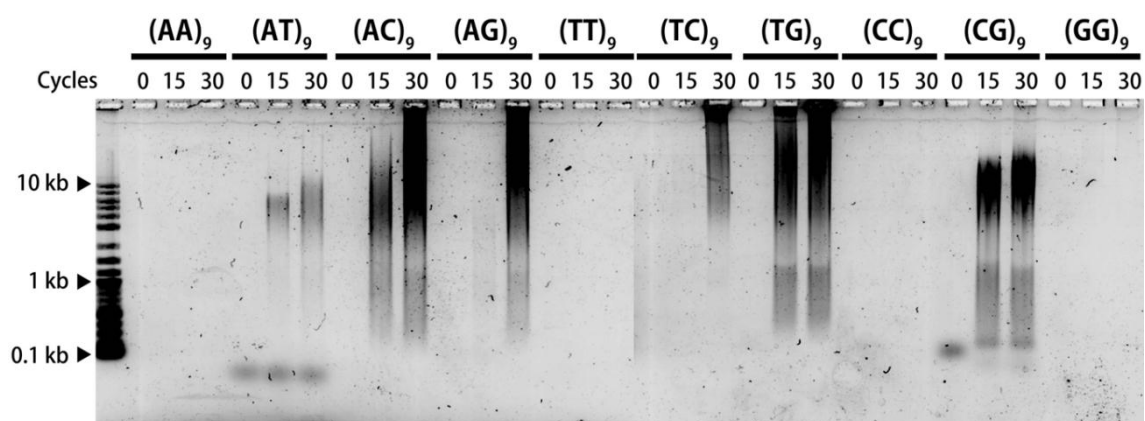


Figure 2-11. Elongation of short ssDNA under PCR condition. Cycle 0 indicates samples collected immediately after reaction start. Reaction conditions: Initial = 98°C 30 sec., Cycle phase Melt / Anneal / Extension = 98°C 10 sec. / 60°C 30 sec. / 72°C 45 sec. (30 cycles) Termination = 72°C 5 min. Solution conditions: 20 U/mL Vent(exo-) DNA polymerase, 0.5 mM each dNTPs, 100 nM ODN, 1x Thermopol buffer.

To avoid such undesired products, using other polymerase is effective. In Figure 2-12, short ssDNAs were reacted with 4 types of various polymerases at 70°C. DNA polymerases used here were Vent(exo-), 9°N_m, KOD dash and Pfu DNA polymerase. These polymerases belong in Family B and are highly homologous among each other.³¹⁻³³

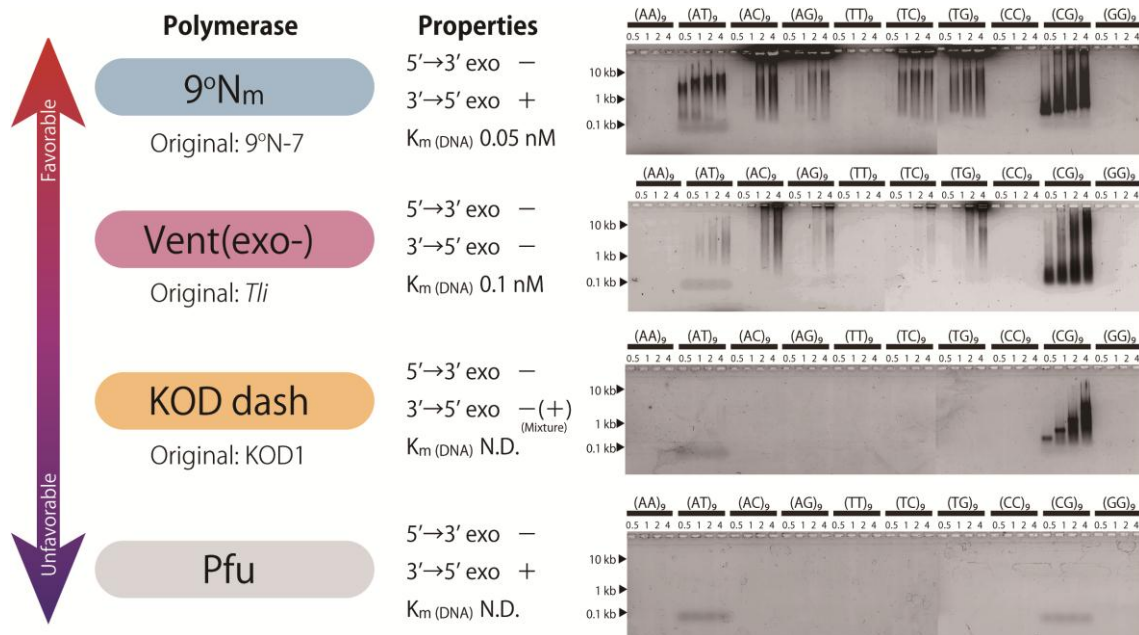


Figure 2-12. Gel patterns of elongation of various short ssDNA by different four polymerases. K_m (DNA) was referred from manufacturers and reference 34.

The short ssDNAs were elongated efficiently in the order of $9^\circ N_m > \text{Vent}(\text{exo}^-) > \text{KOD dash} > \text{Pfu}$. Interestingly, the efficiency of elongation was greatly variable despite of highly conserved homology among these polymerases. The difference on elongation efficiency cannot be explained well by properties of polymerase, however, the lower $K_m(\text{DNA})$ would be favorable to elongate various short ssDNA by catching them efficiently owing to the strong affinity. In other words, if $K_m(\text{DNA})$ of polymerase is low, it could catch DNA and elongate short ssDNA efficiently, by contrast, if $K_m(\text{DNA})$ of polymerase is higher, it would be difficult to catch DNA and elongate them. As described, elongation of short ssDNA highly depended on the type of polymerase. Especially Pfu exhibited no elongation of short ssDNA. Therefore, optimization of reaction conditions particularly DNA polymerase will be effective to prevent unexpected non-specific amplification.

2-3-4 The unusual elongation mechanism of short single strand DNA

In previous section, it was confirmed that short ssDNAs were elongated in unusual way and its efficiency depended on the reaction temperature. The elongated products contained palindromic sequences with various lengths and it suggested that the elongation mechanism involved hairpin formation like self-priming (back-priming).

Here, for clarifying mechanism of elongation of short ssDNA, dA₁₂ (5'-AAAAAAAAAAAAA-3') and/or dT₁₂ (5'-TTTTTTTTTTTTT-3') were reacted with DNA polymerase and dATP under isothermal conditions. Since it was difficult to directly observe the elongation steps of other sequences like (TG)₉ due to the high efficiency of elongation, short poly dA and poly dT strands with reaction solution containing only dATP were used here to slow down the reaction speed. For sensitive detection, radio isotope labeled dATP was used. 100 nM of dA₁₂ and/or dT₁₂ were reacted with dATP containing α -³²PdATP by DNA polymerase under isothermal condition at 50°C. An aliquot of reaction solution was collected and analyzed on denaturing 20% PAGE containing 8 M Urea (Figure 2-13).

Table 2-4. Name and sequences of short ssDNA used here.

Name	Sequence
dA ₁₂	5' - AAAAAAAAAAAAAA - 3'
dT ₁₂	5' - TTTTTTTTTTTTTT - 3'
dA ₁₈	5' - AAAAAAAAAAAAAAAAAA - 3'
dT ₁₈	5' - TTTTTTTTTTTTTTTTTT - 3'
dT ₁₂ +A	5' - TTTTTTTTTTTTTTA - 3'
dT ₁₂ +A ₂	5' - TTTTTTTTTTTTTTAA - 3'
dT ₁₂ +A ₃	5' - TTTTTTTTTTTTTTAAA - 3'
dT ₅	5' - TTTTTT - 3'
dT ₆	5' - TTTTTT - 3'
dT ₈	5' - TTTTTTTT - 3'

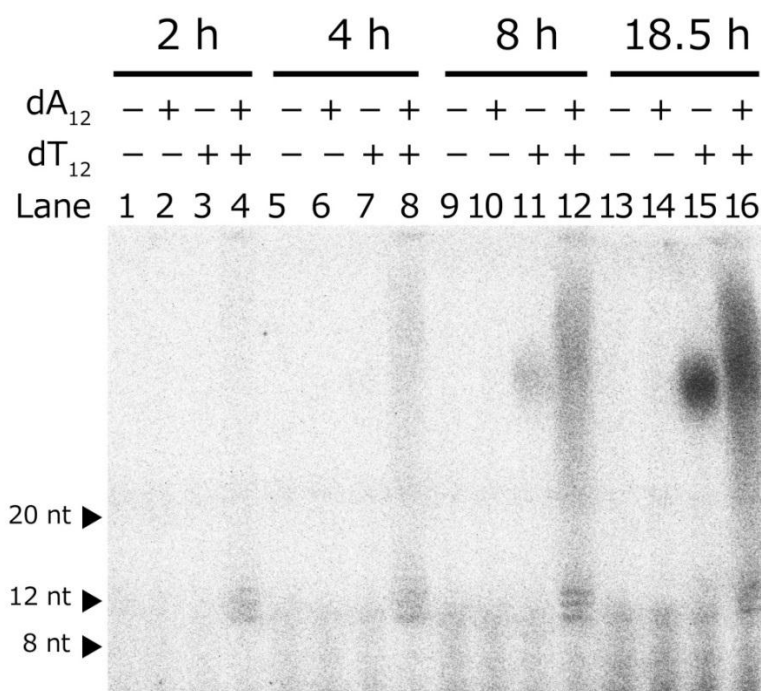


Figure 2-13. Gel patterns of synthesized DNA on 20% denaturing PAGE. Conditions: 50°C, 20 U/mL Vent(exo-) DNA polymerase, 0.5 mM dATP, 100 nM oligonucleotides, 0.2 $\mu\text{Ci}/\mu\text{L}$ $\alpha\text{-}^{32}\text{P}$ dATP, in 1 \times Thermopol buffer. Lane 1, 5, 9 and 13 show the reaction in the total absence of added DNA. Lane 2, 6, 10 and 14 show elongation reaction in the presence of only dA₁₂. Lane 3, 7, 11 and 15 show that of only dT₁₂. Lane 4, 8, 12 and 16 show that of dA₁₂ and dT₁₂.

When no DNA was added (Lane 1, 5, 9, 13) and only dA₁₂ was added (Lane 2, 6, 10, 14), synthesized DNA were not detected, whereas in the presence of dT₁₂ (Lane 3, 7, 11, 15) and dA₁₂&dT₁₂ (Lane 4, 8, 12, 16), synthesized DNA could be observed. For dA₁₂&dT₁₂, synthesized long poly dA was widely smeared.

Interestingly, DNA synthesis was observed even though only dT₁₂ was added (Lane 11, 15). The synthesized product in the presence of only dT₁₂ seems like a spot and less efficient than the case of dA₁₂&dT₁₂. Synthesis of long poly dA in the presence of only dT₁₂ was surprising because dT₁₂ cannot form any template/primer structure and it will be intact for polymerase. It must be involved abnormal elongation mechanism. On the other hand, in the presence of dA₁₂&dT₁₂, the widely smeared product of poly dA would be synthesized by slippage mechanism, however, T_m of dA₁₂/dT₁₂ duplex was 31.8°C (measurement conditions: 5 μM each dA₁₂ and dT₁₂ in 1 \times Thermopol Detergent Free buffer) and the result of theoretical calculation on DINAMelt Web Server

(<http://dinamelt.bioinfo.rpi.edu/>) was 22.3°C at 100 nM. Therefore dA₁₂ and dT₁₂ could hardly form duplex during reaction at high temperature of 50°C. It may be because polymerase would clamp dA₁₂/dT₁₂ duplex and it would enable DNA synthesis. If poly dA could be elongated by sufficient length, dT₁₂ would be also able to behave as a primer.

In addition, dA₁₈ and dT₁₈, which are little longer than dT₁₂ were also tested (Figure 2-14). Similar to dT₁₂, unusual elongation of dT₁₈ was observed in the absence of dA₁₈. Reaction efficiency of dT₁₈ seemed to be higher than that of dT₁₂ and the elongated products were longer than the products of dT₁₂.

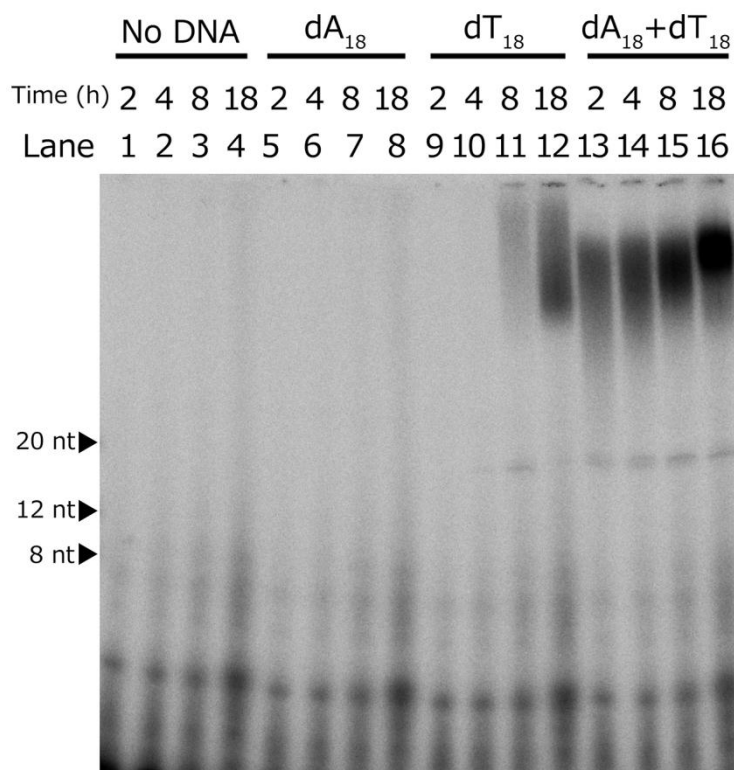


Figure 2-14. Elongation of dA₁₈ and dT₁₈. Reaction condition was the same as described above.

As shown above, thermophilic DNA polymerases could elongate short ssDNA such as dT₁₂ in unusual way. To confirm the synthesized poly dA was really originated from dT₁₂, 5'-ends of dA₁₂ and dT₁₂ were labeled with γ -³²P ATP by T4PNK. After purification, 5'-labelled ODNs were added to the reaction solution under 50°C (Figure 2-15).

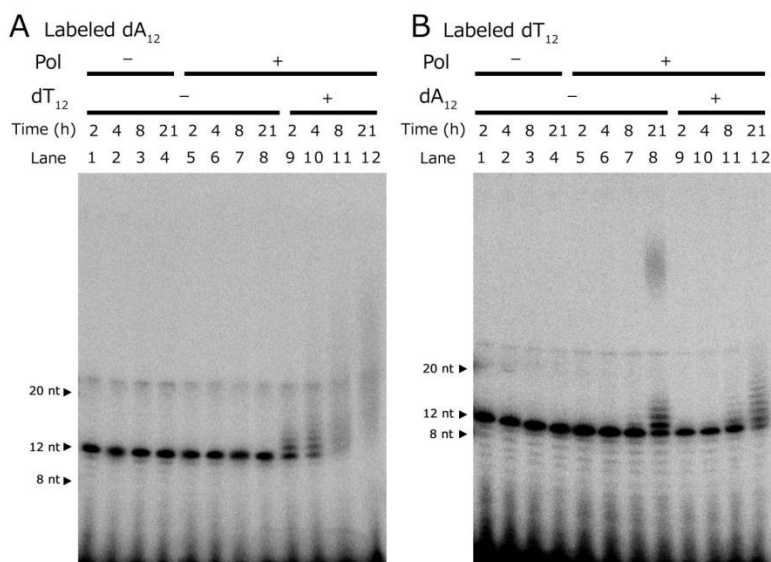


Figure 2-15. Elongation of 5'-labeled dA₁₂ (Panel A) and dT₁₂ (Panel B). dA₁₂ and dT₁₂ were labeled independently with 0.2 μ Ci/ μ L of γ -³²P ATP by T4 Polynucleotide Kinase. Reaction conditions were the same as described in Figure. 2-13.

As expected, labeled dA₁₂ could not be elongated without dT₁₂ (Figure 2-15A, Lane 9-12). When in the presence of dT₁₂, labeled dA₁₂ was added several dATPs (Panel A, Lane 9, 10). These shorter products were disappeared after 8 hours and longer products over 20 nt were synthesized (Panel A, Lane 11, 12). By contrast, labeled dT₁₂ was elongated without dA₁₂ (Panel B, Lane 8) indicating that the smeared spots shown in Figure 2-13 lane 11, 15 were elongated dT₁₂. Note that several bands slightly longer than 12 nt were observed in lane 8. These were also derived from dT₁₂ and several dATPs were added at 3'-end of dT₁₂. In other words, after addition of several dATPs, dT₁₂ could be efficiently elongated after incubation of 21 hours. For in the presence of dA₁₂, labeled dT₁₂ remained shorter length and only several dATP were added (Panel B Lane 11, 12). It indicated that the synthesized longer DNA shown in Figure 2-13 lane 12 and 16 were mainly elongated dA₁₂. It would be because that dA₁₂/dT₁₂ duplex allowed elongation in Template/Primer manner and dA₁₂ was preferentially elongated using dT₁₂ as a template.

Again, unusual elongation of dT₁₂ was due to addition of dATPs at 3'-end of dT₁₂. To know how dT₁₂ could be elongated, a series of dT₁₂ derivatives which were attached several dATPs in advance, dT₁₂+A (5'-TTTTTTTTTTTTTA-3'), dT₁₂+A₂ (5'-TTTTTTTTTTTTTAA-3'), dT₁₂+A₃ (5'-TTTTTTTTTTTTTAAA-3') were prepared. The shorter bands around 12 nt shown in Figure 2-15B lane 8 indicated that addition of dATP was a rate-limiting step. After three dATPs were added, dT₁₂ would be elongated efficiently. If it is true, dT₁₂+A_n series will be able to shorten the lag time until detection of longer products. For easy comparison, 1 μM of ODNs were added here. Other conditions were the same as previous experiment.

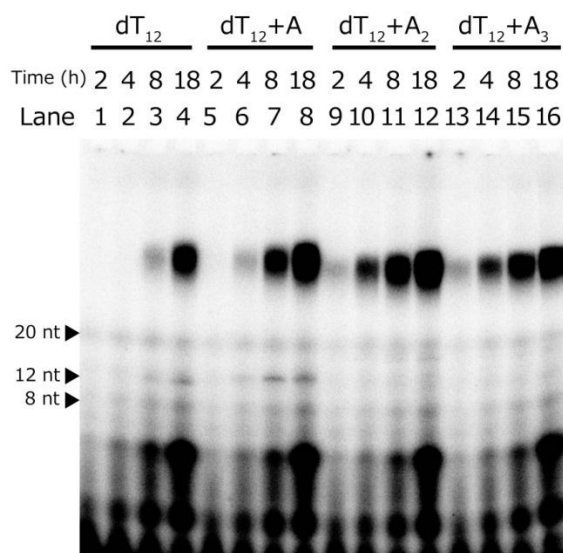


Figure 2-16. Elongation of dT₁₂, dT₁₂+A, dT₁₂+A₂ and dT₁₂+A₃. Reaction condition was same as described above except for ODN concentration was 1 μM. dT₁₂+A₂ and dT₁₂+A₃ could synthesize longer DNA as early as < 2 h. dT₁₂+A could be elongated in 2-4 h, while dT₁₂ needed 8 h to be elongated.

Obviously, dT₁₂+A₂ and dT₁₂+A₃ could successfully shorten the lag time until detection of longer products (Figure 2-16). The elongated products were observed as short as within 2 hours (Lane 9, 13, respectively), whereas dT₁₂ required 8 hours of incubation (lane 3). dT₁₂+A also shortened the lag time, the longer products were observed after incubation of 4 hours (Lane 6). These results showed that first and second dATP additions are relatively low efficient and following third addition and efficient elongation are fast. As shown above, it was confirmed that addition of dATPs allowed elongation of dT₁₂.

Next, the requirements of length of poly dT for elongation was investigated. Shorter three types of ssDNA dT₅, dT₆, dT₈ were compared with dT₁₂ (Figure 2-17). As a result, only dT₁₂ was able to be elongated (Lane 15, 16) and others were not (Lane 1-12). These results showed that the nucleotide addition followed by elongation requires 9~12 nt ssDNA at least.

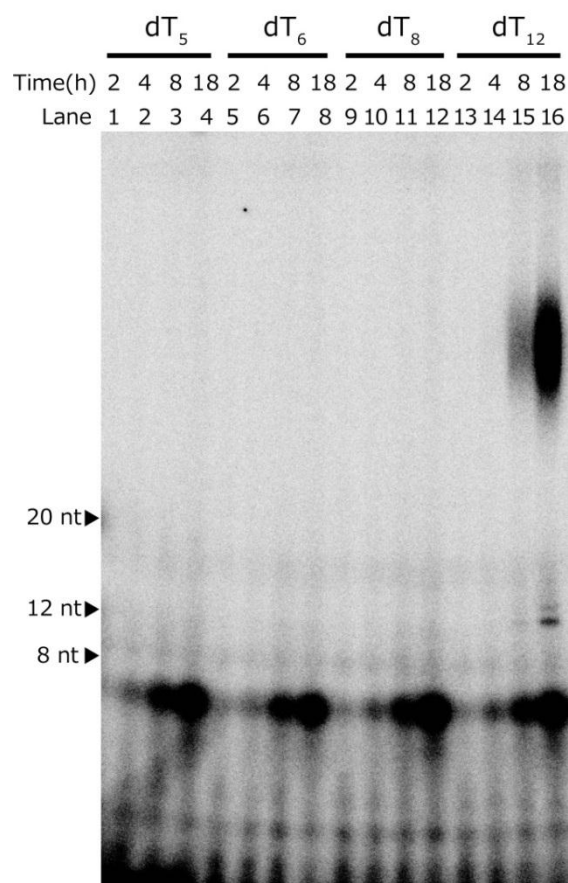


Figure 2-17. Elongation of dT₅, dT₆, dT₈ and dT₁₂. Reaction condition was same as described previously. Only dT₁₂ was elongated in Lane 15, 16.

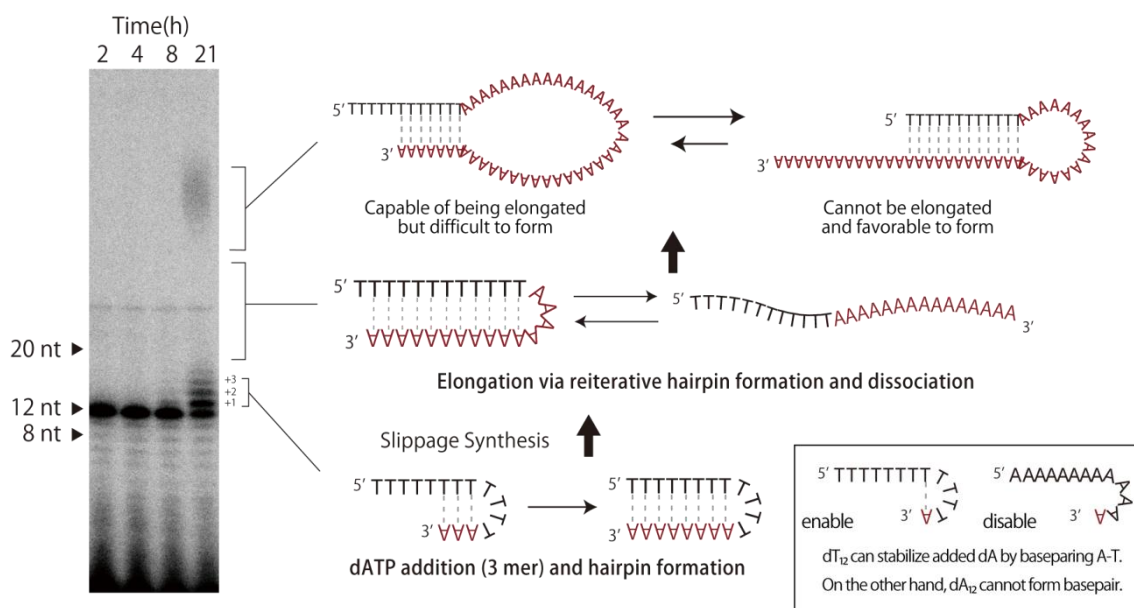


Figure 2-18. Proposed elongation mechanism of dT₁₂. dT₁₂ was slowly added three dATPs by DNA polymerase, then hairpin was formed and stabilized by A-T base pairing or clamping by polymerase. Then dATP added dT₁₂ can be elongated by reiterative cycles of hairpin formation, primer extension and dissociation of hairpin. Once elongated dT₁₂ attained sufficient length, very long dA tail would disturb formation of 5'-overhang, which is similar to primer/template structure and elongation of dT₁₂ would be inhibited.

Finally, the elongation mechanism of dT₁₂ was discussed based on above results. At first, dATP is added at 3'-end of dT₁₂. This process is the rate-limiting step and it required more than 8 hours of incubation at 50°C. Amounts of these intermediate measured from band intensity at 21 h were dT₁₂(+0) 31%, +1 dATP 27%, +2 dATPs 14%, +3 dATPs 8%, smeared band 20%. Unexpectedly, for dA₁₂, the addition of dATP was not detected even after several days of incubation. dA₁₂ could be elongated only in the presence of dT₁₂. It is interesting that only dT₁₂ could be added dATPs without its complementary strand. These results suggested that dT₁₂ would be able to stabilize dATP to be added next by hairpin formation, whereas dA₁₂ could not stabilize dATP to be added due to steric hindrance of A·A mismatch and it inhibited nucleotide addition of dA₁₂. Such stabilization of dATP by dT₁₂ would be available within only a short time therefore it was the rate-limiting step. The band intensity at position of +1 and +2 were relatively higher. Hairpin structure with only 1 or 2 base pair is too unstable at 50°C even though polymerase could clamp it. Nucleotide addition by DNA polymerase is

known as “TdT like activity” that an extra dATP is added after usual primer extension.³⁵⁻³⁷ However this is the template-dependent nucleotide addition and it will not be appropriate for the explanation of nucleotide addition of dT₁₂.

Secondly, more stable hairpin would be able to form after three dATPs were incorporated. Self-priming with 5'-overhanged shape allowed primer extension using its own sequence as template. Once primer extension started, dT₁₂ can be elongated by stepwise reaction of reiterative cycle of hairpin formation, self-primed extension and dissociation. This process was invisible on the gel since it was relatively higher efficiency and too fast to observe. However, once the elongated dT₁₂ reached at sufficient length, formation of back-primed 5'-overhang structure would be restricted since probability of formation of 5'-overhang structure would be decrease owing to long poly dA. The narrow spot like smeared bands observed in Figure2-13 demonstrated that restriction of elongation efficiency.

In summarize, the elongation mechanism of dT₁₂ was involved with nucleotide addition at 3'-end and intermittent elongation by formation/dissociation of hairpin structure.

As shown in the previous section, various types of short ssDNA were elongated although the sequences of short ssDNAs could NEVER form any secondary structures by themselves. The elongated products of dT₁₂ were much shorter than that of short ssDNAs in the previous section due to the limitation of substrate; only dATP was added to the reaction solution. Though considering such limitation, elongated products of ssDNAs like (TG)₉ were too long (>10 kb). As described above, intermittent elongation by formation/dissociation of hairpin would limit the length of products within < 300 nt because the probability of 5'-overhang hairpin formation which can be elongated would be decreased. Therefore, after short ssDNA grew sufficient length by formation/dissociation of hairpin, elongation mechanism should be changed for efficient elongation as long as over 10 kb. Namely, another mechanism for such efficient elongation should be proposed to explain how the long products > 10 kb were synthesized from short ssDNA.

efficient elongation. Hairpin formation at each end is available even under isothermal condition and relatively lower temperature than T_m . Hairpin structure at 3'-end and strand displacement activity of DNA polymerase allows usual primer extension and the product length will be doubled. After elongation, the product sequence contains palindromic sequence at each end and formation of hairpin enables successive elongation again. Successive elongation via terminal hairpin formation and primer extension from self-primed 3'-end gives high elongation efficiency. It is also important that this model do not require complete dissociation of duplex; only termini should dissociate and form hairpin structure. Therefore this model is applicable for elongation under lower temperature than T_m .

2-3-5 Elongation of short DNA containing hairpins at each end

In this section, to check validity of THSP model, elongation of short DNA containing hairpins at each end was investigated.³⁸ Sequence design of short seed sequences for elongation was shown in Figure 2-20.

For continuous DNA synthesis after the initiation, the 5' end is also important. A palindromic sequence at the 5' end can increase the probability of self-priming after the primer extension reaches the 5' end because the newly synthesized 3' end contains also the palindromic sequence. Accordingly, a 28-nt-long ODN (**S28**) with palindromic sequences at both 5' and 3' ends for forming hairpin structures (Figure 2-20) was designed. At relatively high concentrations, the ODN can also form intermolecular duplex (self-dimer). To avoid unexpected mis-pairing during elongation, **S28** is AT rich (71% AT content). For the 14-nt-long sequence at 5' end of **S28**, the AT content is 85.7%. To investigate in detail the effect of hairpin formation on elongation, a series of modified sequences based on **S28** were also used (Figure 2-20).

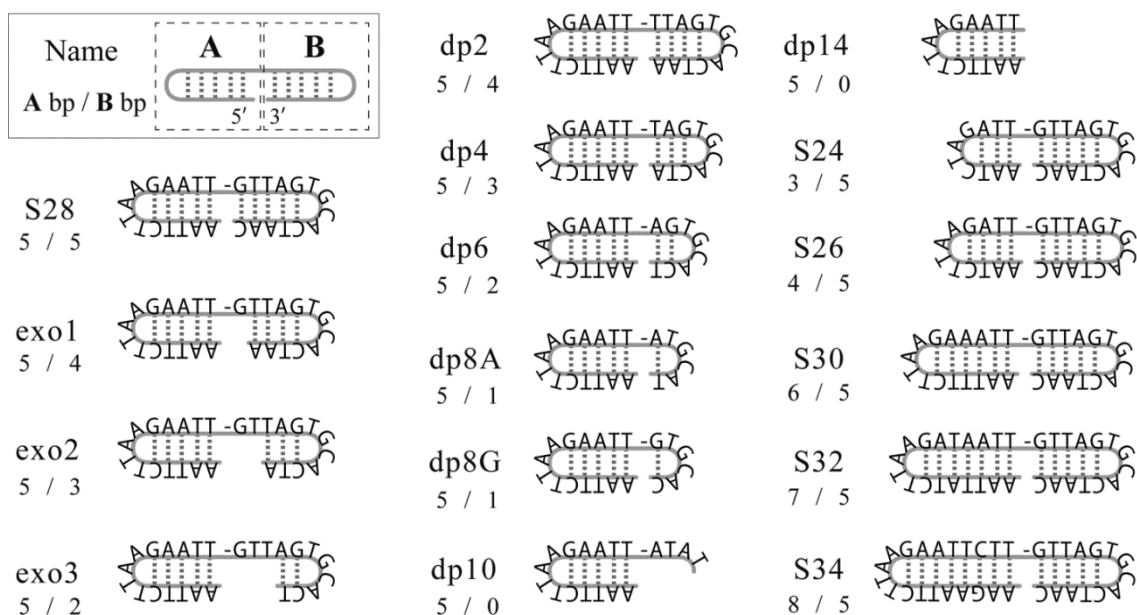


Figure 2-20. Design of DNA sequences used in this study. These ODNs have a hairpin at only the 5' end or at both ends. The 5' half of the ODN is referred to as Part A and 3' half as Part B. The hairpins in **S28** have 5 base pairs. Part A in **exo1**, **exo2**, and **exo3** and **dp2**, **dp4**, **dp6**, **dp8A**, **dp8G**, and **dp10** are identical to that of **S28** and are modified in Part B. **dp14** is only the 5' half of **S28**. **S24**, **S26**, **S30**, **S32**, and **S34** have the Part B sequence of **S28** and vary in the 5' region. The numbers of base pairs formed in each hairpin are indicated below of the name of ODNs in the manner of Part A/Part B.

Table 2-5. DNA sequences used in this section.

Name	Sequence
S28	5'-AATTCTTAAGAATT-GTTAGTGCCTAAC-3'
exo1	5'-AATTCTTAAGAATT-GTTAGTGCCTAA-3'
exo2	5'-AATTCTTAAGAATT-GTTAGTGCCTA-3'
exo3	5'-AATTCTTAAGAATT-GTTAGTGCCT-3'
dp2	5'-AATTCTTAAGAATT-TTAGTGCCTAA-3'
dp4	5'-AATTCTTAAGAATT-TAGTGCCTA-3'
dp6	5'-AATTCTTAAGAATT-AGTGCCT-3'
dp8A	5'-AATTCTTAAGAATT-ATGCAT-3'
dp8G	5'-AATTCTTAAGAATT-GTGCAC-3'
dp10	5'-AATTCTTAAGAATT-ATAT-3'
dp14	5'-AATTCTTAAGAATT-3'
S14	5'-GTTAGTGCCTAAC-3'
S24	5'-AATCTAGATT-GTTAGTGCCTAAC-3'
S26	5'-AATCTTAAGATT-GTTAGTGCCTAAC-3'
S30	5'-AATTTCTTAAGAAATT-GTTAGTGCCTAAC-3'
S32	5'-AATTATCTTAAGATAATT-GTTAGTGCCTAAC-3'
S34	5'-AAGAATTCTTAAGAATTCTT-GTTAGTGCCTAAC-3'
T-S14	5'-TTTTTTTTTTTTTTT-GTTAGTGCCTAAC-3'
RnA	5'-AATTCTTAAGAATTAATTCCTTAAGAATTAGATTGAACTCTCGAACTAT-3'
RnB	5'-AATTCTTAAGAATTAATTCCTTAAGAATTATAGTTCGAGAGTTCAATCT-3'

The elongation reaction by Vent (exo-) DNA polymerase was first performed at 70 °C using 100 nM **S28** and 0.5 mM dNTPs. A higher concentration of dNTPs was used here for producing more elongation products, especially for a long reaction time. The elongation products were analyzed by 1.0% agarose gel (Figure 2-21a). Smear bands were observed close to the well of the gel indicating that very long DNA was synthesized. The short fragment observed at the bottom of the gel was non-elongated **S28**. **S28** was elongated very efficiently and products of longer than 10 kb were observed within only 10 min (Figure 2-21a, Lane 1). Similar results were also obtained when a denaturing agarose gel (30 mM NaOH) was used (data not shown). As shown by the time course in Figure 2b, elongation continued after 20 hours. As intermolecular duplex formation may result in extension, the concentration dependence of the elongation was also evaluated (Figure 2-22). When 100 pM of **S28** was used, DNA products longer than 10 kb was observed in 20 min. Even with 10 pM, much lower than K_m (90 pM) of Vent (exo-) DNA polymerase,²⁹ **S28** was elongated efficiently, and the elongated products were detected after 1.0 hour.

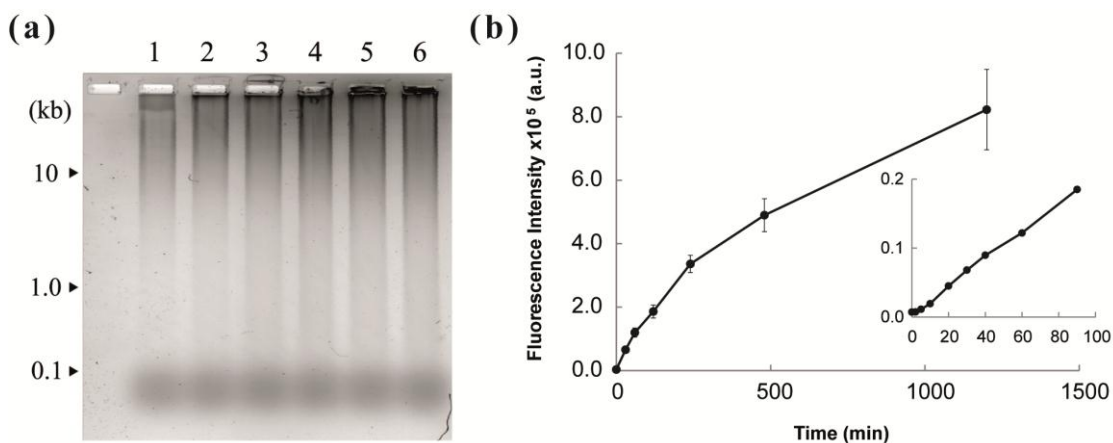


Figure 2-21. Time course of the elongation of **S28** by Vent (exo-) DNA polymerase at 70 °C. (a) Image of the gel resolving elongation products after staining with SYBR Green I. Lane 1: 10 min; Lane 2: 30 min; Lane 3: 60 min; Lane 4: 90 min; Lane 5: 120 min; Lane 6: 150 min. (b) Quantitative analysis of elongation of **S28**. Fluorescence intensity after staining with SYBR Green I was measured. The inset shows the result of first 100 min.

In addition, the product sequences were checked. For sequencing, elongated products were purified, digested by slight amount of DNase I, and cloned into SmaI site of the pUC19 vector. In order to obtain blunt ended fragments, Mn²⁺ ion was added into the DNase I digestion buffer. As shown in Figure 2-23, the sequences of elongated products were tandem repeats of **S28**, although several point mutations were observed. In clones 4, 5, and 6, 6-13-nt-long deletions occurred, probably due to the ligation of digested fragments before insertion into the plasmid. Point mutations may arise due to mis-incorporation by Vent (exo-) DNA polymerase, which lacks proof-reading activity.

Moreover, to determine whether longer products were elongated from **S28**, the elongated DNA was digested by restriction enzyme Tsp509I with recognition site 5'-↓AATT-3' (Figure 2-24a). All DNA products were digested efficiently and no DNA longer than 50 nt remained, indicating that all elongated products contained the 5'-AATT-3' sequence at short intervals. The electrophoresis pattern of Tsp509I digestion products indicated that the elongation products consisted of repeats of the sequence of **S28**. The possible fragments were also depicted in Figure 2-24b. All of the short bands could be assigned to digested fragments derived from elongated S28 (Lane 6, 18 nt and 28 nt).

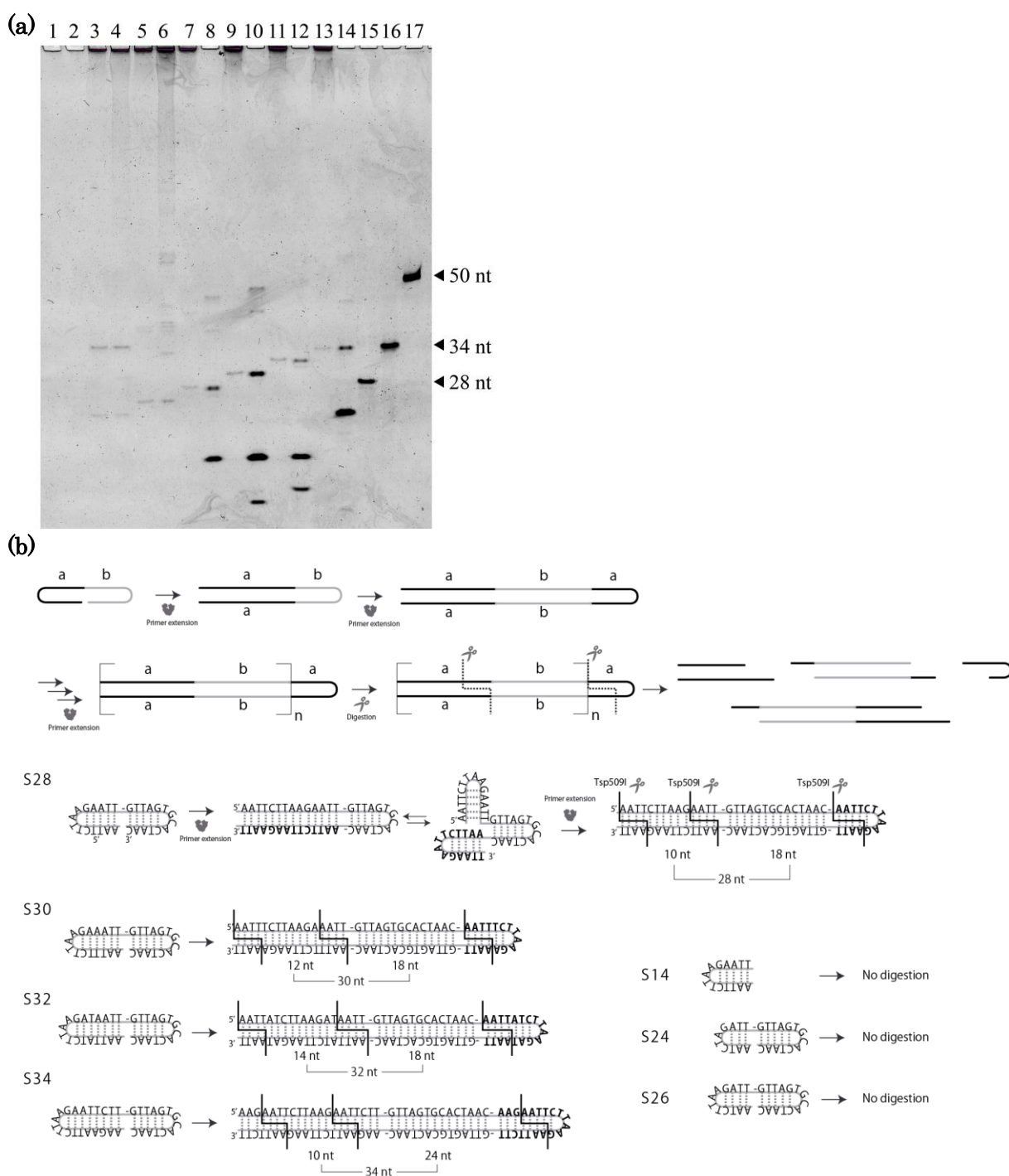


Figure 2-24. Assignment of the elongated products. (a) Elongated products of Short Seeds were digested by Tsp509I followed by purification. Samples were analyzed on 10% denatured PAGE with 8 M Urea in 0.5× TBE buffer. Gel was stained by SYBR Green II. Odd numbered lanes are after elongation of Short Seeds (purified) and even numbered lanes are after digestion by Tsp509I at 65°C for overnight. Lane 1&2: **dp14**, Lane 3&4: **S24**, Lane 5&6: **S26**, Lane 5&6: **S28**, Lane 7&8: **S30**, Lane 11&12: **S32**, Lane 13&14: **S34**, Lane 15: Marker 28 nt, Lane 16: Marker 34 nt, Lane 17: Marker 50 nt. (b) The possible fragments of digestion by Tsp509I. **dp14**, **S24** and **S26** cannot be digested because they do not contain the recognition sequence (AATT). **S28**, **S30**, **S32** and **S34** can be readily digested and the length of the fragment was in good agreement with the length of Short Seeds (e.g. 18 nt and 28 nt, for **S28**).

Next, temperature dependence of elongation of **S28** was investigated to check elongation mechanism of **S28**. If elongation of **S28** was based on THSP model, **S28** can be elongated efficiently under lower temperature than its T_m . As shown in Figure 2-25a, long DNA was only obtained during elongation of **S28** within a narrow range of temperature (66-74 °C), indicating that the elongation efficiency was very sensitive to the reaction temperature. The optimal reaction temperature was 68.8 °C, and the amount of elongation product decreased abruptly when the temperature was outside the optimal range by only 1 to 2 °C (Figure 2-25b). Interestingly, at temperatures lower than 66.2 °C, distinct bands were observed, and all the elongation products were shorter than 500 bp. At temperatures higher than 74 °C, however, almost no elongation was observed (Figure 2-25b, lane 10-12). In addition to the bands due to **S28**, another band of approximately 42 nt was observed at all temperatures (Figure 4a). This band is the product with elongation stopped after replication of 5' part of **S28**.

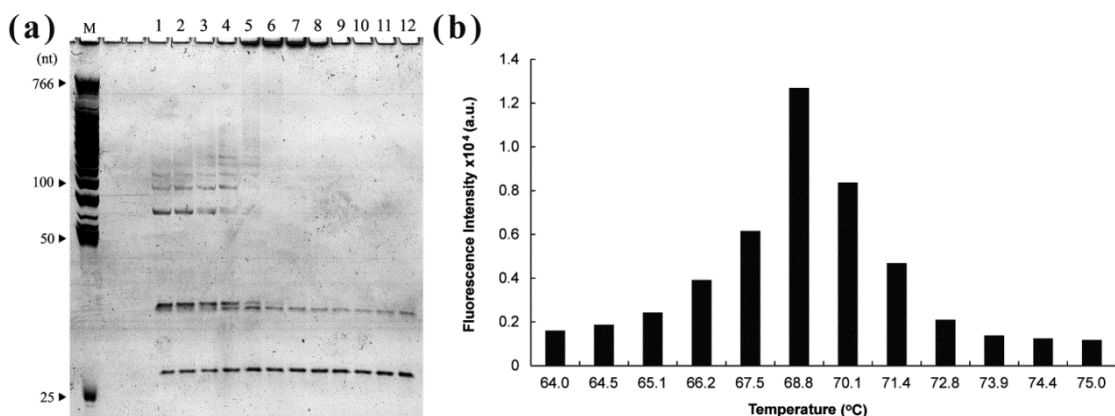


Figure 2-25. Temperature dependence of elongation of **S28**. (a) Image of a gel stained by SYBR Green II separating products of elongation of **S28** at various temperatures. Lane 1: 64.0 °C; Lane 2: 64.5 °C; Lane 3: 65.1 °C; Lane 4: 66.2 °C; Lane 5: 67.5 °C; Lane 6: 68.8 °C; Lane 7: 70.1 °C; Lane 8: 71.4 °C; Lane 9: 72.8 °C; Lane 10: 73.9 °C; Lane 11: 74.4 °C; Lane 12: 75.0 °C. The elongation reaction was stopped at 30 min and analysed on a 10% denaturing PAGE containing 8.0 M urea in 1×TBE buffer. The bands with highest mobility are assigned to be **S28**. The bands between 25 and 50 nt are the 42-nt-long intermediate of elongation. (b) Quantitative analysis of elongated products under various temperatures using fluorescence measurement stained by SYBR Green I. The fluorescence background in the absence of short oligos was not subtracted. The elongation reaction was performed for 60 min.

Then, melting temperatures (T_m) of both short seeds and the elongated products were measured. For these experiments, Thermopol Detergent Free (D.F.) buffer was used as Triton X-100, a nonionic surfactant, causes turbid at temperatures higher than 65 °C. Figure 2-26 shows an example of T_m curves of **S28** and the purified products obtained from elongation by Vent (exo-) DNA polymerase at 70 °C for 4.0 h. T_m s of **S28** and the product were 53.1 °C and 79.4 °C, respectively. As the elongation of **S28** was carried out at a temperature below 73 °C, the elongated products should be mostly in duplex states, suggesting that the mechanism such as hairpin-coil transition or DEME model does not explain the elongation of **S28**. In the absence of DNA polymerases at the elongation reaction temperature (>64 °C), **S28** will not have a hairpin structure (shown in Figure 2-20) as the T_m is significantly lower than the reaction temperature. Thus, binding of DNA polymerase must promote and stabilize self-priming of **S28**. It was confirmed that **S28** was elongated based on THSP model and this model can explain efficient elongation of palindromic sequences under relatively lower temperature than T_m .

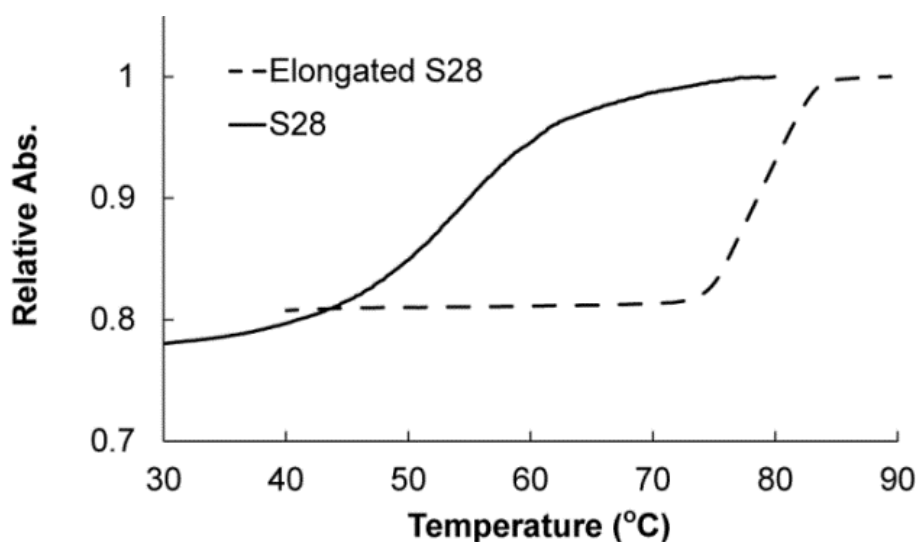


Figure 2-26. T_m curves of **S28** (solid line) and elongated products (dashed line). Samples for T_m measurements were prepared in 1×Thermopol D.F. buffer. The T_m s for **S28** and the product were 53.1 °C and 79.4 °C, respectively.

Furthermore, to investigate in detail the effect of the hairpin structure of the short seed template, 16 ODNs were used as elongation templates (see detailed structure in Figure 2-20). Sequences of these short seeds were designed based on **S28**. Since the self-priming at the 3' end should be the key step in initiation of elongation, sequences able to form hairpins of various stabilities at the 3' end were used. For example, **exo1**, **exo2**, and **exo3** lack 1 to 3 bases relative to the 3' end of **S28**; **dp2**, **dp4**, **dp6**, **dp8A**, **dp8G**, **dp10**, and **dp14** are sequences lacking 1 to 6 base pairs (Figure 2-20). **dp8A** has the potential to form only a single A-T pair, and **dp8G** can form one G-C pair at the 3' end. For **S24**, **S26**, **S30**, **S32**, **S34**, the length of 5' hairpin was varied. As shown in Figure 2-27a, all short seeds except for **dp8A**, **dp10**, and **dp14** were elongated at 70 °C within 1.0 h, and long smeared bands were observed. The T_{ms} of **S24**, **S26**, **S30**, **S32**, and **S34** and their elongated products were measured (Table 2-6). As expected, for all these sequences, T_{ms} of short seeds were lower and T_{ms} of the elongated products were higher than 70 °C (the reaction temperature).

Table 2-6. T_m values and GC% of short seeds and their elongated products.

Seq.	GC%	T_m of Short Seeds (°C)	T_m of Elongated Product (°C)
S24	33.3	53.1	80.4
S26	30.8	52.4	80.1
S28	28.6	53.1	79.4
S30	26.7	53.1	79.2
S32	25.0	54.8	77.8
S34	31.3	57.9	80.0

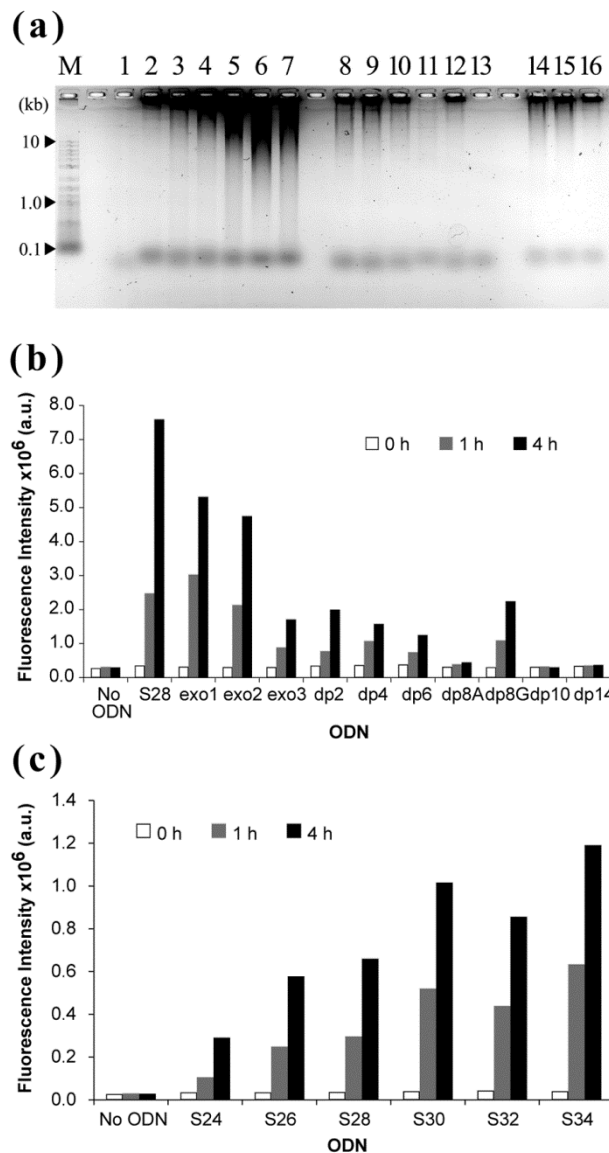


Figure 2-27. Elongation of short seeds with various sequences. (a) Separation of elongation products on a 1.0% agarose gel stained by SYBR Green I. The elongation was carried out at 70 °C for 1.0 h. Lane 1: **dp14**; Lane 2: **S24**; Lane 3: **S26**; Lane 4: **S28**; Lane 5: **S30**; Lane 6: **S32**; Lane 7: **S34**; Lane 8: **dp2**; Lane 9: **dp4**; Lane 10: **dp6**; Lane 11: **dp8A**; Lane 12: **dp8G**; Lane 13: **dp10**; Lane 14: **exo1**; Lane 15: **exo2**; Lane 16: **exo3**. (b) Quantitative analysis of products elongated from **S28** derivatives of **exo** and **dp** series (stained with SYBR Green D). (c) Quantitative analysis of products elongated from **S28** derivatives of **S** series of short seeds.

As shown in Figure 2-27b, the elongation efficiency depended on the number of base pairs in the hairpin at 3' end of the short seed template. For **exo1**, **exo2**, and **exo3**, elongation efficiency decreased with the number of deleted bases. Similarly, elimination of base pairs caused a significant decline of elongation efficiency for the series **dp2**, **dp4**,

dp6, dp8A, and dp8G. For **dp10** and **dp14**, no elongation was observed even after 20 h (data not shown), demonstrating that self-priming at 3' end is necessary for initiating the elongation. Interestingly, even for **dp8G**, in which only 6-nt-long sequence (5'-GTGCAC-3') was left at 3' end, very long DNA product was obtained in 1.0 h (lane 12, Figure 2-27a). Even at a low concentration of 1.0 nM, relatively efficient elongation of **dp8G** was also observed (data not shown). More interestingly, for **dp8A** which has also 6-nt-long sequence (5'-ATGCAT-3') at 3' end but lower GC content, elongation was also observed, although the efficiency was very low (lane 11, Figure 2-27a).

Hairpin length in the 5' half region also affected the elongation efficiency. Reaction from longer sequences such as **S30**, **S32**, and **S34** yielded greater amounts of elongated products (Figure 2-27c) than that of **S28**. By contrast, **S26** and **S24**, which have fewer base pairs than **S28** at 5' end, were elongated less efficiently. Reaction with **S24**, which has a 10-nt-long palindromic sequence, provided significantly less product than that with **S28**. As a control, the sequence without the 5' half region (**S14**: 5'-GTTAGTGCCTAAC-3') was also tested; no elongated product was observed within 1.0 hour (Figure 2-28). Furthermore, the sequence with 14 thymines at 5' end that cannot form a hairpin (**T-S14** in Figure 2-28) was not elongated. Hence it was concluded that hairpin formation in the 5' half region is necessary for elongation.

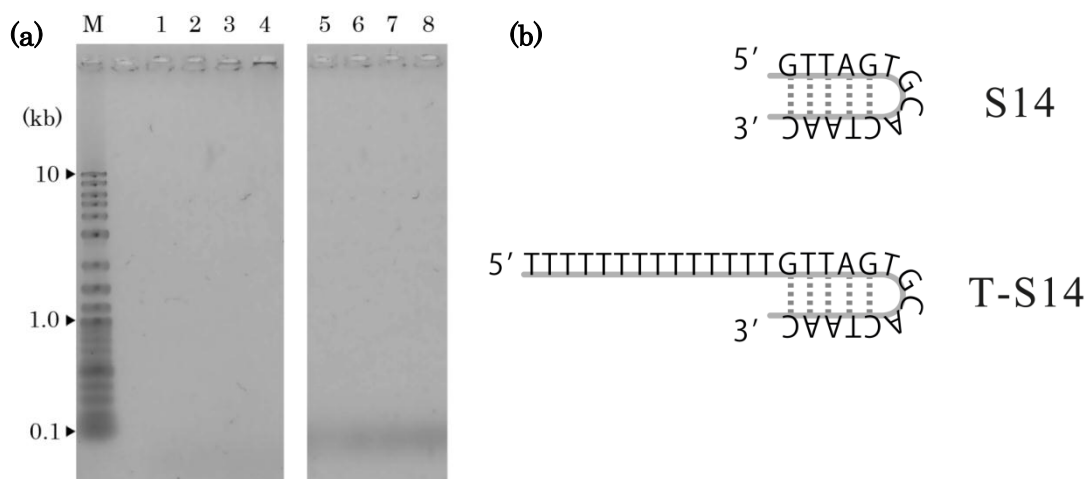


Figure 2-28. Elongation of **S14** and **T-S14**. Sequences are shown in panel B. Reaction conditions were as follows; 100 nM **S14** or **T-S14**, 20 U/mL Vent(exo-), 0.5 mM dNTP in 1×Thermopol buffer. Samples were electrophoresed on 1.0% agarose gel and the gel was stained by SYGR Green I. Lane 1: **S14**, 0 h. Lane 2: **S14**, 0.5 h. Lane 3: **S14**, 1 h. Lane 4: **S14**, 2 h. Lane 5: **T-S14**, 0 h. Lane 6: **T-S14**, 0.5 h. Lane 7: **T-S14**, 1 h. Lane 8: **T-S14**, 2 h.

Short 20 to 30 nt long DNA sequences that can form hairpins at either end due to the palindromic nature of the sequence were efficiently elongated by DNA polymerases. In some cases, elongation products longer than 10 kb were observed within only 10 min. The elongation efficiency depended on the stability of hairpin at both ends of the short seed template. During elongation, DNA is mostly in a duplex state as shown by our analysis of melting temperatures of short seeds and products. This suggests that the elongation is not due to simple back-primed primer extension caused by slippage. Other previously reported elongation mechanisms do not explain well why long DNA products are obtained so quickly. Here, a new model, Terminal Hairpin formation and Self-Priming extension or THSP, is able to explain this unusual elongation (Figure 2-29).

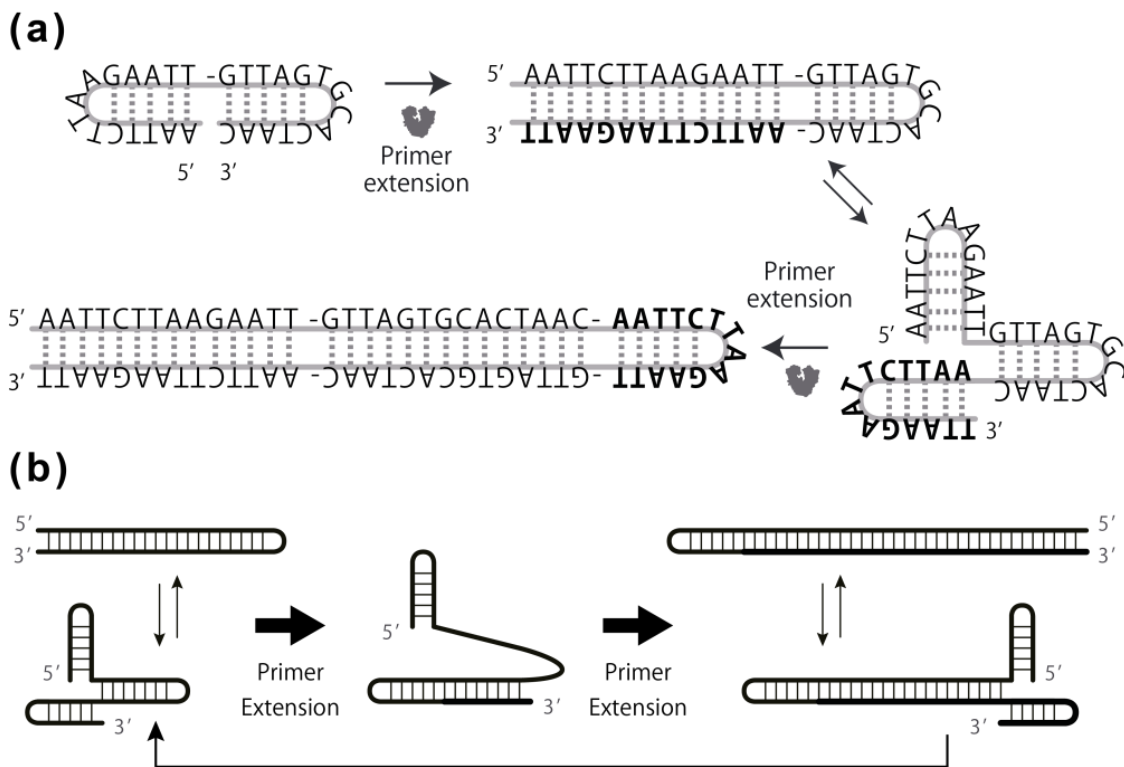


Figure 2-29. Proposed terminal hairpin formation and self-priming extension (THSP) model for efficient elongation of short seeds. (a) Self-priming and elongation of S28 at the initiation step. Once elongation starts, conserved palindromic sequences at 5'-end enable efficient elongation. (b) Continuous elongation according to THSP model. A hairpin structure forms at the 3' terminus and the primer extension occurs. The duplex stem of the hairpin opens during primer extension due to the strand displacement activity of DNA polymerase. When the primer extension reaches the 5' end, a longer hairpin structure is formed and a new elongation cycle starts.

As shown in Figure 2-29a, once the hairpin at 3' end forms, primer extension to the 5' end of the short seed template will first give a 42-nt-long product that can form longer hairpin structure. This 42-nt product is clearly observed in Figure 2-25a. Self-priming from this product occurs when hairpins form at each end; each of these hairpins has the same sequence as the 5' half of **S28** (Figure 2-29a). The hairpin at 3' end is similar to a usual template/primer structure that can be elongated by primer extension. After extension to a 70-nt-long sequence, a larger hairpin can form. Obviously, this self-priming and elongation can be carried out continuously with the length of ODN almost doubled after each cycle (Figure 2-29b). The above process, including dissociation of some base pairs, self-priming, and primer extension, enables successive efficient elongation under isothermal conditions. It is noteworthy that the DNA forms the duplex and only the termini melt transiently in this model. According to the THSP model, the hairpin formation at 3' end plays the role of initiation of elongation, and the hairpin at the 5' end allows successive elongation. Obviously, even mis-pairing at the 3' end can initiate elongation. Once the initiation starts, the sequence at 5' end will dominate the elongation.

Strand displacement activity of DNA polymerase is likely required to dissociate the hybridized non-template regions prior to elongation. To confirm this, the elongation by other thermophilic DNA polymerases Deep Vent (exo-), 9^oN_m, Taq, and Phusion was examined. Like Vent (exo-), Deep Vent (exo-) and 9^oN_m have strand displacement activity, but the other polymerases do not. As expected, DNA polymerases with strand displacement activity efficiently elongated **S28**, but no elongation was observed in the presence of DNA polymerases Taq and Phusion, which do not have strand displacement activity (Figure 2-30). The requirement for strand displacement activity strongly supports the THSP model.

Other results can also be explained by the THSP model. The intramolecular self-priming and primer extension enable elongation at a low DNA concentration (Figure 2-22). The elongated products can be digested completely by Tsp509I to give very clear bands of 28 and 18 nucleotides (Figure 2-24), indicating that the elongated products consist of the repeated sequence of **S28** (Figure 2-23).

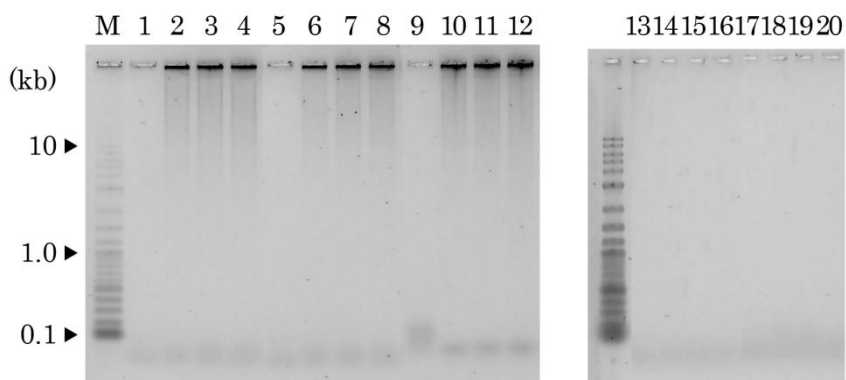


Figure 2-30. Elongation of **S28** by various DNA polymerases. Reaction conditions were as follows; 100 nM **S28**, 20 U/mL DNA polymerase, 0.5 mM dNTP in 1×Thermopol buffer (for Phusion, 1× Phusion HF buffer). Samples were electrophoresed on 1.0% agarose gel and the gel was stained by SYGR Green I. Lane 1: Vent(exo⁻), 0 h. Lane 2: Vent(exo⁻), 0.5 h. Lane 3: Vent(exo⁻), 1 h. Lane 4: Vent(exo⁻), 2 h. Lane 5: Deep Vent(exo⁻), 0 h. Lane 6: Deep Vent(exo⁻), 0.5 h. Lane 7: Deep Vent(exo⁻), 1 h. Lane 8: Deep Vent(exo⁻), 2 h. Lane 9: 9°N_m, 0 h. Lane 10: 9°N_m, 0.5 h. Lane 11: 9°N_m, 1 h. Lane 12: 9°N_m, 2 h. Lane 13: Taq, 0 h. Lane 14: Taq, 0.5 h. Lane 15: Taq, 1 h. Lane 16: Taq, 2 h. Lane 17: Phusion, 0 h. Lane 18: Phusion, 0.5 h. Lane 15: Phusion, 1 h. Lane 16: Phusion, 2 h.

Efficient elongation occurred in the temperature range of 66-77°C; **S28** is in a single-stranded state in this range, whereas the elongated products are in a duplex state. As the T_m of **S28** is 53.1°C, the hairpin with the sequence of 5'-AATTCTTAAGAATT-3' does not form at the reaction temperature in buffer. Binding of DNA polymerase likely promotes hairpin formation and allows self-priming. At lower temperatures, the duplex is stable, and it was observed that elongation did not occur after the initial primer extension. The end of a long DNA duplex can partly dissociate by breathing even at a temperature lower than its T_m .³⁹ Smolina *et al.* reported that a 13-nt-long PNA could even invade at 37°C to the end of a DNA duplex longer than 100 bp.⁴⁰ At higher temperatures, hairpin does not form even in the presence of polymerase, and no primer extension was detected.

The sequences used here are different from previously reported sequences that result in unusual products; those sequences are usually simple repetitive sequences.^{23,41-46} Obviously, the mechanisms previously proposed cannot explain the unusual elongation of short single-stranded ODNs used here. For the *in vitro* elongation of short duplex with repetitive sequence, slippage may be the main model (Figure 2-31A).^{23,41-47} In the case of **S28**, however, slippage cannot happen because the strands would have to move 28 nt to find another point for primer extension, and the activation

energy is too high. Similarly, bulge migration (Figure 2-31B)^{26,46-48} is unlikely to occur through the long repeats of **S28**. The previously proposed hairpin-coil transition model^{25,26} is close to our model; however, hairpin formation only occurs at the initiation of priming in that model. The template switching model (Figure 2-31D)²⁴ requires high concentrations of DNA. The DEME model (Figure 2-31C)²⁸ can only explain the elongation at a temperature close to the T_m of the elongated product. In contrast, our proposed mechanism explains the elongation of single-stranded simple repetitive sequence to some extent.

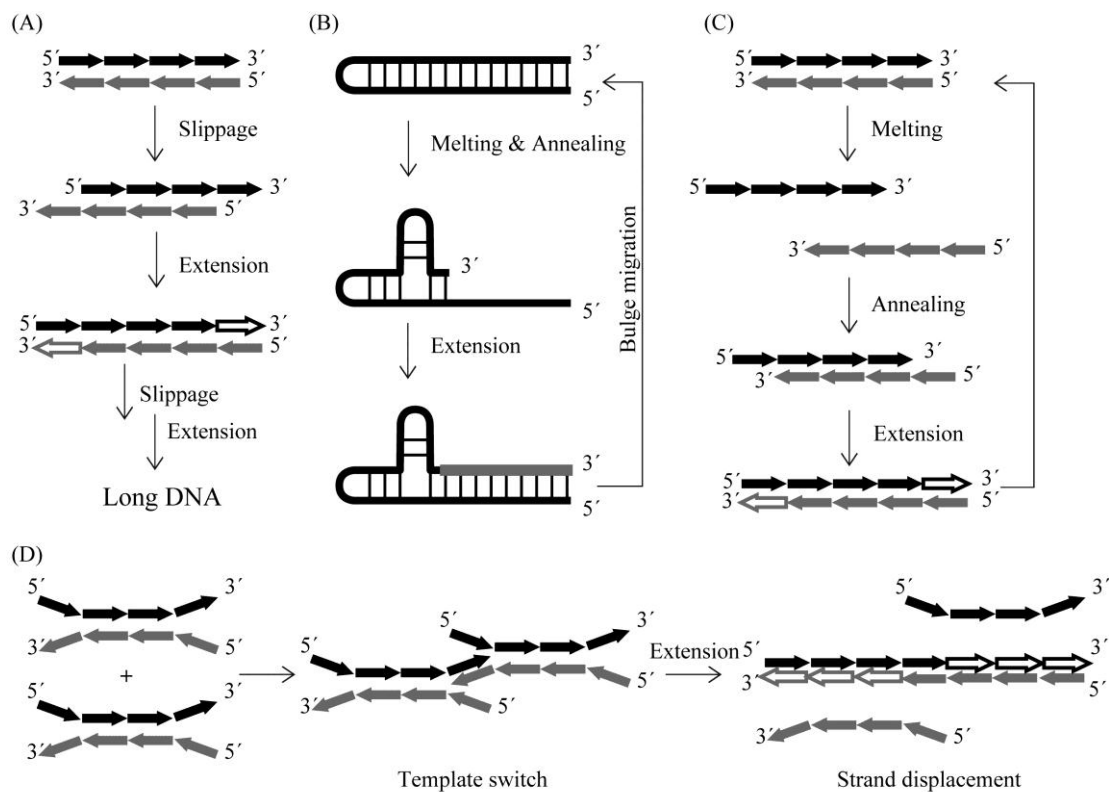


Figure 2-31 Elongation mechanisms supposed by other groups. (A) Slippage synthesis model by Kornberg A *et al.* (B) Hairpin-elongation model by Kornberg A and Ogata N *et al.* (C) DEME (Duplex Elongation at Melting Equilibrium) model by Ogata N *et al.* at a higher temperature. (D) Template switching and strand displacement model by Tuntiwechapikul W *et al.*

According to the THSP mechanism, palindromic sequences at the 5' and 3' ends of the template are important for successive elongation. To verify this, two sequences **RnA** and **RnB** with palindromic sequence only at the 5' end (Table 2-5) were prepared. At their 3'-ends, **RnA** and **RnB** have two 20-nt-long random (non-palindromic) sequences that are complementary to each other. For sequence analysis, the recognition site of Taq^oI (5'-T↓GCA-3') was also present. During elongation, the 3' ends of **RnA** and **RnB** hybridize and allow primer extension. To simulate the 70-nt-long intermediate as shown in Figure 2-25a, two repeats of the 5' half of **S28** were designed. When both **RnA** and **RnB** were added, efficient elongation was observed in 30 min (lane 7-9, Figure 2-32a). If only **RnA** was added, elongation was barely detected. A slight amount of elongation of **RnB** was also observed in the absence of **RnA**, probably due to the mis-priming from the 3'-end of **RnB** (lane 4-6, Figure 2-32a). To analyze the sequence of the elongation product from **RnA/RnB**, digestion by restriction enzyme Taq^oI (5'-T↓GCA-3') was carried out. As shown in Figure 2-32b, the elongated product was digested efficiently, indicating that it has the repetitive sequence of **RnA/RnB**. The fragment length deduced from bands on the gel also coincided well with the possible fragments when the elongation was carried out according to our THSP model.

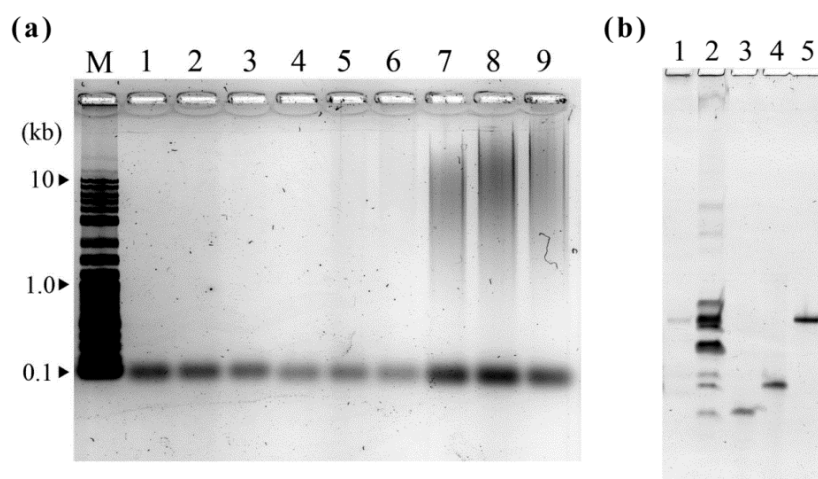
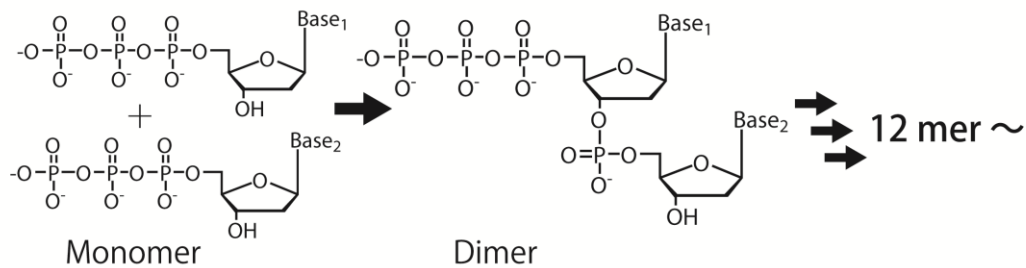


Figure 2-32. Elongation of DNA sequences (**RnA** and **RnB**) with palindromic sequences at the 5' ends and mixed sequence at the 3' ends. (a) Image of gel separation of elongation products. Samples were electrophoresed on 1.0% agarose gel and stained by SYBR Green I. Lane 1: **RnA** only, 0.5 h; Lane 2: **RnA** only, 1.0 h; Lane 3: **RnA** only, 2.0 h; Lane 4: **RnB** only, 0.5 h; Lane 5: **RnB** only, 1.0 h; Lane 6: **RnB** only, 2.0 h; Lane 7: **RnA** and **RnB**, 0.5 h; Lane 8: **RnA** and **RnB**, 1.0 h; Lane 9: **RnA** and **RnB**, 2.0 h. The reaction was performed at 67.0 °C. (b) Digestion of elongated product from **RnA/RnB** by restriction enzyme Taq^oI. Samples were analyzed on a 10% denatured PAGE containing 8.0 M urea in 0.5× TBE buffer. The gel was stained by SYBR Green II. Lane 1: After elongation (purified); Lane 2: after digestion; Lane 3: 28-nt marker; Lane 4: 34-nt marker; Lane 5: 50-nt marker.

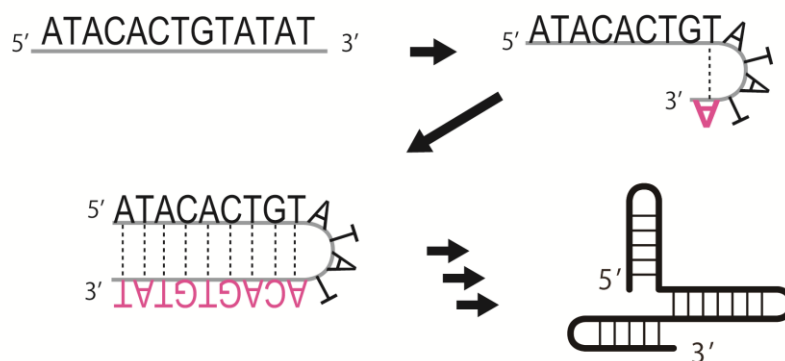
2-3-6 Proposed mechanism of unexpected DNA amplification

According to above results, the mechanism of *de novo* DNA synthesis was discussed here (Figure 2-33).

(a) Early stage of initiation step



(b) Late stage of initiation step



(c) Elongation step

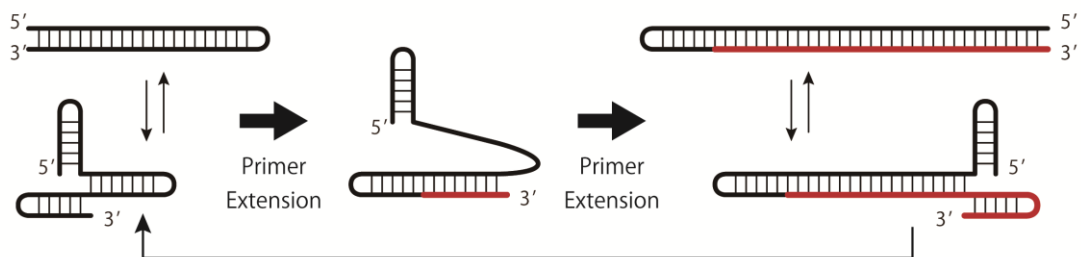


Figure 2-33. Supposed mechanism of *de novo* DNA synthesis. (a) In the early stage of initiation step, 2 monomers are somehow polymerized and form dimer. The dimer is next added a monomer and form trimer, tetramer... at last about 12-nt-long ssDNA may be synthesized. (b) In the late stage of initiation step, short ssDNA is added dNTP and formed hairpin. This make palindromic sequence on the basis of *de novo* DNA synthesized tandem repeat products. Then short ssDNA is elongated by formation/dissociation of hairpin, at last the elongated DNA can form hairpin at each termini. (c) In the elongation step, synthesized DNA is applicable to be elongated by THF-SPE model and very long DNA is produced.

In the early stage of initiation step (Figure 2-33a), short ssDNA will be polymerized from dNTP step by step. This stage is still obscure due to limitation of detection sensitivity, however, a new strand should be synthesized. Since DNA polymerase also contains some contaminant DNA fragment, it would assist and involve such abnormal reaction. About 12-nt-long ssDNA can be elongated by reiterative formation/dissociation of hairpin. As the probability of hairpin formation and nucleotide addition is low especially at high temperature, this step is rate-limiting and requires long time of incubation. At this step, random sequence of ssDNA would be synthesized, however, the stability of hairpin is very important factor, so the sequence of ssDNA highly depends on the reaction temperature in this step. For instance, if poly dA was synthesized, it cannot form hairpin at 80°C and would not become major product since nucleotide addition requires stabilization by forming hairpin as shown in section 2-3-4. The moderate balance of the stability of hairpin and reaction temperature is required during synthesis of short ssDNA. Therefore the product sequence of *de novo* DNA synthesis correlated with the reaction temperature and GC% shown in Table 2-1. Namely, the sequences of measure products were selected here.

In the late stage of initiation step (Figure 2-33b), short ssDNA would grow a palindromic sequence by self-primed extension. As shown in section 2-3-4, palindromic sequences can be synthesized from short ssDNAs which can never form usual Watson-Click base pairs by cycles of nucleotide addition and hairpin formation/dissociation followed by self-primed primer extension. After that, the synthesized product would contain repetitious palindromic sequences which can form hairpin structures at each end. In this step, the stability of hairpin also affects reaction efficiency because this step requires both formation and dissociation of hairpin structures.

Once the palindromic sequence containing hairpins at each end was synthesized, efficient elongation by THSP model can be available (Figure 2-33c). Here, since only termini of duplex should be dissociated, elongation reaction can be carried out under lower temperature than the T_m of the product DNA. In addition, unlike PCR, THSP model does not require complete dissociation of duplex, hence *de novo* DNA synthesis and unexpected amplification of ssDNA can be carried out under isothermal conditions.

2-4 Conclusions

In this chapter, an unexpected DNA amplification, *de novo* DNA synthesis and elongation of short ssDNA were closely investigated. As a result, the mechanisms of unexpected DNA amplification were clarified.

De novo DNA synthesis, which is assumed to be a cause of unexpected DNA amplification, was closely investigated. It was found that *de novo* DNA synthesis could be carried out in a wide range of temperature (25-94°C). The reaction efficiency of *de novo* DNA synthesis by **Vent** highly depended on the reaction temperature and the optimal temperature was around 50 °C. The products were remarkably long >10 kb and contained highly repetitious palindromic sequences. The product sequences were highly correlated with the reaction temperature, GC% tended to be larger in higher temperature.

To clarify the mechanism of *de novo* DNA synthesis, elongation mechanism of short ssDNA was studied. Some thermophilic DNA polymerases can elongate short ssDNA such as (AC)₉, (AG)₉, (TC)₉, (TG)₉ which can NEVER form general Watson-Crick base pair. This phenomenon also involves unexpected amplification of primer. Even if the primers were designed well so as not to cause mis-priming or form self-dimer, DNA polymerase could synthesize palindromic sequences from primers and it would cause unexpected amplification. The sequence to be elongated was greatly varied with the reaction temperature. AT-rich sequences were elongated efficiently at relatively lower temperatures, whereas the sequences containing higher GC% was favorable to be elongated at higher temperature. Elongation of short ssDNA also depended on polymerases. A great difference in elongation efficiency among 4 thermophilic DNA polymerases was observed despite of their highly conserved homology. From these results, optimizing the reaction temperature according to the primer sequence and using appropriate DNA polymerase will be effective to avoid such unexpected reaction.

The elongation mechanisms of both short ssDNA and *de novo* DNA synthesis would be quite similar. Elongation of short ssDNA could be divided into 2 steps; first, elongation would start by nucleotide addition and reiterative formation/dissociation of hairpin, secondly, extended palindromic sequence would be elongated according to

THSP model. It could also be applied to the mechanism of *de novo* DNA synthesis after synthesis of short ssDNA from dNTP monomers.

THSP model was proposed to explain efficient elongation under isothermal condition. Successive elongation from self-primed 3'-end and formation of terminal hairpin enable efficient elongation. This model was verified using short DNA containing hairpins at each end. The temperature dependence and the product sequences were consistent with the products of *de novo* DNA synthesis and elongated short ssDNAs.

Short single-stranded DNA with sequences able to form hairpin structures at each end was elongated efficiently by a thermophilic DNA polymerase under isothermal conditions. Even an ODN with a palindromic sequence only at the 5' end could be elongated once priming from the 3' end occurs. THSP can explain well the results presented here. The high efficiency under isothermal conditions is due to hairpin formation that allows self-priming and primer extension. THSP may also explain *in vitro* elongation of simple repetitive sequence as long as a short hairpin structure can form at 5' end of the DNA strand after the initiation step. This model may clarify the molecular evolution of nucleic acids and explain the observation of non-specific amplification observed during PCR reactions. These results would be beneficial for designing reaction conditions in precise and highly sensitive DNA amplification techniques.

2-5 Experimental section

Materials

pUC19, NEB 5-alpha Competent *E.coli* (High Efficiency) was purchased from New England BioLabs. GenElute Plasmid Miniprep Kit was from Invitrogen, SeaKem GTG Agarose was from TaKaRa Bio Inc. All DNA oligonucleotides (ODNs) used in this study were purchased from Integrated DNA Technologies. ODNs were dissolved in sterile Milli-Q water to a concentration of 100 μ M and frozen until use. Usually, the ODNs were diluted to 1.0 μ M as the stock for elongation and to a final concentration of 100 nM. Vent (exo⁻) DNA polymerase, Taq DNA polymerase, Deep Vent (exo⁻) DNA polymerase, and 9^oN_m DNA polymerase were obtained from New England Biolabs. Phusion DNA polymerase was purchased from Finnzymes. KOD dash DNA polymerase was from TOYOBO, *Pfu* DNA polymerase was from Promega, dNTP was from GE Healthcare Bio Science.

Elongation conditions of ODNs

The standard reaction solution contained 100 nM ODN, 0.5 mM each dNTPs (GE Healthcare), and 20 U/mL DNA Polymerase in 100 μ L 1 \times Thermopol buffer (20 mM Tris-HCl, 10 mM (NH₄)₂SO₄, 10 mM KCl, 2.0 mM MgSO₄, 0.1% Triton X-100, pH 8.8). Elongation by Phusion DNA polymerase was carried out in 1 \times Phusion HF buffer supplied by Finnzymes (the contents are not declared). Before starting the elongation reaction, the reaction mixture lacking of only dNTPs was prepared and incubated at the reaction temperature for several minutes, then the reaction was started by addition of dNTPs (in a 25 mM stock solution). Elongation was performed on a Thermal Cycler Dice (Takara Bio) or a PCR-320 (Astec). To quench the reaction, aliquots of the reaction solution were mixed with an equal volume of the 2 \times loading dye or 60-fold excess volume of 0.5 \times TAE buffer. In cases of low concentrations, the products were ethanol precipitated and analysed on an agarose gel. In some cases, products were analysed on a denaturing agarose gel (30 mM NaOH, 1.0 mM EDTA).

Quantitative analysis of DNA products

Elongated DNA products were analyzed by fluorescence measurement after staining with SYBR Green I (Lonza). An aliquot of the reaction mixture was diluted 60-fold with 2× SYBR Green I solution in 0.5× TAE buffer. A 100 μL aliquot of the sample was transferred into a well of a 96-well clear-bottom microplate, and fluorescence measurement was performed on FLA-3000 (Fujifilm). When the DNA concentration was too high to measure, the samples were diluted until the fluorescence intensity was in a proper range.

Materials for radio-isotope labeling experiments

Vent(exo-) DNA polymerase was purchased from New England Bio Labs. T4 Poly Nucleotide Kinase was purchased from Fermentas. dATP was GE Healthcare and α -³²P dATP and γ -³²P ATP were from Perkin Elmer. All ODNs were synthesized by Integrated DNA Technology with desalting grade.

Elongation reactions of short ssDNA with radio-isotope

Standard reaction conditions were as below: 20 U/mL **Vent(exo-)**, 0.5 mM dATP containing 0.2 μCi/μL α -³²P dATP, 100 nM ODN in 1x Thermopol buffer, total volume 25 μL, on PC-320 (ASTECC).

Analysis on PAGE: 20 % denaturing PAGE containing 8 M Urea in 1x TBE buffer was used. Acrylamide was polymerized by addition of 15 μL of TEMED and 150 μL of 10% APS. Electrophoresis was at 750 V for 120 minutes in 1x TBE buffer. After electrophoresis, the gel was wrapped by cellophane wrap and exposed to Imaging Plate (IP) for 120 minutes. IP was filmed on FLA-3000 in IP mode.

Labeling by phosphorylation at 5'-end of short ssDNA

Reaction conditions: 1/2.5 volume of 1 μM ODN, 0.2 μCi/μL γ -³²P ATP, 1/25 volume of PNK in 1x T4 Ligase buffer (40 mM Tris-HCl, 10 mM MgCl₂, 10 mM DTT, 0.5 mM ATP,

pH 7.8@25°C) for 2 hours. After the reaction, the reaction solution was treated with PCI and CIA three times each. The purified product was precipitated with ethanol and suspended again in an equal volume of sterile water of firstly added ODN.

Molecular cloning for sequencing

Elongated products was purified by PCI (phenol:chloroform:isoamylalcohol = 25:24:1, Invitrogen), CIA (chloroform:isoamylalcohol = 24:1, Fluka Chemicals) treatment and precipitated with ethanol (Wako). Small molecules were removed with a sephadex G-25 spin column (GE Healthcare). The purified DNA was fragmented by 0.08 U/mL of DNase I (New England Biolabs) at 15 °C for 30 min in the presence of 10 mM MnCl₂. The fragments, which have blunt ends, were cloned into the SmaI site of pUC19 plasmid (New England Biolabs) by ligation with T4 DNA Ligase (Invitrogen) at 16 °C for 20 h. After harvesting, inserted plasmids were purified with GenElute plasmid extraction kit (Invitrogen). Sequencing reactions were performed by MacroGen Japan Inc. Reaction conditions for sequencing were as follows: a BioRad DNA Engine Dyad PTC-220 Peltier Thermal Cycler by using an ABI BigDye™ Terminator v3.1 Cycle Sequencing Kit. Single-pass sequencing was performed on an ABI 3730xl sequencer (Applied Biosystems) according to the protocols supplied by the manufacturer.

***T_m* measurements**

After PCI/CIA treatment, the products were purified by ethanol precipitation and spin column G-25 or G-50. The purified products were dissolved into 1×Thermopol Detergent Free buffer (10 mM KCl, 10 mM (NH₄)₂SO₄, 20 mM Tris-HCl, 2 mM MgSO₄, pH 8.8). The mid-point of thermal melting transition (*T_m*) was determined by monitoring the change of absorbance at 260 nm with temperature on a UV/Vis spectrometer (UV-1800) equipped with temperature-controlling device TMSPC-8 (Shimadzu). *T_m*s of short seed DNAs used as elongation substrates were also measured under the same conditions. The concentration of DNA was adjusted to A₂₆₀ ≈ 1.0.

Elongation of RnA and/or RnB

Elongation of **RnA** (5'-AATTCTTAAGAATTAATTCTTAAGAATTAGATTGAACTCTCG AACTAT-3') and **RnB** (5'-AATTCTTAAGAATTAATTCTTAAGAATTATAGTTCGAGAG TTCAATCT-3') was performed at 70 °C under following conditions: 100 nM **RnA** and/or **RnB**, 0.5 mM each dNTPs, 20 U/mL Vent (exo-) DNA polymerase in 1× Thermopol buffer. Samples were electrophoresed on 1.0 % agarose gels and stained by SYBR Green I. The elongation products were purified by treatment with PCI, CIA, ethanol precipitation, and a sephadex G-25 spin column before digestion by Taq^qI.

Digestion by restriction enzyme of elongated products

After purification, elongated products were digested by the restriction enzyme Tsp509I (New England Biolabs). The reaction was carried out at 65 °C overnight with 10 U Tsp509I in 50 µL 1× NEBuffer 1 (10 mM bis-Tris-propane-HCl, pH 7.0, 10 mM MgCl₂, 1.0 mM dithiothreitol). For the elongation products of **RnA** and **RnB**, restriction enzyme Taq^qI (New England Biolabs) was used. After purification, the elongation product was digested at 65 °C overnight by 20 U Taq^qI in 50 µL 1× NEBuffer 4 (50 mM potassium acetate, 20 mM Tris-acetate, 10 mM magnesium acetate, pH 7.9, 1.0 mM dithiothreitol).

2-6 References

- (1) Morlinghem, J. E.; Harbers, M.; Traeger-Synodinos, J.; Lezhava, A. *Pharmacogenomics*, **2011**, *12*, 845-860.
- (2) Asiello, P. J.; Baeumner, A. J. *Lab Chip*, **2011**, *11*, 1420-1430.
- (3) Gill, P.; Ghaemi, A. *Nucleos. Nucleot. Nucl.*, **2008**, *27*, 224-243.
- (4) Schachman H. K. *J. Biol. Chem.*, **1960**, *235*, 3242-3249.
- (5) Radding, C. M.; Kornberg, A. *J. Biol. Chem.*, **1962**, *237*, 2869-2876.
- (6) Radding, C. M.; Kornberg, A. *J. Biol. Chem.*, **1962**, *237*, 2877-2882.
- (7) Kornberg, A.; Jackson, J. F.; Khorana, H. G.; Bertsch, L. L. *Proc. Natl. Acad. Sci. U.S.A.*, **1964**, *51*, 315-323.
- (8) Kornberg, A.; Baker, T.A. *DNA Replication*, 2nd ed., W.H.Freeman, NY., **1992**.
- (9) Burd, J. F.; Wells, R.D. *J. Biol. Chem.*, **1970**, *53*, 435-459.
- (10) Henner, D.; Furth, J. J. *J. Biol. Chem.*, **1977**, *252*, 1932-1937.
- (11) Nazarenko, I. A.; Potapov, V. A.; Romaschenko, A. G.; Salganik, R. I. *FEBS letters*, **1978**, *86*, 201-204.
- (12) Nazarenko, I. A.; Bobko, L. E.; Romashchenko, A. G.; Khripin, Y. L.; Salganik, R. I. *Nucleic Acids Res.*, **1979**, *6*, 2545-2560.
- (13) Ogata, N.; Miura, T. *Biochem. J.*, **1997**, *324*, 667-671.
- (14) Ogata, N.; Miura, T. *Nucleic Acids Res.*, **1998**, *26*, 4652-4656.
- (15) Ogata, N. Miura, T. *Nucleic Acids Res.*, **1998**, *26*, 4657-4661.
- (16) Liang, X. G.; Jensen, K.; Frank-Kamenetskii, M. D. *Biochemistry*, **2004**, *43*, 13459-13466.
- (17) Liang, X. G.; Jensen, K.; Frank-Kamenetskii, M. D. *Nucleic Acids Symp. Ser.*, **2006**, *50*, 95-96.
- (18) Zyrina, N. V.; Zheleznaya, L. A.; Dvoretzky, E. V.; Vasiliev, V. D.; Chernov, A.; Matvienko, N. I. *Biol. Chem.*, **2007**, *388*, 367-372.

- (19) Hanaki, K.; Odawara, T.; Muramatsu, T.; Kuchino, Y.; Masuda, M.; Yamamoto, K.; Nozaki, C.; Mizno, K.; Yoshikura, H. *Biochem. Bioph. Res. Co.*, **1997**, *238*, 113-118.
- (20) Hanaki, K.; Odawara, T.; Nakajima, N.; Shimizu, Y. K.; Nozaki, C.; Mizuno, K.; Muramatsu, T.; Kuchino, Y.; Yoshikura, H. *Biochem. Bioph. Res. Co.*, **1998**, *244*, 210-219.
- (21) Hanaki, K.; Nishihara, T.; Odawara, T.; Nakajima, N.; Yamamoto, K.; Yoshikura, H. *BioTechniques*, **2001**, *31*, 734-738.
- (22) Ramadan, K.; Shevelev, I. V.; Maga, G.; Hubscher, U. *J. Mol. Biol.*, **2004**, *339*, 395-404.
- (23) Hartig, J. S.; Kool, E. T. *Nucleic Acids Res.*, **2005**, *33*, 4922-4927.
- (24) Tuntiwechapikul, W.; Salazar, M. *Biochemistry*, **2002**, *41*, 854-860.
- (25) Ogata, N.; Morino, H. *Nucleic Acids Res.*, **2000**, *28*, 3999-4004.
- (26) Ogata, N.; Miura, T. *Biochemistry*, **2000**, *39*, 13993-14001.
- (27) Ogata, N. *Biochimie*, **2007**, *89*, 702-712.
- (28) Liang, X. G.; Kato, T.; Asanuma, H. *Nucleic Acids Symp. Ser.*, **2007**, *51*, 351-352.
- (29) Kong, H.; Kucera, R. B.; Jack, W. E. *J. Biol. Chem.*, **1993**, *268*, 1965-1975.
- (30) Sambrook, J.; Fritsch, E. F.; Maniatis, T. *Molecular Cloning: A laboratory Manual*, 2nd ed., Cold Spring Harbor Laboratory Press, Cold Spring Harbor, NY., **1989**
- (31) Rodriguez A. C.; Park, H. W.; Mao, C.; Beese, L. S. *J. Mol. Biol.*, **2000**, *299*, 447-462.
- (32) Kim, S. W.; Kim, D.-U.; Kim, J. K.; Kang, L.-W.; Cho, H.-S. *Int. J. Biol. Macromol.*, **2008**, *42*, 356-361.
- (33) Rothwell, P. J.; Waksman, G. *Adv. Protein Chem.*, **2005**, *71*, 401-440.
- (34) Hogrefe, H. H.; Cline, J.; Lovejoy, A. E.; Nielson, K. B. *Method. Enzymol.*, **2001**, *334*, 91-116.
- (35) García, P. B.; Robledo, N. L.; Islas, Á. L. *Biochemistry*, **2004**, *43*, 16515-16524.
- (36) Faucett, A. M.; Islas, A. L. *Biochem. Bioph. Res. Co.*, **2005**, *337*, 1030-1037.

- (37) Clark, J. M. *Nucleic Acids Res.*, **1988**, *16*, 9677-9686.
- (38) Kato, T.; Liang, X. G.; Asanuma, H. *Biochemistry*, **2012**, *51*, 7846-7853.
- (39) Frank-Kamenetskii, M. D. *Nature*, **1987**, 328, 17-18.
- (40) Smolina, I. V.; Demidov, V. V.; Soldatenkov, V. A.; Chasovskikh, S. G.; Frank-Kamenetskii, M. D. *Nucleic Acids Res.*, **2005**, *33*, e146.
- (41) Kornberg, A.; Bertsch, L. R. L.; Jackson, J. F.; Khorana, H. G. *Proc. Natl. Acad. Sci. U.S.A.* **1964**, *51*, 315-323.
- (42) Wells, R. D.; Ohtsuka, E.; Khorana, H. G. *J. Mol. Biol.* **1965**, *14*, 221-237.
- (43) Wells, R. D.; Büchi, H.; Kössel, H.; Ohtsuka, E.; Khorana, H. G. *J. Mol. Biol.* **1967**, *27*, 265-272.
- (44) Wells, R. D.; Jacob, T. M.; Narang, S. A.; Khorana, H. G. *J. Mol. Biol.* **1967**, 27, 237-263.
- (45) Kotlyar, A. B.; Borovok, N.; Molotsky, T.; Fadeev, L.; Gozin, M. *Nucleic Acids Res.* **2005**, *33*, 525-535.
- (46) Kurihara, H.; Nagamune, T. *Biotechnol. Prog.* **2004**, *20*, 1855- 1860.
- (47) Lyons-Darden, T.; Topal, M. D. *Nucleic Acids Res.* **1999**, *27*, 2235-2240.
- (48) Heidenfelder, B. L.; Makhov, A. M.; Topal, M. D. *J. Biol. Chem.* **2003**, *278*, 2425-2431.
- (49) Bohlke, K.; Pisani, F. M.; Vorgias, C. E.; Frey, B.; Sobek, H.; Rossi, M.; Antranikian, G. *Nucleic Acids Res.*, **2000**, *28*, 3910-3917.
- (50) Freisinger, E.; Grollman, A. P.; Miller, H.; Kisker, C. *EMBO Journal*, **2004**, *23*, 1494-1505.
- (51) Pisani, F. M.; De Felice, M.; Rossi, M.; *Biochemistry*, **1998**, *37*, 15005-15012.

2-7 Appendixes

The product of *de novo* DNA synthesis at 50°C was measured on AFM (tapping mode).

Measurement buffer: 1x TAE buffer containing 100 mM MgSO₄

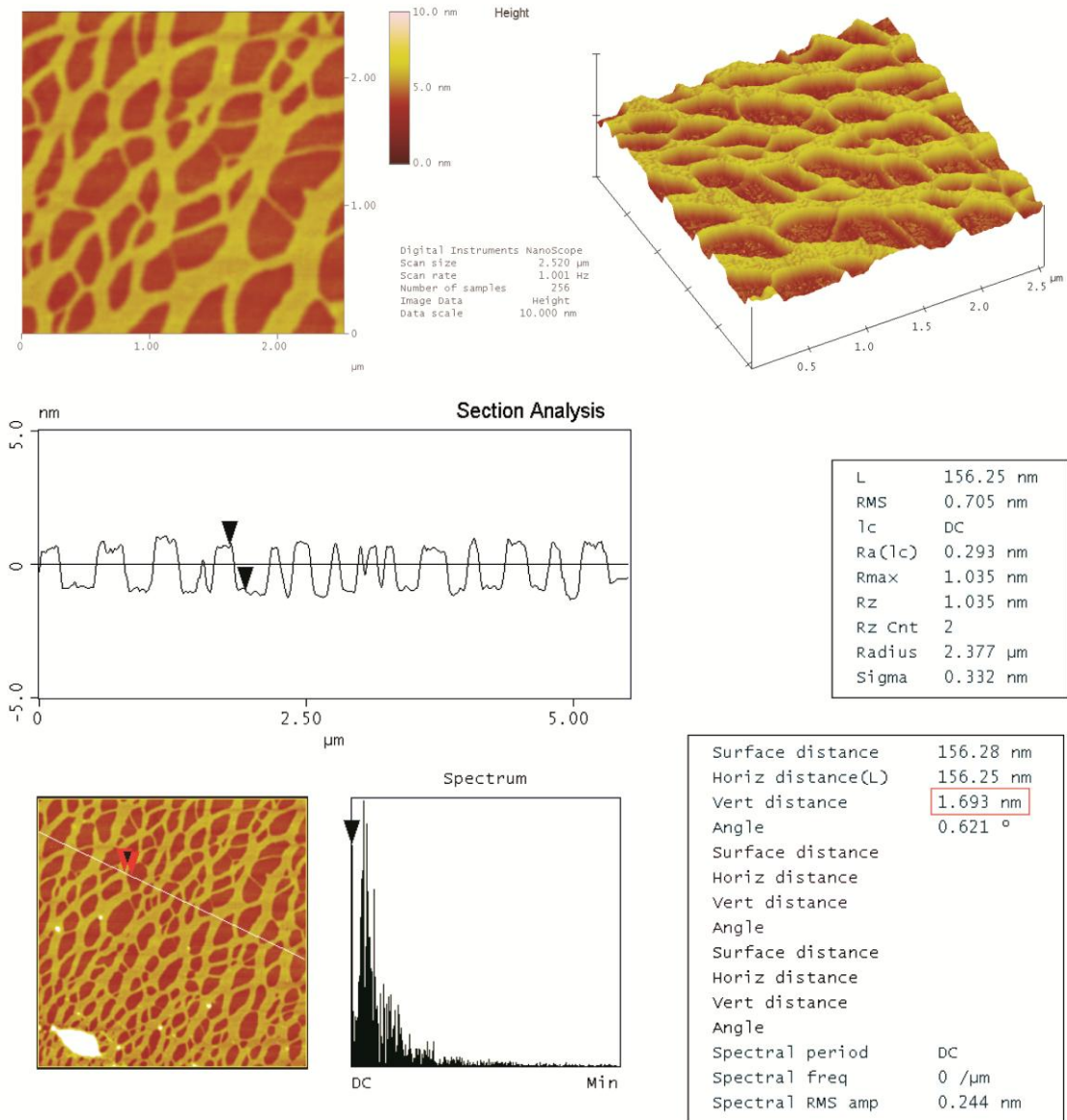


Figure 2-34. AFM images of the product of *de novo* DNA synthesis at 50°C.

The product was intertwined mesh structure. The height of the mesh was 1.7 nm, which corresponds to typical radius of B-type DNA helix (2 nm).

Some polymerase could elongate short ssDNA such as (TG)₉. This reaction highly depended on the type of DNA polymerase. Although 4 polymerase used here were highly conserved homologous, however, the reaction efficiency was significantly different. Here, sequence alignment of the 4 polymerases was performed (Figure 2-35). Red colored region is common part which is highly conserved. Yellow color shows a little different residues and no colored region is variable. In yellow region, red letters have relatively high homology and black letters are residues which have obviously different properties. The variable regions in these polymerases were identified by amino acid sequence alignment. Confining to residues in the variable regions which can interact, Y-GG/A motif which lies around 385 was found.⁴⁹ The residue of “-“ in Y-GG/A is variable in each polymerases. It is worthy of note that polymerases which are favorable to elongate short ssDNA have hydrophobic residue at this position, in contrast, polymerases which are unfavorable to elongate short ssDNA have hydrophilic residue (Figure 2-36 upper right part). Comparing with RB69 DNA polymerase,⁵⁰ which also belongs to Family B, X-ray crystallographic data shows that Y-GG/A motif can touch Template DNA strand (Figure 3-36 left bottom part). In addition, Pisani FM *et al.* reported that mutations introduced around Y-GG/A motif affected $K_m(\text{DNA})$ of polymerases.⁵¹ Taken together, it was suggested that the 385th residues are different from each other and the difference affects $K_m(\text{DNA})$, which may be an important factor of elongation of short ssDNA.

Amino acid sequence alignment

		Y-GG/A motif			
		360	370	380	390
favorable to elongate {	9°N-7	RKAYKRNE	LAPNKP	DERELARR	-RGGYAGGYV
	Vent	RVAYARNE	LAPNKP	DEEEYKRRL	RTTYLGGYV
unfavorable to elongate {	KOD	RKAYERNE	LAPNKP	DEKELARR	-RQSYEGGYV
	Pfu	RKAYERNE	VAPNKP	SEEEYQRRL	RESYTTGGFV

Y-GG/A motif can be in contact with template

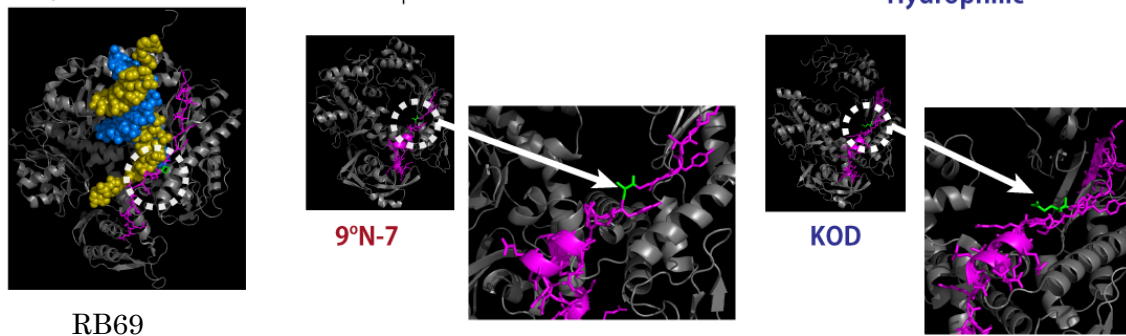


Figure 2-36. Amino acid sequence alignment around Y-GG/A motif and molecular modeling data of RB69 DNA polymerase, 9°N-7 DNA polymerase and KOD DNA polymerase. Magenta chain indicates a region which has Y-GG/A motif and the green one is a variable residue in Y-GG/A motif.

CHAPTER 3. LIGHTING-UP OF FLUOROPHORE BY “INSULATOR” BASE-SURROGATES

3-1 Abstract

Fluorescent-labeled DNA is strong and facile tools for biological research. However, some fluorescent dyes are significantly quenched by natural nucleobases. In order to protect fluorophores, a new base-surrogate molecule which can shield dyes from influence of natural base pair should be developed. Here, we propose “insulator base pairs” that can shield a fluorescent dye from nucleobases and recover the quantum yield of dye from severe quenching. Insulator base pair is generally designed so as not to have aromatic ring because such π -conjugated system should mediate electron or hole transfer between dye and nucleobase. The introduction of a single pair of isopropylcyclohexanes into the middle of DNA slightly destabilized the duplex. Interestingly, as the number of the “base pairs” increased, the duplex was highly stabilized. From the results of NMR analysis and spectroscopic measurements, the cyclohexyl moieties formed base pairs within DNA duplex without severely disturbing the helical structure of natural B-type DNA helix. Next, we introduced cyclohexyl base pairs between pyrene and nucleobases as an “insulator” that inhibits electron transfer. A massive increase in the quantum yield of pyrene due to efficient shielding of pyrene from nucleobases was observed. Although isopropylcyclohexane moiety has an excellent shielding ability between dyes and nucleobases, however, when insulator basepairs were introduced between two pyrenes, weak emission of excimer was observed. This indicated that shielding of dye-dye interaction was not sufficient because of dynamic molecular mobility of insulator basepairs. Interestingly, *tert*-butyl cyclohexane moiety possessed good shielding ability of interaction between dyes and no excimer was observed. The insulator base pairs have the potential to prepare highly fluorescent labeling agents by multiplying fluorophores and insulators alternately into DNA duplexes.

3-2 Introduction

Natural DNA forms a stable double-helical structure by hydrophobic interaction, hydrogen bonding and aromatic stacking interactions. In 1995, Kool *et al.* firstly reported that hydrogen bonding is not essential for the stability of the DNA duplex.¹ They reported that an artificial base pair which has aromatic rings but no hydrogen bonding sites could stabilize duplex. Since then, a wide variety of artificial base pair that use aromatic stacking interaction have been reported.²⁻⁹ Recently, Leumann *et al.* reported that a non-planar artificial base-surrogate, cyclohexylbenzene conjugated with D-ribose, greatly stabilize the duplex by stacking interaction.¹⁰ In addition, non-ribose scaffolds were also utilized to design various base-surrogates containing functional molecules.¹¹⁻¹⁸ Asanuma *et al.* have reported a variety of base-surrogates bearing functional molecules via D-threoninol scaffold.¹⁹ These artificial nucleotides have the potential to serve as novel nanomaterials and biological tools.²⁰⁻²⁴

Fluorescent-labeled oligonucleotides are now widely accepted in biological research. However, some fluorophores cannot be utilized for the labeling of nucleic acids due to strong quenching by nucleobases despite of their high potential. Kool *et al.* reported an “insulator molecule” which can enhance the emission of pyrene in a single strand oligo nucleotide.²⁵ They synthesized a trimer which contains 5,6-dihydro-2'-deoxythymidine (DHT) inserted between pyrene and thymine. Note that DHT does not contain aromatic ring and the nucleobase has non-planar structure. This trimer exhibited a quantum yield approximately 70 times higher than that of a dimer directly conjugated pyrene and thymine. However, structural fluctuations of the single strand oligo nucleotide still prevented complete recovery of the quantum yield of pyrene.

One solution for improving emission intensity is introduction of multiple dyes to raise the extinction coefficients. However, simple accumulation of fluorophores does not necessarily enhance the emission intensity because most of the dyes are self-quenched dimerization. Kashida *et al.* reported various fluorophore assemblies which were strictly regulated within rigid DNA duplex.²⁶ Inter strand wedged motif, the dyes are alternately aligned with natural base pairs, efficiently shielded dimerization of dyes, however, shielding by natural base pairs also caused quenching. Hence a new methodology that can restrict dye-dye interaction without quenching even within DNA duplex is necessary.

Here, some novel designs of “insulator base pairs” that can shield fluorophores from nucleobases were proposed in order to achieve a high quantum yield within DNA duplex. As these molecules contain non-planar structure, the influence on duplex stability caused by introduction of such bulky moieties should be studied in detail. The shielding ability of insulators and stability of DNA duplex were systematically investigated. A mechanism which affects to the stability of DNA duplex was also discussed. Additionally, shielding various dyes from nucleobases and restriction of dimerization within DNA duplex were performed.

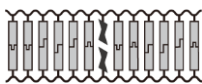
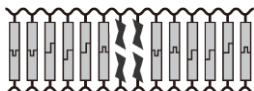
3-3 Results and Discussions

3-3-1 Structural analysis and thermo dynamic stability of duplex containing insulator basepairs

At first, the structure of a duplex containing a cyclohexyl base pair was investigated. If cyclohexyl moieties behave as a “base pair”, the moieties should be closely located inside the DNA duplex and interact with each other. For confirming the solution structure of modified DNA, NMR structural analysis was conducted with a 7 mer duplex containing **H** and **K** in Figure 3-1. *trans*-methylcyclohexane (**K**) and *trans*-isopropylcyclohexane (**H**) were tethered at the center position of duplex via D-threoninol scaffold. In order to monitor imino protons that are exchangeable with water molecules, NMR was measured in H₂O/D₂O 9:1 at 275 K with a 3-9-19 WATERGATE pulse sequence for H₂O suppression.²⁷ Most of the signals of the duplex, except for the protons of the cyclohexane rings, could be assigned from the NOEXY, DQFCOSY and TOCSY spectra. The one-dimensional NMR chart of the imino proton region is shown in Figure 3-1. Six peaks corresponding natural base pairs were observed in the imino proton region. Overlapping between the signals of imino protons of G4 and G7 was also observed, indicating that the DNA duplex **H1c/K1d** was not largely inclined and base pairing of natural base pairs was not severely disturbed despite of introduction of non-natural bulky moieties at the center. NOEs between imino protons and protons of **H** and **K** are also shown in Figure 3-1. Methyl protons of **H** showed NOEs to imino protons of both G4 and T10. Similarly, distinct NOEs were observed between methyl protons of **K** and imino protons of G4 and T10. These NOEs clearly demonstrated that both the isopropyl group of **H** and the methyl group of **K** were located adjacent to both G4 and T10. Therefore, **H** and **K** moieties should be located within DNA duplex. Moreover, both H_a of

K and H_b of **H** showed NOE with an imino proton of T10 and G4, respectively, suggesting that the orientations of the cyclohexane rings were reversed each other. Intermolecular NOEs between **H** and **K** were also observed. These results definitely demonstrated that **H** and **K** formed a “base pair” inside the DNA duplex and these moieties interact with each other. Computer simulation without any restraints by Insight II/Discover 3 was also consistent with the results of NOESY (Figure 3-2).

Table 3-1. Sequence of synthesized DNA in this section.

Name	Sequence	Representation
H1c/K1d	5' - CGA H GTC - 3' 3' - GCT K CAG - 5'	
Nt/S0	5' - GGTATC GCAATC - 3' 3' - CCATAG CGTTAG - 5'	
H1a/H1b	5' - GGTATC H GCAATC - 3' 3' - CCATAG H CGTTAG - 5'	
K1a/K1b	5' - GGTATC K GCAATC - 3' 3' - CCATAG K CGTTAG - 5'	
A1a/T1b	5' - GGTATC A GCAATC - 3' 3' - CCATAG T CGTTAG - 5'	
G1a/C1b	5' - GGTATC G GCAATC - 3' 3' - CCATAG C CGTTAG - 5'	
H2a/H2b	5' - GGTATC HH GCAATC - 3' 3' - CCATAG HH CGTTAG - 5'	
K2a/K2b	5' - GGTATC KK GCAATC - 3' 3' - CCATAG KK CGTTAG - 5'	
A2a/T2b	5' - GGTATC AA GCAATC - 3' 3' - CCATAG TT CGTTAG - 5'	
H6a/H6b	5' - GGTATC HHHHHH GCAATC - 3' 3' - CCATAG HHHHHH CGTTAG - 5'	
K6a/K6b	5' - GGTATC KKKKKK GCAATC - 3' 3' - CCATAG KKKKKK CGTTAG - 5'	
A6a/T6b	5' - GGTATC AAAAAA GCAATC - 3' 3' - CCATAG TTTTTT CGTTAG - 5'	

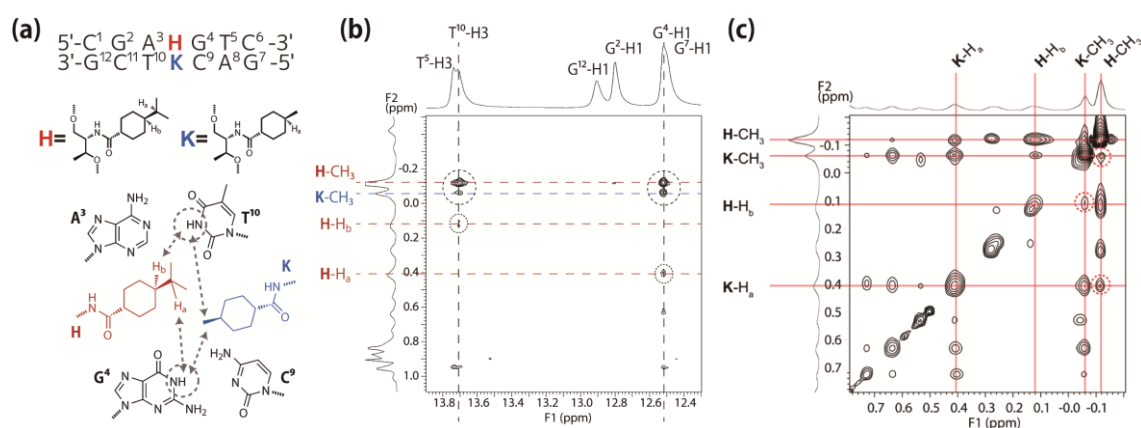


Figure 3-1. NMR analysis of modified DNA containing **H** and **K**. NMR spectra were measured with a Varian INOVA spectrometer (700 MHz) equipped for triple resonance at a probe temperature of 275 K. NMR samples were prepared by dissolving three-times-lyophilized DNA in an H₂O/D₂O (9:1) solution containing 10mM sodium phosphate (pH 7.0) to give a duplex concentration of 1.7 mM. NaCl was added to give a final sodium concentration of 200 mM. Resonances were assigned by standard methods using a combination of 1D, TOCSY (60 ms of mixing time), DQF-COSY and NOESY (150 ms of mixing time) experiments. All spectra in the H₂O/D₂O 9:1 solution were recorded using the 3-9-19 WATERGATE pulse sequence for water suppression. (a) The sequence and structure of modified DNA (**H1c/K1d**). The residue numbers and proton numbers of **H** and **K** residues are shown. (b) 2D NOESY spectra of DNA duplex **H1c/K1d** containing **H** and **K** between the aliphatic protons and imino protons in H₂O/D₂O (9:1) at 275K. 1D spectra of the imino protons and aliphatic protons are shown at the top and left of the chart, respectively. (c) 2D NOESY spectra of modified DNA **H1c/K1d**. 1D spectra of aliphatic protons are shown at the top and left of the chart.

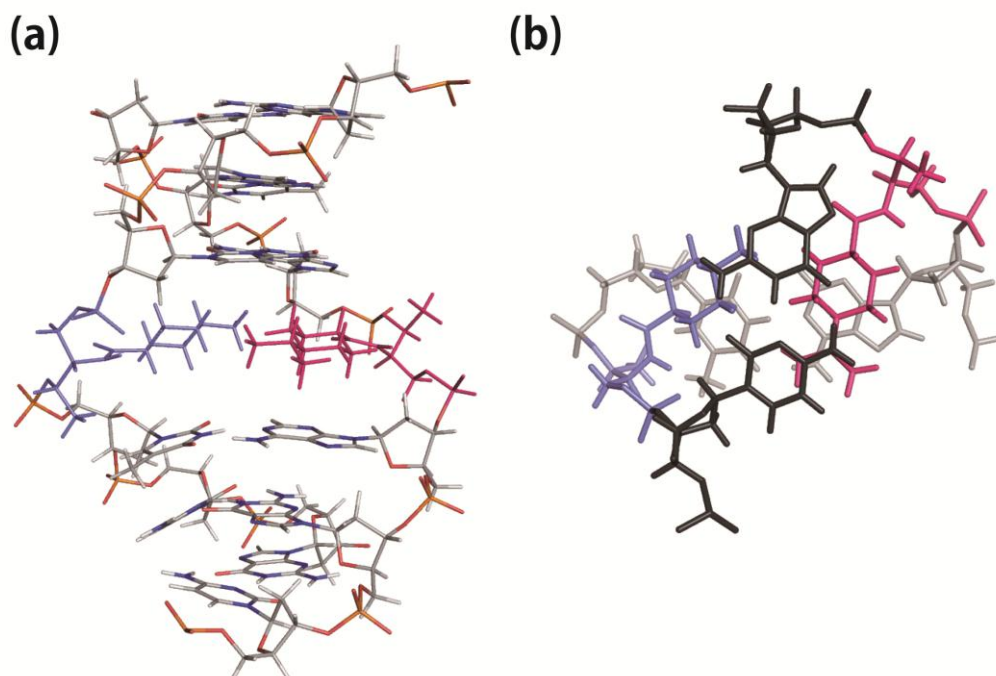


Figure 3-2. Energy-minimized structure of **H1c/K1d** duplex containing single **H-K** pair calculated by Insight II / Discover 3. The **H** and **K** residues are colored in magenta and blue, respectively. (a) Side view of the duplex. (b) The enlarged view of **H-K** pair and neighboring bases.

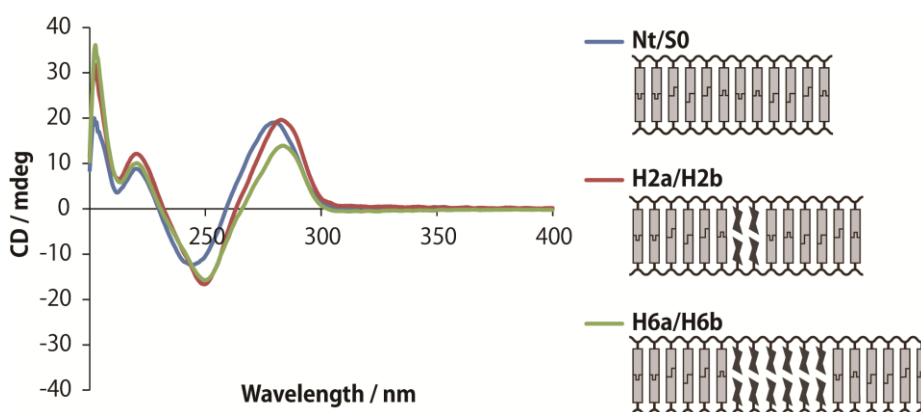


Figure 3-3. CD spectra of **Nt/S0**, **H2a/H2b** and **H6a/H6b** at 20°C. Conditions: [ODN] = 5.0 μ M, [NaCl] = 100 mM, pH 7.0 (10 mM phosphate buffer).

Next, in order to investigate the structure of a DNA duplex containing of a DNA duplex tethering multiple cyclohexyl base pairs, the CD spectra of duplex containing **H-H** pairs were measured (Figure 3-4). Sequences of synthesized DNAs in this section were described in Table 3-1. **H2a/H2b** carrying two **H-H** pairs showed a similar positive couplet to that of native duplex (**Nt/S0**). In addition, **H6a/H6b** carrying six **H-H** pairs also exhibited similar spectra. These results indicated that the incorporation of **H-H** pairs did not disturb the basic B-form helix structure of DNA. From NMR and CD analyses, it was confirmed that cyclohexyl moieties behave as “base pairs” without disturbing natural DNA structure, although they had non-planar bulky structures.

Moreover, the thermal stability of duplexes containing cyclohexyl base pairs were investigated (Table 3-1). Here, multiple numbers of **H-H** and **K-K** homo pairs were introduced into the middle of DNA duplex. When a single **H-H** pair was introduced (**H1a/H2b**), T_m was slightly decreased (44.7°C) comparing with that of the native duplex (47.7°C). The T_m of **K-K** pair (**K1a/K1b**) was also further lowered to 41.1°C, suggesting that cyclohexyl rings in **H-H** and **K-K** pair destabilized DNA due to its non-planar structure. However, as the number of the **H-H** pairs increased, the duplex was stabilized. For example, the T_m of **H2a/H2b** which contains two **H-H** pairs was 47.1°C, it was 2.4°C higher than that of **H1a/H1b**. Surprisingly, the introduction of six **H-H** pairs massively stabilized the DNA duplex; the T_m of **H6a/H6b** was as high as 61.3°C, which was 13.6°C higher than that of native duplex. To compare the stabilizing effect of **H-H** with natural base pairs, T_m of the native duplexes containing A-T or G-C pairs instead of **H-H** pairs were also measured. **A1a/T1b** and **G1a/C1b** gave higher T_m than that of **H1a/H2b** and **A2a/T2b** exhibited the same result comparing with **H2a/H2b**. However, the T_m of six A-T pairs (**A6a/T6b**) was 53.6°C, which was lower than that of six **H-H**

pairs (**H6a/H6b**: 61.3°C). It is noteworthy that **H-H** pairs were more stable than A-T pairs when multiple **H-H** pairs were introduced.

The thermodynamic parameters of these duplexes determined from $1/T_m$ v.s. $\ln(C_T/4)$ plots were also listed in Table 3-1. The $-\Delta G_{37}^{\circ}$ value of **H1a/H1b** was 10.1 kcal mol⁻¹, which was less than that of the native duplex (**Nt/S0**: 11.2 kcal mol⁻¹), however, when two **H-H** pairs were introduced (**H2a/H2b**), $-\Delta G_{37}^{\circ}$ increased by 0.6 kcal mol⁻¹. Furthermore, $-\Delta G_{37}^{\circ}$ of **H6a/H6b** was as high as 15.4 kcal mol⁻¹, which was 4.2 kcal mol⁻¹ higher than that of **Nt/S0** without artificial base pairs. In addition, the $-\Delta G_{37}^{\circ}$ was even 0.5 kcal mol⁻¹ larger than that of **A6a/T6b**. The larger $-\Delta G_{37}^{\circ}$ of **H6a/H6b** was mainly attributed to the $-\Delta S$, which was 106 cal K⁻¹ mol⁻¹ smaller than that of **A6a/T6b**, whereas its $-\Delta H$ was 32.2 kcal mol⁻¹ smaller. These results strongly suggested that a smaller loss in entropy due to hydrophobic interaction between **H** moieties contributed to the large T_m . The striking difference between **H** and **K** could also be explained by the difference of hydrophobicity of **H** and **K**. As shown in Table 1, **K6a/K6b** showed obviously less stable T_m than that of **H6a/H6b** indicating that isopropyl group should contribute to form stable duplex. The difference of $-\Delta G_{37}^{\circ}$ between **H6a/H6b** and **K6a/K6b** was as high as 4.7 kcal mol⁻¹. It was because methyl group of **K** is less hydrophobic than isopropyl group of **H**, therefore multiple introduction of **K** possessed only weakly contribute to the stability of duplex. Namely, hydrophobic interaction between isopropyl groups contributed strongly to the stabilization of the duplex.

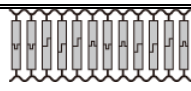
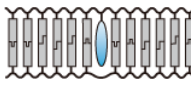
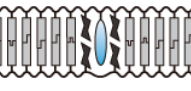
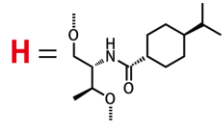
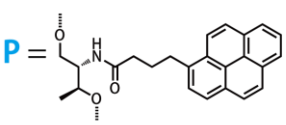
Table 3-2. Thermodynamic parameters of duplexes containing natural of artificial base pairs.

Sequence	$T_m / ^\circ\text{C}^a$	$-\Delta H / \text{kcal mol}^{-1}$	$-\Delta S / \text{cal K}^{-1} \text{mol}^{-1}$	$-\Delta G_{37}^{\circ} / \text{kcal mol}^{-1}$
Nt/S0	47.7	89.9	254	11.2
H1a/H1b	44.7	86.2	245	10.1
K1a/K1b	41.1	79.0	226	8.8
A1a/T1b	49.4	94.0	266	11.6
G1a/C1b	53.4	100.5	282	13.1
H2a/H2b	47.1	86.9	246	10.7
K2a/K2b	40.3	81.8	235	8.8
A2a/T2b	49.2	101.6	289	11.9
H6a/H6b	61.3	102.0	279	15.4
K6a/K6b	47.4	85.4	241	10.7
A6a/T6b	53.6	134.2	385	14.9

a: Solution conditions: [ODN] = 5.0 μM, [NaCl] = 100 mM, pH 7.0 (10 mM phosphate buffer)

3-3-2 Shielding efficiency of cyclohexyl base pairs as insulators

Table 3-3. Sequence of synthesized DNA in this section.

Name	Sequence	Representation
Nt/S0	5' -GGTATC GCAATC-3' 3' -CCATAG CGTTAG-5'	
P1a/S0	5' -GGTATC P GCAATC-3' 3' -CCATAG CGTTAG-5'	
H2Pa/H2b	5' -GGTATC H P HGCAATC-3' 3' -CCATAG H H CGTTAG-5'	
H6Pa/H6b	5' -GGTATC HHH P HHH GCAATC-3' 3' -CCATAG HHH HHH CGTTAG-5'	
	<div style="display: flex; justify-content: space-around; align-items: center;"> <div style="text-align: center;"> <p>H = </p> <p>Isopropylcyclohexane</p> </div> <div style="text-align: center;"> <p>P = </p> <p>Pyrene</p> </div> </div>	

Next, shielding efficiency of cyclohexyl base pair was investigated. To suppress electron transfer in DNA, isopropylcyclohexane basepairs (**H**) were applied as “Insulator”. Natural nucleobases are known to be good mediators for hole/electron transfer.²⁸⁻³² However, since the cyclohexyl base pair has no π electrons and does not mediate electron transfer, it should be an “insulator” of electron transfer when it is located next to natural base pairs. The insulator molecules were introduced into both strands of a DNA duplex to form tentative “base pairs”. Because these molecules have high hydrophobicity, they should face to the inside of the duplex and form “base pairs”. These insulator base pairs would therefore be expected to shield a fluorophore from quenching by nucleobases. We chose the fluorophore pyrene (**P**) to examine the shielding effect of these insulators. Pyrene has good photostability and highly planar structure hence the pyrene moiety intercalates in the middle of DNA duplex by strong π - π stacking interaction. For evaluation of the insulating ability of **H**, the fluorescence recovery of pyrene by the incorporation of **H** was measured. Pyrene-conjugated DNAs have been widely utilized for fluorescent probes and labeling agents.³³⁻³⁸ Kashida *et al.* have also introduced pyrene between natural base pairs to develop fluorescent probe,^{26,39,40} however, pyrene was strongly quenched by natural nucleobases and it severely limited the detection sensitivity. The quantum yield of pyrene within DNA duplex was as low as 0.003, especially when multiple pyrenes are introduced between natural base pairs.⁴⁰ Fluorescence enhancement by insulator base pairs has the potential to improve the sensitivity of pyrene-based probes and labeling agents.

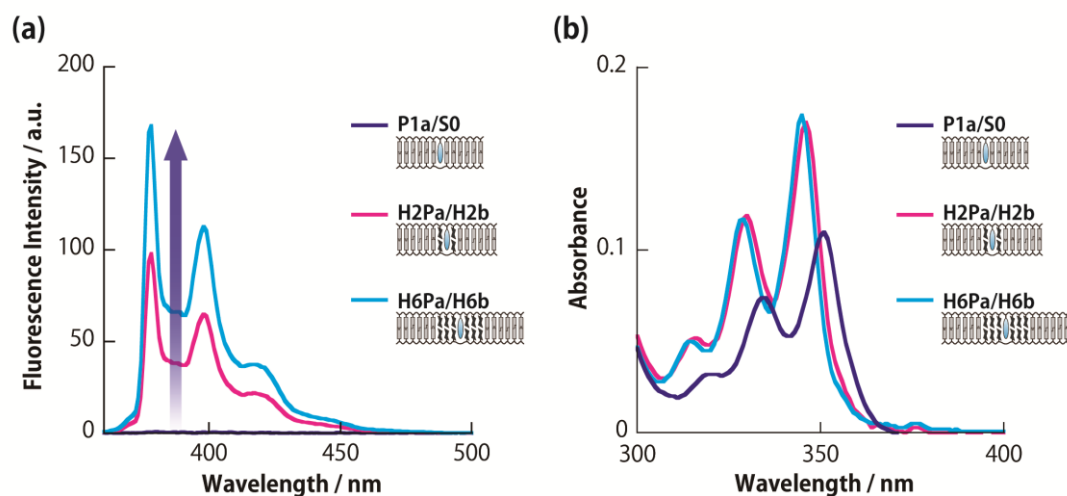


Figure 3-4. Evaluation of insulation ability of modified DNA. (a) Fluorescence spectra of **P1a/S0**, **H2Pa/H2b** and **H6Pa/H6b** at 20°C. Conditions: [ODN] = 1.0 μ M, [NaCl] = 100 mM, pH 7.0 (10 mM phosphate buffer). Excitation wavelength was 345 nm. (b) UV-Vis spectra of **P1a/S0**, **H2Pa/H2b** and **H6Pa/H6b** at 20°C. Conditions: [ODN] = 5.0 μ M, [NaCl] = 100 mM, pH 7.0 (10 mM phosphate buffer).

Table 3-3. Spectroscopic behaviors and thermodynamic stabilities of modified DNA.

Sequence	Relative Intensity ^a	Φ ^b	λ_{\max} / nm ^c	T_m / °C ^d	ΔT_m / °C ^e
Nt/S0	—	—	—	47.7	—
P1a/S0	< 0.01	< 0.01	351	48.7	+1.0
H2Pa/H2b	1	0.19	346	48.5	+0.8
H6Pa/H6b	1.71	0.32	345	62.0	+14.3

^a: Emission intensity at 378 nm relative to that of **H2Pa/H2b**. Solution conditions: [DNA] = 1 μ M each, [NaCl] = 100 mM, pH 7.0 (10 mM phosphate buffer), 20°C. Excitation wavelength: 345 nm. ^b: Quantum yield determined from the quantum yield of pyrene in N₂-bubbled cyclohexane (0.65) used as a reference. ^c: Absorption maxima of pyrene in the UV-Vis spectra at 20°C. ^d: Solution conditions: [DNA] = 5 μ M each, [NaCl] = 100 mM, pH 7.0 (10 mM phosphate buffer). ^e: The difference of T_m values between modified ODNs and native duplex **Nt/S0**.

Sequences of synthesized DNA in this section were shown in Table3-3. Here, two or six **H** base pairs were introduced between pyrene and natural base pairs. **P1a/S0**, which contains no **H** base pairs but one pyrene, was synthesized as a control. **P1a/S0** exhibited almost no fluorescence due to strong quenching by neighboring G-C pairs (purple line in Figure 3-4). UV-Vis spectra of **P1a/S0** also indicated strong interaction between pyrene and nucleobases. Absorption maximum of **P1a/S0** was largely red-shifted owing to exciton coupling between pyrene and nucleobases. Obvious hypochromic effect of **P1a/S0**

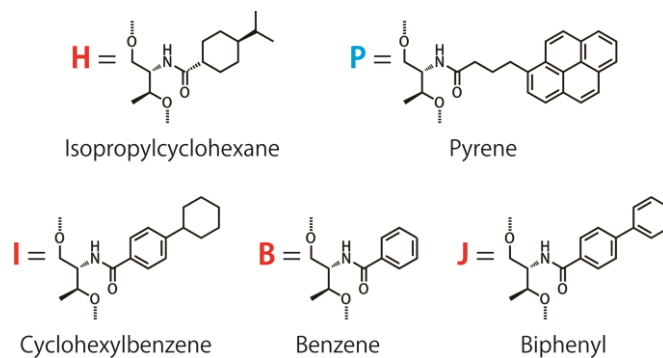
also represented strong π - π stacking interaction. On the other hand, incorporation of **H·H** pairs greatly increased the emission of pyrene. **H2Pa/H2b**, which contains two **H·H** pairs showed intense peaks at around 380-400 nm (magenta line in Figure 3-4). The quantum yield was highly recovered to 0.19 (Table 3-3). Furthermore, **H6Pa/H6b**, which contained six **H·H** pairs between the pyrene and nucleobases, showed a 1.7 times greater emission intensity than that of **H2Pa/H2b** (cyan line in Figure 3-4), and its quantum yield was as high as 0.32 (Table 3-3). UV-Vis spectra of **H2Pa/H2b** and **H6Pa/H6b** showed very sharp bands at 346 nm and 345 nm, respectively. The absorption maxima of **H·H** conjugated ODNs were about 5 nm shorter than that of **P1/S0** supporting the shielding of pyrene from neighboring nucleobases. Such blue shift of dye strongly indicated interruption of excitonic interaction and π - π stacking. The melting temperatures of these duplexes were also shown in Table 3-3. The T_{ms} of duplexes containing pyrene sandwiched by **H·H** pairs were stable enough as expected. This is because the hydrophobic interactions of **H·H** pairs efficiently worked even when pyrene was inserted between them.

3-3-3 The molecular design of insulator 1; requirement of cyclohexyl ring

Here, to confirm shielding effect by cyclohexyl group, several insulator molecules, 4-cyclohexylbenzene (**I**), benzyl moiety (**B**) and biphenyl moiety (**J**) were synthesized in addition to **H** moiety as shown in Table 3-5. **H** and **I** have one rigid cyclohexane ring with no π electrons. **B** and **J** containing no cyclohexane rings were used as controls.

Table 3-5. Sequences of synthesized DNA in this section.

Name	Sequence	Representation
P1a/S0	5' - GGTATC P GCAATC - 3' 3' - CCATAG CGTTAG - 5'	
H2Pa/H2b	5' - GGTATC H P HGCAATC - 3' 3' - CCATAG H H CGTTAG - 5'	
I2Pa/I2b	5' - GGTATC I P I GCAATC - 3' 3' - CCATAG I I CGTTAG - 5'	
B2Pa/B2b	5' - GGTATC B P B GCAATC - 3' 3' - CCATAG B B CGTTAG - 5'	
J2Pa/J2b	5' - GGTATC J P J GCAATC - 3' 3' - CCATAG J J CGTTAG - 5'	



As shown in Figure 3-5a and Table 3-6, the emission of pyrene was quenched as low as background level. On the other hand, **H2Pa/H2b** and **I2Pa/I2b** duplex exhibited highly intense emission of pyrene more than 100 times and the quantum yield of pyrene in **H2Pa/H2b** duplex was recovered from < 0.01 to 0.19. The emission intensity of **I2Pa/I2b** was 0.7 relative to **H2Pa/H2b**, suggesting the effect of aromatic ring. By contrast, duplexes of **B2Pa/B2b** and **J2Pa/J2b** showed quite low fluorescence intensity due to electron transfer mediated by π electrons of aromatic ring. These results

indicated that at least one cyclohexyl group is required for shielding and the aromatic ring surely mediated electron transfer.

The shielding effect by insulators could also be estimated by UV-Vis spectra (Figure 3-5b). **P1a/S0** showed red shifted spectrum due to the exciton coupling between pyrene and nucleobases. While modified DNA containing **H**, **I**, **B** and **J** exhibited clearly blue shifted spectra owing to restriction of the exciton coupling between nucleobases and pyrene. Interestingly, **H2Pa/H2b** showed the shortest λ_{\max} among them and it was consistent with the results of fluorescence measurement. It is noteworthy that other three moieties containing benzene ring had the same shorter λ_{\max} and thus these moieties could shield the pyrene from neighboring base pairs, however, they have aromatic ring and it could also interact with pyrene by stacking. Indeed, bands of pyrene in **J2Pa/J2b** showed strong hypochromicity compared to other duplexes demonstrating π - π stacking interactions. However, note that blue-shift of absorption maximum was not derived from the excitonic interaction. As a result, **B** and **J** moieties mediated electron transfer through π -electrons of benzene ring and pyrene was severely quenched, however, interestingly **I** moiety still kept good shielding ability. It is likely that the benzene ring of **I** moiety might slightly quench the fluorescence of pyrene.

The T_{ms} of artificial base pairs are also listed in Table 3-6. Artificial base pairs carrying aromatic moieties stabilized the duplex by stacking interaction. One exception was **B** moiety, having only one benzene ring. T_{m} of **B2Pa/B2b** was significantly dropped because **B** is too small and vacant space would have destabilized the duplex. The T_{ms} of duplex sandwiched with two insulator pairs were in the following order: **J2Pa/J2b** (52.6°C) \approx **I2Pa/I2b** (52.2°C) > **H2Pa/H2b** (48.5°C) \approx **P1a/S0** (48.6°C) \gg **B2Pa/B2b** (35.8°C). The $-\Delta G_{37}^{\circ}$ of the base pairs synthesized here was in the order of **I-I** (11.2 kcal mol⁻¹) \approx **Nt/S0** > **J-J** (10.5 kcal mol⁻¹) \approx **H-H** (10.1 kcal mol⁻¹) > **K-K** (8.8 kcal mol⁻¹) (data not shown see reference 41). From these results, it did not necessarily coincide with the number of benzene rings in the base-surrogate. Stability of **K-K** base pair was 1.3 kcal mol⁻¹ lower than that of **H-H** pair. Furthermore, **H6a/H6b** and **K6a/K6b** was as high as 4.7 kcal mol⁻¹, demonstrating that hydrophobic interactions between isopropyl groups contributed strongly to the stabilization of the duplex.

In summary, aromatic ring should be avoided for suppression of electron transfer and rigid hydrophobic molecule such as cyclohexane is appropriate to shielding dyes.

Table 3-6. Spectroscopic behaviors and thermodynamic stabilities of the modified ODNs.

Sequence	Relative Intensity ^a	Φ^b	$\lambda_{\max} / \text{nm}^c$	$T_m / ^\circ\text{C}^d$
H2Pa/H2b	1	0.19	346	48.5
I2Pa/I2b	0.70	n.d.	347	52.2
B2Pa/B2b	0.03	n.d.	347	35.8
J2Pa/J2b	< 0.01	n.d.	347	52.6
P1a/S0	< 0.01	< 0.01	351	48.6

a: Emission intensity at 378 nm relative to that of **H2Pa/H2b**. Solution conditions: [DNA] = 1.0 μM each, [NaCl] = 100 mM, pH 7.0 (10 mM phosphate buffer), 20°C. Excitation wavelength: 345 nm. *b*: Quantum yield determined from the quantum yield of pyrene in N₂-bubbled cyclohexane (0.65) used as a reference. *c*: Absorption maximum of pyrene in the UV-Vis spectrum at 20°C. *d*: Solution conditions: [DNA] = 5.0 μM each, [NaCl] = 100 mM, pH 7.0 (10 mM phosphate buffer).

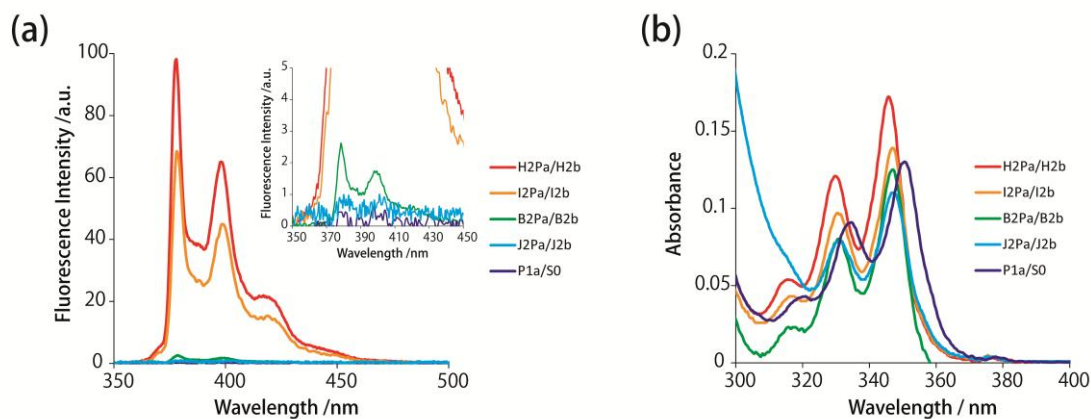
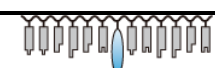
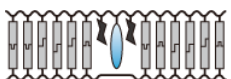
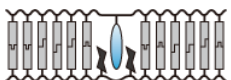


Figure 3-5. Spectrum behaviors of synthesized DNA containing insulator base pairs with a pyrene moiety. (a) Fluorescence spectra of modified DNAs. Solution conditions were as follows: [DNA] = 1 μM each, [NaCl] = 100 mM, pH 7.0 (10 mM phosphate buffer), 20°C. Excitation wavelength: 345 nm. (b) UV-Vis spectra of modified DNAs. Solution conditions were as follows: [DNA] = 5 μM each, [NaCl] = 100 mM, pH 7.0 (10 mM phosphate buffer), 20°C.

3-3-4 The molecular design of insulator 2; necessity of forming pairs

As described in 3-3-1, the cyclohexyl moieties were located in close proximity of each other within DNA duplex and could behave like “base pair” by hydrophobic interaction. For further applications, introduction of artificial base-surrogates to both strands may limit molecular design of probes or labeling agents. For considering such situation, the requirement of forming insulator pair was discussed here. The combination of modified DNA and name of duplexes were listed in Table 3-7.

Table 3-7. Sequence of modified DNA involving the topic in this section.

Name	Sequence	Representation
P1a single	5' - GGTATC P GCAATC - 3'	
H2Pa single	5' - GGTATC H P H GCAATC - 3'	
H2Pa/S0	5' - GGTATC H P H GCAATC - 3' 3' - CCATAG CGTTAG - 5'	
P1a/H2b	5' - GGTATC P GCAATC - 3' 3' - CCATAG H H CGTTAG - 5'	
H2Pa/H2b	5' - GGTATC H P H GCAATC - 3' 3' - CCATAG H H CGTTAG - 5'	
H6Pa single	5' - GGTATC H H H P H H H GCAATC - 3'	
H6Pa/H6b	5' - GGTATC H H H P H H H GCAATC - 3' 3' - CCATAG H H H H H H CGTTAG - 5'	

Kool *et al.* reported that single stranded ODNs containing pyrene and dihydrothymidine (DHT) enhanced fluorescence emission of pyrene because DHT shielded pyrene from quenching by nucleobases.²⁵ However, single stranded DNA is flexible and thus shielding by DHT is not sufficient. In their system, pyrene was located outside of DNA and the restriction of dye mobility would be weak. On the other hand, isopropylcyclohexane moiety reported in this paper may be able to retain shielding ability owing to its hydrophobic rigid bulky structure even if DNA duplex was not formed. To confirm this, the shielding ability in single stranded DNA was investigated.

Figure 3-6a shows fluorescence spectra of single stranded DNAs. **H2Pa/H2b** duplex was also shown as control. **P1a single** exhibit quite low fluorescence intensity, however,

it was less severely quenched than **P1a/S0** duplex. This is because the interaction between pyrene and nucleobases were not sufficient in single strand, whereas pyrene in **P1a/S0** was strongly intercalated in duplex and efficiently quenched. Shorter λ_{\max} than that of **P1a/S0** (Table 3-8) and hyperchromicity of **P1a single** in UV-Vis spectra (Figure 3-6b) also supported weak interaction between pyrene and nucleobases in **P1a single**. As expected, **H2Pa single** showed approximately 8 times higher emission intensity than that of **P1a single**. Absorption maximum was also slightly blue-shifted indicating that pyrene was shielded from nucleobases. Moreover, **H6Pa single** exhibited higher fluorescence emission, however, its intensity was lower than that of **H2Pa/H2b**. Multiple pairs of **H** moiety in **H6Pa single** could surely disturb the interaction between pyrene and nucleobases, however, it was not sufficient due to the flexibility of single strand DNA. Therefore, duplex formation is necessary for efficient shielding. The core structure of pyrene was tethered with D-threoninol scaffold via C3 linker, which is relatively long and flexible. Such long flexible linker would enable interaction over multiple **H** moieties.

Next, necessity of forming **H-H** pair was confirmed. Here, duplex containing pyrene and two **H** moieties without forming **H-H** pair was prepared. Pyrene in **H2Pa/S0** was sandwiched by two **H** but its complementary strand contains no **H** moieties. Similarly, in **P1a/H2b**, neighboring bases of pyrene is nucleobase but **H** moieties were introduced on its complementary strand. As shown in Figure 3-7, these duplexes exhibited obviously lower fluorescence intensity than that of the duplex containing two **H-H** pairs (**H2Pa/H2b**). Interestingly, fluorescence emission of **H2Pa/S0** was lower than that of

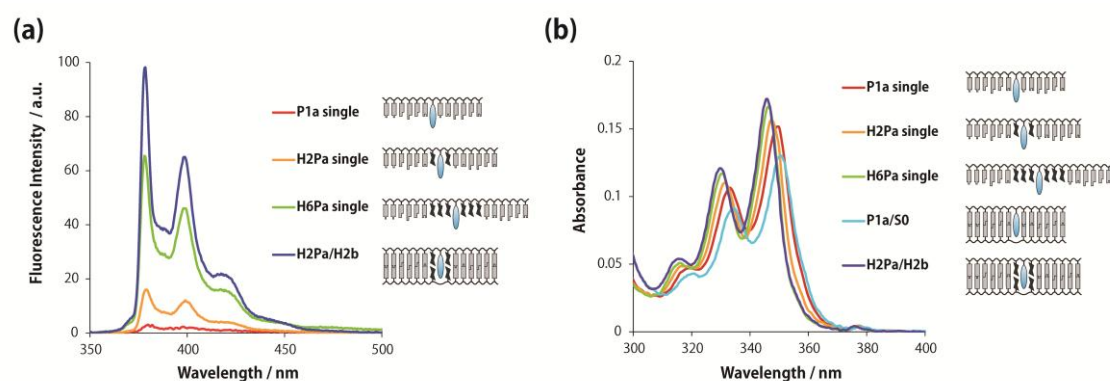


Figure 3-6. Spectrum behaviors of synthesized DNA containing insulator base pairs with a pyrene moiety. (a) Fluorescence spectra of modified DNAs. Solution conditions were as follows: [DNA] = 1 μ M each, [NaCl] = 100 mM, pH 7.0 (10 mM phosphate buffer), 20°C. Excitation wavelength: 345 nm. (b) UV-Vis spectra of modified DNAs. Solution conditions were as follows: [DNA] = 5 μ M each, [NaCl] = 100 mM, pH 7.0 (10 mM phosphate buffer), 20°C.

P1a/H2b. In **H2Pa/S0**, C3 linker of pyrene was longer than **H** group and pyrene core could interact with nucleobases on the complementary strand. On the other hand, in **P1a/H2b**, pyrene would be located in close proximity of two bulky **H** moiety and it disturbed stacking interaction between pyrene and nucleobases. Larger T_m of **P1a/H2b** than that of **H2Pa/S0** also suggested hydrophobic interaction between pyrene and **H** moiety. In summarize, formation of **H-H** pair was also required for efficient shielding. Again, to enhance fluorescence emission by protecting fluorophores from nucleobases, shielding by rigid hydrophobic bulky structure like cyclohexane without any p-electron should be effective. For effective shielding, the position of those hydrophobic groups should be regulated within well-organized structure like DNA duplex and they should be formed pairs to avoid structural inclinations.

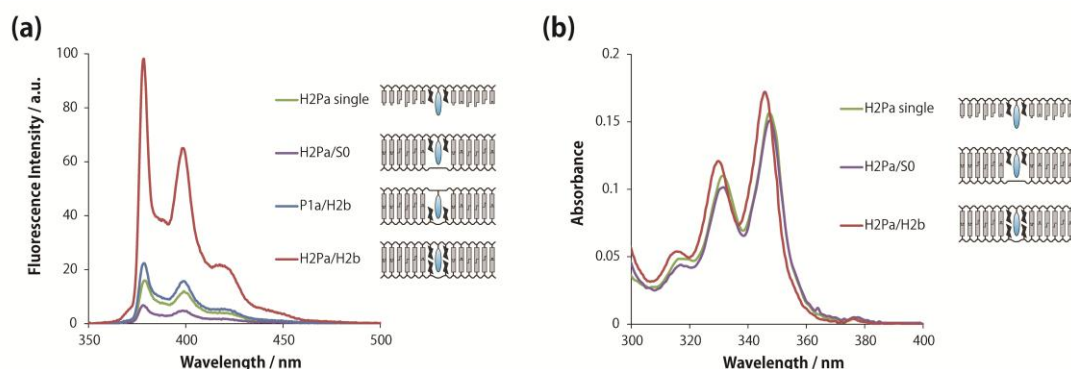


Figure 3-7. Spectrum behaviors of synthesized DNA containing insulator base pairs with a pyrene moiety. Measurement conditions were the same with Figure 3-6. (a) Fluorescence spectra of modified DNAs. (b) UV-Vis spectra of modified DNAs.

Table 3-8. Spectroscopic behaviors and thermodynamic stabilities of modified DNA.

Sequence	Relative Intensity ^a	Φ^b	$\lambda_{\max} / \text{nm}^c$	$T_m / ^\circ\text{C}^d$	$\Delta T_m / ^\circ\text{C}^e$
P1a single	0.02	n.d.	350	—	—
P1a/S0	< 0.01	< 0.01	351	48.7	+1.0
H2Pa single	0.16	n.d.	348	—	—
H2Pa/S0	0.07	0.02	348	43.2	-4.5
P1a/H2b	0.22	0.05	348	47.5	-0.2
H2Pa/H2b	1	0.19	346	48.5	+0.8
H6Pa single	0.67	n.d.	346	—	—
H6Pa/H6b	1.71	0.32	345	62.0	+14.3

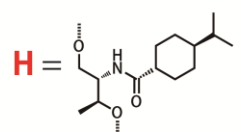
^a: Emission intensity at 378 nm relative to that of **H2Pa/H2b**. Solution conditions: [DNA] = 1 μM each, [NaCl] = 100 mM, pH 7.0 (10 mM phosphate buffer), 20°C. Excitation wavelength: 345 nm. ^b: Quantum yield determined from the quantum yield of pyrene in N_2 -bubbled cyclohexane (0.65) used as a reference. ^c: Absorption maxima of pyrene in the UV-Vis spectra at 20°C. ^d: Solution conditions: [DNA] = 5 μM each, [NaCl] = 100 mM, pH 7.0 (10 mM phosphate buffer). ^e: The difference of T_m values between modified ODNs and native duplex **Nt/S0** (47.7 °C).

3-3-5 Shielding dye-dye interactions

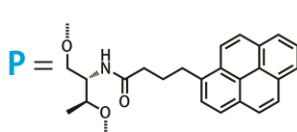
Fluorescence quenching by neighboring base pair was mainly discussed above, however, interaction between dyes also restricts fluorescence emission. For example, dimerization of perylene exhibit efficient quenching.⁴⁰ Interaction between pyrene also exhibit notable excimer emission and monomer emission is significantly dropped. One conceivable solution to enhance fluorescence emission is to conjugate multiple fluorophores. However, such interaction between dyes tends to cause self-quenching, therefore shielding individual dyes by separating with the insulator should be effective. Here, two pyrenes were introduced within DNA duplex and the insulator base pairs were also introduced not only between nucleobases and dye but also between dyes as shown in Table 3-9.

Table 3-9. Sequence of modified DNA synthesized in this section.

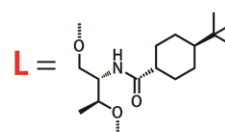
Name	Sequence	Representation
H2Pa/H2Pb	5' -GGTAT HP HGCAATC -3' 3' -CCATAG H PH CGTTAG -5'	
H3Pa/H3Pb	5' -GGTAT HPH HGCAATC -3' 3' -CCATAG H HPH CGTTAG -5'	
H4Pa/H4Pb	5' -GGTAT HPHH HGCAATC -3' 3' -CCATAG H HHPH CGTTAG -5'	
H5Pa/H5Pb	5' -GGTAT PHHH HGCAATC -3' 3' -CCATAG H HHH PHCGTTAG -5'	
L3Pa/L3Pb	5' -GGTAT LPL LGCAATC -3' 3' -CCATAG L LPL CGTTAG -5'	
L1a/L1b	5' -GGTAT L GCAATC -3' 3' -CCATAG L CGTTAG -5'	
L2a/L2b	5' -GGTAT LL GCAATC -3' 3' -CCATAG LL CGTTAG -5'	
L6a/L6b	5' -GGTAT LLLLLL GCAATC -3' 3' -CCATAG LLLLLL CGTTAG -5'	
L2Pa/L2b	5' -GGTAT LPL GCAATC -3' 3' -CCATAG L L CGTTAG -5'	



Isopropylcyclohexane



Pyrene



Tertiarybutylcyclohexane

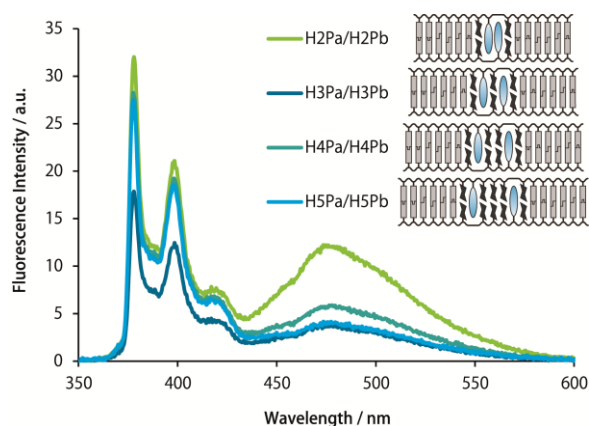


Figure 3-8. Fluorescence spectra of synthesized DNA containing insulator base pairs with two pyrene moiety. Solution conditions were as follows: [DNA] = 1 μ M each, [NaCl] = 100 mM, pH 7.0 (10 mM phosphate buffer), 20°C. Excitation wavelength: 345 nm.

Table 3-10. Spectroscopic behaviors and thermodynamic stabilities of modified DNA.

Sequence	Relative Monomer Intensity ^a	Relative Excimer Intensity ^b	Monomer/Excimer Ratio ^c	T_m / °C ^d	ΔT_m / °C ^e
H2Pa/H2Pb	1	1	2.6	51.6	+3.9
H3Pa/H3Pb	0.56	0.31	4.8	55.0	+7.3
H4Pa/H4Pb	0.87	0.49	4.7	58.1	+10.4
H5Pa/H5Pb	0.84	0.33	6.8	62.7	+15.0

a: Emission intensity at 378 nm relative to that of **H2Pa/H2Pb**. Solution conditions: [DNA] = 1 μ M each, [NaCl] = 100 mM, pH 7.0 (10 mM phosphate buffer), 20°C. Excitation wavelength: 345 nm. *b:* Emission intensity at 478 nm relative to that of **H2Pa/H2Pb**. *c:* Relative ratio of the monomer emission intensity at 378 nm / excimer emission intensity at 478 nm. *d:* Solution conditions: [DNA] = 5 μ M each, [NaCl] = 100 mM, pH 7.0 (10 mM phosphate buffer). *e:* The difference of T_m values between modified ODNs and native duplex **Nt/S0** (47.7 °C).

Fluorescence spectra of **H2Pa/H2Pb**, **H3Pa/H3Pb**, **H4Pa/H4Pb** and **H5Pa/H5Pb** were shown in Figure 3-8. All these duplex has one pair of **H** between pyrene and nucleobases. **H3Pa/H3Pb**, **H4Pa/H4Pb** and **H5Pa/H5Pb** have 1, 2, 3 pairs of **H-H** between dyes, respectively, while **H2Pa/H2Pb** has no **H-H** pairs between pyrenes. T_m s of these duplexes were stable enough relative to native duplex (Table 3-10) indicating that artificial base surrogates of **P** and **H** stabilized the duplex by hydrophobic interaction. Obviously, pyrenes in **H2Pa/H2Pb** could directly interact and thus large excimer emission around 450-500 nm was observed. Relative intensity of monomer emission / excimer emission was as low as 2.6 due to strong excimer emission. On the other hand, **H3Pa/H3Pb**, **H4Pa/H4Pb** and **H5Pa/H5Pb** showed relatively lower excimer emission than **H2Pa/H2Pb** indicating that **H** moieties between pyrene suppressed

excimer formation, however, excimer emission demonstrates pyrenes were somehow interacted and shielding by introduction of **H** moieties between dyes was insufficient. Moreover, monomer emission was also decreased e.g. **H3Pa/H3Pb**. Generally, inhibition of excimer formation would bring recovery of monomer emission. This decline of monomer emission suggested that pyrenes could interact with not only each other but also nucleobases. Introduction of multiple **H** and **P** might distort the structure of DNA duplex even though higher T_m of duplex due to hydrophobic interaction. Namely, **H** moiety cannot maintain rigid well-organized B-type helix of DNA by only hydrophobic interaction. Thermodynamic mobility of **H-H** pair disrupted the shielding by insulator and collisional contact of pyrenes would exhibit weak excimers, in addition, disruption of **H-H** pair also would cause quenching by nucleobases.

To resolve this problem, a wide variety of insulators has been designed and synthesized (see 3-7 Appendixes). Here, tertiarybutylcyclohexane moiety (**L**) was focused on. This moiety has only small difference in one methyl group with **H**. However, surprisingly, insertion of **L-L** pair between pyrenes completely inhibited excimer emission and highly intense monomer emission was recovered (Figure 3-9). λ_{max} of **L3Pa/L3Pb** was slightly blue-shifted comparing with **H3Pa/H3Pb** indicating that pyrenes were completely separated each other and shielded from nucleobases. Hyperchromicity of **L3Pa/L3Pb** also supported that stacking interaction was highly restricted by **L** moiety. However, the reason why **L** moiety gave such excellent shielding effect was still obscure. It might be because of good symmetry with bulkier structure of tertiarybutyl group would contribute to restriction of mobility of insulator and pyrene.

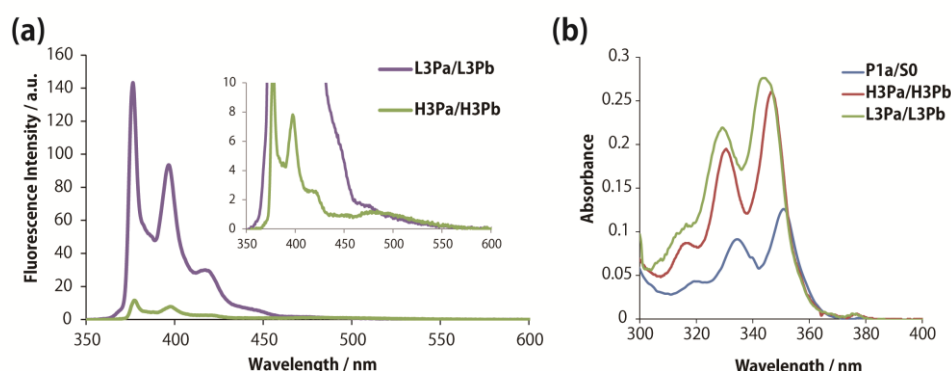


Figure 3-9. Comparison of spectroscopic behaviors of **H3Pa/H3Pb** and **L3Pa/L3Pb**. (a) Fluorescence spectra of modified DNA. The inset shows magnified view of **H3Pa/H3Pb**. Solution conditions were as follows: [DNA] = 1.0 μ M each, [NaCl] = 100 mM, pH 7.0 (10 mM phosphate buffer), 0°C. Excitation wavelength: 345 nm. (b) UV-Vis spectra of modified DNA. Solution conditions were as follows: [DNA] = 5.0 μ M each, [NaCl] = 100 mM, pH 7.0 (10 mM phosphate buffer), 0°C.

In addition, shielding ability of **L** between pyrene and nucleobase was also studied. As shown in Figure 3-10, emission intensity of **L2Pa/L2b** was less than that of **H2Pa/H2b**, however, **L** moiety has sufficient shielding ability between pyrene and nucleobases. Moreover, thermal stabilities of modified DNAs containing **H** and **L** were shown in Table 3-9. T_m values of modified DNA containing **L** moiety was quite similar with that of **H**. **L** moiety seems to be a little bit more stable than **H** due to greater hydrophobicity of *tert*-butyl group, especially for **L6a/L6b** exhibited high stability of 63.4 °C (+15.7 °C). Such stable duplex formation would inhibit molecular mobility within duplex and it provides efficient shielding ability. Complete shielding effect from nucleobase-dye and dye-dye interaction by incorporation of multiple **L** or **H** moieties could be expected.

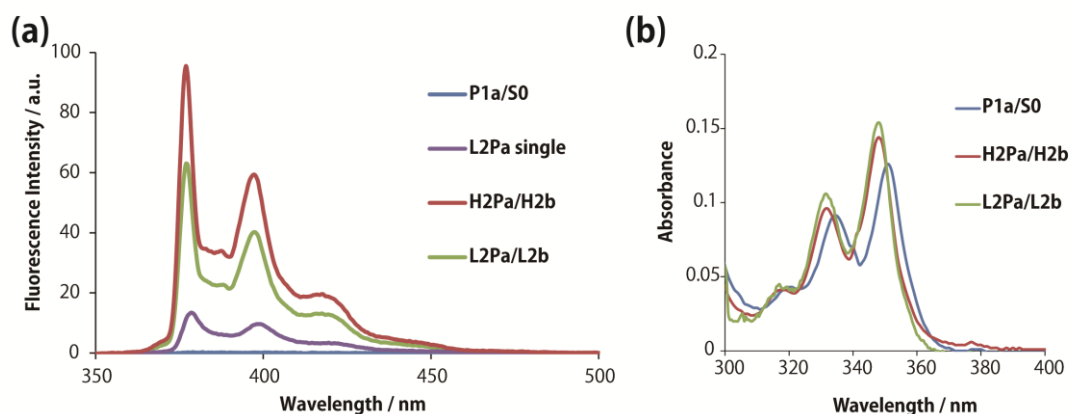


Figure 3-10. Comparison of spectroscopic behaviors of **H2Pa/H2b** and **L2Pa/L2b**. Solution conditions were the same with that of in Figure 3-9. (a) Fluorescence spectra of modified DNA. Excitation wavelength: 345 nm. (b) UV-Vis spectra of modified DNA.

Table 3-11. Comparison of thermal stabilities of modified DNA containing H or L moieties.

Sequence	Representation	X = H [†]	X = L [†]
X1a/X1b		44.9 °C (-2.8)	45.8 °C (-1.9)
X2a/X2b		47.1 °C (-0.6)	46.9 °C (-0.8)
X6a/X6b		61.3 °C (+13.6)	63.4 °C (+15.7)
X2Pa/X2b		48.5 °C (+0.8)	48.8 °C (+1.1)
X3Pa/X3Pb		55.0 °C (+7.3)	55.3 °C (+7.6)

[†]: T_m values of the duplex. The round bracket indicates ΔT_m , the difference of T_m values between modified ODNs and native duplex **Nt/S0** (47.7 °C). Solution conditions: [DNA] = 5 μ M each, [NaCl] = 100 mM, pH 7.0 (10 mM phosphate buffer).

3-3-6 Protection of various dyes

So far, a fluorophore pyrene was used for evaluating shielding ability of insulators because pyrene was very sensitive to electron transfer between nucleobases. Indeed, many fluorophore could be more or less quenched by neighboring nucleobases. Practical fluorophores such as FITC or Rhodamine contain non-planar structures not like pyrene. In this section, to confirm versatility of insulator moiety, modified DNAs containing a wide variety of fluorophores shielded by **H** moieties were synthesized.

First, the fluorophore perylenediimide (PDI: **D**) was tested because it has highly planar structure similar to pyrene and it has been widely applied to material use because of its high electron affinity, high brightness, strong π - π stacking interaction and excellent photostability.⁴²⁻⁴⁴ Furthermore, PDI has also been used for the functionalization of DNA.⁴⁵⁻⁵⁴ Even though the PDI monomer shows a high quantum yield, however, electron transfer from nucleobases severely quenched PDI. Here, as described the previous section, isopropylcyclohexane (**H**) was used as insulator to enhance fluorescence of PDI. Sequences of synthesized DNA were shown in Table 3-12.

Spectrum behaviors of those PDI-conjugated duplex was shown in Figure 3-11. For **D1a/S0**, which contains only one **D** moiety, almost no fluorescence emission was detected (dark purple line in Figure 3-11). This extremely low emission is due to quenching of PDI by nucleobases. However, when two **H-H** pairs were inserted between PDI and its neighboring nucleobases (**H2Da/H2b**), distinct emission at 550 nm was observed. As summarized in Table 3-12, the quantum yield of **H2Da/H2b** was 0.020 whereas that **D1a/S0** was as low as < 0.001 . Furthermore, the emission intensity of **H6Da/H6b** was drastically higher than that of **H2Da/H2b**. Quantum yield of **H6Da/H6b** was as high as 0.59, which was approximately 30 times higher than that of **H2Da/H2b**. This bright orange fluorescence emission could also be detected even by the naked eye (Figure 3-12). Shielding of **D** from nucleobases was also confirmed by the UV-Vis spectra. λ_{\max} of **H2Da/H2b** and **H6Da/H6b** were 535 nm and 532 nm, respectively whereas that of **D1a/S0** was 546 nm. These blue-shift and hyperchromic effect showed that interactions between **D** and nucleobases were disturbed by insulator. The T_m of **H2Da/H2b** was 44.2°C, which was 3.2°C higher than that of **D1a/S0**. Furthermore, the introduction of six **H-H** pairs greatly enhanced the thermal stability of the duplex: the T_m of **H6Da/H6b** was as high as 62.0°C. These results were similar to that of pyrene, demonstrating versatility of effective shielding by insulator base pairs.

Table 3-12. Sequence of modified DNA containing D and H moieties.

Name	Sequence	Representation	
D1a/S0	5' - GGTATC D GCAATC - 3' 3' - CCATAG CGTTAG - 5'		 Perylenediimide (D)
H2Da/H2b	5' - GGTATC HDH GCAATC - 3' 3' - CCATAG H HCGTTAG - 5'		
H6Da/H6b	5' - GGTATC HHH HHH GCAATC - 3' 3' - CCATAG HHH HHH CGTTAG - 5'		

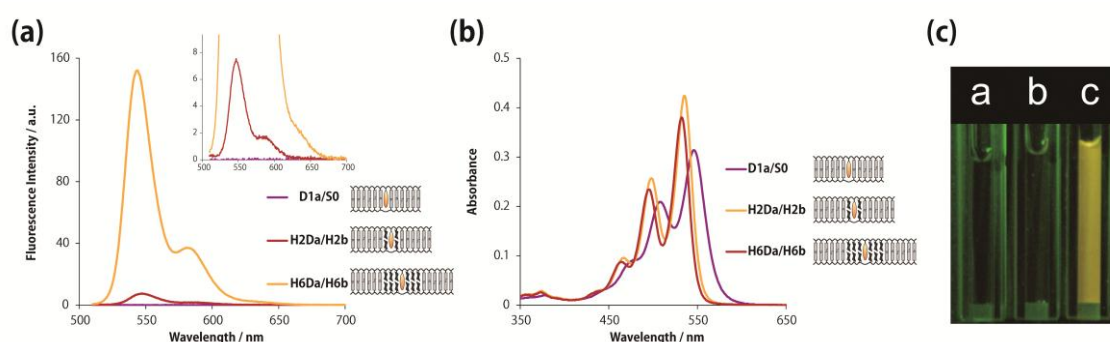


Figure 3-11. Spectrum behaviors of synthesized DNA containing insulator base pairs with a PDI moiety. (a) Fluorescence spectra of modified DNAs. The inset shows magnified view. Solution conditions were as follows: [DNA] = 1.0 μM each, [NaCl] = 100 mM, pH 7.0 (10 mM phosphate buffer), 20°C. Excitation wavelength: 500 nm. (b) UV-Vis spectra of modified DNAs. Solution conditions were as follows: [DNA] = 5 μM each, [NaCl] = 100 mM, pH 7.0 (10 mM phosphate buffer), 20°C. (c) A photograph of a: **D1a/S0**, b: **H2Da/H2b** and c: **H6Da/H6b**. Solution conditions were as follows: [DNA] = 1.0 μM each, [NaCl] = 100 mM, pH 7.0 (10 mM phosphate buffer), 20°C. Excitation wavelength: 520 nm.

Table 3-13. Spectroscopic behaviors and thermodynamic stabilities of modified DNA.

Sequence	Representation	Φ^a	$\lambda_{\text{max}} / \text{nm}^b$	$T_m / ^\circ\text{C}^c$	$\Delta T_m / ^\circ\text{C}^d$
D1a/S0		< 0.001	546	41.0	-6.7
H2Da/H2b		0.020	535	44.2	-3.5
H6Da/H6b		0.59	532	62.0	+14.3

a: Quantum yield determined from the quantum yield of rhodamine6G in EtOH (0.94) as a reference. *b*: Absorption maxima of PDI in the UV-Vis spectra at 20°C. *c*: Solution conditions: [DNA] = 5 μM each, [NaCl] = 100 mM, pH 7.0 (10 mM phosphate buffer). *d*: The difference of T_m values between modified ODNs and native duplex **Nt/S0** (47.7 °C).

Next, the fluorophore Nile Red (**R**) was used because it has unique solvatochromism effect (Figure 3-12a). Modified DNA containing this fluorophore would provide important environmental information around insulator basepairs. As shown in Figure 3-12, Fluorescence emission of **R1a/S0** was not completely quenched, however, its intensity was weak. On the other hand, emission intensity of **H2Ra/H2b** and **H6Ra/H6b** was higher than that of **R1a/S0**. It is noteworthy that λ_{\max} s of these duplexes in fluorescence spectra were almost the same but only intensity was changed. These results indicated that **R** moiety was quenched by neighboring base pair and shielding effect of **H** brought enhancement of fluorescence emission of **R**. Changes in fluorescence intensity without spectral shift demonstrate that solvation environment around **R** was not largely changed in the presence or absence of **H** moieties. Therefore **R** was quenched by electron transfer, not by difference of solvation environment.

Table 3-14. Sequence of modified DNA containing R and H moieties.

Name	Sequence	Representation
R1a/S0	5' -GGTATC R GCAATC-3' 3' -CCATAG CGTTAG-5'	
H2Ra/H2b	5' -GGTATC HRH GCAATC-3' 3' -CCATAG H CGTTAG-5'	
H6Ra/H6b	5' -GGTATC HHHRHHH GCAATC-3' 3' -CCATAG HHH HHHCGTTAG-5'	

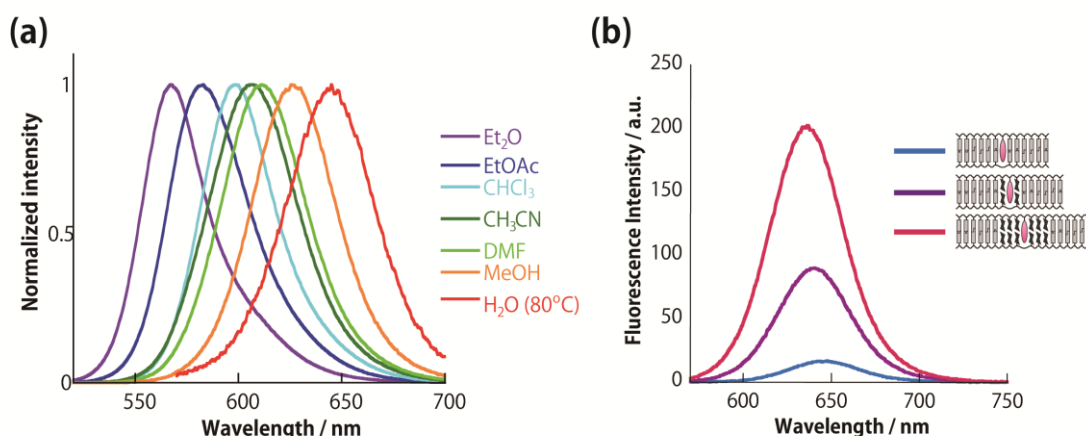
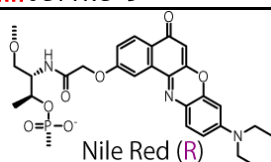


Figure 3-12. Spectrum behaviors of synthesized DNA containing insulator base pairs with a Nile Red moiety. (a) Solvation polarity dependence in fluorescence spectra of Nile Red. (b) Fluorescence spectra of modified DNAs. The inset shows magnified view. Solution conditions were as follows: [DNA] = 1.0 μ M each, [NaCl] = 100 mM, pH 7.0 (10 mM phosphate buffer), 20°C. Excitation wavelength: 560 nm.

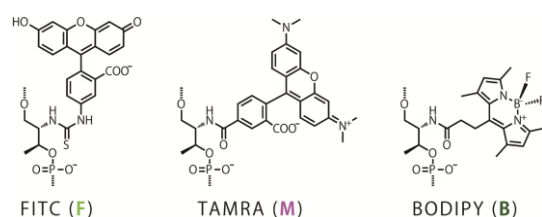


Figure 3-13. Structures of fluorophores conjugated with DNA strands in this topic.

Table 3-14. Sequence of modified DNA containing F, M, B and H moieties.

Name	Sequence	Representation
F1H0	5' - F GGCAGCGTAGGTCCT - 3' 3' - CCGTCGCATCCAGGA - 5'	
F1H1	5' - FH GGCAGCGTAGGTCCT - 3' 3' - CCGTCGCATCCAGGA - 5'	
F1H2	5' - FHH GGCAGCGTAGGTCCT - 3' 3' - CCGTCGCATCCAGGA - 5'	
M1	5' - TGCATG M GTACAC - 3' 3' - ACGTAC CATGTG - 5'	
AMA	5' - TGCATG MA GTACAC - 3' 3' - ACGTACT TCATGTG - 5'	
HMH	5' - TGCATG HM HGTACAC - 3' 3' - ACGTACH HCATGTG - 5'	
HMMH	5' - TGCATG HMM HGTACAC - 3' 3' - ACGTACH HCATGTG - 5'	
HMHMH	5' - TGCATG HMMH HGTACAC - 3' 3' - ACGTACH H HCATGTG - 5'	
HMHMHMH	5' - TGCATG HMHMH HGTACAC - 3' 3' - ACGTACH HHH HCATGTG - 5'	
B1	5' - TGCATG B GTACAC - 3' 3' - ACGTAC CATGTG - 5'	
ABA	5' - TGCATG BA GTACAC - 3' 3' - ACGTACT TCATGTG - 5'	
HBH	5' - TGCATG HB HGTACAC - 3' 3' - ACGTACH HCATGTG - 5'	

In addition, more practical fluorophores which have longer excitation wavelength were tested. Here, insulation effect on FITC (**F**), TAMRA (**M**) and BODIPY (**B**), which are popular and widely accepted conventional fluorophores due to their large extinction coefficients and good quantum yields. However, these fluorophores could also be quenched by nucleobases, for example, **F** and **M** are often quenched by Guanine base owing to electron transfer from G to fluorophores. Moreover, **F** and **M** have larger size of molecule and non-planer structure of vertically conjugated benzene ring. This structural difference from pyrene may affect the insulation ability of **H** because those fluorophores are not suitable to be intercalated within duplex and they tend to destabilize and flip out from inside of DNA duplex.

First, one of the most popular fluorophore, FITC was examined, however, it has already known that FITC cannot intercalate between base pairs owing to its non-planar structure, negative charge and hydrophilic properties. In general, FITC was tethered with DNA via long flexible linker and it was located within grooves, outside of DNA duplex. Herein, FITC was attached at the end of DNA (**F1H0**). Its neighboring base pair is G-C pair, which is known to be a quencher of FITC. As shown in Figure 3-14, **F1H0** was quenched by G-C pair and its fluorescence emission was limited (green line in Figure 3-14a). Red-shifted UV-Vis spectrum also supported interaction between **F** and nucleobases (Figure 3-14b). However, when single **H** moiety was inserted between **F** and nucleobases (**F1H1**), fluorescence intensity of **F** was increased and relative intensity vs. **F1H0** was as high as 3.0, indicating that **F** was protected from G-C quenching by insertion of only one **H** moiety even though outside of DNA duplex. Furthermore, when two **H** moieties were inserted (**F1H2**), fluorescence emission was further enhanced and the relative intensity was 3.6. Unfortunately, insertion of more than three **H** moieties did not affect because dyes attached to the end of DNA can freely move and flexible structure of tandem incorporated **H** moieties could not perfectly shield the dye from nucleobases. One reason why **F** tends to flip out from inside of DNA duplex is because **F** has non-planar structure. Its intercalation would destabilize and disrupt the structure of DNA duplex. However, it is likely that the flexibility of **H** moiety would be able to compensate the inclination caused by intercalation of **F**. To confirm this, **F** moiety sandwiched between two **H-H** pairs was introduced within DNA duplex (data not shown). As expected, enhancement of fluorescence was observed, however, the duplex was significantly destabilized. Therefore **F** was not suitable to be tethered within DNA duplex, however, fluorescence of end-attached **F** was successfully enhanced.

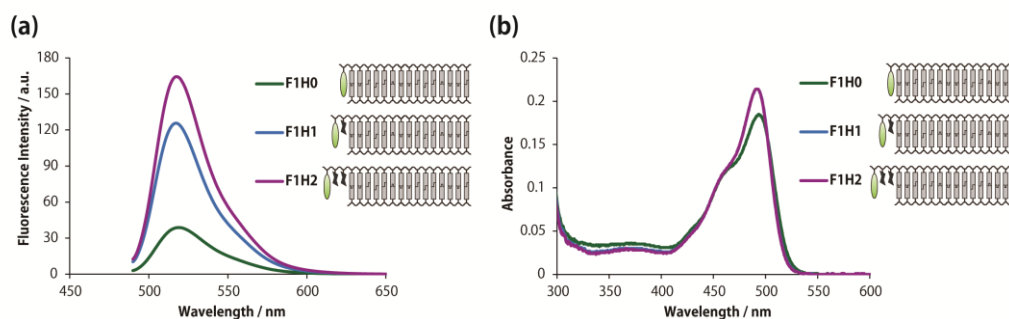


Figure 3-14. Spectrum behaviors of synthesized DNA containing insulator base pairs with a FITC moiety. (a) Fluorescence spectra of modified DNAs. Solution conditions were as follows: [DNA] = 1.0 μM each, [NaCl] = 100 mM, pH 8.0 (10 mM Tris buffer), 20°C. Excitation wavelength: 480 nm. (b) UV-Vis spectra of modified DNAs. Solution conditions were as follows: [DNA] = 5 μM each, [NaCl] = 100 mM, pH 8.0 (10 mM Tris buffer), 20°C.

Next, TAMRA, which has similar structure to FITC. FITC is anionic and inadequate for intercalation due to the electric repulsion with phosphate backbone of DNA. On the other hand, since TAMRA has both negative charge and positive charge, it would be able to compensate such electric repulsion. Here, not like FITC, TAMRA (**M**) was introduced in the middle of DNA duplex. **M** moiety in DNA duplex was quenched by neighboring G-C pair and the absorption maximum was red-shifted (**M1**, cyan lines in Figure 3-15). In the case of neighboring base pairs were A-T pair, fluorescence emission was slightly increased and red-shifted. This is because A-T base pair could have still mediated electron transfer between **M** and G-C pair. However, when two H moieties were inserted between **M** and G-C pair, fluorescence emission was greatly enhanced and the absorption spectrum was also blue-shifted and sharpened up indicating that **H** could successfully protect TAMRA from quenching by G-C pair. T_m value of **M1** was significantly dropped by insertion of **M** (Table 3-15), however, **HMH** duplex possessed relatively stable T_m which was compatible with corresponding native duplex. Flexibility and hydrophobic interaction of **H** could compensate the inclination caused by insertion of TAMRA.

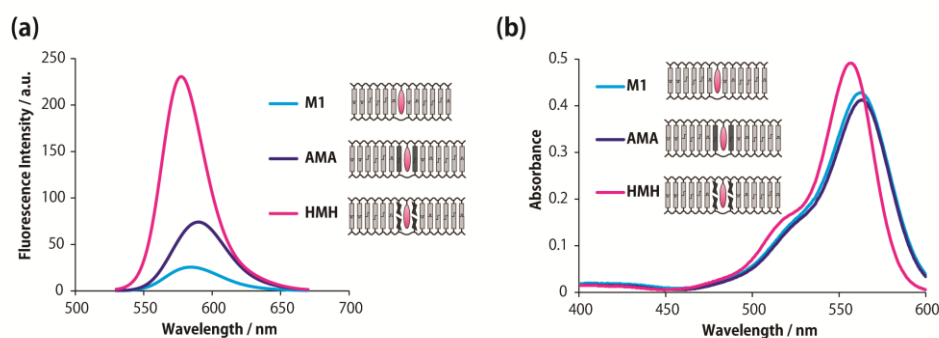


Figure 3-15. Spectrum behaviors of synthesized DNA containing insulator base pairs with a TAMRA moiety. (a) Fluorescence spectra of modified DNAs. Solution conditions were as follows: [DNA] = 1.0 μM each, [NaCl] = 100 mM, pH 7.0 (10 mM Phosphate buffer), 20°C. Excitation wavelength: 520 nm. (b) UV-Vis spectra of modified DNAs. Solution conditions were as follows: [DNA] = 5 μM each, [NaCl] = 100 mM, pH 7.0 (10 mM Phosphate buffer), 20°C.

Table 3-15. Spectroscopic behaviors and thermodynamic stabilities of modified DNA.

Sequence	Relative Int. ^a	$\lambda_{\text{max}} / \text{nm}^b$	$T_m / ^\circ\text{C}^c$	$\Delta T_m / ^\circ\text{C}^d$
M1	1	562	41.4	-10.2
AMA	2.8	563	45.9	-5.7
HMH	8.3	556	51.4	-0.2

^a: Emission intensity at 584 nm relative to that of **M1**. Solution conditions: [DNA] = 1 μM each, [NaCl] = 100 mM, pH 7.0 (10 mM phosphate buffer), 20°C. Excitation wavelength: 520 nm. ^b: Absorption maxima of TAMRA in the UV-Vis spectra at 20°C. ^c: Solution conditions: [DNA] = 5 μM each, [NaCl] = 100 mM, pH 7.0 (10 mM phosphate buffer). ^d: The difference of T_m values between modified ODNs and corresponding native duplex (51.6 °C).

Moreover, since TAMRA is also quenched by dimerization, shielding ability of dye-dye interaction by **H** was examined. Dimerized **M** was obviously quenched in **HMMH** (cyan line in Figure 3-16). Note that quenching by nucleobase was shielded by adjacent two **H-H** pairs. When one **H-H** pairs were inserted between **M** moieties (**HMHMH**, dark blue line), fluorescence emission was highly recovered. Furthermore, for three pairs of **H-H** were inserted, there was no difference from **HMHMH**. Unexpectedly, the fluorescence intensity of **HMHMH** was smaller than that of **HMH**. The absorption spectra of **HMHMH** and **HMHHMH** were also still red-shifted suggesting that shielding of dye-dye interaction was not enough, although the duplexes were highly stabilized (Table 3-16). As discussed in 3-3-5, multiple incorporation of **H** tends to corrupt the alignment of **HMHMH** owing to high mobility of **H** moieties and dyes could dynamically contact each other. Taken together, **M** could be certainly shielded from nucleobases, however, restriction of dimerization was still insufficient. For further enhancement of fluorescent emission, shielding ability by tertiarybutylcyclohexane (**L**) should be estimated.

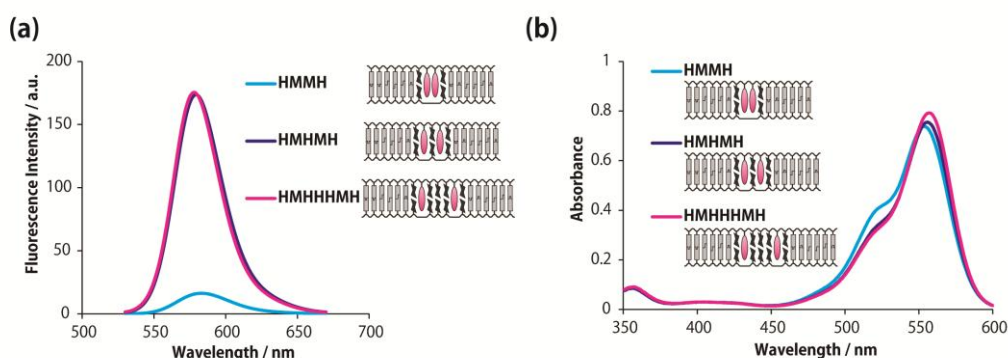


Figure 3-16. Spectrum behaviors of synthesized DNA containing insulator base pairs with two TAMRA moieties. (a) Fluorescence spectra of modified DNAs. Solution conditions were as follows: [DNA] = 1.0 μM each, [NaCl] = 100 mM, pH 7.0 (10 mM Phosphate buffer), 20°C. Excitation wavelength: 520 nm. (b) UV-Vis spectra of modified DNAs. Solution conditions were as follows: [DNA] = 5 μM each, [NaCl] = 100 mM, pH 7.0 (10 mM Phosphate buffer), 20°C.

Table 3-16. Spectroscopic behaviors and thermodynamic stabilities of modified DNA.

Sequence	Relative Int. ^a	λ_{max} / nm ^b	T_m / °C ^c	ΔT_m / °C ^d
HMMH	1	554	52.0	+0.4
HMHMH	10.2	556	55.7	+4.1
HMHHMH	10.0	557	63.9	+12.3

^a: Emission intensity at 584 nm relative to that of **HMMH**. Solution conditions: [DNA] = 1 μM each, [NaCl] = 100 mM, pH 7.0 (10 mM phosphate buffer), 20°C. Excitation wavelength: 520 nm. ^b: Absorption maxima of TAMRA in the UV-Vis spectra at 20°C. ^c: Solution conditions: [DNA] = 5 μM each, [NaCl] = 100 mM, pH 7.0 (10 mM phosphate buffer). ^d: The difference of T_m values between modified ODNs and corresponding native duplex (51.6 °C).

Finally, another fluorophore, BODIPY (**B**) was tested. BODIPY has relatively planar and smaller structure than FITC or TAMRA. As shown in Figure 3-17, BODIPY was quenched by neighboring G-C pair (**B1**). Unlike TAMRA, insertion of A-T pair (**ABA**) could enhance fluorescence emission. Slightly destabilized T_m of **B1** and **ABA** duplex and small difference in UV-Vis spectra between them suggested that **B** moiety was not correctly intercalated within DNA duplex. However, insertion of **H-H** pairs between **B** and G-C pairs was still effective for fluorescence enhancement (**HBH**).

As described above, protection of fluorophores by **H** insulator has wide versatility and potential of improvement of detection sensitivity in DNA analyses.

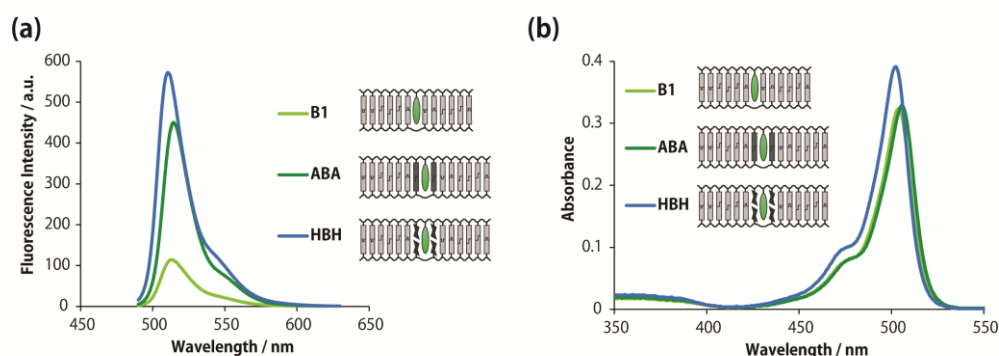


Figure 3-17. Spectrum behaviors of synthesized DNA containing insulator base pairs with a BODIPY moiety. (a) Fluorescence spectra of modified DNAs. Solution conditions were as follows: [DNA] = 1.0 μM each, [NaCl] = 100 mM, pH 7.0 (10 mM Phosphate buffer), 20°C. Excitation wavelength: 480 nm. (b) UV-Vis spectra of modified DNAs. Solution conditions were as follows: [DNA] = 5 μM each, [NaCl] = 100 mM, pH 7.0 (10 mM Phosphate buffer), 20°C.

Table 3-16. Spectroscopic behaviors and thermodynamic stabilities of modified DNA.

Sequence	Relative Int. ^a	$\lambda_{\text{max}} / \text{nm}^b$	$T_m / ^\circ\text{C}^c$	$\Delta T_m / ^\circ\text{C}^d$
B1	1	504	49.5	-2.1
ABA	3.9	506	49.9	-1.7
HBH	4.8	502	51.1	-0.5

a: Emission intensity at 513 nm relative to that of **B1**. Solution conditions: [DNA] = 1 μM each, [NaCl] = 100 mM, pH 7.0 (10 mM phosphate buffer), 20°C. Excitation wavelength: 480 nm. *b:* Absorption maxima of BODIPY in the UV-Vis spectra at 20°C. *c:* Solution conditions: [DNA] = 5 μM each, [NaCl] = 100 mM, pH 7.0 (10 mM phosphate buffer). *d:* The difference of T_m values between modified ODNs and corresponding native duplex (51.6 °C).

3-4 Conclusions

To enhance fluorescence intensity, novel artificial bases that formed a pair through hydrophobic interactions have been successfully developed. These “base pairs” of isopropylcyclohexane moieties showed even higher stability than natural A-T pairs, although the moiety had neither aromatic rings nor hydrogen bonds. When the artificial base pairs were introduced between fluorophores and nucleobases, cyclohexyl moieties worked as “insulators”, and the emission intensity of fluorophore was remarkably improved. The cyclohexyl base pairs efficiently disturbed the electron transfer between fluorophore and nucleobases. This shielding effect by cyclohexyl moiety is applicable to a wide variety of fluorophores including conventional dyes.

3-5 Experimental section

3-5-1 Materials

All of the conventional phosphoramidite monomers, CPG columns, reagents for DNA synthesis and Poly-Pak II cartridges were purchased from Glen Research. Other reagents for the synthesis of phosphoramidite monomers were purchased from Tokyo Kasei Co., Ltd and Sigma-Aldrich. Native oligodeoxyribonucleotides (ODNs) were purchased from Integrated DNA Technologies.

3-5-2 Synthesis of the DNA modified with fluorophores and insulators

All of the modified ODNs were synthesized on an automated DNA synthesizer (ABI-3400 DNA synthesizer, Applied Bio systems) using phosphoramidite monomers bearing fluorophores and insulators. Phosphoramidite monomer tethering fluorophores and insulators were synthesized as described below. The coupling efficiency of the monomers corresponding to the modified residues was as high as that of the conventional monomers, as judged from the coloration of the released trityl cation. After the recommended work-up, they were purified by reversed phase (RP)-HPLC and were characterized by MALDI-TOFMS (Autoflex, Bruker Daltonics). Purities of all the ODNs are estimated over 99% from HPLC analysis.

The MALDI-TOFMS data for the DNA were as follows:

m/z: **H1a**: Obsd 3962 (calcd for [**H1a** + H⁺]: 3964). **H2a**: Obsd 4283 (calcd for [**H2a** + H⁺]: 4283). **H6a**: Obsd 5558 (calcd for [**H6a** + H⁺]: 5560). **H1b**: Obsd 3962 (calcd for [**H1b** + H⁺]: 3964). **H2b**: Obsd 4281 (calcd for [**H2b** + H⁺]: 4283). **H6b**: Obsd 5559 (calcd for [**H6b** + H⁺]: 5560). **K1a**: Obsd 3936 (calcd for [**K1a** + H⁺]: 3936). **K1b**: Obsd 3937 (calcd for [**K1b** + H⁺]: 3936). **K2a**: Obsd 4225 (calcd for [**K2a** + H⁺]: 4227). **K2b**: Obsd 4227 (calcd for [**K2b** + H⁺]: 4227). **K6a**: Obsd 5391 (calcd for [**K6a** + H⁺]: 5391). **K6b**: Obsd 5393 (calcd for [**K6b** + H⁺]: 5391). **P1a**: Obsd 4081 (calcd for [**P1a** + H⁺]: 4082). **H1c**: Obsd 2112 (calcd for [**H1c** + H⁺]: 2112). **K1d**: Obsd 2084 (calcd for [**K1d** + H⁺]: 2084).

H2Pa: Obsd 4719 (calcd for [**H2Pa** + H⁺]: 4720). **I2Pa**: Obsd 4788 (calcd for [**I2Pa** + H⁺]: 4788). **J2Pa**: Obsd 4776 (calcd for [**J2Pa** + H⁺]: 4776). **H6Pa**: Obsd 5995 (calcd for [**H6Pa** + H⁺]: 5997). **B2Pa**: Obsd 4623 (calcd for [**B2Pa** + H⁺]: 4625). **B2b**: Obsd 4187 (calcd for [**B2b** + H⁺]: 4186). **H3Pa**: Obsd. 5039 (Calcd. for [**H3Pa** + H⁺]: 5039). **H3Pb**: Obsd. 5039 (Calcd. for [**H3Pb** + H⁺]: 5039). **H4Pa**: Obsd. 5357 (Calcd. for [**H4Pa** + H⁺]: 5358). **H4Pb**: Obsd. 5357 (Calcd. for [**H4Pb** + H⁺]: 5358). **H5Pa**: Obsd. 5675 (Calcd. for [**H5Pa** + H⁺]: 5678). **H5Pb**: Obsd. 5675 (Calcd. for [**H5Pb** + H⁺]: 5678).

L1a: Obsd 3979 (calcd for [**L1a** + H⁺]: 3977). **L1b**: Obsd 3979 (calcd for [**L1b** + H⁺]: 3977). **L2a**: Obsd 4312 (calcd for [**L2a** + H⁺]: 4310). **L2b**: Obsd 4312 (calcd for [**L2b** + H⁺]: 4310). **L6a**: Obsd 5643 (calcd for [**L6a** + H⁺]: 5645). **L6b**: Obsd 5646 (calcd for [**L6b** + H⁺]: 5643). **L2Pa**: Obsd 4755 (calcd for [**L2Pa** + H⁺]: 4749). **L3Pa**: Obsd 5083 (calcd for [**L3Pa** + H⁺]: 5081). **L3Pb**: Obsd 5083 (calcd for [**L3Pb** + H⁺]: 5081).

D1a: Obsd 4227 (calcd for [**D1a** + H⁺]: 4227). **H2Da**: Obsd 4864 (calcd for [**H2Da** + H⁺]: 4865). **H6Da**: Obsd 6141 (calcd for [**H6Da** + H⁺]: 6142).

R1a: Obsd 4185 (calcd for [**R1a** + H⁺]: 4187). **H2Ra**: Obsd 4823 (calcd for [**H2Ra** + H⁺]: 4824). **H6Ra**: Obsd 6100 (calcd for [**H6Ra** + H⁺]: 6100).

F1H0: Obsd 5164 (calcd for [**F1H0** + H⁺]: 5163). **F1H1**: Obsd 5483 (calcd for [**F1H1** + H⁺]: 5482). **F1H2**: Obsd 5803 (calcd for [**F1H2** + H⁺]: 5801). Complementary strand “z” for these ODNs: Obsd 4533 (calcd for [**z** + H⁺]: 4534).

M1x: Obsd 4225 (calcd for [**M1x** + H⁺]: 4223). **M1y**: Obsd 3643 (calcd for [**M1y** + H⁺]: 3644). **AMAx**: Obsd 4849 (calcd for [**AMAx** + H⁺]: 4849). **AMAy**: Obsd 4256 (calcd for [**AMAy** + H⁺]: 4252). **HMHx**: Obsd 4862 (calcd for [**HMHx** + H⁺]: 4861). **HMHy**: Obsd 4284 (calcd for [**HMHy** + H⁺]: 4282). **HMMHx**: Obsd 5443 (calcd for [**HMMHx** + H⁺]:

5440). **HMMHy**: Obsd 4284 (calcd for [**HMMHy** + H⁺]: 4282). **HMHMHx**: Obsd 5767 (calcd for [**HMHMHx** + H⁺]: 5760). **HMHMHy**: Obsd 4603 (calcd for [**HMHMHy** + H⁺]: 4601). **HMHHMHx**: Obsd 6403 (calcd for [**HMHHMHx** + H⁺]: 6398). **HMHHMHy**: Obsd 5243 (calcd for [**HMHHMHy** + H⁺]: 5240).

B1x: Obsd 4114 (calcd for [**B1x** + H⁺]: 4113). **B1y**: Obsd 3643 (calcd for [**B1y** + H⁺]: 3644). **ABAx**: Obsd 4738 (calcd for [**ABAx** + H⁺]: 4739). **ABAy**: Obsd 4256 (calcd for [**ABAy** + H⁺]: 4252). **HBHx**: Obsd 4749 (calcd for [**HBHx** + H⁺]: 4751). **HBHy**: Obsd 4284 (calcd for [**HBHy** + H⁺]: 4282).

3-5-3 Spectroscopic measurements

Fluorescence spectra were measured on a JASCO model FP-6500 with a microcell. The sample solutions were as follows: [NaCl] = 100 mM, pH 7.0 (10 mM phosphate buffer), [ODN] = 1.0 mM. Quantum yields were determined from the quantum yield of pyrene in N₂-bubbled cyclohexane (0.65) or Rhodamine6G in EtOH (0.94) as a reference. UV-Vis and CD spectra were measured on a Shimadzu UV-1800 and a JASCO model J-820, respectively, with a 10-mm quartz cell equipped with programmed temperature controllers. The sample solutions were as follows: [NaCl] = 100 mM, pH 7.0 (10 mM phosphate buffer), [ODN] = 5.0 mM.

3-5-4 Measurement of the melting temperature

The melting curve of duplex DNA was obtained with a Shimadzu UV-1800 by measurement of the change in absorbance at 260 nm versus temperature. The melting temperature (T_m) was calculated from the maximum in the first derivative of the melting curve. Both the heating and the cooling profiles were measured and its average was determined as T_m . The temperature ramp was 0.5 °C min⁻¹ and the T_m s determined from heating and cooling profiles agreed to within 2.0 °C. The sample solutions were as follows: [NaCl] = 100 mM, pH 7.0 (10 mM phosphate buffer), [ODN] = 5.0 mM.

Thermodynamic parameters of duplexes (ΔH , ΔS) were determined from $1/T_m$ versus $\ln(C_T/4)$ plots by the following equation: $1/T_m = R/\Delta H \ln(C_T/4) + \Delta S/\Delta H$, where C_T is the total concentration of ODNs. ΔG^{0}_{37} was calculated from the ΔH and ΔS values. The sample solutions were as follows: [NaCl] = 100 mM, pH 7.0 (10 mM phosphate buffer). The range of DNA concentrations was 2–64 mM.

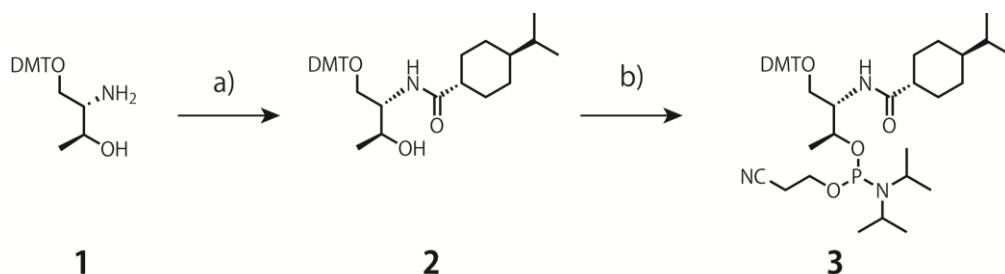
3-5-5 NMR measurements

NMR samples were prepared by dissolving three-times lyophilized DNA in an H₂O/D₂O 9 : 1 solution containing 10 mM sodium phosphate (pH 7.0) to give a duplex concentration of 1.7 mM. NaCl was added to give a final sodium concentration of 200 mM. NMR spectra were measured with a Varian INOVA spectrometer (700 MHz) equipped for triple resonance at a probe temperature of 275 K. Resonances were assigned by standard methods using a combination of 1D, TOCSY (60ms of mixing time), DQFCOSY, and NOESY (150 ms of mixing time) experiments. All spectra in the H₂O/D₂O 9 : 1 solution were recorded using the 3-9-19 WATERGATE pulse sequence for water suppression.

3-5-6 Computer modeling

Molecular modeling by conformational energy minimization was performed with Insight II/Discover 3 software (Molecular Simulation, Inc.) on a Silicon Graphics Octane workstation with the operating system IRIX64 Release 6.5 and AMBER was used for the calculations. The results of the NMR analyses served as a starting point for the modeling (no restraints were used for energy minimization).

3-5-7 Synthesis of phosphoramidite monomers tethering insulators and dyes

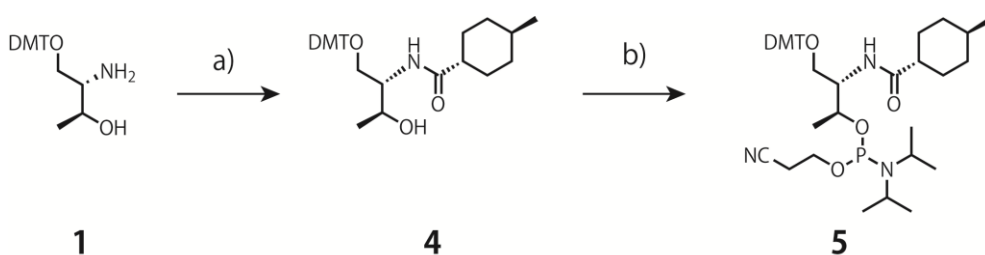


Scheme 3-1. Synthesis of phosphoramidite monomer tethering *trans*-4-isopropylcyclohexanecarboxylic acid (**H**). Reagents and conditions: a) *trans*-4-isopropylcyclohexanecarboxylic acid, PyBOP, Et₃N, CH₂Cl₂, r.t., over night, 89 %; b) (iPr)₂NP(Cl)(OCH₂CH₂CN), Et₃N, CH₃CN, 0 °C → r.t., 1h, 92 %

The phosphoramidite monomer tethering *trans*-4-isopropylcyclohexanecarboxylic acid (**H**) was synthesized as follows: Synthesis of compound **1** will be reported elsewhere.

trans-4-Isopropylcyclohexanecarboxylic acid (0.20 g, 1.2 mmol) was reacted with PyBOP (0.62 g, 1.2 mmol) in CH₂Cl₂ (5.0 ml) for 10 min. Then, a solution of Et₃N (5.0 ml) and compound **1** (0.41 g, 1.0 mmol) in CH₂Cl₂ (5.0 ml) were added to the above mixture. After a night of vigorous stirring, the organic solution was washed with saturated aqueous solution of NaHCO₃. The solvent was removed by evaporation, followed by silica gel column chromatography (AcOEt : hexane : Et₃N = 40:60:3, *R_f* = 0.37) to afford **2** (0.50 g, yield 89 %). ¹H-NMR [CDCl₃, 500 MHz] δ = 7.38-6.82 (m, 13H), 6.13 (d, *J* = 8.5 Hz, 1H), 4.07 (m, 1H), 3.91 (m, 1H), 3.79 (s, 6H), 3.44 (dd, *J* = 4 Hz, 10 Hz, 1H), 3.25 (dd, *J* = 4 Hz, 10 Hz, 1H), 3.16 (br, 1H), 2.08 (m, 1H), 1.96 (m, 2H), 1.82 (m, 2H), 1.52-1.41 (m, 3H), 1.11 (d, *J* = 6.5 Hz, 3H), 1.09-0.99 (m, 3H), 0.88 (d, *J* = 7 Hz, 6H). HRMS(FAB) Calcd for C₃₅H₄₅NO₅ (M⁺) 559.3298. Found 559.3301.

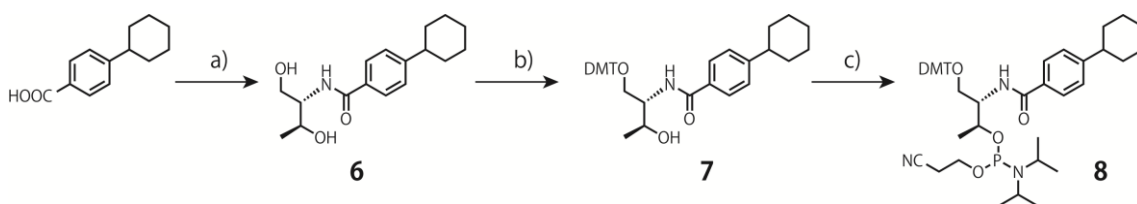
Et₃N (0.69 ml, 5.0 mmol) and 2-cyanoethyl diisopropylchlorophosphoramidite (0.45 ml, 2.0 mmol) were added to a solution of compound **2** (0.56 g, 1.0 mmol) in CH₃CN (5.0 ml) at 0 °C. After 20 min of vigorous stirring, the solution was stirred for 40 min at room temperature. Then, an excess of AcOEt was added to the reaction mixture and was washed with saturated aqueous solution of NaHCO₃ and of NaCl. After drying over MgSO₄, the solvent was removed by evaporation, followed by silica gel column chromatography (AcOEt : hexane : Et₃N = 30:70:3, *R_f* = 0.59) to afford **3** (0.70 g, yield 92 %). ³¹P-NMR [121 MHz, CDCl₃] δ = 148.0, 147.9. HRMS(FAB) Calcd for C₄₄H₆₂N₃O₆PNa (M + Na⁺) 782.4274. Found 782.4300.



Scheme 3-2. Synthesis of phosphoramidite tethering 4-methylcyclohexanecarboxylic acid (**K**). Reagents and conditions: a) DCC, HOBT, DMF, r.t., overnight, quant.; b) $(iPr)_2NP(Cl)(OCH_2CH_2CN)$, Et_3N , THF, $0\text{ }^\circ\text{C} \rightarrow \text{r.t.}$, 1h, 78 %.

The phosphoramidite monomer tethering 4-methylcyclohexanecarboxylic acid (**K**) was synthesized as follows: *trans*-4-Methylcyclohexanecarboxylic acid (0.83 g, 5.83 mmol) was coupled with DMT-D-threoninol (compound **1**) (2.0 g, 4.90 mmol) in the presence of *N,N'*-dicyclohexylcarbodiimide (1.50 g, 7.27 mmol) and 1-hydroxybenzotriazole (0.99 g, 7.32 mmol) in DMF (40 ml). After the reaction mixture was stirred at room temperature for overnight, the solvent was removed and the remained oil was subjected to silica gel column chromatography (AcOEt : hexane : Et_3N = 50:50:3, R_f = 0.32) to afford compound **4** (yield quant.). $^1\text{H-NMR}$ [CDCl_3 , 500 MHz] δ = 7.37 (m, 2H, aromatic protons of DMT), 7.30-7.22 (m, 7H, aromatic protons of DMT), 6.84-6.82 (m, 4H, aromatic protons of DMT), 6.13 (d, J = 9 Hz, 1H, - NHCO -), 4.07 (m, 1H, - $\text{CH}(\text{CH}_3)\text{OH}$), 3.91 (m, 1H, - $\text{CH}_2\text{CH}(\text{NHCO})\text{CH}$), 3.79 (s, 6H, - OCH_3), 3.43 (dd, J = 4 Hz, 10 Hz, 1H, - CH_2ODMT), 3.40 (dd, J = 3.5 Hz, 9.5 Hz, 1H, - CH_2ODMT), 3.16 (br, 1H, - $\text{CH}(\text{CH}_3)\text{OH}$), 2.07 (m, 1H, - $\text{COCH}(\text{CH}_2)_2$), 1.90 (m, 2H, - $\text{COCH}(\text{CH}_2)_2$), 1.79 (m, 2H, - $(\text{CH}_2)_2\text{CHCH}_3$), 1.50 (m, 2H, - $\text{COCH}(\text{CH}_2)_2$), 1.39 (m, 1H, - $(\text{CH}_2)_2\text{CHCH}_3$), 1.11 (d, 3H, J = 6.5 Hz, - $\text{CH}(\text{CH}_3)\text{OH}$), 0.97 (m, 2H, - $(\text{CH}_2)_2\text{CHCH}_3$), 0.90 (d, J = 6.5 Hz, 3H, - $(\text{CH}_2)_2\text{CHCH}_3$). HRMS(FAB) Calcd for $\text{C}_{33}\text{H}_{41}\text{NO}_5$ (M^+) 531.2985. Found 531.2980.

DIPEA (1.06 ml, 4.70 mmol) and 2-cyanoethyl-diisopropylchlorophosphoramidite (0.55 ml, 2.45 mmol) were added to a solution of compound **4** (0.65 g, 1.22 mmol) in THF (5 ml) at $0\text{ }^\circ\text{C}$. After 20 min of vigorous stirring on ice, the solution was stirred for 40 min at room temperature. Then, an excess of AcOEt was added to the reaction mixture and was washed with saturated aqueous solution of NaHCO_3 and of NaCl. After drying over MgSO_4 , the solvent was removed by evaporation, followed by silica gel column chromatography (AcOEt : hexane : Et_3N = 30:70:3, R_f = 0.70) to afford **5** (0.70 g, yield 78 %). $^{31}\text{P-NMR}$ [121 MHz, CDCl_3] δ = 148.8, 148.7. HRMS(FAB) Calcd for $\text{C}_{42}\text{H}_{58}\text{N}_3\text{O}_6\text{PNa}$ ($\text{M} + \text{Na}^+$) 754.3961. Found 754.3975.



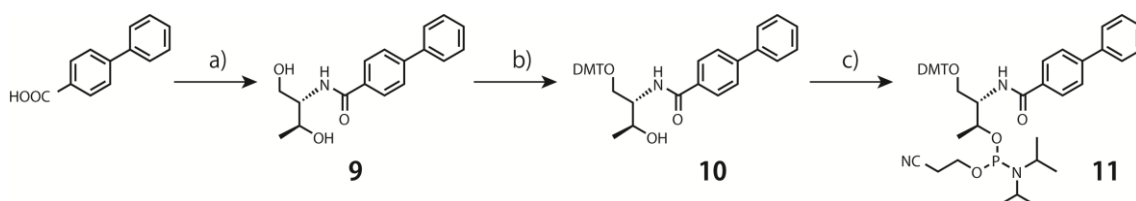
Scheme 3-3. Synthesis of phosphoramidite monomer tethering 4-cyclohexylbenzoic acid (**I**). Reagents and conditions: a) D-threoninol, DCC, HOBT, DMF, r.t., 3d, 83%; b) DMT-Cl, DIPEA, DMAP, CH₂Cl₂, pyridine, 0 °C→r.t., 74 %; c) (*t*Pr₂N)₂PO(CH₂)₂CN, 1*H*-tetrazole, CH₃CN, 0 °C→r.t., 3h, 73 %

The phosphoramidite monomer tethering 4-cyclohexylbenzoic acid (**I**) was synthesized as follows: 4-Cyclohexylbenzoic acid (1.04 g, 5.1 mmol) was coupled with D-threoninol (0.50 g, 4.6 mmol) in the presence of dicyclohexylcarbodiimide (1.24 g, 6.0 mmol) and 1-hydroxybenzotriazole (0.81 g, 6.0 mmol) in DMF. After the reaction mixture was stirred at room temperature for 3 days, the solvent was removed and the remained oil was subjected to silica gel column chromatography (CH₃OH : CHCl₃ = 1:5, *R_f* = 0.44) to afford compound **6** (1.11g, yield 83%). ¹H-NMR [CDCl₃, 500 MHz] δ = 7.74 (d, *J* = 8.5 Hz, 2H), 7.27 (d, *J* = 8 Hz, 2H), 6.89 (d, *J* = 8.5 Hz, 1H), 4.28 (m, 1H), 4.03 (m, 1H), 3.93 (d, *J* = 3.5 Hz, 2H), 2.84 (br, 1H), 2.77 (br, 1H), 2.55 (m, 2H), 1.86 (m, 4H), 1.41 (m, 4H), 1.26 (d, 3H, *J* = 6.5 Hz). HRMS(FAB) Calcd for C₁₇H₂₅NO₃ (M⁺) 292.1841. Found 292.1834.

Dry pyridine solution containing **6** (1.11 g, 3.81 mmol) and *N,N*-diisopropylethylamine (1.0 ml, 5.71 mmol) was cooled on ice under nitrogen. Then, 4,4'-dimethoxytrityl chloride (DMT-Cl) (1.94 g, 5.71 mmol) and 4-(dimethylamino)pyridine (0.058 g, 0.48 mmol) in CH₂Cl₂ was added to the above mixture. After 3 h of vigorous stirring, the solvent was removed by evaporation, followed by silica gel column chromatography (AcOEt : hexane : Et₃N = 50:50:3, *R_f* = 0.43) to afford **7** (1.68 g, yield 74 %). ¹H-NMR [CDCl₃, 500 MHz] δ = 7.74 (d, *J* = 8.5 Hz, 2H), 7.38 (m, 2H), 7.31-7.20 (m, 9H), 6.82-6.77 (m, 5H), 4.20 (m, 1H), 4.11 (m, 1H), 3.77 and 3.76 (s, 6H), 3.57 (dd, *J* = 4 Hz, 9.5 Hz, 1H), 3.34 (dd, *J* = 3.5 Hz, 10 Hz, 1H), 3.22 (d, *J* = 2.5Hz, 1H), 2.57 (m, 1H), 1.90-1.75 (m, 5H), 1.46-1.28 (m, 5H), 1.19 (d, *J* = 6 Hz, 3H). HRMS(FAB) Calcd for C₃₈H₄₃NO₅ (M⁺) 593.3141. Found 593.3144.

In dry acetonitrile (10 mL) under nitrogen, **7** (0.35 g, 0.59 mmol) and 2-cyanoethyl *N,N,N',N'*-tetraisopropylphosphordiamidite (0.22 ml, 0.71 mmol) were reacted with 1*H*-tetrazole (0.054 g, 0.77 mmol). Prior to the reaction, **7** and 1*H*-tetrazole were dried by coevaporation with dry acetonitrile (three times). After 2 h, the product was taken into ethyl acetate. The organic solution was washed with saturated aqueous solution of

NaHCO₃ and of NaCl, and dried over MgSO₄. Finally the solvent was removed *in vacuo*, and the oily product was purified by column chromatography (AcOEt: hexane: Et₃N = 50:50:3, *R_f* = 0.74) to afford **8** (0.34 g, yield 73 %) and used for the DNA synthesis. ³¹P-NMR [121 MHz, CDCl₃] *d* = 149.0, 148.5. HRMS(FAB) Calcd for C₄₇H₆₀N₃O₆PNa (M + Na⁺) 816.4117. Found 816.4141.



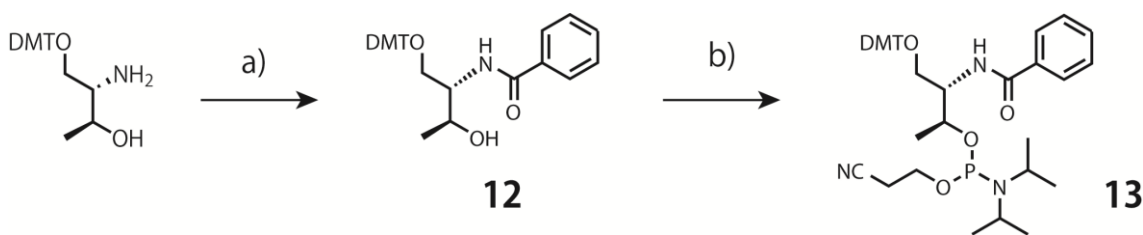
Scheme 3-4. Synthesis of phosphoramidite tethering biphenyl-4-carboxylic acid (**J**). Reagents and conditions: a) D-threoninol, DCC, HOBt, DMF, r.t., 3d, quant.; b) DMT-Cl, DIPEA, DMAP, CH₂Cl₂, pyridine, 0→r.t., 78 %; c) (iPr₂N)₂PO(CH₂)₂CN, 1*H*-tetrazole, CH₃CN, 0 °C→r.t., 1.5h, 74 %

The phosphoramidite monomer tethering biphenyl-4-carboxylic acid was synthesized as follows: Biphenyl-4-carboxylic acid (1.37 g, 6.91 mmol) was coupled with D-threoninol (0.575 g, 5.30 mmol) in the presence of *N,N*-dicyclohexylcarbodiimide (1.64 g, 7.95 mmol) and 1-hydroxybenzotriazole (1.08 g, 7.95 mmol) in DMF. After the reaction mixture was stirred at room temperature for 3 days, the solvent was removed and the remained oil was subjected to silica gel column chromatography (CH₃OH : CHCl₃ = 1:5, *R_f* = 0.50) to afford compound **9** (yield quant.). ¹H-NMR [CDCl₃, 500 MHz] *δ* = 7.86 (d, *J* = 8.5 Hz, 2H), 7.61 (d, *J* = 9 Hz, 2H), 7.57 (m, 2H), 7.45 (m, 2H), 7.39 (m, 1H), 7.10 (d, *J* = 8 Hz, 1H), 4.38 (br, 2H), 4.32 (m, 1H), 4.08 (m, 1H), 3.97 (m, 2H), 1.28 (d, 3H, *J* = 6.5 Hz). HRMS(FAB) Calcd for C₁₇H₂₀NO₃ (M + H⁺) 286.1443. Found 286.1385.

Dry pyridine solution containing **9** (1.51 g, 5.30 mmol) and *N,N*-diisopropylethylamine (1.53 ml, 8.74 mmol) was cooled on ice under nitrogen. Then, 4,4'-dimethoxytrityl chloride (DMT-Cl) (2.97 g, 8.68 mmol) and 4-(dimethylamino)pyridine (0.09 g, 0.73 mmol) in CH₂Cl₂ was added to the above mixture. After 3 h of vigorous stirring, the solvent was removed by evaporation, followed by silica gel column chromatography (AcOEt : hexane : Et₃N = 50:50:3, *R_f* = 0.32) to afford **10** (2.43 g, yield 78 %). ¹H-NMR [CDCl₃, 500 MHz] *δ* = 7.90 (d, *J* = 8.5 Hz, 2H), 7.70 (d, *J* = 8.5 Hz, 2H), 7.64 (m, 2H), 7.49 (t, *J* = 2Hz, 2H), 7.42 (m, 3H), 7.32-7.20 (m, 7H), 6.91 (d, *J* = 8.5 Hz, 2H), 6.83-6.80 (m, 4H), 4.25 (m, 1H), 4.16 (m, 1H), 3.77 and 3.77 (s, 6H), 3.62 (dd, *J* = 4 Hz, 9.5 Hz, 1H), 3.40 (dd, *J* = 3 Hz, 9.5 Hz, 1H), 3.27 (br, 1H),

1.24 (d, $J = 6.5$ Hz, 3H). HRMS(FAB) Calcd for $C_{38}H_{37}NO_5$ (M^+) 587.2672. Found 587.2659.

In dry acetonitrile (10 mL) under nitrogen, **10** (0.77 g, 1.31 mmol) and 2-cyanoethyl N,N,N,N' tetraisopropylphosphordiamidite (0.50 ml, 1.57 mmol) were reacted with 1*H*-tetrazole (0.12 g, 1.71 mmol). Prior to the reaction, **10** and 1*H*-tetrazole were dried by coevaporation with dry acetonitrile (three times). After 2 h, the product was taken into ethyl acetate. The organic solution was washed with saturated aqueous solution of $NaHCO_3$ and of NaCl, and dried over $MgSO_4$. Finally the solvent was removed *in vacuo*, and the oily product was purified by column chromatography (AcOEt: hexane: $Et_3N = 50:50:3$, $R_f = 0.55$) to afford **11** (0.76 g, yield 74 %) and used for the DNA synthesis. ^{31}P -NMR [121 MHz, $CDCl_3$] $\delta = 149.1, 148.7$. HRMS(FAB) Calcd for $C_{47}H_{54}N_3O_6PNa$ ($M + Na^+$) 810.3648. Found 810.3655.

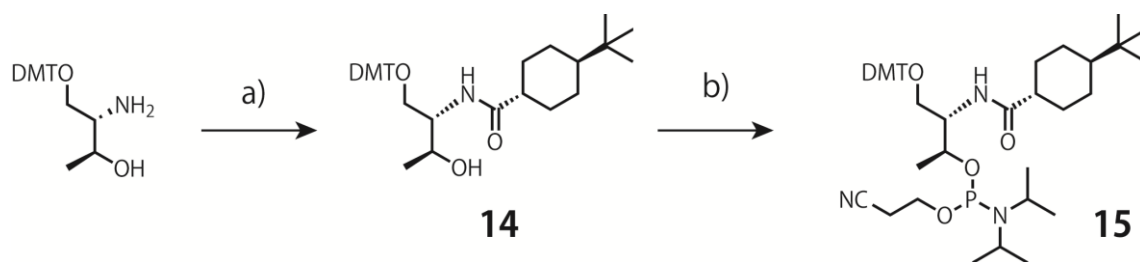


Scheme 3-5. Synthesis of phosphoramidite monomer tethering benzoic acid (**B**). Reagents and conditions: a) benzoic acid, DCC, HOBT, DMF, r.t., overnight, 63%; b) $(iPr)_2NP(Cl)(OCH_2CH_2CN)$, Et_3N , CH_3CN , $0^\circ C \rightarrow r.t.$, 1h, 61 %

The phosphoramidite monomer tethering benzoic acid (**B**) was synthesized as follows: Benzoic acid (215 mg, 1.76 mmol, 1.2 eq) was coupled with DMT-D-threoninol (compound **1**, 0.60 g, 1.47 mmol) in the presence of dicyclohexylcarbodiimide (364 mg, 1.76 mmol, 1.2 eq) and 1-hydroxybenzotriazole (270 mg, 1.76 mmol, 1.2 eq) in 12 mL DMF. After a night of vigorous stirring, the organic solution was washed with saturated aqueous solution of $NaHCO_3$ and of NaCl. The solvent was removed by evaporation, followed by silica gel column chromatography (AcOEt : hexane : $Et_3N = 25:75:3$, $R_f = 0.06$) to afford **12** (0.48 g, yield 63 %). 1H -NMR [$CDCl_3$, 500 MHz] $\delta = 7.82$ -7.46 (m, 5H, benzene ring), 7.39-7.18 (m, 9H, aromatic protons of DMT), 6.85 (d, $J = 8.8$ Hz, 1H, amide) 6.81-6.77 (m, 4H, aromatic protons of DMT), 4.22 (m, 1H), 4.12 (m, 1H), 3.77 (s, 6H), 3.58 (dd, $J = 4$ Hz, 10 Hz, 1H), 3.37 (dd, $J = 4$ Hz, 10 Hz, 1H), 3.19 (br, 1H), 1.21 (d, $J = 6.5$ Hz, 3H). LRMS(FAB) Calcd for $C_{32}H_{33}NO_5$ (M^+) 511.2359. Found 511.

DIPEA (0.4 ml, 2.3 mmol, 5 eq) and 2-cyanoethyl diisopropylchlorophosphoramidite (0.2 ml, 0.94 mmol, 2 eq) were added to a solution of compound **12** (0.24 g, 0.47 mmol) in

CH₃CN (5.0 ml) at 0 °C. After 20 min of vigorous stirring, the solution was stirred for 40 min at room temperature. Then, an excess of AcOEt was added to the reaction mixture and was washed with saturated aqueous solution of NaHCO₃ and of NaCl. After drying over MgSO₄, the solvent was removed by evaporation, followed by silica gel column chromatography (AcOEt : hexane : Et₃N = 20:80:3, *R_f* = 0.11) to afford **13** (0.2 g, yield 61%).

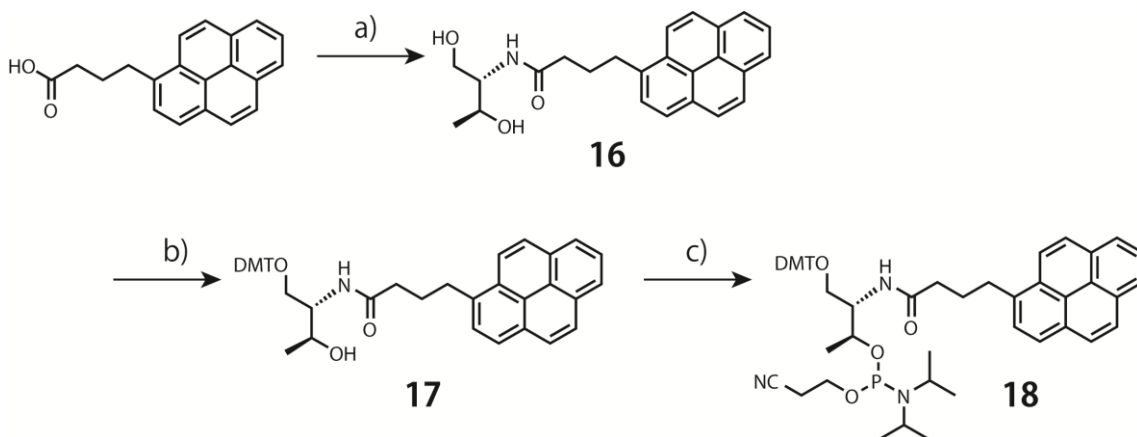


Scheme 3-6. Synthesis of phosphoramidite monomer tethering *trans*-4-*tert*-butylcyclohexanecarboxylic acid (**L**). Reagents and conditions: a) *trans*-4-*tert*-butylcyclohexanecarboxylic acid, DCC, HOBT, DMF, r.t., overnight, 85%; b) (iPr)₂NP(O)Cl, DIPEA, dry CH₃CN, 0 °C → r.t., 1h, 71 %

The phosphoramidite monomer tethering *trans*-4-*tert*-butylcyclohexanecarboxylic acid (**L**) was synthesized as follows: *trans*-4-*tert*-butylcyclohexanecarboxylic acid (190 mg, 1.032 mmol) was coupled with DMT-D-threoninol (compound **1**, 0.35 g, 0.86 mmol) in the presence of dicyclohexylcarbodiimide (213 mg, 1.032 mmol) and 1-hydroxybenzotriazole (158 mg, 1.032 mmol) in DMF (10 mL). After a night of vigorous stirring, the organic solution was washed with saturated aqueous solution of NaHCO₃ and of NaCl. The solvent was removed by evaporation, followed by silica gel column chromatography (AcOEt : hexane : Et₃N = 33:66:3, *R_f* = 0.33) to afford **14** (0.42 g, yield 85 %). ¹H-NMR [CDCl₃, 500 MHz] δ = 7.39-6.83 (m, 13H), 6.16 (d, *J* = 8 Hz, 1H), 4.09 (m, 1H), 3.92 (m, 1H), 3.81 (s, 6H), 3.45 (dd, *J* = 4 Hz, 10 Hz, 1H), 3.26 (dd, *J* = 4 Hz, 10 Hz, 1H), 3.18 (br, 1H), 2.04-1.84 (m, 4H), 1.54-1.42 (m, 2H), 1.12 (d, *J* = 6.5 Hz, 3H), 1.09-0.99 (m, 3H), 0.87 (s, 9H).

DIPEA (0.9 ml, 5.3 mmol) and 2-cyanoethyl-diisopropylchlorophosphoramidite (0.48 ml, 2.1 mmol) were added to a solution of compound **12** (0.61 g, 1.06 mmol) in CH₃CN (10.0 ml) at 0 °C. After 30 min of vigorous stirring, the solution was stirred for 30 min at room temperature. Then, an excess of AcOEt was added to the reaction mixture and was washed with saturated aqueous solution of NaHCO₃ and of NaCl. After drying over

MgSO₄, the solvent was removed by evaporation, followed by silica gel column chromatography (AcOEt : hexane : Et₃N = 33:66:3, *R_f* = 0.26) to afford **15** (0.78 g, yield 71 %).



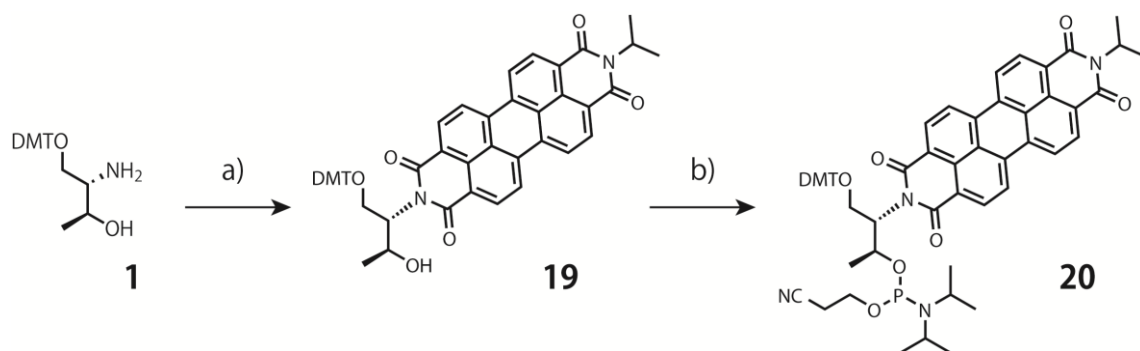
Scheme 3-7. Synthesis of phosphoramidite monomer tethering 1-pyrenebutyric acid (**P**). Reagents and conditions: a) D-threoninol, DCC, HOBT, DMF, r.t., overnight, quant.; b) DMT-Cl, DIPEA, DMAP, CH₂Cl₂, pyridine, 0→r.t., 62 %; c) *(iPr*₂*N)*₂PO(CH₂)₂CN, 1*H*-tetrazole, CH₃CN, 0→r.t., 1.5h, 77 %

The phosphoramidite monomer tethering 1-pyrenebutyric acid (**P**) was synthesized as 1-pyreneacetic acid reported previously (H. Kashida, H. Asanuma, M. Komiyama, *Chem. Commun.* **2006**, 2768-2770): 1-Pyrenebutyric acid (2.53 g, 8.51 mmol) was coupled with D-threoninol (1.00 g, 9.23 mmol) in the presence of dicyclohexylcarbodiimide (2.11 g, 10.2 mmol) and 1-hydroxybenzotriazole (1.38 g, 10.2 mmol) in DMF. After the reaction mixture was stirred at room temperature for 1 week, the solvent was removed and the remained oil was subjected to silica gel column chromatography (CH₃OH : CHCl₃ = 1:5, *R_f* = 0.53) to afford compound **16** (yield quant.). ¹H-NMR [CDCl₃, 500 MHz] δ = 8.16-7.20 (m, 9H, aromatic protons of pyrene), 6.63 (d, 1H, -NHCO-), 5.80 (br, 2H, -CH₂OH, -CH(CH₃)OH), 4.10 (m, 1H, -CH(OH)CH₃), 3.83 (m, 1H, HOCH₂CH(NHCO-)), 3.75 (d, 2H, ³*J*(H,H) = 5 Hz, -CH₂-OH), 3.25 (t, 2H, ³*J*(H,H) = 9 Hz, -CH₂C₁₆H₉), 2.32 (m, 2H, -CH₂CO-), 2.11 (m, 2H, -CH₂-CH₂-CH₂), 1.13 (d, 3H, ³*J*(H,H) = 7 Hz, -CH(OH)CH₃). HRMS(FAB) Calcd for C₂₄H₂₅NO₃ (M⁺) 375.1834. Found 375.1823.

Dry pyridine solution containing **16** (3.20 g, 8.51 mmol) and *N,N*-diisopropylethylamine was cooled on ice under nitrogen. Then, 4,4'-dimethoxytrityl chloride (DMT-Cl) (4.33 g, 12.8 mmol) and 4-(dimethylamino)pyridine (0.13 g, 1.1 mmol) in CH₂Cl₂ was added to the above mixture. After 3 h of vigorous stirring, the solvent

was removed by evaporation, followed by silica gel column chromatography (AcOEt : hexane : Et₃N = 50:50:3, *R_f* = 0.09) to afford **17** (yield 62 %). ¹H-NMR [CDCl₃, 500 MHz] δ = 8.30-6.74 (m, 22H, aromatic protons of DMT, pyrene), 6.07 (d, 1H, -NHCO-), 4.12 (m, 1H, -OCH₂CH(NHCO-)), 3.98 (m, 1H, -CH(OH)CH₃), 3.68 and 3.65 (s, 6H, -C₆H₄-OCH₃), 3.41-3.29 (m, 4H, -CH₂-ODMT, -CH₂C₁₆H₉), 2.36 (m, 2H, -CH₂CO-), 2.23 (m, 2H, -CH₂-CH₂-CH₂-), 1.15 (d, 3H, -CH(OH)CH₃). HRMS(FAB) Calcd for C₄₅H₄₃NO₅ (M⁺) 677.3141. Found 677.3127

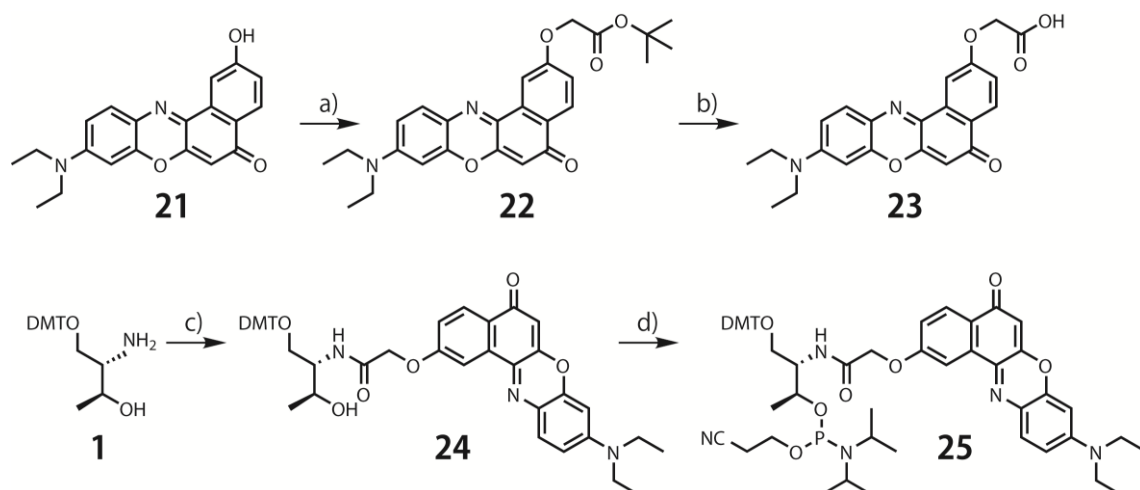
In dry acetonitrile (10 mL) under nitrogen, **17** (0.34 g, 0.50 mmol) and 2-cyanoethyl *N,N,N',N'*-tetraisopropylphosphordiamidite (0.20 g, 0.65 mmol) were reacted with 1*H*-tetrazole (0.046 g, 0.65 mmol). Prior to the reaction, **17** and 1*H*-tetrazole were dried by coevaporation with dry acetonitrile (three times). After 2 h, the product was taken into ethyl acetate. The organic solution was washed with saturated aqueous solution of NaHCO₃ and of NaCl, and dried over MgSO₄. Finally the solvent was removed *in vacuo*, and the oily product **18** was purified by column chromatography (AcOEt: hexane: Et₃N = 50:50:3) and used for the DNA synthesis. ³¹P-NMR [121 MHz, CDCl₃] δ = 148.7, 148.6. HRMS(FAB) Calcd for C₅₄H₆₀N₃O₆P (M⁺) 877.4220. Found 877.4235.



Scheme 3-8. Synthesis of phosphoramidite monomer tethering perylenediimide (**D**): a) perylene-3, 4, 9, 10-tetracarboxylic acid, isopropylamine, $\text{Zn}(\text{OAc})_2 \cdot 2\text{H}_2\text{O}$, Et_3N , pyridine, reflux, 2d, 28 %; b) $(i\text{Pr})_2\text{NP}(\text{Cl})(\text{OCH}_2\text{CH}_2\text{CN})$, Et_3N , CH_2Cl_2 , $0\text{ }^\circ\text{C} \rightarrow \text{r.t.}$, 1h, quant.

The phosphoramidite monomer tethering perylenediimide (**D**) was synthesized as follows: After desiccation of $\text{Zn}(\text{OAc})_2 \cdot 2\text{H}_2\text{O}$ (0.25 g, 1.1 mmol) and molecular sieve 3\AA in oven at $130\text{ }^\circ\text{C}$, dry pyridine solution (20 ml) containing compound **1** (0.23 g, 0.57 mmol), perylene-3, 4, 9, 10-tetracarboxylic acid (0.22 g, 0.57 mmol), $\text{Zn}(\text{OAc})_2$, Et_3N (5.0 ml) and molecular sieve 3\AA was refluxed for 1 day. Then after addition of isopropylamine (1.0 ml, 12 mmol), the reaction mixture was refluxed for 1 day. The solution was filtered and evaporated, the red residue was dissolved by CHCl_3 and the organic solution was washed with 1M KOH aqueous solution. After drying over MgSO_4 , the solvent was removed by evaporation, followed by silica gel column chromatography (CHCl_3 : hexane : Et_3N = 50:50:3, R_f = 0.11) to afford **19** (0.13 g, yield 28 %). $^1\text{H-NMR}$ [CDCl_3 , 500 MHz] δ = 8.66-8.18 (m, 8H), 7.28-6.60 (m, 13H), 5.61 (m, 1H), 5.43 (sept, J = 7 Hz, 1H), 4.40 (m, 2H), 3.86 (dd, J = 9 Hz, 10 Hz, 4H), 3.69 and 3.67 (s, 6H), 3.62 (dd, J = 4 Hz, 10 Hz, 1H), 1.68 and 1.67 (d, J = 7 Hz, 6H), 1.29 (d, J = 6 Hz, 3H). HRMS(FAB) Calcd for $\text{C}_{52}\text{H}_{42}\text{N}_2\text{O}_8$ (M^+) 822.2941. Found 822.2913.

Et_3N (0.56 ml, 4.0 mmol) and 2-cyanoethyl *N,N*-diisopropylchlorophosphoramidite (0.27 ml, 1.2 mmol) were added to a solution of compound **19** (0.33 g, 0.40 mmol) in dry CH_2Cl_2 (10 ml) at $0\text{ }^\circ\text{C}$. After 20 min of vigorous stirring, the solution was stirred for 40 min at room temperature. Then, an excess of CHCl_3 was added to the reaction mixture and was washed with saturated aqueous solution of NaHCO_3 and NaCl . After drying over MgSO_4 , the solvent was removed by evaporation, followed by silica gel column chromatography (AcOEt : hexane : Et_3N = 40:60:3, R_f = 0.44) to afford **20** (yield quant.). $^{31}\text{P-NMR}$ [121 MHz, CDCl_3] δ = 147.0. HRMS(FAB) Calcd for $\text{C}_{61}\text{H}_{59}\text{N}_4\text{O}_9\text{P}$ (M^+) 1022.4020. Found 1022.4019. $\epsilon_{\text{PDI}} = 0.293 \times 10^5 \text{ M}^{-1}\text{cm}^{-1}$



Scheme 3-9. Synthesis of phosphoramidite tethering Nile Red (**R**). Reagents and conditions: a) $\text{ClCH}_2\text{CO}_2^t\text{Bu}$, K_2CO_3 , acetone, reflux, 6h, 74%; b) TFA, Et_3SiH , CH_2Cl_2 , rt, overnight, 86 %; c) PyBOP, DIPEA, CH_2Cl_2 , rt, overnight, 58 %; d) $(i\text{Pr})_2\text{NP}(\text{Cl})(\text{OCH}_2\text{CH}_2\text{CN})$, Et_3N , THF, $0^\circ\text{C} \rightarrow \text{r.t.}$, 1h, 91 %.

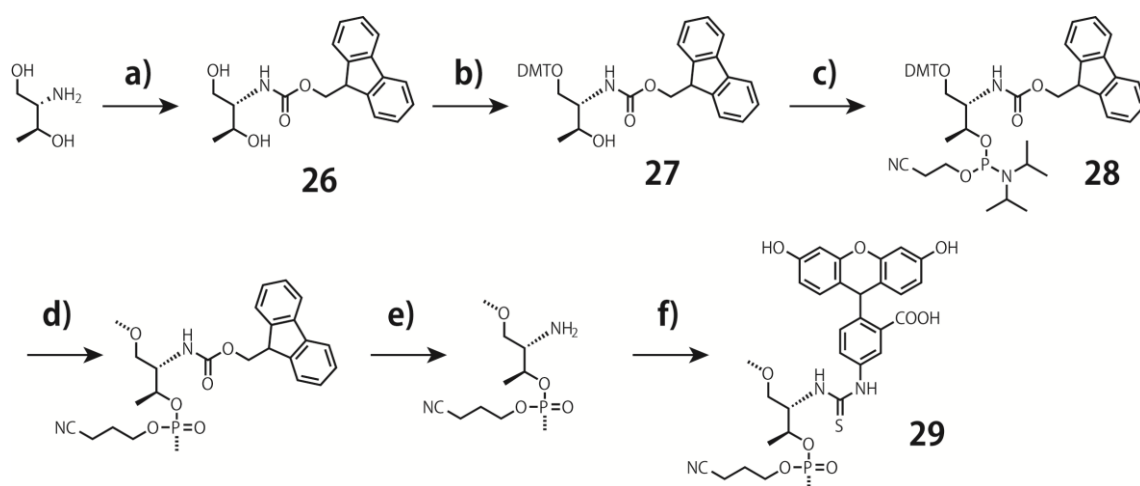
The phosphoramidite monomer tethering Nile Red was synthesized as follows: Compound **21** was synthesized according to the previous report (M. S. J. Briggs, I. Bruce, J. N. Miller, C. J. Moody, A. C. Simmonds and E. Swann, *J. Chem. Soc. Perkin Trans. 1*, 1997, 1051-1058.). Compound **21** (0.73 g, 2.18 mmol), *tert*-butyl chloroacetate (0.63 ml, 4.38 mmol) and potassium carbonate (1.21 g, 8.75 mmol) were dissolved in 10 ml of acetone. After 6 hr of reflux, the solvent was removed *in vacuo*. Then the solid was redissolved in CHCl_3 and washed twice with brine. After drying over MgSO_4 , the solvent was removed by evaporation, followed by silica gel column chromatography ($\text{CHCl}_3 : \text{MeOH} = 20:1$, $R_f = 0.48$) to afford **22** (0.73 g, yield 74 %). $^1\text{H-NMR}$ [CDCl_3 , 500 MHz] $\delta = 8.17$ (d, $J = 9$ Hz, 1H), 7.94 (d, $J = 2.5$ Hz, 1H), 7.47 (d, $J = 9$ Hz, 1H), 7.17 (dd, $J = 2.5$ Hz, 9 Hz, 1H), 6.56 (dd, $J = 3$ Hz, 9 Hz, 1H), 6.34 (d, 2.5 Hz, 1H), 6.22 (s, 1H), 4.69 (s, 2H), 3.38 (q, $J = 7.5$ Hz, 4H), 1.52 (s, 9H), 1.21 (t, $J = 7$ Hz, 6H). $^{13}\text{C-NMR}$ [CDCl_3 , 126 MHz] $\delta = 183.2, 167.8, 160.6, 152.2, 151.0, 147.0, 139.6, 134.2, 131.2, 131.2, 128.0, 127.9, 126.4, 124.9, 118.7, 109.9, 109.7, 106.8, 106.6, 106.0, 105.4, 105.3, 104.8, 96.5, 96.3, 82.9, 66.0, 45.3, 28.3, 12.8$. HRMS(FAB) Calcd for $\text{C}_{26}\text{H}_{29}\text{N}_2\text{O}_5$ ($\text{M} + \text{H}^+$) 449.2076. Found 449.2066.

Trifluoroacetic acid (3.2 ml, 42.4 mmol) was added to a solution of compound **22** (0.73 g, 1.63 mmol) and triethylsilane (1.3 ml, 8.17 mmol) in CH_2Cl_2 (10 ml). After vigorous stirring for overnight, the solvent was removed by evaporation, followed by silica gel column chromatography ($\text{CHCl}_3 : \text{MeOH} : \text{AcOH} = 100:10:1$, $R_f = 0.08$) to afford **23** (0.55

g, yield 86 %). $^1\text{H-NMR}$ [CDCl_3 , 500 MHz] δ = 8.00 (d, J = 9 Hz, 1H), 7.86 (d, J = 2.5 Hz, 1H), 7.55 (d, J = 9 Hz, 1H), 7.22 (dd, J = 3 Hz, 9 Hz, 1H), 6.76 (dd, J = 2.5 Hz, 9.5 Hz, 1H), 6.61 (d, 3 Hz, 1H), 6.15 (s, 1H), 4.77 (s, 2H), 3.38 (q, J = 7 Hz, 4H), 1.16 (t, J = 7 Hz, 6H). HRMS(FAB) Calcd for $\text{C}_{33}\text{H}_{41}\text{NO}_5$ ($\text{M} + \text{H}^+$) 393.1450. Found 393.1434.

Compound **23** (0.55 g, 1.40 mmol) was reacted with PyBOP (0.89 g, 1.71 mmol) in CH_2Cl_2 (5.0 ml) for 10 min. Then, a solution of diisopropylethylamine (5.0 ml) and compound **1** (0.70 g, 1.72 mmol) in CH_2Cl_2 (5.0 ml) were added to the above mixture. After a night of vigorous stirring, the organic solution was washed with saturated aqueous solution of NaHCO_3 . The solvent was removed by evaporation, followed by silica gel column chromatography ($\text{AcOEt} : \text{Et}_3\text{N} = 100 : 3$, $R_f = 0.33$) to afford **24** (0.64 g, yield 58 %). $^1\text{H-NMR}$ [CDCl_3 , 500 MHz] δ = 8.14 (d, J = 8.5 Hz, 1H), 8.00 (d, J = 2.5 Hz, 1H), 7.47 (d, J = 9 Hz, 1H), 7.40 (d, J = 7 Hz, 2H), 7.32 (d, J = 9 Hz, 1H), 7.26 (m, 6H), 7.18 (t, J = 7.5 Hz, 1H), 7.11 (dd, J = 8.5 Hz, 2.5 Hz, 1H), 6.80 (m, 4H), 6.57 (dd, J = 9.5 Hz, 3 Hz, 1H), 6.36 (d, J = 2.5 Hz, 1H), 6.21 (s, 1H), 4.72 (d, J = 9.5 Hz, 1H), 4.67 (d, J = 10 Hz, 1H), 4.09 (m, 1H), 3.73 and 3.72 (s, 6H), 3.44-3.33 (m, 6H), 1.23 (t, J = 7 Hz, 6H), 1.18 (d, J = 8.5 Hz, 3H). HRMS(FAB) Calcd for $\text{C}_{47}\text{H}_{47}\text{N}_3\text{O}_8$ (M^+) 781.3363. Found 781.3337.

DIPEA (0.29 ml, 1.66 mmol) and 2-cyanoethyl-diisopropylchlorophosphoramidite (0.15 ml, 0.66 mmol) were added to a solution of compound **24** (0.26 g, 0.33 mmol) in THF (5.0 ml) at 0 °C. After 20 min of vigorous stirring on ice, the solution was stirred for 40 min at room temperature. Then, an excess of AcOEt was added to the reaction mixture and was washed with saturated aqueous solution of NaHCO_3 and of NaCl. After drying over MgSO_4 , the solvent was removed by evaporation, followed by silica gel column chromatography ($\text{AcOEt} : \text{hexane} : \text{Et}_3\text{N} = 90:10:3$, $R_f = 0.54$) to afford **25** (0.30 g, yield 91 %). $^1\text{H-NMR}$ [CDCl_3 , 500 MHz] δ = 8.23 (d, J = 9 Hz, 1H), 8.09 (m, 1H), 7.47 (d, J = 9 Hz, 1H), 7.57 (d, J = 9 Hz, 1H), 7.42 (m, 1H), 7.30 (m, 6H), 7.20 (m, 1H), 7.14 (m, 1H), 6.88 (m, 1H), 6.79 (m, 4H), 6.68 (m, 1H), 6.46 (m, 1H), 6.31 (s, 1H), 4.71 (m, 2H), 4.36 (m, 1H), 4.30 (m, 1H), 3.76 and 3.75 (s, 6H), 3.47 (m, 8H), 3.29 (m, 1H), 3.19 (m, 1H), 2.37 (t, J = 6.5 Hz, 2H), 1.27 (m, 10H), 1.13-0.97 (m, 11H). $^{31}\text{P-NMR}$ [121 MHz, CDCl_3] δ = 149.5, 147.9. HRMS(FAB) Calcd for $\text{C}_{56}\text{H}_{64}\text{N}_5\text{O}_9\text{P}$ (M^+) 981.4442. Found 981.4436.



Scheme 3-10. Synthesis of DNA strand containing FITC. Reagents and conditions: a) D-threoninol, Fmoc-Cl, THF, triethylamine 0°C→r.t., 17 hr, 73%; b) DMT-Cl, DIPEA, DMAP, CH₂Cl₂, pyridine, 0°C→r.t., 83 %; c) (iPr)₂NP(Cl)(OCH₂CH₂CN), Et₃N, dry CH₃CN, 0°C → r.t., 1.5h, 42 %; d) DNA synthesis on automated DNA synthesizer.; e) DMF, piperidine.; f) FITC, DMF, DIPEA, 3 days.

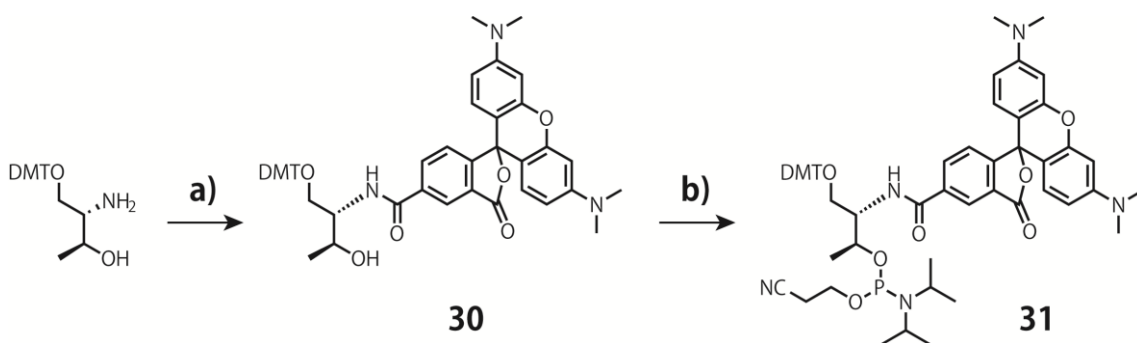
DNA strand containing FITC was prepared by coupling with D-threoninol scaffold after DNA synthesis and Fmoc deprotection. For DNA synthesis, the phosphoramidite monomer tethering Fmoc was synthesized as follows: THF (10 mL) solution of Fmoc-Cl (1.51 g, 5.82 mmol) was added to THF (40 mL) solution D-threoninol (0.51 g, 4.85 mmol) in the presence of triethylamine (4 mL) on ice. After the reaction mixture was stirred on ice for 15 min and at room temperature for 17 hr, the solvent was removed and the remained oil was suspended into certain amount of AcOEt. The organic solution was washed with saturated aqueous solution of NaHCO₃ twice and of NaCl, and dried over MgSO₄. Finally the solvent was removed *in vacuo*, and the oily product was purified by column chromatography (CHCl₃: MeOH = 15:1) to afford **26** (1.44 g, yield 73 %).

Dry pyridine solution containing **26** (1.44 g, 4.22 mmol) and *N,N*-diisopropylethylamine (1.78 ml, 6.33 mmol) was cooled on ice under nitrogen. Then, 4,4'-dimethoxytrityl chloride (DMT-Cl) (1.72 g, 5.06 mmol) and 4-(dimethylamino)pyridine (0.10 g, 0.84 mmol) in CH₂Cl₂ was added drop wise to the above mixture. After 3 h of vigorous stirring, the solvent was removed by evaporation and a certain amount of AcOEt was added. The organic solution was washed with saturated aqueous solution of NaHCO₃ twice and of NaCl, and dried over MgSO₄. Finally the solvent was removed *in vacuo*, and followed by silica gel column chromatography (AcOEt : hexane : Et₃N = 50:50:3) to afford **27** (2.12 g, yield 83 %).

Triethylamine (2.3 ml) and 2-cyanoethyl-diisopropylchlorophosphoramidite (1.1 ml, 5.06 mmol) were added to a solution of compound **27** (2.12 g, 3.37 mmol) in dry CH₃CN (5.0 ml) at 0 °C. After 15 min of vigorous stirring on ice, the solution was stirred for 80 min at room temperature. Then, an excess of AcOEt was added to the reaction mixture and was washed with saturated aqueous solution of NaHCO₃ and of NaCl. After drying over MgSO₄, the solvent was removed by evaporation, followed by silica gel column chromatography (AcOEt : hexane : Et₃N = 100:50:1) to afford **28** (1.16 g, yield 41.5 %).

After DNA synthesis, DMF/piperidine mixture (80:20) was added to CPG tethering DNA strands to deprotect Fmoc. Then organic solution was removed by filtration and washed with DMF and CH₂Cl₂, DMF (450 μL) solution of FITC (100 μmol, 38.9 μg) with 50 μL DIPEA was added to CPG and vigorously stirred for 3 days to afford **29**.

ϵ_{260} of FITC = $0.209 \times 10^5 \text{ } \mu\text{L cm}^{-1} \text{ mol}^{-1}$.



Scheme 3-11. Synthesis of phosphoramidite monomer tethering TAMRA (**R**). Reagents and conditions: a) TAMRA, PyBOP, DIPEA, CH₂Cl₂, rt, overnight.; b) (*i*Pr)₂NP(Cl)(OCH₂CH₂CN), DIPEA, dry CH₃CN, 0 °C → r.t., 1h, 71 %

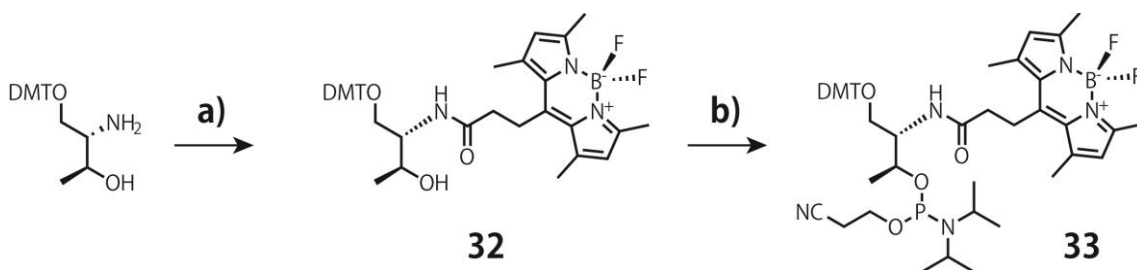
The phosphoramidite monomer tethering TAMRA (**R**) was synthesized as follows: TAMRA-COOH was synthesized according to previous literatures. (Maksim V. Kvach, Irina A. Stepanova, Igor A. Prokhorenko and Aleksander P. Stupak *et al.*, *Bioconjugate Chem.*, **2009**, *20*, 1673-1682. Bashar Mullah and Alex Andrus, *Tetrahedron Letters*, **1997**, *38*, 5751-5754.)

TAMRA-COOH (215 mg, 0.5 mmol) was reacted with PyBOP (260 mg, 0.5 mmol) in DMF for 5 min. Then, a solution of diisopropylethylamine (5.0 ml) and compound **1** (203 mg, 0.5 mmol) in DMF (5.0 ml) were added to the above mixture. After a night of vigorous stirring, the solvent was removed by evaporation and an excess of CHCl₃ was added and the organic solution was washed with saturated aqueous solution of NaHCO₃

and of NaCl. After drying over MgSO₄, the solvent was removed by evaporation, followed by silica gel column chromatography (acetone : MeOH = 1:1, *R_f* = 0.25) to afford **30** (0.05 g, yield 13%). ¹H-NMR [CDCl₃, 500 MHz] δ = 1.25 (d, *J* = 6.5 Hz, 3H), 3.00 (s, 12H), 3.45 (dd, *J* = 9.5, 4 Hz, 1H), 3.57 (dd, *J* = 10, 4.5 Hz, 1H), 3.78 (d, *J* = 1.0, 6H), 4.18 (m, 1H), 4.26 (dq, *J* = 6.5, 2.5 Hz, 1H), 6.39 (dd, *J* = 5.0, 2.5 Hz, 2H), 6.49 (d, *J* = 2.5 Hz, 2H), 6.57 (d, *J* = 11.0, 2H), 6.92 (d, *J* = 8.5 Hz, 1H), 7.20-7.24 (m, 1H), 8.13 (dd, *J* = 8.0, 1.5 Hz, 1H), 8.35 (d, *J* = 1.0, 1H), 7.0-7.6 (m, DMT-13H).

2-Cyanoethyl-diisopropylchlorophosphoramidite (0.13 ml, 0.6 mmol, 2 eq) and triethylamine (0.2 ml, 1.5 mmol, 5 eq) were added to a solution of compound **30** (0.05 g, 0.3 mmol) in dry CH₂Cl₂ (1.0 ml) at 0 °C. After 20 min of vigorous stirring, the solution was stirred for 40 min at room temperature. Then, an excess of CHCl₃ was added to the reaction mixture and was washed with saturated aqueous solution of NaHCO₃ and of NaCl. After drying over MgSO₄, the solvent was removed by evaporation, followed by silica gel column chromatography (acetone, *R_f* = 0.40) to afford **31** (0.2 g, yield 65%).

ε₂₆₀ of TAMRA = 0.323 × 10⁵ μL cm⁻¹ mol⁻¹.



Scheme 3-12. Synthesis of phosphoramidite monomer tethering BODIPY (**B**). Reagents and conditions: a) BODIPY, PyBOP, DIPEA, CH₂Cl₂, rt, overnight.; b) (iPr)₂NP(Cl)(OCH₂CH₂CN), DIPEA, dry CH₃CN, 0 °C → r.t., 1h, 71 %.

The phosphoramidite monomer tethering TAMRA (**R**) was synthesized as follows: BODIPY-COOH was synthesized according to previous literatures. (Dongchuan Wang, Jiangli Fan, Xinqin Gao and Bingshuai Wang *et al.*, *J. Org. Chem.*, **2009**, *74*, 7675-7683. Kha Tram, Daniel Twohig and Hongbin Yan, *Nucleosides, Nucleotides and Nucleic Acids*, **2011**, *30*, 1-11.)

BODIPY-COOH (320 mg, 1 mmol) was reacted with PyBOP (520 mg, 1 mmol) in DMF for 5 min. Then, a solution of diisopropylethylamine (5.0 ml) and compound **1** (406 mg, 1 mmol) in DMF (5.0 ml) were added to the above mixture. After a night of vigorous stirring, an excess of AcOEt was added to the reaction mixture and was washed with

saturated aqueous solution of NaHCO₃ and of NaCl. After drying over MgSO₄, the solvent was removed by evaporation, followed by silica gel column chromatography (AcOEt : hexane : Et₃N = 1:2) to afford **32** (0.24 g, yield 78.9%). ¹H-NMR [CDCl₃, 500 MHz] δ = 1.12 (d, 3H), 2.43 (s, 6H), 2.51 (s, 6H), 2.74 (t, 2H), 3.06 (t, 2H), 3.32 (m, 1H), 3.46 (m, 1H), 3.76 (d, 6H), 4.12 (m, 1H), 6.06 (s, 2H), 6.15 (d, 1H), 6.81 (m, 4H), 7.27 (m, 7H), 7.36 (m, 2H).

2-Cyanoethyldiisopropylchlorophosphoramidite (0.35 ml, 1.58 mmol, 2 eq) and triethylamine (0.55 ml, 3.95 mmol, 5 eq) were added to a solution of compound **30** (0.24 g, 0.79 mmol) in THF (1.0 ml) at 0 °C. After 20 min of vigorous stirring, the solution was stirred for 40 min at room temperature. Then, an excess of AcOEt was added to the reaction mixture and was washed with saturated aqueous solution of NaHCO₃ and of NaCl. After drying over MgSO₄, the solvent was removed by evaporation, followed by silica gel column chromatography (AcOEt : hexane = 1:1, *R_f* = 0.40) to afford **31** (0.42 g, yield 58%).

ϵ_{260} of BODIPY = $0.0167 \times 10^5 \text{ } \mu\text{L cm}^{-1} \text{ mol}^{-1}$.

3-6 References

- (1) Schweitzer, B. A. and Kool, E. T. *J. Am. Chem. Soc.*, **1995**, *117*, 1863–1872.
- (2) Brotschi, C.; Häberli, A.; Leumann, C. *Angew. Chem., Int. Ed.*, **2001**, *40*, 3012-3014.
- (3) Liu, H.; Gao, J.; Lynch, S. R.; Saito, Y. D.; Maynard L.; Kool, E. T. *Science*, **2003**, *302*, 868-871.
- (4) Minakawa, N.; Kojima, N.; Hikishima, S.; Sasaki, T.; Kiyosue, A.; Atsumi, N.; Ueno, Y.; Matsuda, A. *J. Am. Chem. Soc.*, **2003**, *125*, 9970-9982.
- (5) Matsuda, S.; Romesberg, F. E. *J. Am. Chem. Soc.*, **2004**, *126*, 14419-14427.
- (6) Amann, N.; Huber, R.; Wagenknecht, H. A. *Angew. Chem., Int. Ed.*, **2004**, *43*, 1845-1847.
- (7) Yang, Z.; Hutter, D.; Sheng, P.; Sismour, A. M.; Benner, S. A. *NucleicAcids Res.*, **2006**, *34*, 6095-6101.
- (8) Hirao, I.; Mitsui, T.; Kimoto M.; Yokoyama, S. *J. Am. Chem. Soc.*, **2007**, *129*, 15549-15555.
- (9) Hainke S.; Seitz, O. *Angew. Chem., Int. Ed.*, **2009**, *48*, 8250–8253.
- (10) Kaufmann, M.; Gisler M.; Leumann, C. J. *Angew. Chem., Int. Ed.*, **2009**, *48*, 3810-3813.
- (11) Lewis, F. D.; Wu, T.; Burch, E. L.; Bassani, D. M.; Yang, J.-S.; Schneider, S.; Jaeger W.; Letsinger, R. L. *J. Am. Chem. Soc.*, **1995**, *117*, 8785–8792.
- (12) Lewis, F. D.; Zhang Y.; Letsinger, R. L. *J. Am. Chem. Soc.*, **1997**, *119*, 5451–5452.
- (13) Langenegger, S. M.; Häner, R. *Helv. Chim. Acta*, **2002**, *85*, 3414–3421.
- (14) Christensen, U. B.; Pedersen, E. B. *Helv. Chim. Acta*, **2003**, *86*, 2090–2097.
- (15) Christensen, U. B.; Pedersen, E. B. *Nucleic Acids Res.*, **2002**, *30*, 4918–4925.
- (16) Langenegger, S. M.; Häner, R. *Chem. Commun.*, **2004**, 2792–2793.
- (17) Hrdlicka, P. J.; Babu, B. R.; Sorensen, M. D.; Harrit N.; Wengel, J. *J. Am. Chem. Soc.*, **2005**, *127*, 13293–13299.
- (18) Häner, R.; Garo, F.; Wenger, D.; Malinovskii, V. L. *J. Am. Chem. Soc.*, **2010**, *132*, 7466–7471.

- (19) Kashida, H.; Liang, X. G.; Asanuma, H. *Curr. Org. Chem.*, **2009**, *13*, 1065–1084.
- (20) Benner, S. A. *Acc. Chem. Res.*, **2004**, *37*, 784–797.
- (21) Tanaka, K.; Shionoya, M. *Chem. Lett.*, **2006**, *35*, 694–699.
- (22) Krueger, A. T.; Kool, E. T. *Curr. Opin. Chem. Biol.*, **2007**, *11*, 588–594.
- (23) Štambaský, J.; Hocek M.; Kočovský, P. *Chem. Rev.*, **2009**, *109*, 6729–6764.
- (24) Malinovskii, V. L.; Wenger, D.; Häner, R. *Chem. Soc. Rev.*, **2010**, *39*, 410–422.
- (25) Wilson, J. N.; Cho, Y.; Tan, S.; Cuppoletti, A.; Kool, E. T. *ChemBioChem* **2008**, *9*, 279 – 285.
- (26) Kashida, H.; Sekiguchi, K.; Liang, X.G.; Asanuma, H. *J. Am. Chem. Soc.* **2010**, *132*, 6223 –6230.
- (27) Liu, M.; Mao, X.-A.; Ye, C.; Huang, H.; Nicholson J. K.; Lindon, J. C. *J. Magn. Reson.*, **1998**, *132*, 125–129.
- (28) Schuster, G. B. *Acc. Chem. Res.*, **2000**, *33*, 253–260.
- (29) Lewis, F. D.; Letsinger R. L.; Wasielewski, M. R. *Acc. Chem. Res.*, **2000**, *34*, 159–170.
- (30) Giese, B. *Annu. Rev. Biochem.*, **2002**, *71*, 51–70.
- (31) Wagenknecht, H.-A. *Nat. Prod. Rep.*, **2006**, *23*, 973–1006.
- (32) Genereux, J. C.; Barton, J. K. *Chem. Rev.*, **2010**, *110*, 1642–1662.
- (33) Manoharan, M.; Tivel, K. L.; Zhao, M.; Nafisi, K.; Netzel, T. L. *J. Phys. Chem.*, **1995**, *99*, 17461–17472.
- (34) Paris, P. L.; Langenhan, J. M.; Kool, E. T. *Nucleic Acids Res.*, **1998**, *26*, 3789–3793.
- (35) Yamana, K.; Iwai, T.; Ohtani, Y.; Sato, S.; Nakamura, M.; Nakano, H. *Bioconjugate Chem.*, **2002**, *13*, 1266–1273.
- (36) Fujimoto, K.; Shimizu, H.; Inouye, M. *J. Org. Chem.*, **2004**, *69*, 3271–3275.
- (37) Okamoto, A.; Kanatani, K.; Saito, I. *J. Am. Chem. Soc.*, **2004**, *126*, 4820–4827.
- (38) Raunkjær, M.; Haselmann, K. F.; Wengel, J. *J. Carbohydr. Chem.*, **2005**, *24*, 475–502.

- (39) Kashida, H.; Asanuma, H.; Komiyama, M. *Chem. Commun.*, **2006**, 2768–2770.
- (40) Kashida, H.; Takatsu, T.; Sekiguchi, K.; Asanuma, H. *Chem. Eur. J.*, **2010**, *16*, 2479–2486.
- (41) Kashida, H.; Sekiguchi, K.; Higashiyama, N.; Kato, T.; Asanuma, H. *Org. Biomol. Chem.*, **2011**, *9*, 8313–8320.
- (42) Würthner, F. *Chem. Commun.* **2004**, 1564 – 1579.
- (43) De Schryver, F. C.; Vosch, T.; Cotlet, M.; Van der Auweraer, M.; Mullen, K.; Hofkens, J. *Acc. Chem. Res.* **2004**, *37*, 514 –522.
- (44) Zang, L.; Che, Y.; Moore, J. S. *Acc. Chem. Res.* **2008**, *41*, 1596 – 1608.
- (45) Bevers, S.; O’Dea, T. P.; McLaughlin, L. W. *J. Am. Chem. Soc.* **1998**, *120*, 11004 – 11005.
- (46) Bevers, S.; Schutte, S.; McLaughlin, L. W. *J. Am. Chem. Soc.* **2000**, *122*, 5905 – 5915.
- (47) N. Rahe, C. Rinn, T. Carell, *Chem. Commun.* **2003**, 2120 –2121.
- (48) Wang, W.; Wan, W.; Zhou, H.-H.; Niu, S.; Li, A. D. Q. *J. Am. Chem. Soc.* **2003**, *125*, 5248 –5249.
- (49) Abdalla, M. A.; Bayer, J.; Rädler, J. O.; Müllen, K. *Angew. Chem.* **2004**, *116*, 4057 – 4060; *Angew. Chem. Int. Ed.* **2004**, *43*, 3967 –3970.
- (50) Wagner, C.; Wagenknecht, H.-A. *Org. Lett.* **2006**, *8*, 4191 – 4194.
- (51) Baumstark, D.; Wagenknecht, H.-A. *Angew. Chem.* **2008**, *120*, 2652 – 2654; *Angew. Chem. Int. Ed.* **2008**, *47*, 2612 – 2614.
- (52) Zheng, Y.; Long, H.; Schatz, G. C.; Lewis, F. D. *Chem. Commun.* **2006**, 3830 – 3832.
- (53) Zeidan, T. A.; Carmieli, R.; Kelley, R. F.; Wilson, T. M.; Lewis, F. D.; Wasielewski, M. R. *J. Am. Chem. Soc.* **2008**, *130*, 13945 –13955.
- (54) Bouquin, N.; Malinovskii, V. L.; Häner, R. *Chem. Commun.* **2008**, 1974 – 1976.
- (55) Lewis, F. D.; Zhu, H.; Daublain, P.; Cohen, B.; Wasielewski, M. R.; *Angew. Chem. Int. Ed.* **2006**, *45*, 7982-7985.

3-7 Appendixes

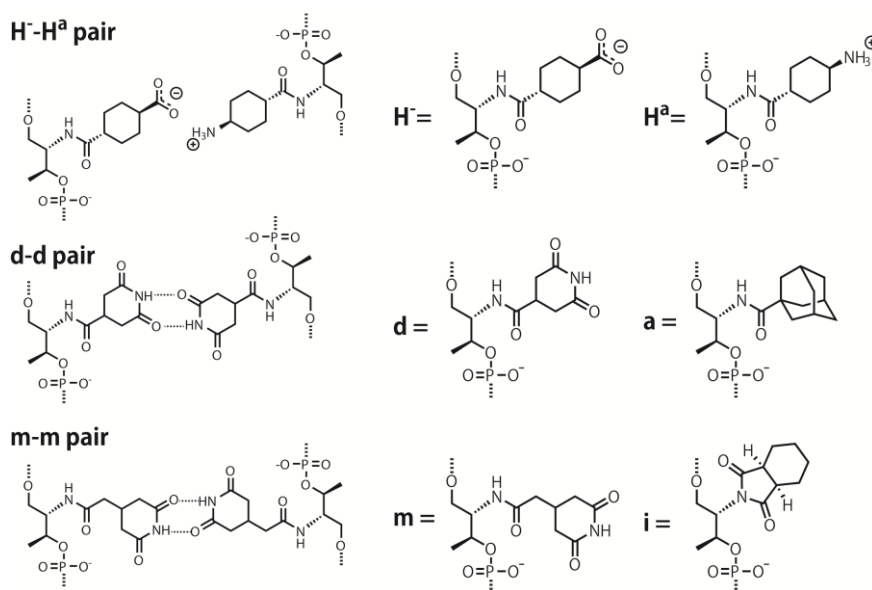
3-7-1 Other miscellaneous insulators

Here, other miscellaneous insulators developed for shielding dye-dye interaction were summarized. **H⁻** and **H^a** contain anionic and cationic groups, respectively. These insulators were designed to form pair by electrostatic interaction. Formation of pair would restrict mobility of cyclohexane moiety and improve shielding efficiency between dyes. Similarly, **m** and **d**, which are mimicking dihydrouracil group, can form a pair themselves by hydrogen bonding. Those 4 insulator “base pairs” are worthy of the name since they have recognition sites and the pairs can be formed via hydrogen bonding or electrostatic interaction in addition to hydrophobic interaction. **a** carries adamantane, which has bulkier and more hydrophobic structure. This bulky group would reduce a space to move and be strongly incorporated within duplex by hydrophobicity. For **i** moiety, cyclohexane was conjugated via imide ring to enhance rigidity since amide bond allows rotation of cyclohexane group.

Table 3-17. Sequences of synthesized DNA in this section.

Name	Sequence	Representation
<i>X1a/X1b</i>	5' -GGTATC X GCAATC-3' 3' -CCATAG X CGTTAG-5'	
<i>X2Pa/X2b</i>	5' -GGTATC XPX GCAATC-3' 3' -CCATAG X X CGTTAG-5'	
<i>X3Pa/X3Pb</i>	5' -GGTATC XPX X GCAATC-3' 3' -CCATAG X XPX CGTTAG-5'	

“**X**” corresponds to various insulators as shown below.



The thermodynamic stabilities of various insulators were summarized in Table 3-18. **H-H^a**, **m-m**, **d-d** and **i-i** pairs destabilized duplex significantly. Since **H-H^a**, **m-m** and **d-d** pairs are relatively more hydrophilic than **H-H** pair, these insulators could not form stable “base pairs” inside of DNA. Hydrophobicity of insulator is very important to form stable pair within DNA duplex as discussed in Table 3-2. Those moieties may be flipped out from the duplex, therefore electrostatic bonding and hydrogen bonding would not be formed. For **i-i** pair, as **i** moiety was too short to form pair and imide bond would roll toward helical axis, the duplex structure may be inclined and destabilized. In contrast, **a1a/a1b** containing one **a-a** pair was more stabilized than **H-H** pair due to stronger hydrophobicity of adamantane, however, the duplex was still slightly destabilized comparing with native duplex.

The shielding ability of various insulators was judged from fluorescence and UV-Vis spectra (Figure 3-18). **H-H^a**, **m-m**, **d-d** and **i-i** pairs could not exhibit sufficient shielding abilities, however, these 4 pairs showed blue-shifted bands in UV-Vis spectra. Hence static interaction between pyrene and nucleobases were disturbed by insulator moieties, however, unstable structure around pyrene would be cause dynamic contact between pyrene and nucleobases. **H2Pa/H^a2b** showed largely blue-shifted spectrum around pyrene, this may be because pyrene was almost completely flipped out from the duplex owing to disruption of structure around pyrene caused by electric repulsion between **H** and phosphate back bone. On the other hand, **a-a** pair showed good shielding effect as high as **H-H** pairs. Unexpectedly, bulkiness of insulator moiety did not largely influence on the shielding ability.

Table 3-18. Thermodynamic stabilities of modified DNA.

Sequence	$T_m / ^\circ\text{C}^a$	$\Delta T_m / ^\circ\text{C}^b$
H1a/H1b	44.9	-2.8
H1a/H^a1b	29.5	-18.2
m1a/m1b	31.4	-16.3
d1a/d1b	29.5	-18.2
a1a/a1b	45.9	-1.8
i1a/i1b	31.3	-16.4

^a: Solution conditions: [DNA] = 5 μM each, [NaCl] = 100 mM, pH 7.0 (10 mM phosphate buffer). ^b: The difference of T_m values between modified ODNs and native duplex **Nt/S0** (47.7 $^\circ\text{C}$).

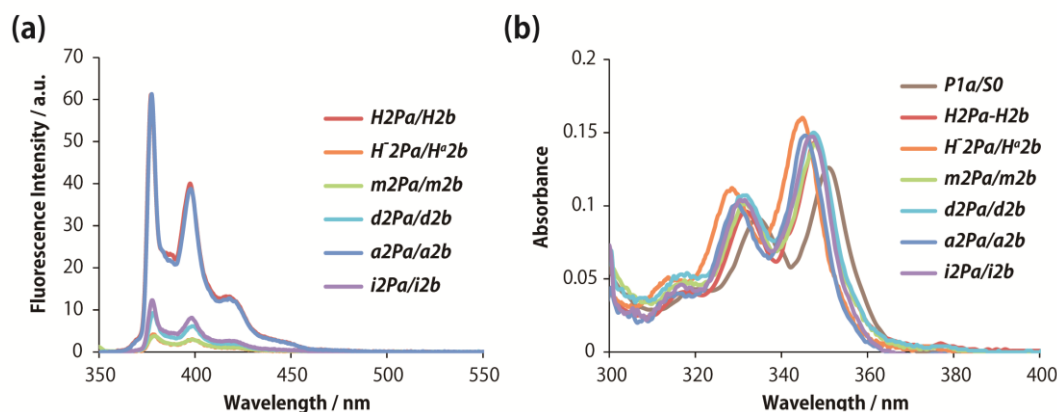


Figure 3-18. Spectrum behaviors of synthesized DNA containing various insulator base pairs with a Pyrene moiety. (a) Fluorescence spectra of modified DNAs. Solution conditions were as follows: [DNA] = 1.0 μ M each, [NaCl] = 100 mM, pH 7.0 (10 mM Phosphate buffer), 20°C. Excitation wavelength: 345 nm. (b) UV-Vis spectra of modified DNAs. Solution conditions were as follows: [DNA] = 5 μ M each, [NaCl] = 100 mM, pH 7.0 (10 mM Phosphate buffer), 20°C.

Table 3-19. Spectroscopic behaviors and thermodynamic stabilities of modified DNA.

Sequence	Relative Intensity ^a	λ_{\max} / nm ^b	T_m / °C ^c	ΔT_m / °C ^d
<i>H2Pa/H2b</i>	1	346	48.5	+0.8
<i>H'2Pa/H'2b</i>	0.07	345	31.6	-16.1
<i>m2Pa/m2b</i>	0.06	348	30.0	-17.7
<i>d2Pa/d2b</i>	0.16	348	28.7	-19.0
<i>a2Pa/a2b</i>	1.02	345	45.5	-2.2
<i>i2Pa/i2b</i>	0.21	347	29.9	-17.8

a: Emission intensity at 378 nm relative to that of **H2Pa/H2b**. Solution conditions: [DNA] = 1 μ M each, [NaCl] = 100 mM, pH 7.0 (10 mM phosphate buffer), 20°C. Excitation wavelength: 345 nm. *b:* Absorption maxima of pyrene in the UV-Vis spectra at 20°C. *c:* Solution conditions: [DNA] = 5 μ M each, [NaCl] = 100 mM, pH 7.0 (10 mM phosphate buffer). *d:* The difference of T_m values between modified ODNs and native duplex **Nt/S0** (47.7 °C).

Shielding ability between dyes were also tested (Figure 3-19). **H-H^a**, **a-a** and **i-i** pairs could not shield interaction between dyes. For **a-a** and **i-i** pairs, monomer emission was also largely quenched due to interaction between nucleobases and pyrene since structure around pyrene may be disordered by insulators. Especially in the case of **a3Pa/a3Pb**, excimer emission was very low but monomer emission was not recovered enough. T_m of **a3Pa/a3Pb** was as high as 57.2, the duplex was greatly stabilized by **a-a** pair suggesting that bulky **a** moieties would filled the middle of duplex and it could disturb contact between pyrenes, however, pyrenes may be flipped out and contact with nucleobases. As a result, **a** moiety was too bulky to align with pyrene in DNA duplex.

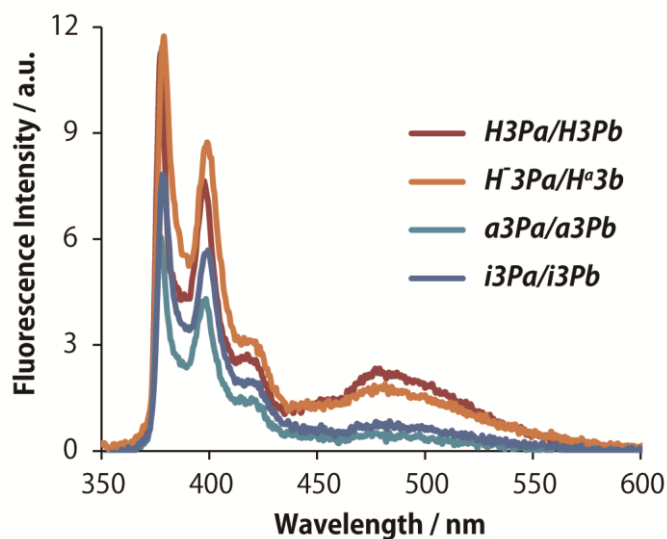


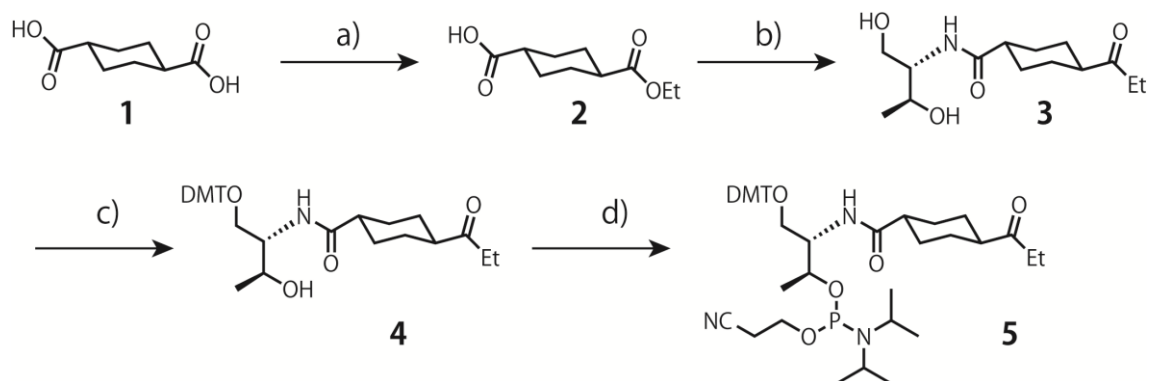
Figure 3-19. Fluorescence spectra of modified DNA containing various insulator base pairs with two Pyrene moieties. Solution conditions were as follows: [DNA] = 1.0 μ M each, [NaCl] = 100 mM, pH 7.0 (10 mM Phosphate buffer), 20°C. Excitation wavelength: 345 nm.

Table 3-20. Spectroscopic behaviors and thermodynamic stabilities of modified DNA.

Sequence	Relative Monomer Intensity ^a	Relative Excimer Intensity ^b	Monomer/Excimer Ratio ^c	$T_m / ^\circ\text{C}^d$	$\Delta T_m / ^\circ\text{C}^e$
<i>H3Pa/H3Pb</i>	1	1	4.8	55.0	+7.3
<i>H3Pa/H3b</i>	1.04	0.81	6.4	33.4	-14.3
<i>a3Pa/a3Pb</i>	0.54	0.23	11.8	57.2	+9.5
<i>i3Pa/i3Pb</i>	0.70	0.31	11.1	33.5	-14.2

a: Emission intensity at 378 nm relative to that of **H2Pa/H2Pb**. Solution conditions: [DNA] = 1 μ M each, [NaCl] = 100 mM, pH 7.0 (10 mM phosphate buffer), 20°C. Excitation wavelength: 345 nm. *b*: Emission intensity at 478 nm relative to that of **H2Pa/H2Pb**. *c*: Relative ratio of the monomer emission intensity at 378 nm / excimer emission intensity at 478 nm. *d*: Solution conditions: [DNA] = 5 μ M each, [NaCl] = 100 mM, pH 7.0 (10 mM phosphate buffer). *e*: The difference of T_m values between modified ODNs and native duplex **Nt/S0** (47.7 °C).

Synthesis of insulators



Scheme 3-13. Synthesis of phosphoramidite monomer tethering Cyclohexane-1,4-dicarboxylic acid monoethyl ester (**H⁻**). Reagents and conditions: a) HOBt, DMAP, DMF, EtOH, DCC, r.t., 24 hr, crude.; b) D-threoninol, DCC, HOBt, DMF, r.t. 24 hr, 9.5%.; c) DMT-Cl, DIPEA, DMAP, CH₂Cl₂, pyridine, 0 °C → r.t., 62 %.; d) (*i*Pr)₂NP(=O)(OCH₂CH₂CN), Et₃N, dry CH₃CN, 0 °C → r.t., 1h, 93 %

The phosphoramidite monomer tethering Cyclohexane-1,4-dicarboxylic acid monoethyl ester (**H⁻**) was synthesized as follows:

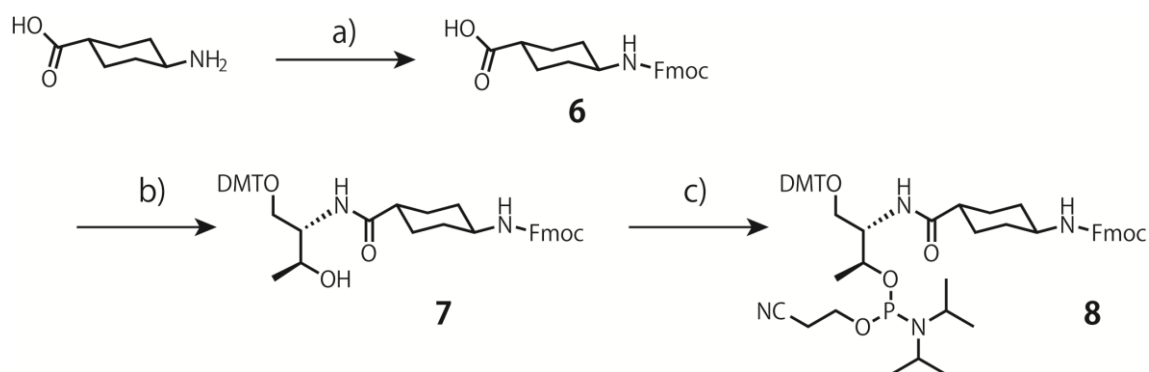
trans-1,4-cyclohexane dicarboxylic acid, compound **1** 1.72 g (10.0 mmol) was dissolved into 50 mL of DMF in the presence of HOBt 1.35 g (10.0 mmol, 1.0 eq.) and DMAP 1.22 g (10.0 mmol, 1.0 eq.). EtOH 17.5 ml (300 mmol, 30 eq.) and DCC 2.06 g (10.0 mmol, 1.0 eq.) were added to the above mixture. After vigorous stirring for 24 hr, the mixture was filtered and the solvent was removed by evaporation. Then, an excess of AcOEt was added and the organic solution was washed with 1N HCl aq. three times. After drying over MgSO₄, the solvent was removed by evaporation to afford **2** (crude).

The compound **2** (10.0 mmol, 1.05 eq.) was coupled with D-threoninol 1.00 g (9.51 mmol) in the presence of HOBt 1.35 g (10.0 mmol, 1.05 eq.) and DCC 2.06 g (10.0 mmol, 1.05 eq.) in DMF (100 mL). After the reaction mixture was stirred at room temperature for 24 hr, the mixture was filtered and the solvent was removed by evaporation. Then, an excess of AcOEt was added and the organic solution was washed with NaHCO₃ aq. and brine. After drying over MgSO₄, the solvent was removed by evaporation, followed by silica gel column chromatography (CHCl₃ : MeOH = 10:1) to afford **3** (0.26 g, yield 9.5 %). HRMS [FAB]: Obsd. 288.1781 (Calcd. for C₁₄H₂₆NO₅ [M+H⁺]: 288.1811), ¹H-NMR [CDCl₃, 500 MHz]: δ = 6.20 (d, *J* = 8.0 Hz, 1H), 4.19 (m, 1H), 4.13 (q, *J* = 7.0 Hz, 2H), 3.87-3.80 (m, 3H), 2.61 (br, 1H), 2.54 (br, 1H), 2.33-2.26 (m, 1H), 2.20-2.14 (m, 1H), 2.10-2.06 (m, 2H), 2.02-1.97 (m, 2H), 1.60-1.44 (m, 4H), 1.26 (t, *J* = 7.0 Hz, 3H), 1.20 (d, *J* = 6.5 Hz, 3H).

Dry pyridine (10 mL) solution containing **3** (0.43 g, 1.50 mmol) and *N,N*-diisopropylethylamine (0.297 ml, 1.80 mmol) was cooled on ice under nitrogen. Then, 4,4'-dimethoxytrityl chloride (DMT-Cl) (0.610 g, 1.80 mmol) and 4-(dimethylamino)pyridine (0.022 g, 0.18 mmol) in CH₂Cl₂ (5 mL) was added to the above mixture. After 3 h of vigorous stirring, the solvent was removed by evaporation, followed by silica gel column chromatography (AcOEt : hexane : Et₃N = 40:60:3) to afford **4** (0.55 g, 0.93 mmol, yield 62 %). HRMS [FAB]: Obsd. 589.3044 (Calcd. for C₃₅H₄₃NO₇ [M⁺]: 589.3040), ¹H-NMR [CDCl₃, 500 MHz]: δ = 7.38-6.82 (m, 13H), 6.10 (d, *J* = 8.5 Hz, 1H), 4.13 (q, *J* = 7.0 Hz, 2H), 4.09 (m, 1H), 3.90 (m, 1H), 3.79 (s, 6H), 3.42 (dd, *J* = 9.5 Hz, 4.0 Hz, 1H), 3.28 (dd, *J* = 9.5 Hz, 3.5 Hz, 1H), 3.09 (br, 1H), 2.30 (m, 1H), 2.12-2.06 (m, 3H), 2.00-1.94 (m, 2H), 1.58-1.46 (m, 4H), 1.26 (t, *J* = 7.0 Hz, 3H), 1.12 (d, *J* = 7.0 Hz, 3H).

Et₃N (0.125 ml, 9.0 mmol) and 2-cyanoethyldiisopropylchlorophosphoramidite (0.134 ml, 0.6 mmol) were added to a solution of compound **4** (0.177 g, 0.3 mmol) in dry CH₃CN (6 ml) at 0 °C. After 20 min of vigorous stirring, the solution was stirred for 40 min at room temperature. Then, an excess of AcOEt was added to the reaction mixture and was washed with saturated aqueous solution of NaHCO₃ and of NaCl. After drying over MgSO₄, the solvent was removed by evaporation, followed by silica gel column chromatography (AcOEt : hexane : Et₃N = 40:60:3) to afford **5** (0.22 g, yield 93 %). HRMS [FAB]: Obsd. 812.4022 (Calcd. for C₄₄H₆₀N₃O₈PNa [M+Na⁺]: 812.4016), ³¹P-NMR [CD₃CN, 121 MHz]: δ = 148.9, 148.3.

After DNA synthesis, to avoid reactions with ammonia, the deprotection was performed as follows. CPG was treated with the mixture (1 mL) of 0.4 M NaOH H₂O / Methanol (H₂O : Methanol = 1 : 4) at room temperature for 17 hr. After that, 1.5 mL 2.0 M TEAA and 13.5 mL of water were added to neutralize the solution followed by purification by PolyPack II.



Scheme 3-14. Synthesis of phosphoramidite monomer tethering 4-(9H-Fluoren-9-ylmethoxy carbonylamino)-cyclohexanecarboxylic acid (**H^a**). Reagents and conditions: a) Fmoc-Cl, NaHCO₃ aq., 1,4-dioxane, overnight, quant.; b) DMT-D-threoninol, PyBOP, Et₃N, DMF, r.t., overnight, quant; b) (*i*Pr)₂NP(O)(Cl)(OCH₂CH₂CN), Et₃N, dry THF, 0 °C → r.t., 1h, 46 %

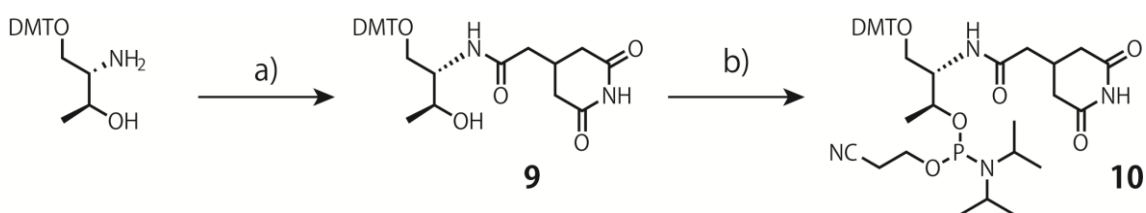
The phosphoramidite monomer tethering 4-(9H-Fluoren-9-ylmethoxycarbonylamino)-cyclohexanecarboxylic acid (**H^a**) was synthesized as follows:

trans-4-Aminocyclohexane carboxylic acid 1.00 g (6.98 mmol) was dissolved into NaHCO₃ aq. (80 ml) and 120 mL of 1,4- dioxane was added to the solution. Fmoc-Cl 2.17 g (8.38 mmol, 1.2 eq.) was added and the mixture was stirred for overnight at room temperature. After removing 1,4-dioxane by evaporation, HCl was added to acidify the solution. The precipitate was filtered and washed with EtOH to afford **6** (2.60 g, 7.11 mmol yield quant). HRMS [FAB]: Obsd. 366.1703 (Calcd. for C₂₂H₂₄NO₄ [M+H⁺]: 366.1705), ¹H-NMR [DMSO, 500 MHz]: δ = 7.93 (d, *J* = 7.5 Hz, 2H), 7.73 (d, *J* = 7.5 Hz, 2H), 7.45 (t, *J* = 7.5 Hz, 2H), 7.37 (t, *J* = 7.5 Hz, 2H), 7.27 (d, *J* = 8.0 Hz, 1H), 4.32 (d, *J* = 7.0 Hz, 2H), 4.24 (t, *J* = 7.0 Hz, 1H), 3.29-3.21 (br, 1H), 1.94-1.90 (br, 2H), 1.87-1.83 (br, 2H), 1.40-1.32 (br, 2H), 1.26-1.18 (br, 2H).

For pre-activation, compound **6** (2.60 g, 6.98 mmol) was reacted with PyBOP (4.36 g, 8.38 mmol) in DMF (150 ml) for 30 min. Then, a solution of Et₃N (2.0 ml) and compound DMT-D-Threoninol (2.84 g, 6.98 mmol) were added to the above mixture. After a night of vigorous stirring, the solvent was removed by evaporation. An excess of AcOEt was added and the organic solution was washed with saturated aqueous solution of NaHCO₃ and brine. After drying over MgSO₄, the solvent was removed by evaporation, the precipitate was filtered and washed with hexane twice to afford **7** (6.19 g, yield quant). HRMS [FAB]: Obsd. 777.3510 (Calcd. for C₄₇H₅₀N₂O₇PNa [M+Na⁺]: 777.3516), ¹H-NMR [CDCl₃, 500 MHz]: δ = 7.77 (d, *J* = 7.5 Hz, 2H), 7.59 (d, *J* = 7.5 Hz, 2H), 7.41-6.82 (m, 18H), 6.14 (d, *J* = 9.0 Hz, 1H), 4.40 (br, 2H), 4.22 (br, 1H), 4.09 (m, 1H), 3.91 (m, 1H),

3.78 (s, 6H), 3.43 (dd, $J = 10$ Hz, 4.5 Hz, 1H) 3.27 (dd, $J = 10$ Hz, 3.5 Hz, 1H), 2.16-2.02 (br, 3H), 1.99-1.90 (br, 2H), 1.67-1.53 (br, 2H), 1.12 (d, $J = 6.5$ Hz, 3H).

Et₃N (0.335 ml, 2.4 mmol) and 2-cyanoethyl-diisopropylchlorophosphoramidite (0.357 ml, 1.6 mmol) were added to a solution of compound **7** (0.604 g, 0.8 mmol) in dry THF (17 ml) at 0 °C. After 20 min of vigorous stirring, the solution was stirred for 40 min at room temperature. Then, an excess of AcOEt was added to the reaction mixture and was washed with saturated aqueous solution of NaHCO₃ and of NaCl. After drying over MgSO₄, the solvent was removed by evaporation, followed by silica gel column chromatography (AcOEt : hexane : Et₃N = 40:60:0.3) to afford **8** (0.35 g, yield 46 %). Note that the concentration of Et₃N was low to avoid unexpected deprotection of Fmoc. HRMS [FAB]: Obsd. 977.4623 (Calcd. for C₅₆H₆₇N₄O₈PNa [M+Na⁺]: 977.4594), ³¹P-NMR [CD₃CN, 121 MHz]: $\delta = 148.9, 148.3$

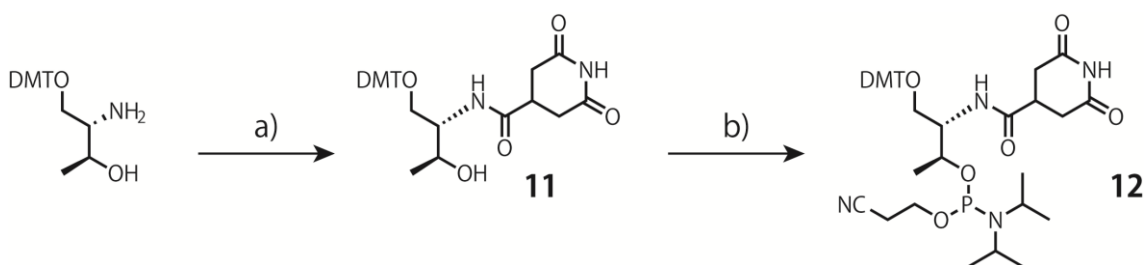


Scheme 3-15. Synthesis of phosphoramidite monomer tethering methylene-glutarimide (**m**). Reagents and conditions: a) glutarimideacetic acid, DCC, HOBT, DMF, r.t., overnight, 49%; b) (iPr)₂NP(O)(Cl)(OCH₂CH₂CN), DIPEA, dry CH₃CN, 0 °C → r.t., 1h, 79 %

The phosphoramidite monomer tethering glutarimideacetic acid (**m**) was synthesized as follows: glutarimideacetic acid was synthesized according to previous report (Xing-yue J. *et al. Chem.Pharm.Bull.* **2010**, *58*, 1436-1441., Bach T. *et al. Chem. Eur. J.* **2001**, *7*, 4512-4521.). Glutarimideacetic acid (0.77 g, 4.51 mmol) was coupled with DMT-D-threoninol (compound **1**, 2.37 g, 3.76 mmol) in the presence of dicyclohexylcarbodiimide (0.77 g, 4.5 mmol) and 1-hydroxybenzotriazole (0.69 g, 4.5 mmol) in DMF (40 mL). After a night of vigorous stirring, an excess AcOEt was added. The organic solution was washed with saturated aqueous solution of NaHCO₃ and of NaCl. The solvent was removed by evaporation, followed by silica gel column chromatography (AcOEt : Et₃N = 100:3) to afford **9** (1.04 g, yield 49 %). ¹H-NMR (500 MHz /CDCl₃) $\delta = 7.37$ - 7.21 ppm (m, 9H, DMT, aromatic), 6.85 - 6.83 ppm (m, 4H, DMT, aromatic), 6.13 ppm (d, 1H, NHCO), 4.10 ppm (q, 1H, threoninol, CH₃-CH-OH), 3.94 ppm (m, 1H, CHNHCO), 3.79 ppm (s, 6H, DMT, MeO), 3.42 - 3.31 ppm (dd, 2H, threoninol, CH₂), 2.90 ppm (s broad, 1H, OH), 2.77 ppm (m, 2H, insulator, CHCH₂CONH), 2.74

ppm (m, 2H, insulator, CH₂CONH), 2.42-2.27 ppm (m, 4H, CH₂CO), 1.13 ppm (d, 3H, threoninol, CH₃), HRMS[FAB]: m/z calcd for C₃₂H₃₆N₂O₇⁺: 560.25 (M⁺+H); found: 560.25.

DIPEA (0.425 ml, 2.5 mmol) and 2-cyanoethyl-diisopropylchlorophosphoramidite (0.22 ml, 1.0 mmol) were added to a solution of compound **9** (0.3 g, 0.5 mmol) in dry CH₃CN (10.0 ml) at 0 °C. After 30 min of vigorous stirring, the solution was stirred for 30 min at room temperature. Then, an excess of AcOEt was added to the reaction mixture and was washed with saturated aqueous solution of NaHCO₃ and of NaCl. After drying over MgSO₄, the solvent was removed by evaporation, followed by silica gel column chromatography (AcOEt : hexane : Et₃N = 66:33:3, R_f = 0.29) to afford **10** (0.3 g, yield 79 %). ¹H-NMR [CDCl₃, 500 MHz]: δ = 7.32-7.26 ppm (m, 9H, DMT, aromatic), 6.84-6.80 ppm (m, 4H, DMT, aromatic), 6.09 ppm (d, 1H, NHCO), 4.3 ppm (m, 1H, threoninol, CH₃-CH-OH), 4.21 ppm (m, 1H, CHNHCO), 3.79 ppm (s, 6H, DMT, MeO), 3.6-3.4 ppm (m, 2H, threoninol, CH₂), 2.8-2.6 ppm (m broad, 1H, OH), 2.4 ppm (m, 1H, insulator, CH-CH₂CONH), 2.4 ppm (m, 6H, insulator), 1.2 ppm (d, 3H, threoninol, Me), 1.15 ppm (t, 12H, N-isopropyl), ³¹P-NMR [CDCl₃, 500 MHz] δ = 147.39 ppm (s), 149.10 ppm (s).

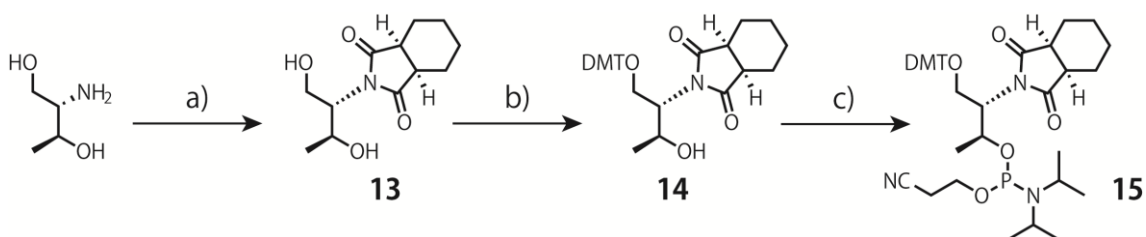


Scheme 3-16. Synthesis of phosphoramidite monomer tethering glutarimidecarboxylic acid (**d**). Reagents and conditions: a) glutarimidecarboxylic acid, DCC, HOBt, DMF, r.t., overnight, 82%; b) (iPr)₂NP(O)Cl, DIPEA, dry CH₃CN, 0 °C → r.t., 1h, 61%.

The phosphoramidite monomer tethering glutarimidecarboxylic acid (**d**) was synthesized as follows: glutarimidecarboxylic acid was synthesized according to previous literature (Rani, B. R. *et al. The Journal of Antibiotics*, **1995**, *48*, 1179-1181.). Glutarimidecarboxylic acid (0.653 g, including salt 1 mmol) was coupled with DMT-D-threoninol (compound **1**, 406 mg, 1 mmol) in the presence of dicyclohexylcarbodiimide (248 mg, 1.2 mmol) and 1-hydroxybenzotriazole (184 mg, 1.2 mmol) in DMF (10 mL). After a night of vigorous stirring, an excess AcOEt was added. The organic solution was washed with saturated aqueous solution of NaHCO₃ and of NaCl. The solvent was removed by evaporation, followed by silica gel column

chromatography (CHCl₃ : MeOH : Et₃N = 100 : 2 : 3) to afford **11** (0.45 g, yield 82%). ¹H-NMR (500 MHz /CDCl₃) δ= 7.37-7.21 ppm (m, 9H, DMT, aromatic), 6.86-6.80 ppm (m, 4H, DMT, aromatic), 6.29 ppm (d, *J* = 9 Hz, 1H, NHCO), 4.36 ppm (m, 1H, threoninol), 3.92 ppm (m, 1H, CHNHCO), 3.80 ppm (s, 6H, DMT, MeO), 3.42-3.32 ppm (dd, *J* = 4, 10 Hz 2H, threoninol), 2.93-2.65 ppm (m 5H), 1.26 ppm (d, *J* = 6.5 Hz, 3H, threoninol, CH₃).

DIPEA (0.34 ml, 2.0 mmol) and 2-cyanoethyl-diisopropylchlorophosphoramidite (0.179 ml, 0.8 mmol) were added to a solution of compound **11** (0.23 g, 0.4 mmol) in dry CH₃CN (10.0 ml) at 0 °C. After 30 min of vigorous stirring, the solution was stirred for 30 min at room temperature. Then, an excess of AcOEt was added to the reaction mixture and was washed with saturated aqueous solution of NaHCO₃ and of NaCl. After drying over MgSO₄, the solvent was removed by evaporation, followed by silica gel column chromatography (AcOEt : hexane : Et₃N = 50:50:3, *R_f* = 0.30) to afford **12** (0.18 g, yield 61 %). ³¹P-NMR [CDCl₃, 500 MHz] δ= 147.74 ppm (s), 149.59 ppm (s).



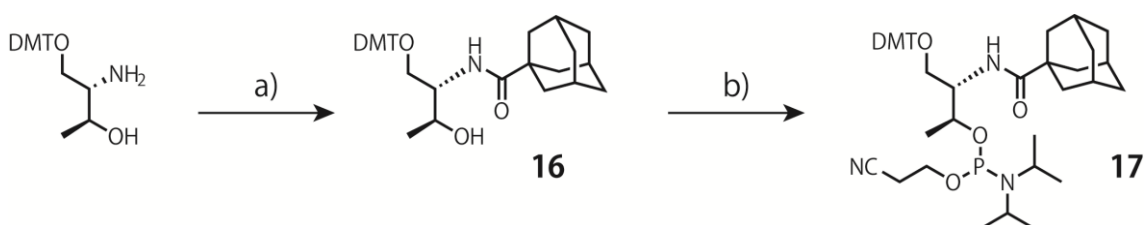
Scheme 3-17. Synthesis of phosphoramidite monomer tethering cyclohexane-*cis*-1,2-dicarboxylic acid (i). Reagents and conditions: a) cyclohexane-*cis*-1,2-dicarboxylic acid, heat, no solvent, 5 min. quant.; b) DMT-Cl, DIPEA, DMAP, CH₂Cl₂, pyridine, 0 °C → r.t., 56%; c) (*i*Pr)₂NP(Cl)(OCH₂CH₂CN), Et₃N, dry CH₃CN, 0 °C → r.t., 1h, 90%

The phosphoramidite monomer tethering cyclohexane-*cis*-1,2-dicarboxylic acid (i) was synthesized as follows: cyclohexane-*cis*-1,2-dicarboxylic acid (275.5 mg, 1.6 mmol) and D-threoninol (157.7 mg, 1.6 mmol) were putted at the bottom of flask without adding any solvent and were heated by heat gun until the solids were melted. Obtained transparent syrup compound **13** was used for next step without purification. (yield quant.) ¹H-NMR [CDCl₃, 500 MHz]: δ = 4.24 (m, 1H), 4.13 (m, 1H), 3.97 (dd, *J* = 12 Hz, 4 Hz, 1H), 3.89 (dd, *J* = 12 Hz, 4 Hz, 1H), 2.96 (m, 2H), 2.30 (m, 1H), 2.00-1.45 (m, 8H), 1.20 (d, *J* = 7.0 Hz, 3H).

Dry pyridine (20 mL) solution containing **13** (0.87 g, 3.6 mmol) and *N,N*-diisopropylethylamine (0.75 ml, 4.32 mmol) was cooled on ice under nitrogen. Then,

4,4'-dimethoxytrityl chloride (DMT-Cl) (1.22 g, 3.6 mmol) and 4-(dimethylamino)pyridine (52.8 mg, 0.432 mmol) in CH₂Cl₂ (20 mL) was added drop wise to the above mixture on ice. After 2.5 h of vigorous stirring, the solvent was removed by evaporation, followed by silica gel column chromatography (AcOEt : hexane : Et₃N = 25:75:3, *R_f* = 0.1) to afford **14** (1.09 g, 2.0 mmol, yield 56%). ¹H-NMR [CDCl₃, 500 MHz]: δ = 7.35-6.79 (m, 13H), 4.40 (m, 1H), 4.04 (m, 1H), 3.78 (s, 6H), 3.54 (dd, *J* = 10 Hz, 4.0 Hz, 1H), 3.46 (dd, *J* = 10 Hz, 4 Hz, 1H), 2.84 (m, 2H), 1.94-1.32 (m, 9H), 1.04 (d, *J* = 7.0 Hz, 3H).

DIPEA (1.7 ml, 10.0 mmol) and 2-cyanoethyl-diisopropylchlorophosphoramidite (0.9 ml, 4.0 mmol) were added to a solution of compound **14** (1.09 g, 2.0 mmol) in dry CH₃CN (20 ml) at 0 °C. After 20 min of vigorous stirring, the solution was stirred for 40 min at room temperature. Then, an excess of AcOEt was added to the reaction mixture and was washed with saturated aqueous solution of NaHCO₃ and of NaCl. After drying over MgSO₄, the solvent was removed by evaporation, followed by silica gel column chromatography (AcOEt : hexane : Et₃N = 25:75:3 *R_f* = 0.23) to afford **15** (1.3 g, yield 90 %).



Scheme 3-18. Synthesis of phosphoramidite monomer tethering 1-adamantanecarboxylic acid (a). Reagents and conditions: a) 1-adamantanecarboxylic acid, DCC, HOBT, DMF, r.t., overnight, 82%; b) (iPr)₂NP(Cl)(OCH₂CH₂CN), DIPEA, dry CH₃CN, 0 °C → r.t., 1h, 79%.

The phosphoramidite monomer tethering 1-adamantanecarboxylic acid (**a**) was synthesized as follows: 1-Adamantanecarboxylic acid (149 mg, 0.824 mmol) was coupled with DMT-D-threoninol (compound **1**, 280 mg, 0.687 mmol) in the presence of dicyclohexylcarbodiimide (170 mg, 0.824 mmol) and 1-hydroxybenzotriazole (126 mg, 0.824 mmol) in DMF (10 mL). After a night of vigorous stirring, an excess AcOEt was added. The organic solution was washed with saturated aqueous solution of NaHCO₃ and of NaCl. The solvent was removed by evaporation, followed by silica gel column chromatography (AcOEt : hexane : Et₃N = 33 : 66 : 3 *R_f* = 0.23) to afford **16** (0.32 g, yield 82%).

DIPEA (0.48 ml, 2.8 mmol) and 2-cyanoethyl-diisopropylchlorophosphoramidite (0.25 ml, 1.12 mmol) were added to a solution of compound **16** (0.32 g, 0.56 mmol) in dry CH₃CN (10.0 ml) at 0 °C. After 30 min of vigorous stirring, the solution was stirred for 30 min at room temperature. Then, an excess of AcOEt was added to the reaction mixture and was washed with saturated aqueous solution of NaHCO₃ and of NaCl. After drying over MgSO₄, the solvent was removed by evaporation, followed by silica gel column chromatography (AcOEt : hexane : Et₃N = 20:80:3, *R_f* = 0.21) to afford **17** (0.34 g, yield 79 %).

The MALDI-TOFMS data for the DNA were as follows:

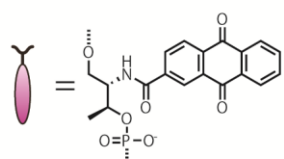
m/z : **H^a1a**: Obsd. 3966 (Calcd. for [**H^a1a**+H⁺]: 3966). **H^a1b**: Obsd. 3966 (Calcd. for [**H^a1b**+H⁺]: 3966). **H^a2Pa**: Obsd. 4725 (Calcd. for [**H^a2Pa**+H⁺]: 4724). **H^a1a**: Obsd. 3937 (Calcd. for [**H^a1a**+H⁺]: 3937). **H^a1b**: Obsd. 3938 (Calcd. for [**H^a1b**+H⁺]: 3937). **H^a2Pa**: Obsd. 4666 (Calcd. for [**H^a2Pa**+H⁺]: 4666). **H^a3Pa**: Obsd. 5046 (Calcd. for [**H^a3Pa**+H⁺]: 5045). **H^a3Pb**: Obsd. 4959 (Calcd. for [**H^a3Pb**+H⁺]: 4958). **m1a**: Obsd. 3966 (Calcd. for [**m1a**+H⁺]: 3965). **m1b**: Obsd. 3966 (Calcd. for [**m1b**+H⁺]: 3965). **m2Pa**: Obsd. 4724 (Calcd. for [**m2Pa**+H⁺]: 4722). **m2b**: Obsd. 4285 (Calcd. for [**m2b**+H⁺]: 4285). **d1a**: Obsd. 3949 (Calcd. for [**d1a**+H⁺]: 3950). **d1b**: Obsd. 3951 (Calcd. for [**d1b**+H⁺]: 3950). **d2Pa**: Obsd. 4693 (Calcd. for [**d2Pa**+H⁺]: 4694). **d2b**: Obsd. 4256 (Calcd. for [**d2b**+H⁺]: 4256). **a1a**: Obsd. 3974 (Calcd. for [**a1a**+H⁺]: 3973). **a1b**: Obsd. 3974 (Calcd. for [**a1b**+H⁺]: 3973). **a2Pa**: Obsd. 4737 (Calcd. for [**a2Pa**+H⁺]: 4739). **a2b**: Obsd. 4302 (Calcd. for [**a2b**+H⁺]: 4304). **a3Pa**: Obsd. 5069 (Calcd. for [**a3Pa**+H⁺]: 5071). **a3Pb**: Obsd. 5069 (Calcd. for [**a3Pb**+H⁺]: 5070). **i1a**: Obsd. 3947 (Calcd. for [**i1a**+H⁺]: 3948). **i1b**: Obsd. 3947 (Calcd. for [**i1b**+H⁺]: 3949). **i2Pa**: Obsd. 4689 (Calcd. for [**i2Pa**+H⁺]: 4689). **i2b**: Obsd. 4252 (Calcd. for [**i2b**+H⁺]: 4250). **i3Pa**: Obsd. 4993 (Calcd. for [**i3Pa**+H⁺]: 4992). **i3Pb**: Obsd. 4992 (Calcd. for [**i3Pb**+H⁺]: 4992).

3-7-2 Restriction of AT hopping hole transfer

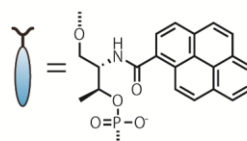
Poly AT sequence can readily mediate electron transfer known as “AT-hopping”.⁵⁵ Here, restriction of AT hopping by insulator was examined to confirm inhibition of electron transfer by shielding ability. The design of system used here was depicted in Table 3-21. Anthraquinone (**Q**), a quencher for pyrene was attached at the end of duplex, whereas pyrene (**p**, note that pyrene used here is direct type, not contain internal linker between dye and threoninol to avoid quenching by nucleobases) was introduced in the middle of duplex. Five AT pairs were inserted between **Q** and **p** to mediate electron transfer (duplex named **QP**). For control, duplex without **Q** was also prepared. To check shielding effect, single **H·H** pair was introduced between **Q** and **p** at various positions (**0HQP**, **2HQP**, **4HQP**).

Table 3-21. Sequences of modified DNA used in this topic.

Name	Sequence	Representation
P1	5' -AAAAA ATAGTCA-3' 3' -TTTTT p TATCAGT-5'	
QP	5' - Q AAAAA ATAGTCA-3' 3' - TTTTT p TATCAGT-5'	
0HQP	5' - QH AAAAA ATAGTCA-3' 3' - H TTTTT p TATCAGT-5'	
2HQP	5' - QAH AAA ATAGTCA-3' 3' - TH TTTT p TATCAGT-5'	
4HQP	5' - QAAAH A ATAGTCA-3' 3' - TTT HT p TATCAGT-5'	



Anthraquinone (**Q**)



Pyrene (direct) (**p**)

Synthesis of **p** was described in Chapter 4.

Synthesis of **Q** was described elsewhere. (Asanuma, H.; Hayashi, H.; Zhao, J.; Liang, X. G.; Yamazawa, A.; Kuramochi, T.; Matsunaga, D.; Aiba, Y.; Kashida, H.; Komiyama, M.; *Chem. Commun.*, **2006**, 5062-5064.)

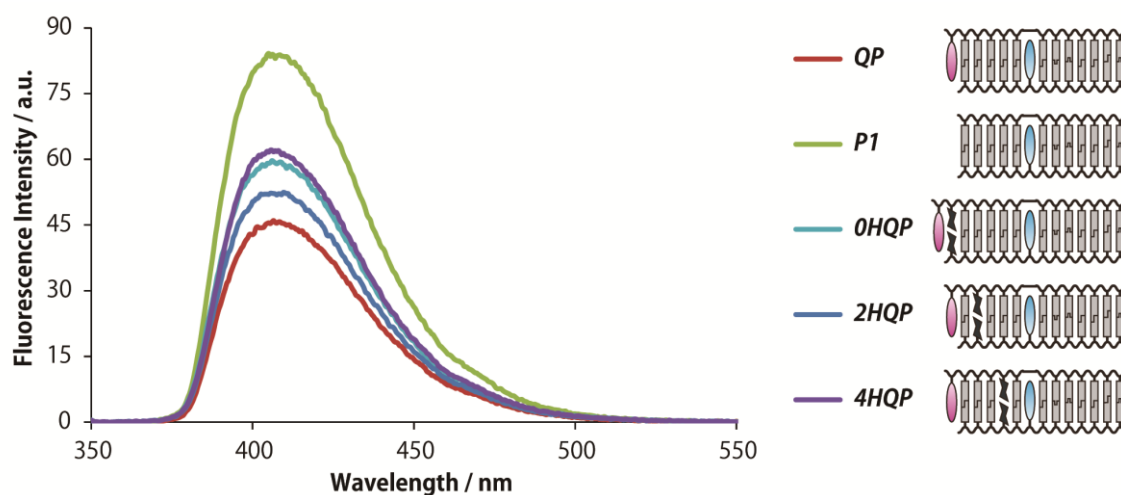


Figure 3-20. Fluorescence spectra of modified DNA containing insulator base pair (**H**) with a pyrene (**p**) and anthraquinone (**Q**). Solution conditions were as follows: [DNA] = 1.0 μ M each, [NaCl] = 100 mM, pH 7.0 (10 mM Phosphate buffer), 20°C. Excitation wavelength: 345 nm.

Table 3-22. Spectroscopic behaviors and thermodynamic stabilities of modified DNA.

Sequence	Relative Intensity ^a
<i>P1</i>	1
<i>QP</i>	0.54
<i>0HQP</i>	0.71
<i>2HQP</i>	0.62
<i>4HQP</i>	0.74

^a: Emission intensity at 406 nm relative to that of **P1**. Solution conditions: [DNA] = 1 μ M each, [NaCl] = 100 mM, pH 7.0 (10 mM phosphate buffer), 20°C. Excitation wavelength: 345 nm.

Under influence of **Q** (**QP**), emission intensity of **p** was dropped about 46% owing to electron transfer mediating AT pairs. Insertion of a **H-H** pair exhibited 8-20% of fluorescence recovery. For **0HQP**, the length between **Q** and **p** was little longer than the others, however, the AT hopping could be successfully shielded. For **2HQP**, since **H-H** pairs were introduced near terminal of duplex, the duplex would be relatively unstable and shielding effect became slightly lower than **4HQP**. **4HQP** exhibited large fluorescence recovery (20%) suggesting that AT hopping was slowed down by insertion of **H-H** pair, however, AT hopping over **H-H** pair may be still possible and the fluorescence could not be fully recovered. Insertion of several insulator pairs will be effective for complete shielding of AT-hopping.

3-7-3 Molecular orbital calculation of dyes and nucleobases

Here, the results of theoretical calculation performed on Gaussian 09W were summarized. Note that these data are rough estimates. In calculation, the command `scrf=(pcm,solvent=water)` was used for solvent parameters.

Table 3-23. Theoretical calculation results by Gaussian 09W.

	HOMO / eV	LUMO / eV	ΔE / eV	λ_{\max} calc. / nm	λ_{\max} exp. / nm	Basis function
A	-6.049 ^a	-0.425	5.625	236.76	-	rb3lyp/6-31g(d)
T	-6.225 ^a	-0.896	5.329	255.46	-	rb3lyp/6-31g(d)
G	-5.619 ^a	-0.100	5.519	248.42	-	rb3lyp/6-31g(d)
C	-6.141	-0.680	5.461	259.68	-	rb3lyp/6-31g(d)
P₃	-5.662	-1.565	4.097	336.36	345	pbe1pbe/6-31g(d)
P₀	-5.851	-1.827	4.024	344.58	345	pbe1pbe/6-31g(d)
B	-6.824	-0.938	5.886	256.94	-	rb3lyp/6-31g(d)
I	-6.627	-0.874	5.753	255.36	-	rb3lyp/6-31g(d)
J	-6.296	-1.302	4.994	273.41	-	rb3lyp/6-31g(d)
Azo	-6.721	-2.502	4.219	342.44	335	pbe1pbe/6-31g(d)
MR	-5.540	-2.208	3.332	425.23	480	pbe1pbe/6-31g(d)
MS	-6.095	-2.480	3.614	399.12	395	pbe1pbe/6-31g(d)
NMR	-6.852	-2.684	4.169 [†]	488.81 [†]	515	pbe1pbe/6-31g(d)
Q	-7.324	-2.958	4.366	332.57	340	pbe1pbe/6-31g(d)
TO	-5.345	-3.455	1.890	541.25	515	pbe1pbe/6-31g(d)
Y₄	-5.199	-3.554	1.645 [†]	507.43 [†]	550	pbe1pbe/6-31g(d)
Y₀	-5.816	-2.681	3.135 [†]	457.9 [†]	550	pbe1pbe/6-31g(d)
BODIPY	-5.779	-2.410	3.370 [†]	414.04 [†]	560	pbe1pbe/6-31g(d)
TAMRA	-6.006	-2.908	3.098 [†]	458.68 [†]	560	pbe1pbe/6-31g(d)
E₂	-5.343	-2.006	3.337	430.25	450	pbe1pbe/6-31g(d)
E₀	-5.477	-2.185	3.293	437.36	450	pbe1pbe/6-31g(d)

[†]: Invalid estimation; more consideration is required.

^a: These data were consistent with the previous report (Kawai, K.; Hayashi, M.; Majima, T. *J. Am. Chem. Soc.*, **2012**, *134*, 4806-4811.).

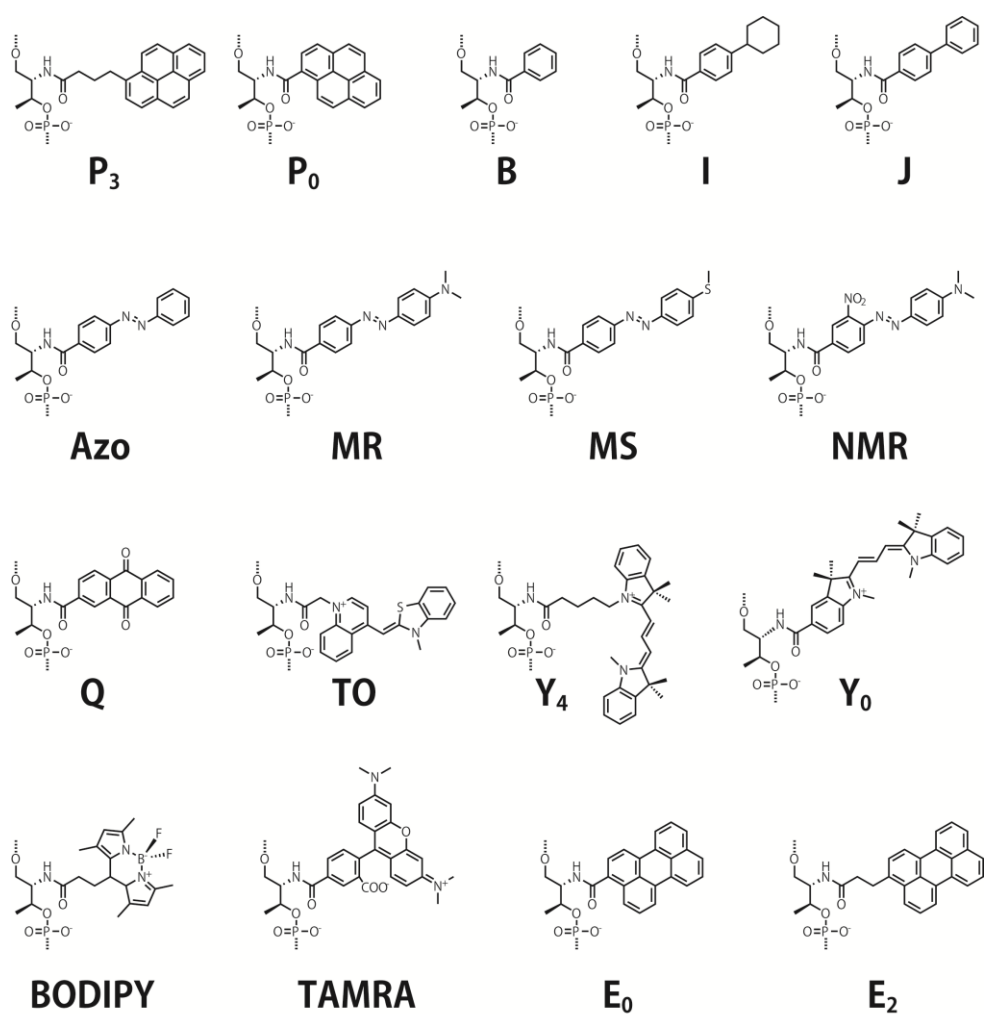


Figure 3-21. Structures and abbreviation names of various dyes tethered on D-threoninol scaffold.

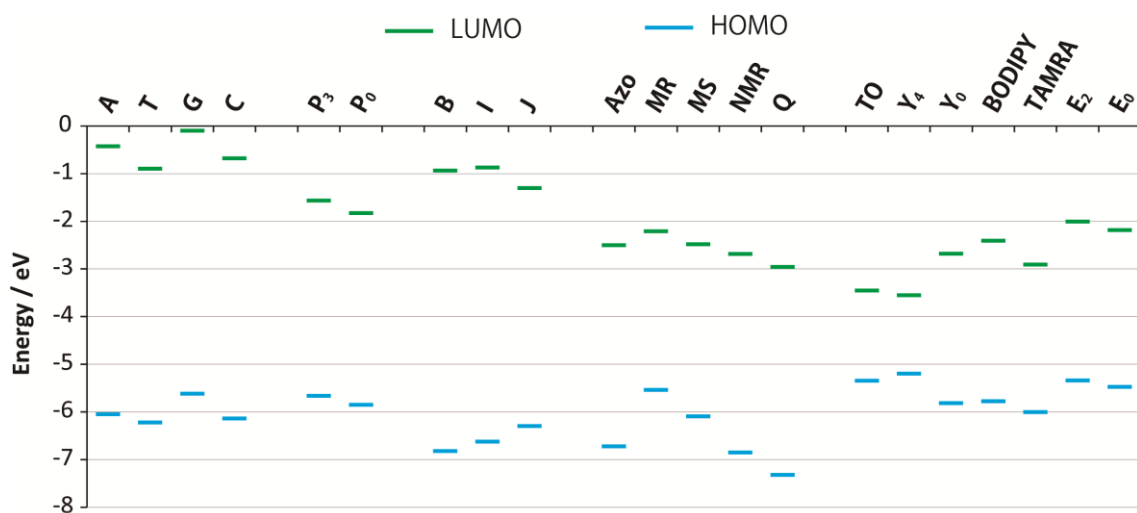


Figure 3-22. Energy diagram of various dyes. LUMO and HOMO were indicated in green and blue line, respectively.

CHAPTER 4. DEVELOPMENT OF A NEW ROBUST DNA-BASED FRET SYSTEM WITH STRICT CONTROL OF DYE MOBILITY WITHIN DNA DUPLEX

4-1 Abstract

One promising solution to enhance detection sensitivity of fluorophore is enlarging apparent Stokes' shift by utilizing FRET. Although distance dependence of FRET is well-studied and FRET has been extensively applied as "molecular ruler", only limited examples of orientation-dependent FRET have been reported. To create a robust FRET system that precisely reflects the orientation between donor and acceptor, donor and acceptor fluorophores were introduced into a DNA via a D-threoninol scaffold. Strong stacking interactions among intercalated dyes and natural base-pairs suppress free movement of the dyes, clamping them in the duplex in a fixed orientation. Pyrene and perylene were used as donor and acceptor, respectively, and both the distance and orientation between these dyes were systematically controlled by varying the number of intervening AT pairs from 1 to 21 (corresponding to two turns of helix). FRET efficiency determined from static fluorescence measurement did not decrease linearly with the number (n) of inserted AT pairs but dropped significantly every 5 base-pairs (i.e., $n = 8, 13, \text{ and } 18$), corresponding to a half-turn of the B-type helix. This clearly demonstrates that FRET efficiency reflects the orientation between pyrene and perylene. Time-resolved fluorescence spectroscopy with a streak camera was also measured and the time-course of the energy transfer could be directly observed. As expected, the FRET efficiencies determined from the life-time of pyrene emission were in good agreement with static measurements. Theoretical calculation of FRET efficiency assuming that the DNA duplex is a rigid cylinder with B-type geometry coincided with the experimental results. This novel FRET system using D-threoninol will contribute to further development of FRET-based measurement techniques.

4-2 Introduction

While the quantum yield of the fluorescent dye is the dominant factor that determines its sensitivity, the Stokes' shift, that is, the difference between the band maxima of absorption and emission of identical dyes, also significantly affects sensitivity because the scattered light of excitation inhibits the detection of emission. Although conventional fluorescent dyes, such as Cy3 and Cy5, have a high quantum yield and can be applied to the labeling of ODNs, their Stokes' shifts are only 15 and 17 nm, respectively. (see ref. 11 in Chap. 1) Since such a small Stokes' shift lowers the sensitivity, efforts have been made to expand the difference between the excitation and emission wavelengths. One promising strategy for this purpose is the utilization of Förster resonance energy transfer (FRET).¹ Several studies on the application of FRET to DNA duplexes have reported an increase in the "apparent" Stokes' shift. (see ref. 12-18 in Chap. 1)

FRET is a physical phenomenon in which excited energy of a donor fluorophore is transferred to an acceptor non-radiatively.¹ FRET is also widely utilized as "molecular ruler" for studying the structure and interactions of macromolecules such as proteins and nucleic acids,^{2,3} since the efficiency of FRET depends on both distance and orientation between donor and acceptor. FRET techniques are used to monitor changes in distance of nano materials or biomolecules (e.g., DNA origami,⁴ molecular probes,⁵ molecular sensors,⁶ ribozymes^{7,8}). Advantages of FRET techniques include 1) high-sensitive fluorescent detection due to extended apparent Stokes' shift, 2) accurate measurement of distance over wide range (10-100 Å), and 3) the ability to monitor molecular dynamics using time resolved fluorescence spectroscopy. However, in many cases, only distance dependence is taken into consideration and orientation is assumed to be averaged owing to free rotation of chromophores.

FRET arises from a coupling of transition dipole moments of the dyes. The efficiency of FRET (Φ_T) and its related parameters are given by following equations.^{9,10}

$$\Phi_T = \frac{1}{1 + (R/R_0)^6} \quad (1)$$

$$R_0 = 0.2108 [J(\lambda) \kappa^2 n^{-4} \Phi_D]^{1/6} \quad (2)$$

$$\kappa^2 = (\cos \theta_T - 3 \cos \theta_D \cos \theta_A)^2 \quad (3)$$

In eq. 1, R is the separation distance between donor and acceptor and R_0 is the distance, where Φ_T equals 0.5, known as Förster radius. Efficiency decreases inversely with the sixth power of the distance, resulting in a significant drop of Φ_T around R_0 . R_0 can be calculated from spectral overlap using a data set of donor emission and acceptor absorption (eq. 2), where $\mathcal{J}(\lambda)$ is spectral overlap at λ (nm) and R_0 (Å). Φ_D is the quantum yield of the donor, and n is refractive index, typically assumed to be 1.4 for biomolecules in aqueous solution¹⁰. κ^2 is the orientation factor given by eq. 3, where θ_T is the total angle of transition dipole moment between donor and acceptor, and θ_D and θ_A are the angles versus distant axis of donor and acceptor, respectively. In principle, FRET efficiency should depend on the mutual orientation (i.e. angle) between the donor and acceptor as well as their distance. However, under conditions in which fluorophores freely move, the orientation factor is assumed to be an averaged value, $\kappa^2 = 2/3$.

DNA is an ideal scaffold for demonstrating orientation-dependence of FRET because DNA forms a rigid double-helical structure.¹¹⁻¹⁹ Generally, the dyes are attached at termini or within grooves of DNA through long flexible linkers, and therefore FRET is assumed to be dependent on distance but not orientation as donor and acceptor should move freely.²⁰⁻²⁶ Lewis *et al.* were first to report orientation-dependent FRET with a capped hairpin system where perylene was attached at a terminus of stilbene-linked hairpin DNA.²⁰ In this system, chromophores are stacked on base pairs, and FRET efficiency changed depending on the chromophore orientation. Iqbal *et al.* introduced fluorescent dyes at each end of DNA duplex; π - π stacking of Cy3 and Cy5 at either end of duplex restricted free rotation of chromophores;²¹ however, stacking onto the end of a DNA duplex tends to slip, and thus the orientation of dye was not sufficiently controlled. In addition, in these end-capped systems, it was difficult to interrogate short distances because of the instability of short duplexes. Börjesson *et al.* designed another excellent FRET system with fluorescent nucleic acid analogs mimicking deoxycytosine.²⁶ Since stacking interactions and hydrogen bonding allowed strict control of the position, they successfully observed the orientation-dependent FRET. However, this design is limited to fluorescent nucleic acid analogs.

Herein, a novel FRET system in which fluorophores are incorporated as base-surrogates using a D-threoninol scaffold²⁷ was proposed. Pyrene and perylene, a well-characterized donor-acceptor pair,^{13,28,29} were covalently inserted at desired positions (Figure 4-1a) as we described previously.^{27,30,31} There are several advantages to this design. First, chromophores on D-threoninol facilitate intercalation between the

nucleobases,³⁰ which inhibits not only free rotation of the dyes but also slip and slide, tilt and roll. Second, donor-acceptor pairs can be incorporated into any position of a DNA duplex. Hence, the distance and orientation between dyes could be readily controlled and estimated from well-known DNA structure parameters. Thirdly, various dyes available as FRET pairs can be covalently tethered to the D-threoninol linker.

In this chapter, we systematically investigated the orientation-dependence of FRET from pyrene to perylene. The distance and orientation were systematically varied by inserting 1 to 21 AT pairs between dyes, and FRET efficiencies were determined both by static fluorescence measurement and time-resolved fluorescent spectroscopy. Comparison with theoretical values calculated based on a cylinder model of DNA is also discussed.

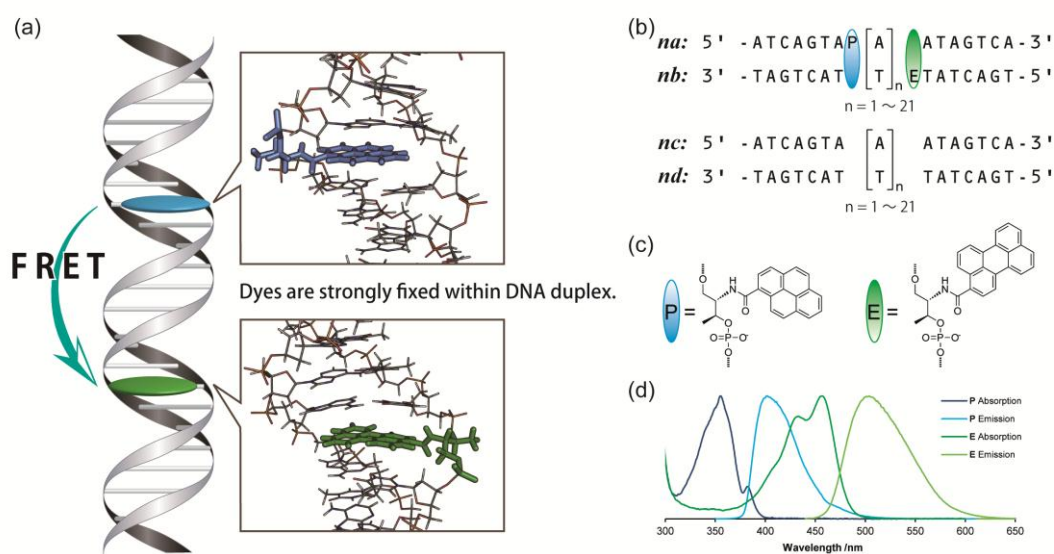


Figure 4-1. Schematic of FRET system used in this study. (a) A graphical representation of our FRET system. (b) Sequence of FRET ODN pair. AT pairs were inserted between **P** (pyrene as donor) and **E** (perylene as acceptor). **P** and **E** moieties were introduced into strands **na** and **nb**, respectively, where *n* indicates the number of inserted A or T residues; **nc** and **nd** were ODNs without fluorophores with sequences identical to **na** and **nb**, respectively. **P** and **E** moieties are inserted into the DNA duplex as single-residue bulges when **na** and **nb** are hybridized. (c) Structure of **P** and **E**. Dyes were directly conjugated via D-threoninol to the DNA strand. (d) Absorption and emission spectra of **P** and **E**.

4-3 Results and Discussions

4-3-1 Strategy and design of the FRET system.

The basic FRET system designed in this study is shown in Figure 4-1a and 4-1b. We synthesized 21 ODN sets that contained from 1 to 21 AT pairs between donor and acceptor. The number of base pairs between donor and acceptor affects both distance and orientation between FRET pairs. Sequences at either end of the ODNs facilitate exact base-pairing and rigid duplex formation. These conserved sequences were carefully designed to avoid undesired intra- or intermolecular structures.

Donor and acceptor were introduced into ODNs *na* and *nb*, respectively. ODNs without fluorophores, *nc* and *nd*, were also synthesized. Control duplexes tethering only a donor or acceptor were prepared by hybridizing pairs *na/nd* or *nc/nb*. We chose 1-pyrenecarboxylic acid (**P**) and 3-perylenecarboxylic acid (**E**) as donor and acceptor, respectively (Figure 4-1c). These fluorophores are photochemically stable and their planar structures are suitable for the intercalation into a DNA duplex. These chromophores were introduced into DNA strands via D-threoninol scaffolds as previously described.^{27,30} **P** and **E** were directly conjugated to D-threoninol in order to suppress free movement of dyes once incorporated into duplex. FRET efficiency depends on the quantum yield of the donor, which is responsible for R_0 ; **P** has a high quantum yield of 0.5 (This value is consistent with a similar pyrene derivative reported in ref. 35 and determined by using 9,10-biphenylanthracene in EtOH (0.95) as a reference.). The spectral overlap of donor (**P**) emission and acceptor (**E**) absorption ($J(\lambda)$) was calculated as 4.50×10^{14} ($M^{-1} \text{ cm}^{-1} \text{ nm}^4$) (Figure 4-1d). Based on these parameters, R_0 was determined 38.8 Å (when $\kappa^2 = 2/3$). This value approximately corresponds to $n = 11$.

In this study, pyrene and perylene were used as a typical example of donor and acceptor, respectively, by intervening only A-T pairs between them to avoid fluorescence quenching of **P** by G-C pair (see Appendix 4-7-2). FRET also occurred even though G-C pair was located in proximity of donor, although Förster radius should decrease due to low quantum yield of the donor. Note that other pairs of dye are also applicable with D-threoninol as a scaffold. By choosing appropriate donor-acceptor pairs, both Förster radius and excitation (emission) wavelength would be controllable.

4-3-2 Spectroscopic behavior of ODN-dye conjugates.

First, UV-Vis and CD spectra were measured in order to investigate the structure of the duplexes modified with dyes. Figure 4-2a shows the temperature dependence of UV-Vis spectra of $n = 10$ FRET system (**10a/10b**). At 80 °C, an absorption maximum (λ_{\max}) of pyrene was observed at 348 nm, while that of perylene appeared at 445 nm. When the temperature was decreased to 0 °C, ODNs formed a duplex, and the λ_{\max} s of pyrene and perylene shifted to 356 and 457 nm, respectively. These red shifts at lower temperature indicated that the dyes were intercalated within DNA duplex.³⁶ Melting temperature (T_m) analyses also supported the intercalation of **P** and **E** moieties (Table 4-1). The duplex containing **P** and **E** moieties (**na/nb**) had a higher T_m than the control duplex without dyes (**nc/nd**), indicating duplexes were stabilized through stacking interactions between dyes and natural base pairs. We also measured CD spectra of **18a/18b** and the control native DNA duplex, **18c/18d** (Figure 4-2b). Very weak signals were observed from **18a/18b** at around 350 nm (**P**) and 450 nm (**E**). These induced CD signals also support intercalation of dyes. Note that induced CD of intercalated dye is usually weak³⁷. In addition, complicated couplets were observed at around 260 nm due to the AT tract. This unique signal near 260 nm was also observed³⁸ in the **18c/18d** duplex, indicating that the structure of surrounding base pairs is not disturbed by the introduction of dyes. These observations are consistent with previous NMR analyses that revealed that a planar *trans*-azobenzene on D-threoninol is intercalated between the base pairs.^{30,32} Thus, structural perturbation by the modification with base surrogates is minimal, and it can assume that the FRET system adopts a typical B-type DNA structure.

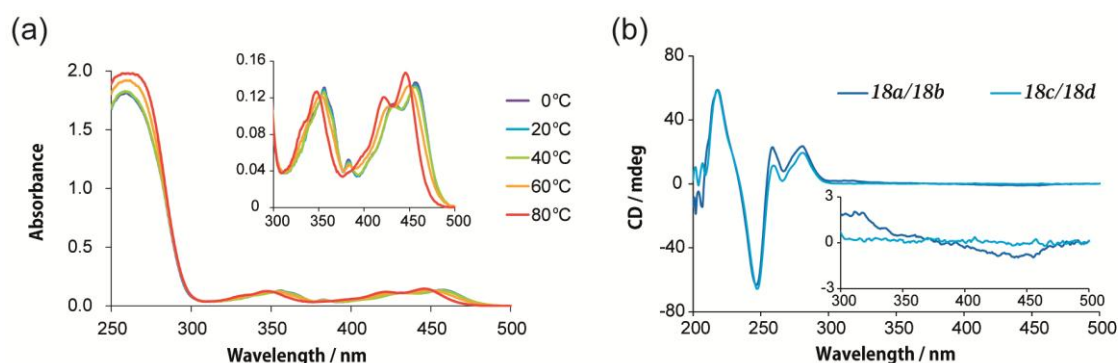


Figure 4-2. Spectroscopic behaviors of FRET system. (a) Temperature dependence of UV-Vis spectra of **10a/10b**. Spectra at 300-500 nm are magnified in the inset. Solution conditions were as follows: 100 mM NaCl, 10 mM phosphate buffer, pH 7.0, 5.0 μ M each ODN. (b) Comparison of CD spectra of **18a/18b** and **18c/18d**. Spectra at 300-500 nm are magnified in the inset. Solution conditions were as follows: 100 mM NaCl, 10 mM phosphate buffer, pH 7.0, 4.0 μ M each DNA strand; 20 °C.

4-3-3 Static measurement of fluorescence spectra.

Next, static fluorescence spectra of FRET duplexes were measured. Figure 4-3a shows fluorescence spectra of duplexes with $n = 5, 10, 15,$ and 20 . Blue emission around 400 nm and green emission around 500 nm result from donor (**P**) and acceptor (**E**), respectively. In the case of $n = 5$, the emission intensity of donor was significantly less than that of the acceptor emission. In contrast, for $n = 20$, acceptor emission was very weak and donor emission was highly intense. This emission intensity of donor was as high as that of the duplex containing only donor (**11a/11d** in Figure 4-3b dark blue line) demonstrating very low FRET efficiency. Duplexes with $n = 10$ and $n = 15$ had certain intensities between those of the $n = 5$ and 20 duplexes. These spectral changes could be clearly observed with naked eyes (Figure 4-4a). **E** could be excited directly by excitation wavelength 345 nm, however, its intensity was sufficiently low and negligible (purple line in Figure 4-b).

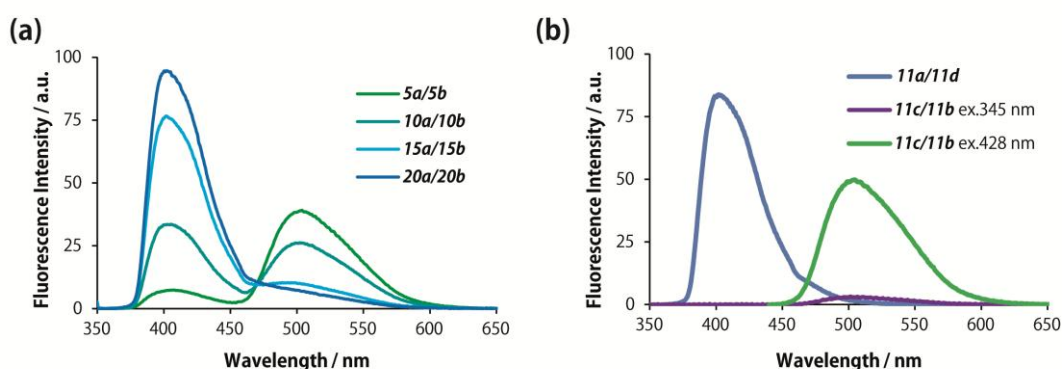


Figure 4-3. Emission spectra of static fluorescence measurement. (a) Fluorescence emission spectra of FRET pairs ($n = 5, 10, 15,$ and 20) at 20 °C. The excitation wavelength was 345 nm. All the fluorescence spectra of FRET pairs ($n = 1-21$) were depicted in 4-7 Appendix section. Solution conditions were as follows: 100 mM NaCl, 10 mM phosphate buffer, pH 7.0 , 1.0 μ M each ODN. Before measurements, samples were heated at 80 °C for 5 min followed by cooling gradually at the rate of 4 °C/min to 20 °C. (b) Static fluorescence spectra of FRET system without donor or acceptor ($n = 11$) at 20 °C. For the duplex containing only **P** (**11a/11d**), the excitation wavelength was 345 nm (blue line). For the duplex containing only **E** the excitation wavelength was either 345 nm (purple line) or 428 nm (green line). Solution conditions were as follows: 100 mM NaCl, 10 mM phosphate buffer, pH 7.0 , 1.0 μ M each DNA strand.

Figure 4-4 shows fluorescence intensities of pyrene and perylene in *na/nb* duplexes. The decrease of donor emission and the increase of acceptor emission were highly correlated. Interestingly, the distance dependence of these emissions was not monotonous (Figure 4-4b and 4-4c). The periodical change in orientation factor as a function of the number of inserted AT pairs induced measurable changes of FRET efficiency. When *n* was 8, 13, and 18, a prominent decline of FRET efficiency was observed. This was visually observed as a color change in Figure 4-4a. For *n* = 8, the sample solution emitted bluish-green fluorescence, which was obviously different from green color of duplexes with *n* = 7 and 9. This cycle of about 5 bp reflected approximately half turns (180°) of the B-type DNA helix indicating that orientation of donor and acceptor was based upon DNA structure. This result is consistent with the previous reports by others.^{23,26}

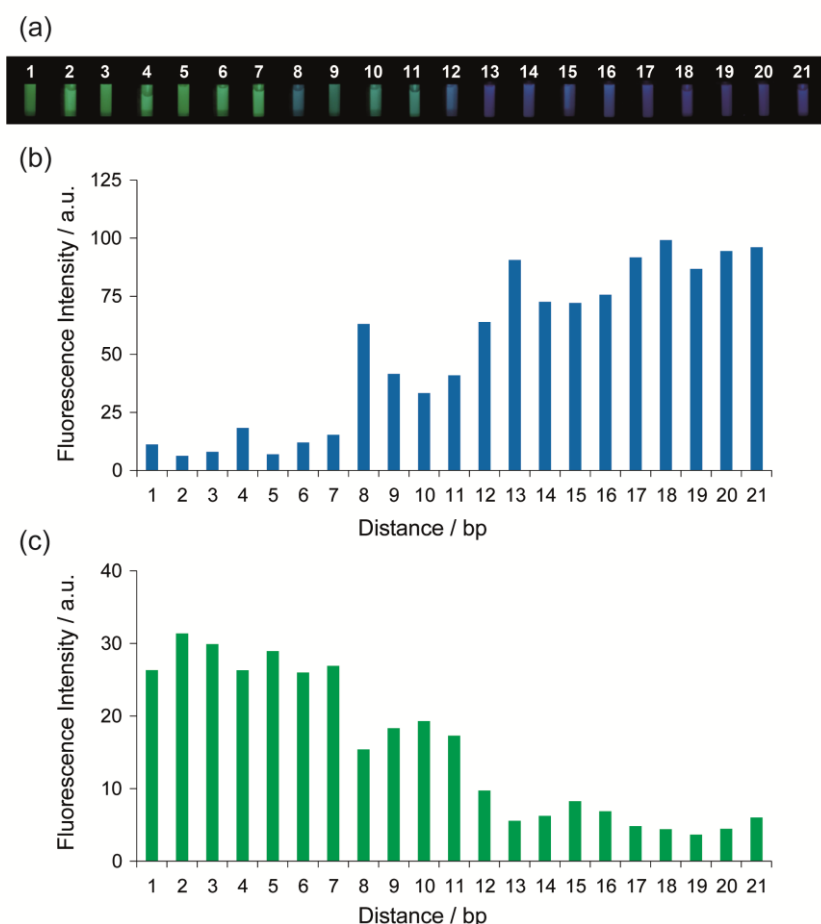


Figure 4-4. Distance dependence of fluorescence intensity of *na/nb* duplexes. Measurement conditions were as follows: 100 mM NaCl, 10 mM phosphate buffer, pH 7.0, 1.0 μ M each ODN. (a) A photograph of samples excited at 340 nm. (b) Fluorescence intensity of **P** (400 nm) at 20 °C. The excitation wavelength was 345 nm. (c) Fluorescence intensity of **E** (530 nm).

4-3-4 Time-resolved fluorescence measurement.

Periodical changes of FRET efficiency were also observed by time-resolved fluorescence measurements using a streak camera. Representative examples are shown in Figure 4-5. Both **P** and **E** had lifetimes of approximately 10 ns. Changes in FRET efficiency were visually apparent in the streak images. For example, for the duplex with $n = 5$ (Fig. 4-5a), the signal of **P** around 400-450 nm disappeared within several ns since the FRET efficiency was very high. On the other hand, for duplexes with $n = 15$ and 20, the decay of **P** was longer due to lower FRET efficiency (Fig. 4-5c and 4-5d). In addition, the time course of energy transfer was observed from delayed fluorescence emission of **E**. Especially in Figure 4-5b, the signal of **E** around 500-600 nm was delayed for several ns compared with the decay of **P**.

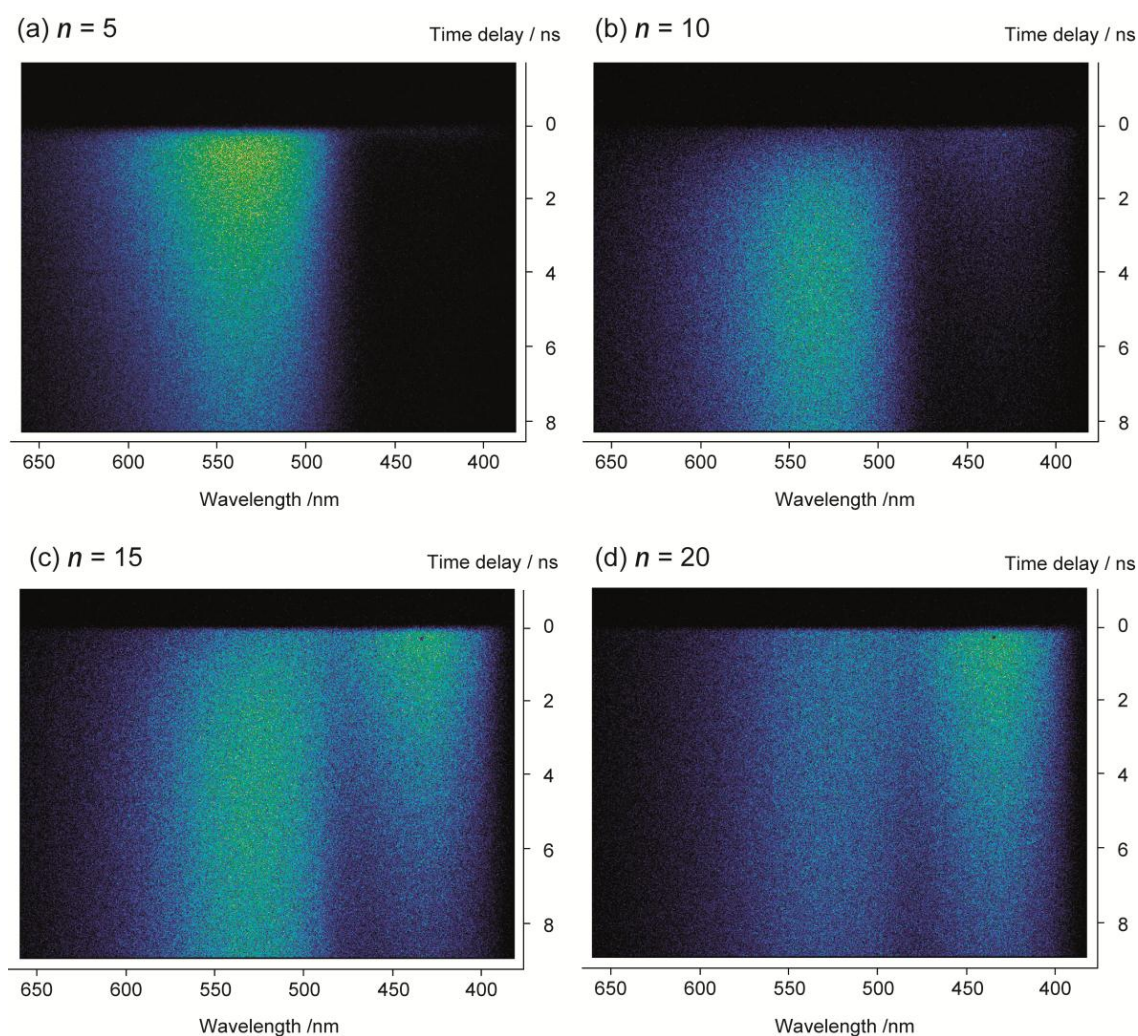


Figure 4-5. Streak images of na/nb ($n = 5, 10, 15,$ and 20). The excitation wavelength was 345 nm. Solution conditions were as follows: 100 mM NaCl, 10 mM phosphate buffer, pH 7.0, 50 μ M each ODN; room temperature.

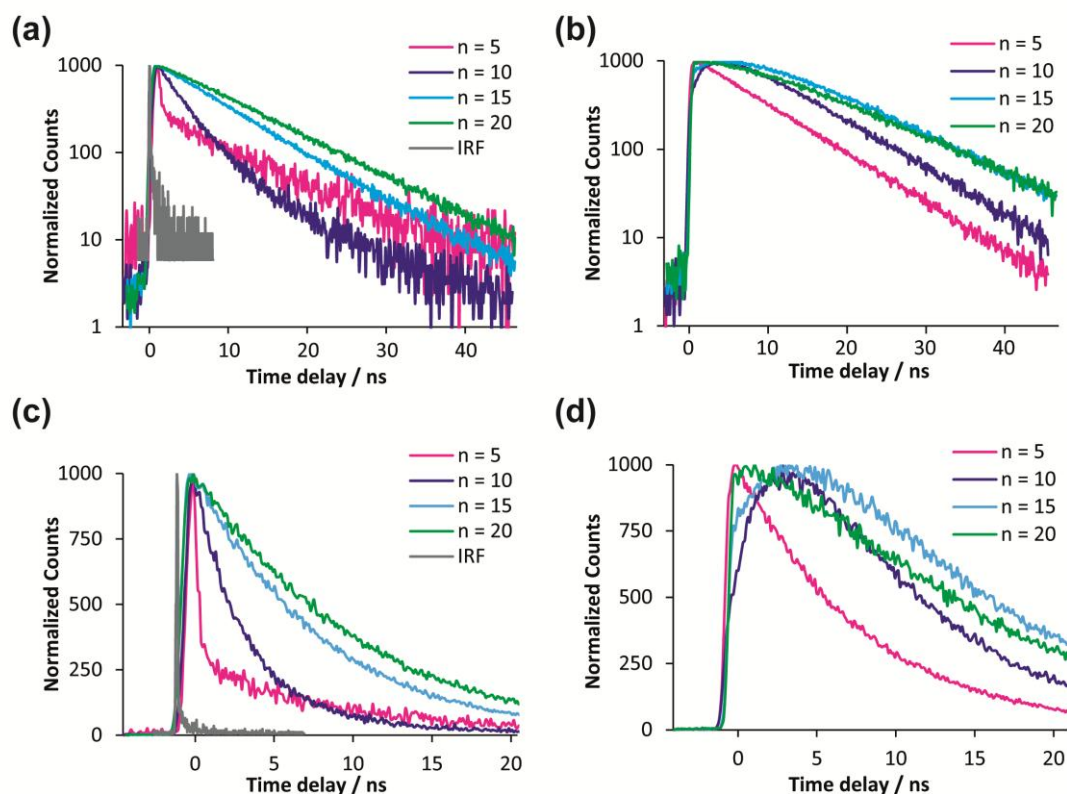
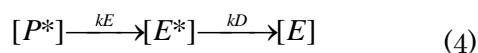


Figure 4-6. Fluorescence decay curves extracted from streak images. Signal counts were normalized by setting maxima to 1000 and plotted on semi-logarithmic scale. (a) Decay curves of **P** obtained from integration of the region from 384.6 to 439.0 nm. The vertical axis is common logarithmic scale. Instrument response factor (IRF) is shown by the gray line. (b) Decay curves of **E** obtained from integration of the region from 469.8 to 603.2 nm. (c) Decay curve of **P** with non-logarithmic vertical scale. Time delay < 20 ns was magnified. (d) Decay curve of **E** with non-logarithmic vertical scale. Time delay < 20 ns was magnified.

The lifetime of **P** was extracted from the streak figures (Figure 4-6a and 4-6c). Fluorescence lifetime of **P** was obviously changed with FRET efficiency. When the dyes were located in close proximity, fluorescence lifetimes were short due to efficient FRET (non-radiative process). As the dyes drew apart, lifetimes became longer and took almost the same value as that of donor-only sample. Lifetime of **E** was also extracted to obtain more information of energy transfer (Figure 4-6b and 4-6d). For $n = 5$, energy transfer occurred within several ns while slow ascent of fluorescence could be observed due to the slow energy transfer for $n = 10$. Then we obtained lifetime values from extracted fluorescence decay. All fitted parameters are summarized in Table 1. Decay curves of **P** exhibit two exponential curves when duplexes with $n < 8$ were analyzed, whereas those curves obtained from duplexes with $n \geq 8$ showed only single exponential curves. The shorter lifetime was caused by FRET, and the longer one was from the donor without energy transfer as it is almost the same as a lifetime of the donor in the

absence of the acceptor (9-10 ns). In addition, the rate constant calculated only from shorter lifetime (k_p) was consistent with that calculated from the acceptor emission (k_E ; *vide infra*). Thus, only shorter lifetimes were utilized for the calculation of k_p and FRET efficiencies (Φ_{T3}). These bi-exponential decays might be caused by unhybridized strand or by experimental errors in measurement of the short lifetime. These fitting results were consistent even if the longer lifetime was fixed known value of donor decay (see Table 4-3 in Appendixes section 4-7-4). Similar bi-exponential decay was observed previously.^{26,39} For the duplex with $n = 1$, the lifetime of **P** was too short to observe, indicating that FRET efficiency was higher than 99%. As expected, k_p did not vary linearly with the distance. For duplexes with $n = 8$ and 13, the lifetimes were longer than those of adjacent duplexes ($n = 8$ vs. $n = 9$ or 10, $n = 13$ vs. $n = 12$ or 14), resulting in the decline of FRET efficiency. These results are totally consistent with static fluorescence measurement.

The rate constant of FRET from acceptor emission (k_E) was also calculated. The increase in acceptor emission was fitted by assuming a step reaction (equation 4) and rate constants were obtained (Table 1).



Here, k_E shows the rate constant of energy transfer from **P** to **E** and k_D is the rate constant of radiative decay of **E**. The population of excited acceptor **E*** was estimated from fluorescence decay of **E** according to the step reaction equation of ($k_E/(k_D - k_E)$) ($\exp(-k_E t) - \exp(-k_D t)$). Curve fitting of **E** was performed on Kaleida Graph Ver. 4.0

Decay curves of the acceptor could not be fitted for longer duplexes ($n > 12$), probably due to weak acceptor emissions. Those rate constants that could be calculated were almost the same as the rate constants calculated from the donor emission (k_p).

Table 4-1. Summary of the results from T_m measurement, from FRET efficiency calculated from static measurement data and time-resolved measurement data, and from fluorescence lifetime curve fitting.

n	T_m (ΔT_m) /°C ^a	τ_1 / ns^b	α_1^b	τ_2 / ns^b	α_2^b	χ^2^b	Φ_{T1} ^c	Φ_{T2} ^d	Φ_{T3} ^e	k_P /ns⁻¹ ^f	k_E /ns⁻¹ ^g
1	54.6 (+8.9)	n.d.	n.d.	n.d.	n.d.	n.d.	0.88	0.89	n.d.	n.d.	18.09
2	58.2 (+9.5)	0.08	0.97	8.80	0.03	1.33	0.95	1.03	0.99	12.82	8.02
3	57.3 (+8.5)	0.37	0.96	7.65	0.04	1.29	0.91	1.04	0.96	2.70	2.51
4	58.0 (+6.4)	0.27	0.98	8.60	0.02	1.37	0.90	0.80	0.97	3.75	3.53
5	57.9 (+6.6)	0.19	0.86	8.46	0.14	1.06	0.92	0.92	0.98	5.18	4.01
6	59.3 (+6.0)	0.36	0.95	6.43	0.05	1.11	0.87	0.85	0.96	2.77	2.67
7	60.9 (+7.0)	1.27	0.92	7.10	0.08	1.26	0.83	0.85	0.86	0.79	0.97
8	59.5 (+5.0)	5.73	1.00			1.43	0.43	0.43	0.37	0.17	0.30
9	60.9 (+5.3)	4.17	1.00			1.27	0.58	0.64	0.54	0.24	0.62
10	60.0 (+4.1)	3.51	1.00			1.29	0.63	0.65	0.61	0.28	0.38
11	61.9 (+5.6)	4.45	1.00			2.38	0.51	0.56	0.51	0.22	0.28
12	57.0 (+0.0)	6.46	1.00			2.32	0.31	0.30	0.29	0.15	0.28
13	62.7 (+5.5)	8.92	1.00			1.21	0.08	0.12	0.07	0.11	-
14	63.2 (+5.5)	8.20	1.00			1.35	0.18	0.15	0.15	0.12	-
15	60.6 (+2.6)	7.64	1.00			1.64	0.21	0.22	0.20	0.13	-
16	63.2 (+4.8)	8.28	1.00			0.99	0.15	0.18	0.14	0.12	-
17	63.0 (+4.3)	9.18	1.00			1.60	0.13	0.09	0.04	0.11	-
18	61.1 (+1.7)	9.27	1.00			1.69	0.05	0.08	0.04	0.11	-
19	63.5 (+4.0)	9.52	1.00			1.50	0.03	0.04	0.01	0.10	-
20	63.7 (+3.9)	9.27	1.00			1.64	0.03	0.08	0.04	0.11	-
21	62.7 (+2.5)	8.75	1.00			1.80	0.08	0.11	0.09	0.11	-

a: Measurement conditions: 100 mM NaCl, 10 mM phosphate buffer, pH 7.0, 5.0 μ M each ODN; 0.5 °C/min. ΔT_m was the difference between T_m s of *na/nb* and control duplexes without dyes (*nc/nd*).

b: Normalized counts were fitted with a bi-exponential curve of $\alpha_1 \exp(-t/\tau_1) + \alpha_2 \exp(-t/\tau_2)$. Where α is amplitude of lifetime component and τ is lifetime. χ^2 is chi-squared value obtained by the fitting program.

c: Donor decrease-based FRET efficiency given by $\Phi_{T1} = 1 - I_{DA,400}/I_D$ (equation 5) where $I_{DA,400}$ is emission intensity of FRET pair *na/nb* at 400 nm, and I_D is that of donor only *na/nd* at 400 nm.

d: Acceptor increase-based FRET efficiency given by $\Phi_{T2} = [A_A/A_D] [I_{DA,530}/I_A - 1]$ (equation 6) where A_A and A_D are absorbance of acceptor and donor at 345 nm, respectively, $I_{DA,530}$ is emission intensity of FRET pair *na/nb* at 530 nm, and I_A is that of acceptor only *nc/nb* at 530 nm.

e: Donor lifetime-based FRET efficiency given by $\Phi_{T3} = 1 - \tau_{DA}/\tau_D$ (equation 7) where τ_{DA} is lifetime of **P** in *na/nb* and τ_D is that of the duplex containing only donor *11a/11d*. Fluorescence lifetime of the duplex containing only donor *11a/11d* was 9.07 ns for $n = 1-12$ and 9.61 ns for $n = 13-21$.

f: The rate constant of donor decay given by $k_P = 1/\tau_1$.

g: The rate constant of acceptor rise (k_E) was calculated from acceptor decay fitting. For more information, see Materials and Methods section. For $n > 12$, emission of **E** could not be fitted correctly because of high background.

4-3-5 Comparison of experimental data with cylinder model.

FRET efficiency in DNA has been estimated based on a rigid cylinder model of the DNA helix (Figure 4-7).^{11,40} Here, some values can be simplified for the theoretical calculation of FRET efficiency. The orientation and distance involving FRET efficiency was defined as shown in Figure 4-7a. The dyes were assumed to be in an almost parallel plane as dyes are intercalated within the DNA duplex. Based on this assumption, θ_b and θ_A in Figure 4-7a are 90° and the orientation factor κ^2 in eq. 3 can be simplified:

$$\kappa^2 = \cos^2 \theta_T \quad (8)$$

Here, θ_T is the angle between dyes in rotational direction of helix. As described above, the distance and orientation of dyes periodically varied with the number of inserted AT pairs. As shown in Figure 4-7b, the distance between the dyes (R) increases by 3.2 \AA/bp , which is slightly shorter than typical B-type DNA duplex owing to the influence of the AT tract.^{17,41} The angle θ_T varies by $-36^\circ/\text{bp}$ (10 bp/turn). Dye angles owing to conjugation with D-threosinol should also be corrected. We determined the transition dipole moments of the two dyes by Gaussian 09W TD-DFT B3LYP 6-31G (Figure 4-7c) and found that the transition dipole moments of pyrene (**P**) and perylene (**E**) were almost parallel to the long axes of each dye.^{42, 43} Next, the angles between transition dipole moment and proximal AT pair were obtained from an energy minimized structure calculated by computer simulation using the Insight II/Discover 98.0 program package. The angle from **P** to the proximal AT was nearly parallel ($\sim 0^\circ$), whereas that of **E** was about -25° (Figure 4-8b and 4-8c). Accordingly, orientation of dyes is given by the following equation:

$$\theta_r = -36^\circ \times (n-1) - 25^\circ \quad (9)$$

And the distance R in \AA is:

$$R = 3.2 \times (n+1) \quad (10)$$

Figure 4-8a shows the computational calculation of energy-minimized structure for the duplex with $n = 10$; dyes are located over a distance of $10 + 1 \text{ bp}$, namely, almost one turn of helix. The dye axes are parallel and intercalated between base pairs. When $n =$

10, θ_T was calculated to be -349° , which was consistent with simulated structure (Figure 4-8d).

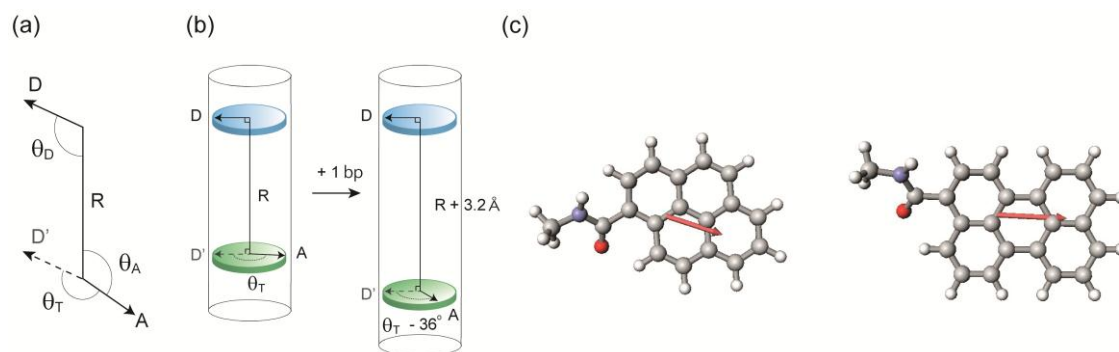


Figure 4-7. Illustrations of the cylinder model. (a) The assignment of angles for calculation of orientation factor. (b) Dyes are assumed to be completely parallel and the helical axis was assumed to penetrate the center of each dye. Insertion of an AT pair affords $+3.2 \text{ \AA}$ in distance and -36° in angle. (c) Calculated transition dipole moments of **P** and **E** by Gaussian 09W. Red arrows indicate the transition dipole moments.

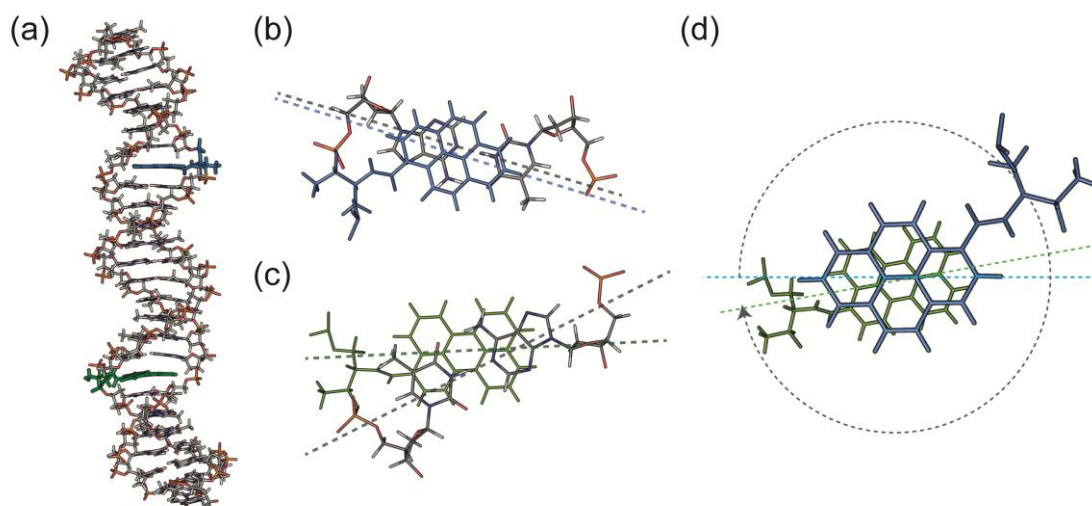


Figure 4-8. Computer simulation of energy-minimized structure of FRET duplex with $n = 10$ by Insight II/Discover 98.0 program package. (a) Structure of duplex with FRET pair. **P** is indicated in blue, and **E** is indicated in green. (b) Angle between **P** and neighboring AT pair (0°). (c) Angle between **E** and neighboring AT pair (25°). (d) Total angle (θ_T) between **P** and **E**. The θ_T of -349° calculated based on the cylinder model was in good agreement with the computer simulation. Right-handed dashed arrow indicates -349° .

The combination of equations 1, 2, 8, 9, and 10 allows calculation of FRET efficiency, Φ_T , of na/nb duplexes. As expected, theoretically calculated curve of cylinder model was obviously different from that the averaged $\kappa^2 = 2/3$ curve (Figure 4-9). This bouncing-ball like curve demonstrated certain influence of the orientation. For comparison of measured FRET efficiency with the cylinder model, FRET efficiency Φ_{T1} (decrease in donor emission), Φ_{T2} (increase in acceptor emission), Φ_{T3} (donor decay lifetime) were experimentally determined (Table 4-1). Observed FRET efficiencies obtained from the different methods showed similar dependency on the number of incorporated AT pairs (n), demonstrating the validity of this model. The exception was Φ_{T2} determined from the increase in acceptor emission, which had relatively large values compared with others, probably due to experimental difficulty in determining Φ_{T2} from small absorbance.

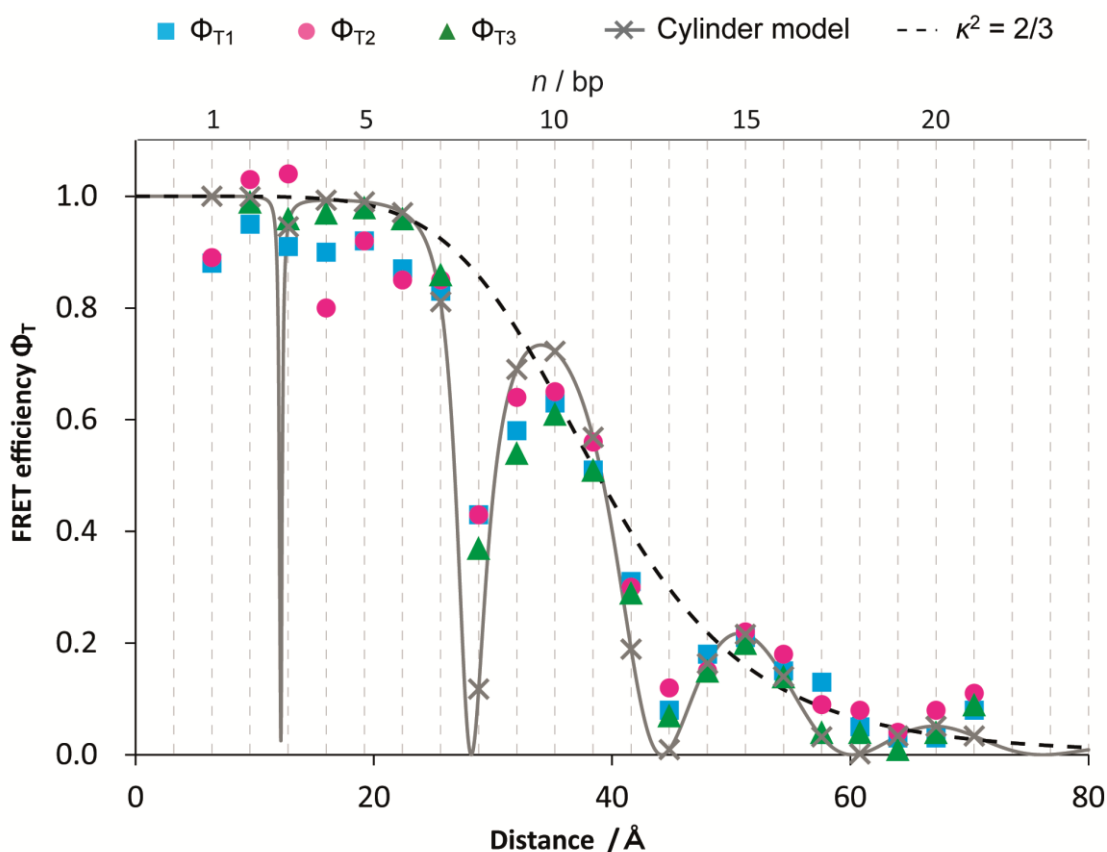


Figure 4-9. Comparison of FRET efficiency obtained from static fluorescence measurement (Φ_{T1} , cyan squares, Φ_{T2} , magenta circles) and time-resolved fluorescence spectroscopy (Φ_{T3} , green triangles) with theoretical values of cylinder model (gray line with cross symbols). The value of averaged orientation is also shown by dashed line.

The comparison of experimental values with the calculated FRET efficiencies is shown in Figure 4-9. The experimental values are in excellent agreement with the calculated values, confirming the validity of the cylinder model. Determination coefficients calculated from the theoretical model and the experimental values were 0.957 for Φ_{T1} , 0.946 for Φ_{T2} and 0.962 for Φ_{T3} indicating good agreement. Significant declines of Φ_T were observed at $n = 8, 13,$ and 18 ; in these duplexes, the two chromophores (i.e., transition dipole moments) were in an approximately perpendicular orientation. The valley observed in Figure 4-9 was much deeper than valleys observed in other studies of duplexes with fluorophores attached at the termini. In our design, dyes are intercalated between base pairs. As a result, stacking interactions of dyes with neighboring base pairs suppress mobility of dyes. The deeper valley observed in this system is evidence of control of dye orientation. FRET efficiency in our system exhibit significant decline of approximately 0.4 in FRET efficiency reflecting strong restriction of dye mobility. Such deep decline was also observed in FRET system using fluorescent nucleotide analog reported by Börjesson *et al.* In their system, fluorescent nucleotide analog was doubly fixed by stacking interaction and hydrogen bonding. The FRET system reported here also showed similar deep decline of FRET efficiency, indicating that mobility of tethered dye within DNA duplex was strictly suppressed. Our DNA modified with base-surrogate chromophores provides a FRET model system that precisely reflects the orientation factor as well as distance, and FRET efficiency can be accurately predicted from a simplified cylinder model of the DNA helix.

From these results, the importance of the orientation factor was further confirmed. The effect of orientation factor should be carefully considered in FRET measurement because disregard of the orientation factor by using averaged value of $\kappa^2 = 2/3$ would cause a considerable error in distance estimation. Hence attention should be paid to unexpected restriction of dye mobility (e.g. groove binding) even though long flexible linkers are used to tether donor and acceptor dyes.

There was a relatively large difference between experimental and calculated Φ_T for duplexes with $n = 1$ and $n = 8$. In the case of the **1a/1b** duplex, the experimental Φ_T was about 0.9, whereas the calculated value was 1.0. The acceptor emission was likely quenched due to the exciton coupling between the dyes due to the close proximity of **P**

and **E** as they are separated by only one AT pair.⁴⁴ **1a/1b** showed bathochromicity of perylene absorption in UV-Vis spectra with respect to those of other duplexes (see section 4-7-5 in Appendixes). For the duplex with $n = 8$, Φ_T was calculated as approximately 0.1 based on the cylinder model because transition dipole moments were nearly perpendicular. However, experimental Φ_{TS} were about 0.4. When the θ_T is around 90° , the orientation factor (κ^2) becomes close to 0. Even small difference in θ_T would cause a large difference in κ^2 .

In this study, dyes were separated with AT base pairs to avoid sequence-dependent quenching of fluorescence. AT tracts are known to induce the curvature in a DNA duplex. However, because the curvature of AT tract is slight ($5^\circ/6$ bp),⁴¹ the difference in orientation factor induced by the AT tract should be small.¹⁷ In addition, the curvature will compensate as the AT tract is lengthened. Accordingly, it was concluded that the effect of AT tract curvature was negligible in this system.

4-3-6 Generality of the FRET system with tethering dyes in DNA duplex

Finally, to confirm generality of the proposed FRET system in which dyes were fixed within DNA duplex, another FRET pair of perylene – Cy3 was examined (Figure 4-10). Similar to **P** and **E**, Cy3 was covalently tethered with D-threoninol via only amide bond and **Y** would have sufficient rigidity within DNA duplex. **Y** was introduced into specific position on the same sequences of **na**. To discriminate carrying dye, ODNs containing **Y** were named **ne** where *n* indicates the number of intervening AT pairs. Short excitation wavelength like UV is harmful for biological molecules. Hence longer excitation wavelength is more applicable for practical use. Here, perylene was used as donor fluorophore and its excitation wavelength is around 450 nm, harmless blue visible light. In addition, the acceptor fluorophore, Cy3 has a large extinction coefficient. The extinction coefficient is responsible for $\mathcal{J}(\lambda)$, spectrum overlap. Improvement of spectrum overlap extends R_0 , therefore FRET efficiency is tunable by designing the pair of dyes. As shown in Figure 4-10c, the pair of **E** and **Y** exhibited good spectrum overlap and $\mathcal{J}(\lambda)$ was $5.4 \times 10^{15} \text{ (M}^{-1} \text{ cm}^{-1} \text{ nm}^4)$, which was more than 10 times larger comparing with **P-E** pair due to large extinction coefficient of Cy3. When Φ_D and κ^2 were assumed to be 0.25 and 2/3 respectively, $\mathcal{J}(\lambda)$ was calculated as high as $5.50 \times 10^{15} \text{ M}^{-1} \text{ cm}^{-1} \text{ nm}^4$ and R_0 of **E-Y** pair was 52.5 \AA , which corresponds to approximately 16 bp.

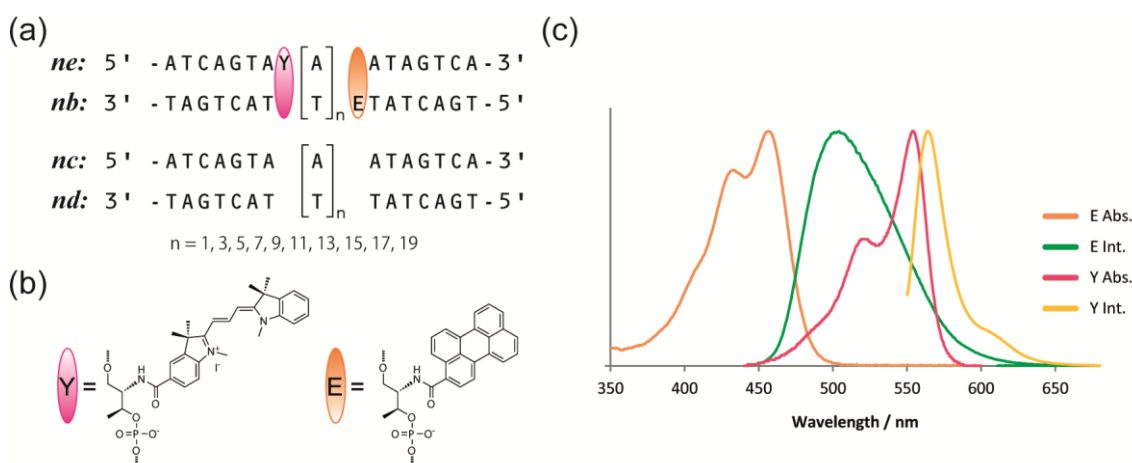


Figure 4-10. Schematic of FRET system used in this study. (a) Sequence of FRET ODN pair. AT pairs were inserted between **E** (perylene as donor) and **Y** (Cy3 as acceptor). **Y** and **E** moieties were introduced into strands **ne** and **nb**, respectively, where *n* indicates the number of inserted A or T residues; **nc** and **nd** were ODNs without fluorophores with sequences identical to **ne** and **nb**, respectively. **E** and **Y** moieties are inserted into the DNA duplex as single-residue bulges when **ne** and **nb** are hybridized. (b) Structure of **Y** and **E**. Dyes were directly conjugated via D-threoninol to the DNA strand. (c) Normalized absorption and emission spectra of **Y** and **E**.

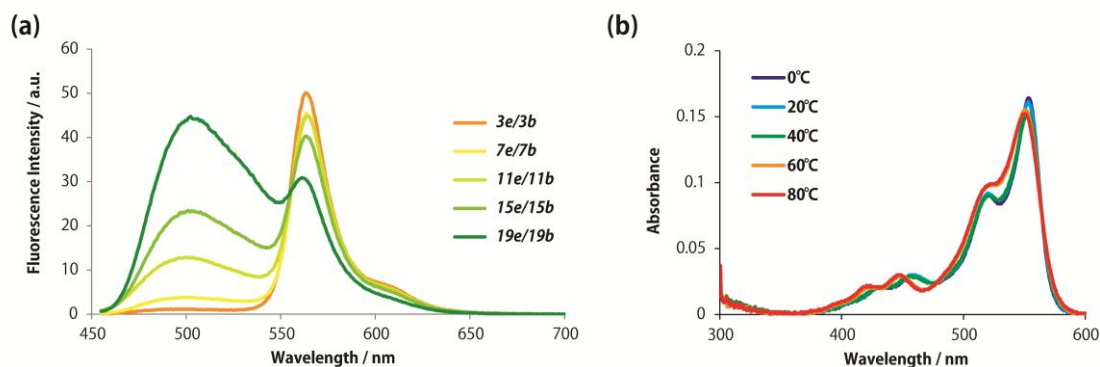


Figure 4-11. Spectroscopic behaviors of **E-Y** FRET pair duplex. (a) Fluorescence emission of FRET pairs containing **Y** and **E** ($n = 3, 7, 11, 15$ and 19) at $0\text{ }^{\circ}\text{C}$. The excitation wavelength was 450 nm . The other fluorescence spectra of FRET pairs were depicted in 4-7 Appendix section. Solution conditions were as follows: 100 mM NaCl , $10\text{ mM phosphate buffer, pH } 7.0$, $1.0\text{ }\mu\text{M}$ each ODN. Before measurements, samples were heated at $80\text{ }^{\circ}\text{C}$ for 5 min followed by cooling gradually at the rate of $4\text{ }^{\circ}\text{C/min}$ to $20\text{ }^{\circ}\text{C}$. (b) Temperature dependence of UV-Vis spectra of **9e/9b**. Spectra at $300\text{-}500\text{ nm}$ are magnified. Solution conditions were as follows: 100 mM NaCl , $10\text{ mM phosphate buffer, pH } 7.0$, $1.0\text{ }\mu\text{M}$ each ODN.

Static fluorescence emission spectra were shown in Figure 4-11. For **3e/3b**, the emission of **E** was significantly dropped and distinct emission of **Y** was observed. Similarly, **7e/7b** also showed efficient FRET. By contrast, **19e/19b** showed low emission of **Y** owing to distance dependence of FRET efficiency, however, comparing with **P-E** FRET pair, obvious FRET has been still observed. Fluorescence of **11e/11b** and **15e/15b** were appropriately changed based on the distance dependence. Temperature dependence of UV-Vis spectra showed sharpening and red-shift of λ_{max} of dyes indicating intercalation (Figure 4-11b). Stabilization of duplex judging from T_m measurement also supported the intercalation (Table 4-2).

Comparison of fluorescence intensity between donor and acceptor emission was shown in Figure 4-12. Similar to **P-E** pair, the decrease of donor emission and the increase of acceptor emission were highly correlated (Figure 4-12b and 4-12c). Non-monotonous change of distance dependence was clearly observed in $n > 11$. This was also observable by naked eye as the change from orange to green emission (Figure 4-12a). In the cases of $n < 12$, changes in the acceptor emission could not be clearly observed since highly efficient FRET within Förster radius. For **1e/1b**, fluorescence of both **E** and **Y** were significantly quenched. This is because photo induced electron transfer (PET) between **E** and **Y**. This quenching by PET was not observed in $n > 1$.

Interestingly, prominent decline of FRET efficiency was observed in $n = 8, 13$ and 18 , similar to **P-E** pair as shown in Figure 4-4. Again, this appearance of irregular point in cycle of 5 bp corresponding to half-turn of DNA helix strongly indicated that orientation dependence of FRET efficiency was regulated by helical structure of DNA. Namely, it was confirmed that the design of FRET system reported here is applicable to any other pairs of fluorophores.

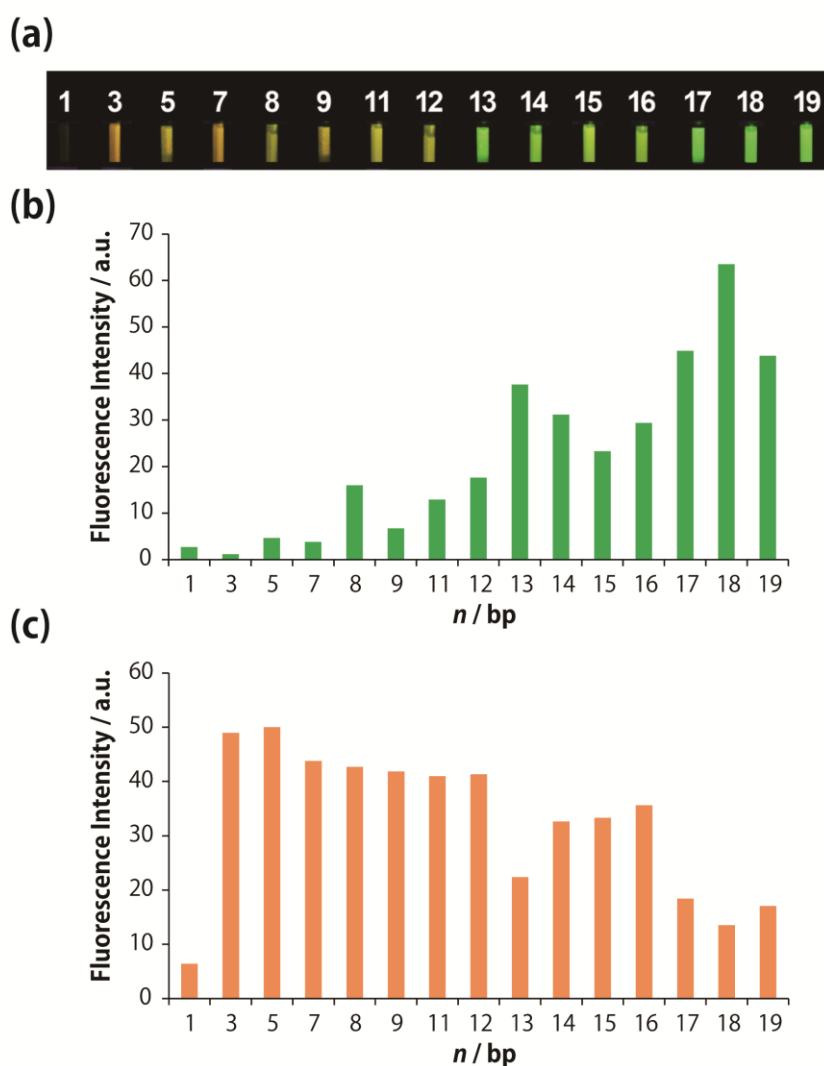


Figure 4-12. Distance dependence of fluorescence intensity of *ne/nb* duplexes. Measurement conditions were as follows: 100 mM NaCl, 10 mM phosphate buffer, pH 7.0, 1.0 μ M each ODN. (a) A photograph of samples excited at 480 nm. (b) Fluorescence intensity of **E** (500 nm) at 0 °C. The excitation wavelength was 450 nm. (c) Fluorescence intensity of **Y** (565 nm). Since the emission of **E** was overlapped with that of **Y** at 565 nm, it was subtracted by using the intensity ratio of **E**: $(I_{DA,565} - I_{DA,500}) / (I_{D,565} / I_{D,500})$, where $I_{DA,565}$ and $I_{DA,500}$ were fluorescence intensity of *ne/nb* (FRET pair) at 565 and 500 nm, respectively and $I_{D,565}$ and $I_{D,500}$ were that of *nc/nb* (Donor only) at 565 and 500 nm.

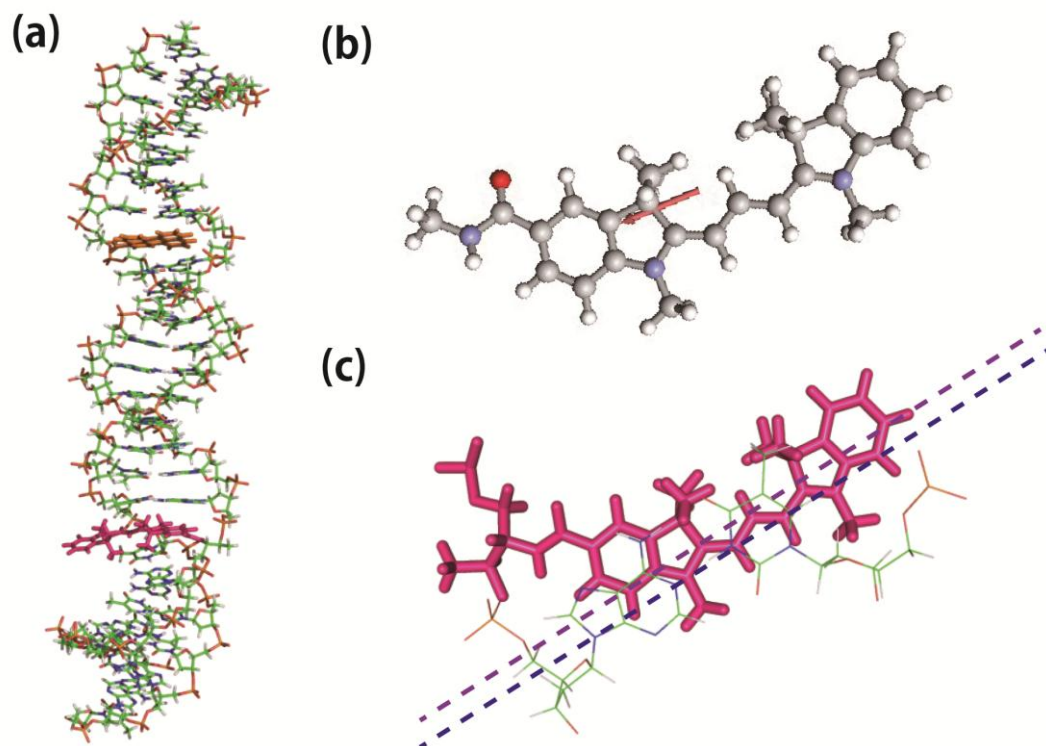


Figure 4-13. Computer simulation of energy-minimized structure of *10e/10b* FRET duplex by Insight II/Discover 98.0 program package. (a) Structure of duplex with FRET pair. **E** is indicated in yellow, and **Y** is indicated in magenta. (b) Calculated transition dipole moments of **Y** by Gaussian 09W. Red arrows indicate the transition dipole moments. (c) Angle between **Y** and neighboring AT pair (0°).

Next, to compare the experimental values of FRET efficiency with the cylinder model, computer calculation of transition dipole moment of **Y** and the angle between proximal AT pair and **Y** were performed (Figure 4-13). Dimethyl groups of Cy3 slightly distorted base pairing of around **Y**, however, **E** and **Y** could be assumed to be almost parallel by stacked within the laminating layer of nucleobases (Figure 4-13a). Transition dipole moment of **Y** was calculated by Gaussian 09W, and it was parallel to the poly methine linker between indole rings. This result was consistent with a previous literature.²¹ From the result of computer simulation of energy-minimized structure of *10e/10b*, the transition dipole moment of **Y** was almost parallel to proximal AT base pair. Therefore, FRET efficiency can be calculated with the same equation (eq. 9 and 10) used for **P-E** pair.

$$\theta_r = -36^\circ \times (n-1) - 25^\circ \quad (9) \quad R = 3.2 \times (n+1) \text{ \AA} \quad (10)$$

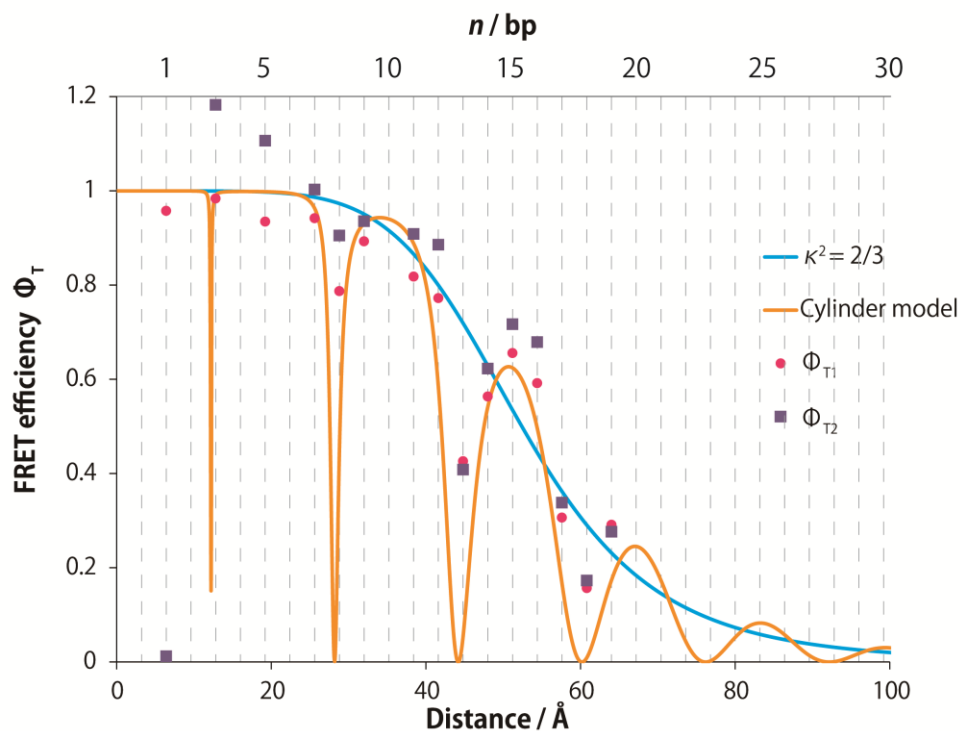


Figure 4-14. Comparison of FRET efficiency obtained from static fluorescence measurement (Φ_{T1} , magenta circles, Φ_{T2} , purple squares) with theoretical values of cylinder model (orange line). The curve of averaged orientation is also shown by cyan line.

Theoretical curve of FRET efficiency of **E-Y** pair based upon cylinder model was depicted in Figure 4-14. Φ_D was 0.25, determined by using perylene in cyclohexane (0.78) as a reference. Helical period and helical pitch were 10 bp/turn and 3.2 Å /bp, respectively. FRET efficiency was still remained over the long distance of 30 bp, approximately 100 Å due to enhancement of Förster radius. As expected, the valley indicating decline of FRET efficiency was located at $n = 3, 8, 13, 18, 23$ and 28. On the other hand, the experimental values were also plotted in Figure 4-14. Here, FRET efficiency based on fluorescence decrease of donor (Φ_{T1}) and based on fluorescence increase of acceptor (Φ_{T2}) were calculated. Experimental values were in good agreement with cylinder model. However, when the distance between donor and acceptor was short, Φ_{T2} tends to be overestimated because the absorption spectra were influenced by interaction between dyes. For $n = 1$, severe quench both **E** and **Y** disabled calculation of accurate FRET efficiency. In addition, the valley of FRET efficiency seems to be relatively shallow comparing with **P-E** pair. This may be because Cy3 could not be fixed

strictly within DNA duplex owing to steric hindrance of bulky dimethyl groups. In the case of **P-E** pair, both **P** and **E** have highly planar structure, which is very suitable for intercalation between base pairs, and they can be strongly stacked and the mobility would be severely restricted. However, non-planar dyes like Cy3 would more or less distort DNA duplex and it would weaken stacking interaction and restriction of mobility of dye. Nevertheless, tethering dyes within DNA duplex is certainly effective even if dye is non-planar, because the orientation dependence of FRET efficiency was clearly observed. Therefore it could be concluded that this FRET system tethering dyes inside of DNA helix has sufficient versatility and is excellent design which can clearly demonstrate the orientation dependence of FRET efficiency.

Table 4-2. Summary of the results from T_m measurement, from FRET efficiency calculated from static fluorescence measurement data.

n	$T_m (\Delta T_m) / ^\circ\text{C}$ ^a	Φ_{T1} ^b	Φ_{T2} ^c
1	51.0 (+5.3)	0.96	0.01
3	54.6 (+5.8)	0.98	1.18
5	55.8 (+4.3)	0.93	1.11
7	56.8 (+3.6)	0.94	1.00
8	56.0 (+1.5)	0.79	0.91
9	56.0 (+0.5)	0.89	0.94
11	57.5 (+1.2)	0.82	0.91
12	57.7 (+0.7)	0.77	0.89
13	58.0 (+0.8)	0.43	0.41
14	57.7 (+1.8)	0.56	0.62
15	58.6 (+0.5)	0.66	0.72
16	60.2 (+1.7)	0.59	0.68
17	59.5 (+0.8)	0.31	0.34
18	59.7 (+0.3)	0.16	0.17
19	60.8 (+1.3)	0.29	0.28

a: Measurement conditions: 100 mM NaCl, 10 mM phosphate buffer, pH 7.0, 1.0 μM each ODN; 0.5 $^\circ\text{C}/\text{min}$. ΔT_m was the difference between T_{ms} of **na/nb** and control duplexes without dyes (**nc/nd**).

b: Donor decrease-based FRET efficiency given by $\Phi_{T1} = 1 - I_{DA,500}/I_D$ (equation 5) where $I_{DA,500}$ is emission intensity of FRET pair **ne/nb** at 500 nm, and I_D is that of donor only **nc/nb** at 500 nm.

c: Acceptor increase-based FRET efficiency given by $\Phi_{T2} = [A_A/A_D] [I_{DA,565}/I_A - 1]$ (equation 6) where A_A and A_D are absorbance of acceptor and donor at 450 nm, respectively. $I_{DA,565}$ is emission intensity of FRET pair **ne/nb** at 565 nm which was subtracted by using the intensity ratio of **E**; $(I_{DA,565} - I_{DA,500}) / (I_{D,565}/I_{D,500})$, where $I_{DA,565}$ and $I_{DA,500}$ were fluorescence intensity of **ne/nb** (FRET pair) at 565 and 500 nm, respectively and $I_{D,565}$ and $I_{D,500}$ were that of **nc/nb** (Donor only) at 565 and 500 nm. I_A is that of acceptor only **ne/nd** at 565 nm.

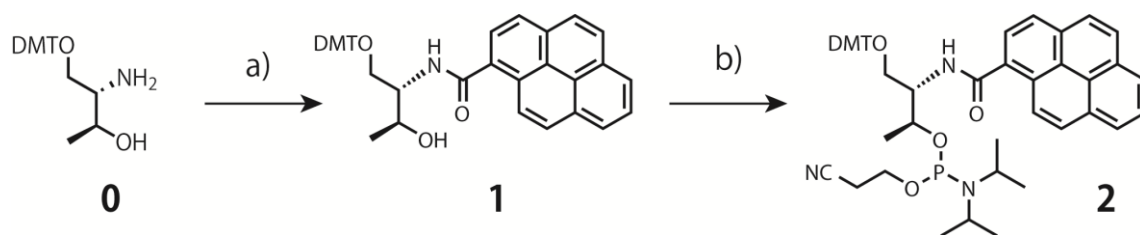
4-4 Conclusions

A robust FRET system, in which dye orientation and distance between chromophores are controlled within a rigid DNA duplex, has been successfully developed. FRET efficiency depended on the orientation of dyes as well as the distance, demonstrating that mobility of the dye was restricted by strong stacking interactions with neighboring base pairs. Experimental FRET efficiencies of our system were in good agreement with theoretical values predicted by the cylinder model of a DNA helix. The orientation factor, which is obscure due to difficulty of strict control of orientation, was reflected in this FRET system. It was also confirmed that regulation of the position and the orientation by tethering dyes via D-threoninol has good generality and would be applicable to any other FRET pairs. In general, FRET is used to determine the distance between dyes. The results presented in this study demonstrated that relative orientation of dyes strongly affects the FRET efficiencies. Our system using D-threoninol as a scaffold of functional molecule will be suitable for experimental verification of theoretical predictions. It can be also applied to structural analyses (such as helical pitch) of supra-molecules and artificial helical polymers as well as oligonucleotides.

4-5 Experimental section

Materials: All the conventional phosphoramidite monomers, CPG columns, reagents for DNA synthesis, and Poly-Pak II cartridges were purchased from Glen Research. Other reagents for the synthesis of phosphoramidite monomers were purchased from Tokyo Chemical Industry, Wako, and Aldrich. Native oligodeoxyribonucleotides (ODNs) were purchased from Integrated DNA Technologies.

4-5-1 Synthesis of pyrene (P), perylene (E) and Cy3 (Y) moiety

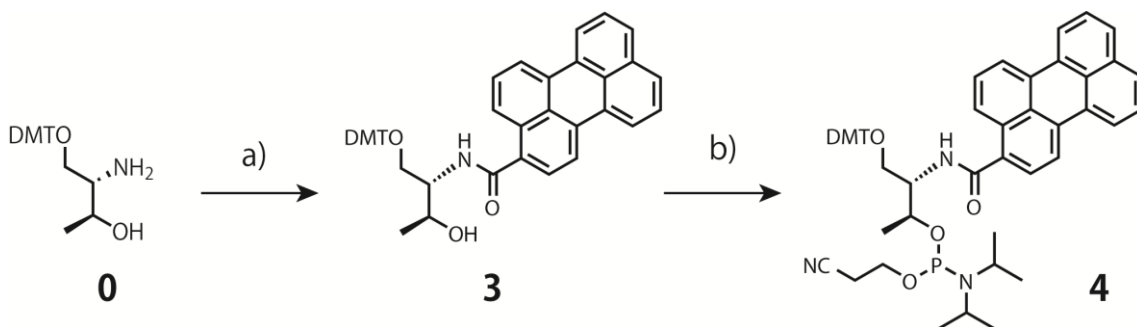


Scheme 4-1. Synthesis of phosphoramidite monomer bearing 1-pyrenecarboxylic acid (P) directly conjugated on D-threoninol through amide bond.; a) DCC, HOBt, DMF, r.t., overnight, 72% b) $(iPr)_2NP(Cl)(OCH_2CH_2CN)$, DIPEA, dry CH_2Cl_2 , 0°C, 1h, 81 %

Compound 1. 1-Pyrenecarboxylic acid (296 mg, xxx mmol) was condensed with DMT-D-threoninol (406 mg, 1.0 mmol) in the presence of DCC (248 mg, 1.2 mmol, 1.2eq) and HOBt·H₂O (184 mg, 1.2 mmol, 1.2eq) in 20 mL of DMF stirred for overnight at room temperature. Then EtOAc was added to the reaction mixture and was washed with saturated solution of NaHCO₃ and that of NaCl. After drying over MgSO₄, the solvent was removed by evaporation, followed by silica gel column chromatography (Hexane: AcOEt: Et₃N = 50: 50: 3 *R_f* = 0.26) to afford compound 1 (460 mg, 0.72 mmol, yield 72%). ¹H-NMR [CDCl₃, 500 MHz] δ = 8.56 (m, 1H, aromatic protons of pyrene), 8.45 (d, 1H, *J* = 9.0 Hz, -NHCO-), 8.37-8.10 (m, 8H, aromatic protons of pyrene), 7.49-6.85 (m, 13H, aromatic protons of DMT), 4.35 (m, 1H, -CH₂CHNH), 4.00 (m, 1H, -CHOH), 3.71 (s, 6H, -OCH₃), 3.36 (dd, *J* = 9 and 4.5 Hz, 1H, -OCH₂-), 3.10 (dd, *J* = 9 and 4.5 Hz, 1H, -OCH₂-), 1.11 (d, *J* = 6.5 Hz, 3H, CH₃-).

Compound 2. 2-cyanoethyl diisopropylchlorophosphoramidite (0.32 mL, 1.45 mmol, 2 eq) and DIPEA (0.62 mL, 3.62 mmol, 5eq) were added to a solution of compound 1 (460 mg, 0.724 mmol) in dry CH₂Cl₂ (10.0 mL) and the solution was stirred for 30 min at 0 °C, and then 30 min at room temperature. Then, EtOAc was added to the reaction mixture and was washed with saturated aqueous solution of NaHCO₃ and that of NaCl. After

drying over MgSO_4 , the solvent was removed by evaporation, followed by silica gel column chromatography (Hexane : AcOEt Et_3N = 66:33:3, R_f = 0.24) to afford **2** (490 mg, 0.59 mmol, yield 81 %).

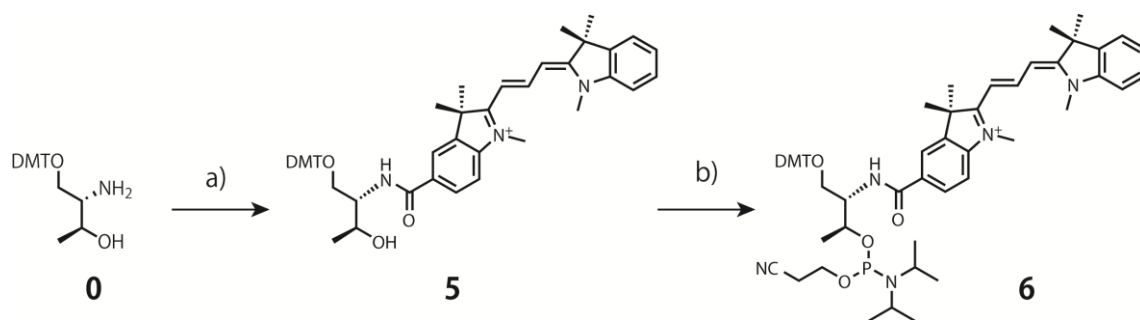


Scheme 4-2. Synthesis of phosphoramidite monomer carrying 3-perylenecarboxylic acid (**E**) directly conjugated on D-threoninol through amide bond.; a) DCC, HOBT, DMF, r.t., overnight, 50 % b) $(i\text{Pr})_2\text{NP}(\text{Cl})(\text{OCH}_2\text{CH}_2\text{CN})$, DIPEA, dry CH_2Cl_2 , 0°C , 1h, 86 %

Compound 3. 3-perylenecarboxylic acid (156 mg, 0.53 mmol) was synthesized according to the previous report (S.S. Bag, Y. Saito, K. Hanawa., S. Kodate, I. Suzuka and I. Saito, *Bioorg. Med. Chem. Lett.*, **2006**, *16*, 6338-6341.) and was condensed with DMT-D-threoninol (285 mg, 0.7 mmol) in the presence of DCC (124 mg, 0.6 mmol, 1.2eq) and HOBT· H_2O (92 mg, 0.6 mmol, 1.2eq) in 20 mL of DMF stirred for overnight at room temperature. Then EtOAc was added to the reaction mixture and was washed with saturated solution of NaHCO_3 and that of NaCl . After drying over MgSO_4 , the solvent was removed by evaporation, followed by silica gel column chromatography (Hexane: CHCl_3 : Et_3N = 50: 50: 3 R_f = 0.14) to afford compound **3** (340 mg, 0.50 mmol, yield 71 %). $^1\text{H-NMR}$ [CDCl_3 , 500 MHz] δ = 8.27 – 7.51 (m, 11H, aromatic protons of perylene), 7.42 – 6.81 (m, 13H, aromatic protons of DMT), 6.72 (d, J = 9.0 Hz, 1H, $-\text{NHCO}-$), 4.26 (m, 1H, $-\text{CH}_2\text{CHNH}$), 3.78 (m, 1H, $-\text{CHOH}$), 3.77 and 3.76 (s and s, 6H, $-\text{OCH}_3$), 3.71 (dd, J = 10

and 3.5 Hz, 1H, -OCH₂-), 3.44 (dd, *J* = 10 and 3.5 Hz, 1H, -OCH₂-), 1.31 (d, *J* = 6.0 Hz, 3H, CH₃-). ¹³C-NMR [CDCl₃, 126 MHz] δ = 170.0, 158.6, 144.5, 135.6, 135.5, 134.3, 133.3, 131.5, 131.1, 130.7, 130.1, 130.0, 128.8, 128.5, 128.2, 128.0, 127.9, 127.32, 127.0, 126.5, 126.5, 126.4, 125.7, 125.2, 120.9, 120.6, 120.5, 118.8, 113.3, 86.8, 68.6, 65.2, 55.2, 54.4, 20.4. HRMS(FAB) Calcd for C₄₆H₃₉NO₅ (M⁺) 685.2828. Found 685.2814.

Compound 4. 2-cyanoethyldiisopropylchlorophosphoramidite (0.22 mL, 0.99 mmol, 2 eq) and DIPEA (0.42 mL, 2.48 mmol, 5eq) were added to a solution of compound **3** (340 mg, 0.50 mmol) in dry CH₂Cl₂ (5.0 mL) and the solution was stirred for 30 min at 0 °C, and then 30 min at room temperature. Then, EtOAc was added to the reaction mixture and was washed with saturated aqueous solution of NaHCO₃ and that of NaCl. After drying over MgSO₄, the solvent was removed by evaporation, followed by silica gel column chromatography (Hexane : CHCl₃ Et₃N = 50:25:3, *R_f* = 0.18) to afford **4** (380 mg, 0.43 mmol, yield 86 %). ¹H-NMR [CDCl₃, 500 MHz] δ = 8.26 – 7.43 (m, 11H, aromatic protons of perylene), 7.37 – 6.79 (m, 13H, aromatic protons of DMT), 6.37 and 6.19 (d and d, *J* = 9.0 Hz, 1H, -NHCO-), 4.54 (m, 1H, -CH₂CHNH), 3.79 (m, 1H, -CHOH), 3.77 (s, 6H, -OCH₃), 3.51 (m, 2H, NC-CH₂-CH₂-O-), 3.54-3.31 (m, 2H, -OCH₂-), 3.46 (m, 2H, N(CH₃CHCH₃)₂), 2.56-2.28 (m, 2H, NC-CH₂-CH₂-O-), 1.34-1.07 (m, 12H, N(CH₃CHCH₃)₂), 0.92 (d, *J* = 6.5 Hz, 3H, CH₃-). ¹³C-NMR [CDCl₃, 176 MHz] δ = 169.5, 158.6, 145.0, 136.2, 134.7, 134.2, 133.6, 131.9, 131.4, 131.1, 130.6, 130.3, 129.2, 128.8, 128.6, 28.4, 128.3, 128.2, 128.0, 127.7, 127.6, 127.0, 126.9, 126.7, 125.8, 121.2, 120.9, 119.3, 113.3, 86.3, 70.3, 69.6, 63.5, 58.1, 55.3, 55.0, 54.6, 43.2, 24.6, 20.3, 19.9. ³¹P-NMR [CDCl₃, 300 MHz] δ = 148.6, 148.7. HRMS(FAB) Calcd for C₅₅H₅₆N₃O₆P (M⁺) 885.3907. Found 885.4226.



Scheme 4-3. Synthesis of phosphoramidite monomer carrying Cy3-carboxylic acid (**Y**) directly conjugated on D-threoninol through amide bond.; a) DCC, HOBt, DMF, r.t., overnight, 58 % b) $(iPr)_2NP(Cl)(OCH_2CH_2CN)$, DIPEA, dry THF, 0°C, 1h, 51 %

Compound 5. Cy3-carboxylic acid (1.06 g, 2.0 mmol) was synthesized according to the previous report (Tomasulo, M.; Kaanumal, S.L.; Sortino, S.; Raymo, F.M. *J. Org. Chem.*, **2007**, *72*, 595-605) and was condensed with DMT-D-threoninol (0.82 g, 2.0 mmol) in the presence of DCC (0.83 g, 4.0 mmol, 2eq) and HOBt·H₂O (0.61 g, 4.0 mmol, 2eq) in DMF stirred for overnight at room temperature. Then EtOAc was added to the reaction mixture and was washed with saturated solution of NaHCO₃ and that of NaCl. After drying over MgSO₄, the solvent was removed by evaporation, followed by silica gel column chromatography (CHCl₃: Et₃N = 100 → CHCl₃: MeOH = 20 : 1) to afford compound **5** (1.06 g, 1.2 mmol, yield 58 %).

Compound 6. 2-cyanoethyl diisopropylchlorophosphoramidite (0.36 mL, 1.6 mmol, 2 eq) and DIPEA (0.79 mL, 4.0 mmol, 5eq) were added to a solution of compound **5** (0.73 g, 0.8 mmol) in dry THF and the solution was stirred for 30 min at 0 °C, and then 30 min at room temperature. Then, EtOAc was added to the reaction mixture and was washed with saturated aqueous solution of NaHCO₃ and that of NaCl. After drying over MgSO₄, the solvent was removed by evaporation, followed by silica gel column chromatography (CHCl₃ : MeOH : Et₃N = 100 : 5 : 3) to afford **6** (0.46 g, 0.41 mmol, yield 51 %).

4-5-2 DNA synthesis containing pyrene (P), perylene (E) and Cy3 (Y)

All dye-conjugated ODNs were synthesized on an automated DNA synthesizer (H-8-SE, Gene World) by using phosphoramidite monomers bearing **P**, **E** or **Y**. Synthesis of **P**, **E** and **Y** were reported above.^{33,34} After workup, synthesized ODNs were purified by reversed phase HPLC and characterized using a MALDI-TOF MS (Autoflex II, Bruker Daltonics). Purities of all the synthesized ODNs were > 99% as estimated by HPLC analysis.

MALDI-TOFMS data for the synthesized ODNs:

The MS data for modified ODNs were as follows:

m/z: **1a**: calcd for [**1a**+H⁺]: 4977: found: 4978; **1b**: calcd for [**1b**+H⁺]: 5000: found: 5001;
2a: calcd for [**2a**+H⁺]: 5290: found: 5292; **2b**: calcd for [**2b**+H⁺]: 5304: found: 5307;
3a: calcd for [**3b**+H⁺]: 5603: found: 5606; **3b**: calcd for [**3b**+H⁺]: 5608: found: 5609;
4a: calcd for [**4a**+H⁺]: 5916: found: 5919; **4b**: calcd for [**4b**+H⁺]: 5912: found: 5918;
5a: calcd for [**5a**+H⁺]: 6229: found: 6231; **5b**: calcd for [**5b**+H⁺]: 6216: found: 6217;
6a: calcd for [**6a**+H⁺]: 6542: found: 6547; **6b**: calcd for [**6b**+H⁺]: 6520: found: 6524;
7a: calcd for [**7a**+H⁺]: 6855: found: 6858; **7b**: calcd for [**7b**+H⁺]: 6824: found: 6828;
8a: calcd for [**8b**+H⁺]: 7168: found: 7170; **8b**: calcd for [**8b**+H⁺]: 7128: found: 7131;
9a: calcd for [**9a**+H⁺]: 7481: found: 7480; **9b**: calcd for [**9b**+H⁺]: 7432: found: 7433;
10a: calcd for [**10a**+H⁺]: 7795: found: 7798; **10b**: calcd for [**10b**+H⁺]: 7736: found: 7741;
11a: calcd for [**11a**+H⁺]: 8108: found: 8111; **11b**: calcd for [**11b**+H⁺]: 8040: found: 8047;
12a: calcd for [**12a**+H⁺]: 8421: found: 8427; **12b**: calcd for [**12b**+H⁺]: 8345: found: 8349;
13a: calcd for [**13a**+H⁺]: 8734: found: 8740; **13b**: calcd for [**13b**+H⁺]: 8649: found: 8651;
14a: calcd for [**14a**+H⁺]: 9047: found: 9049; **14b**: calcd for [**14b**+H⁺]: 8953: found: 8955;
15a: calcd for [**15a**+H⁺]: 9360: found: 9366; **15b**: calcd for [**15b**+H⁺]: 9257: found: 9263;

16a: calcd for [**16a**+H⁺]: 9673: found: 9674; **16b:** calcd for [**16b**+H⁺]: 9561: found: 9863;
17a: calcd for [**17a**+H⁺]: 9986: found: 9988; **17b:** calcd for [**17b**+H⁺]: 9865: found: 9869;
18a: calcd for [**18a**+H⁺]: 10299: found: 10305; **18b:** calcd for [**18b**+H⁺]: 10169: found:
10178; **19a:** calcd for [**19a**+H⁺]: 10612: found: 10614; **19b:** calcd for [**19b**+H⁺]: 10473:
found: 10475; **20a:** calcd for [**20a**+H⁺]: 10925: found: 10930; **20b:** calcd for [**20b**+H⁺]:
10777: found: 10779; **21a:** calcd for [**21a**+H⁺]: 11238: found: 11243; **21b:** calcd for
[**21b**+H⁺]: 11081: found: 11087;

1e: calcd for [**1e**+H⁺]: 5132: found: 5136; **3e:** calcd for [**3e**+H⁺]: 5758: found: 5758;
5e: calcd for [**5e**+H⁺]: 6384: found: 6381; **7e:** calcd for [**7e**+H⁺]: 7011: found: 7012;
8e: calcd for [**8e**+H⁺]: 7324: found: 7324; **9e:** calcd for [**9e**+H⁺]: 7637: found: 7639;
11e: calcd for [**11e**+H⁺]: 8263: found: 8276; **12e:** calcd for [**12e**+H⁺]: 8576: found: 8578;
13e: calcd for [**13e**+H⁺]: 8889: found: 8920; **14e:** calcd for [**14e**+H⁺]: 9202: found: 9199;
15e: calcd for [**15e**+H⁺]: 9515: found: 9516; **16e:** calcd for [**16e**+H⁺]: 9828: found: 9820;
17e: calcd for [**17e**+H⁺]: 10141: found: 10145; **18e:** calcd for [**18e**+H⁺]: 10454: found:
10437; **19e:** calcd for [**19e**+H⁺]: 10767: found: 10783;

4-5-3 Spectroscopic measurements:

Fluorescence spectra were measured on a JASCO model FP-6500 equipped with a micro cell holder. The excitation wavelength was 345 nm. For FRET analyses, experiments were conducted at 20 °C. Before measurement, sample solutions containing DNA duplex were heated at 80 °C, then slowly cooled down to 20 °C by programmable temperature controller. The temperature ramp was 2.5 °C min⁻¹. The sample solutions were as follows: 100 mM NaCl, 10 mM phosphate buffer, pH 7.0, 1.0 μM each DNA strand. Measurement error of fluorescence intensity was within ±1.5 %. UV-Vis spectra were measured in a 10-mm quartz cell on a JASCO model V-530 or V-560 equipped with programmed temperature-controller. The sample solutions were as follows: 100 mM NaCl, 10 mM phosphate buffer, pH 7.0, 5.0 μM each DNA strand. CD spectra were measured in a 10-mm quartz cell on a JASCO model J-820 equipped with programmable temperature controllers. The sample solutions were as follows: 100 mM NaCl, 10 mM phosphate buffer, pH 7.0, 4.0 μM each DNA strand.

4-5-4 Measurement of the melting temperature (T_m):

The melting curve of duplex DNA was obtained with a Shimadzu UV-1800 by measurement of the change in absorbance at 260 nm versus temperature. The temperature ramp was 0.5 °C min⁻¹. The sample solutions were as follows: 100 mM NaCl, 10 mM phosphate buffer, pH 7.0, 5.0 μM each DNA strand.

4-5-4 Analysis of time-resolved fluorescence using a streak camera:

A pulse at 780 nm was generated by a Ti:sapphire amplified laser system Integra-C (Quantronix, 130 fs, 1 kHz). The pulse was changed to a 1380-nm pulse by an optical parametric amplifier (Topas, Light Conversion). The excitation beam had a repetition rate of 1 kHz and a pulse width of 130 fs, and was converted to 345 nm through SHG crystals twice and band pass filters. Fluorescence emission was captured by a streak camera (Hamamatsu C4334) operating in photon counting mode. Measurements were performed at room temperature. The sample solutions contained 100 mM NaCl, 10 mM phosphate buffer, pH 7.0, 50 μ M each ODN *na* and *nb*. The sample solution was placed into a quartz cell with a screw cap (1-mm optical path length, 10-mm width) in order to adjust the absorbance at 345 nm equals to approximately 0.1.

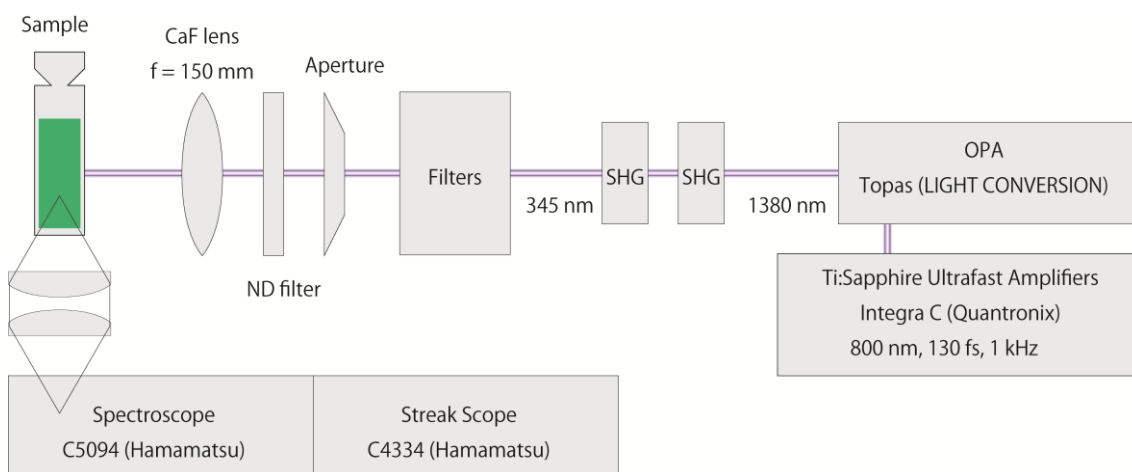


Figure 4-15. Optical system for time-resolved fluorescence spectroscopy used in this study.

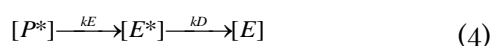
Diffraction grating: Blaze 600 nm (center wavelength = 520 nm to streak camera), 50 g/mm, slit width = 60 μ m.

Excitation wavelength was confirmed by using an optical fiber spectrometer.

Detection wavelength of streak camera was calibrated by standard Hg lamp.

4-5-5 Curve fitting calculation:

The fluorescence decay of **P** was fitted using the U8167-01 program (Hamamatsu). For $n = 1-12$, shorter time-scale data of 10 ns was used and a longer time scale of 50 ns was applied for $n = 13-21$. Decay curves of **P** and **E** were obtained from integration of the region from 384.6 to 439.0 nm and from 469.8 to 603.2 nm, respectively. Signal counts were normalized by setting maxima to 1000 and plotted on semi-logarithmic scale. The donor decay was assumed with the typical single- or bi-exponential function of $\alpha_1 \exp(-t/\tau_1) + \alpha_2 \exp(-t/\tau_2)$. Fluorescence decay of **E**, the population of excited acceptor was estimated by the step reaction as follows:



Here, k_E shows the rate constant of energy transfer from **P** to **E** and k_D is the rate constant of radiative decay of **E**. The population of excited acceptor **E*** was estimated from fluorescence decay of **E** according to the step reaction equation of $(k_E/(k_D - k_E)) (\exp(-k_E t) - \exp(-k_D t))$. Curve fitting of **E** was performed on Kaleida Graph Ver. 4.0 (Synergy Software).

4-5-5 Calculation of transition dipole moment and molecular modeling

The transition dipole moments of **P** and **E** were calculated using an *ab initio* quantum mechanical method in the Gaussian 09W suite of programs. The optimized excited-state geometries and transition dipole moments of **P** and **E** were calculated at the TDDFT B3LYP 6-31G level. The Insight II/Discover 98.0 program package was used for conformational energy minimization. The FRET pair $n = 10$ was built from canonical B-form DNA by a graphical program. The AMBER95 force field was used for the calculation. All the structures were energy-minimized to an RMS derivative of $< 0.001 \text{ kcal } \text{\AA}^{-1}$. Computations were carried out on a Silicon Graphics O2+ workstation with the IRIX64 OS Release 6.5.

4-5-6 Calculation of FRET efficiency:

In this study, FRET efficiency was calculated by three methods. FRET efficiency Φ_{T1} (decrease in donor emission), Φ_{T2} (increase in acceptor emission), and Φ_{T3} (donor decay lifetime) were calculated with following equations:

$$\Phi_{T1} = 1 - I_{DA,400}/I_D \quad (5)$$

where $I_{DA,400}$ is emission intensity of FRET pair **na/nb** at 400 nm, and I_D is that of donor only duplex **na/nd** at 400 nm.

$$\Phi_{T2} = [A_A/A_D] [I_{DA,530}/I_A - 1] \quad (6)$$

where A_A and A_D are absorbance of acceptor and donor at 345 nm, respectively, $I_{DA,530}$ is emission intensity of FRET pair **na/nb** at 530 nm, and I_A is that of acceptor only duplex **nc/nb** at 530 nm.

$$\Phi_{T3} = 1 - \tau_{DA}/\tau_D \quad (7)$$

where τ_{DA} is the lifetime of **P** in **na/nb**, and τ_D is the lifetime of **P** in the duplex without acceptor **11a/11d**. The lifetime of **P** in duplex **11a/11d** was 9.07 ns for $n = 1-12$ and 9.61 ns for $n = 13-21$.

4-6 References

- (1) a) Förster, T. *Naturwissenschaften* **1946**, *6*, 166–175.
b) Jares-Erijman, E.A.; Jovin, T.M. *Nat. Biotechnol.* **2003**, *21*, 1387-1395.
c) Preus, S.; Wilhelmsson, L.M. *ChemBioChem.* **2012**, *13*, 1990-2001.
- (2) Sapsford, K.E.; Berti, L.; Medintz, I.L. *Angew. Chem. Int. ed.* **2006**, *45*, 4562-4588.
- (3) Selvin, P.R. *Methods in Enzymol.* **1995**, *246*, 300-334.
- (4) Stein, I.H.; Schüller, V.; Böhm, P.; Tinnefeld, P.; Liedl, T. *Chem. Phys. Chem.* **2011**, *12*, 689-695.
- (5) Grunwell, J.R.; Glass, J.L.; Lacoste, T.D.; Deniz, A.A.; Chemla, D.S.; Schultz, P.G. *J. Am. Chem. Soc.* **2001**, *123*, 4295-4303.
- (6) Kikuchi, K.; Takakusa, H.; Nagano, T.; *TrAC, Trends Anal. Chem.* **2004**, *26*, 407-415.
- (7) McDowell, S.E.; Jun, J.M.; Walter, N.G. *RNA*, **2010**, *16*, 2414-2426.
- (8) Shu, D.; Zhang, H.; Petrenko, R.; Meller, J.; Guo, P. *ACS NANO* **2010**, *4*, 6843-6853.
- (9) Valeur, B. *Molecular Fluorescence*, Willy-VCH, Weinheim, **2002**.
- (10) Lakowicz, J. R. *Principles of Fluorescence Spectroscopy, 3rd ed.*; Springer: New York, **2006**, p 445.
- (11) Clegg, R. M. *Methods Enzymol.* **1992**, *211*, 353-388.
- (12) Norman, D.G.; Grainger, R.J.; Uhrin, D.; Lilley, D.M.J. *Biochem.* **2000**, *39*, 6317-6324.
- (13) Masuko, M.; Ouchi, S.; Sode, K.; Ohtani, H.; Shimadzu, A. *Nucleic Acids Res.* **2000**, *28*, e34.
- (14) Widengren, J.; Schweinberger, E.; Berger, S.; Seidel, C.A.M. *J. Phys. Chem. A* **2001**, *105*, 6851-6866.
- (15) Dietrich, A.; Buschmann, V.; Müller, C.; Sauer, M. *Rev. Mol. Biotechnol.* **2002**, *82*, 211-231.
- (16) Lee, S.; Lee, J.; Hohng, S. *PLoS one* **2010**, *5*, e12270.
- (17) Di Fiori, N.; Meller, A. *Biophys. J.* **2010**, *98*, 2265-2272.

- (18) Flehr, R.; Kienzler, A.; Bannwarth, W.; Kumke, M.U. *Bioconjugate Chem.* **2010**, *21*, 2347-2354.
- (19) Kupstat, A.; Ritschel, T.; Kumke, M.U. *Bioconjugate Chem.* **2011**, *22*, 2546-2557.
- (20) Lewis, F.D.; Zhang, L.; Zuo, X. *J. Am. Chem. Soc.* **2005**, *127*, 10002-10003.
- (21) Iqbal, A.; Arslan, S.; Okumus, B.; Wilson, T.J.; Giraud, G.; Norman, D.G.; Ha, T., Lilley, D.M.J. *Proc. Nat. Acad. Soc.* **2008**, *105*, 11176-11181.
- (22) Li, X.; Yin, Y.; Yang, X.; Zhi, Z.; Zhao, X.S. *Chem. Phys. Lett.* **2011**, *513*, 271-275.
- (23) Ouellet, J.; Schorr, S.; Iqbal, A.; Wilson, T.J.; Lilley D.M.J. *Biophys. J.* **2011**, *101*, 1148-1154.
- (24) Rindermann, J.J.; Akhtman, Y.; Richardson, J.; Brown, T.; Lagoudakis, P.G. *J. Am. Chem. Soc.* **2011**, *133*, 279-285.
- (25) Urnavicius, L.; McPhee, S.A.; Lilley, D.M.J.; Norman, D.G. *Biophys. J.* **2012**, *102*, 561-568.
- (26) Börjesson, K.; Preus, S.; El-Sapheer, A.H.; Brown, T.; Albinsson, B.; Wilhelmsson, L.M. *J. Am. Chem. Soc.* **2009**, *131*, 4288-4293.
- (27) Kashida, H.; Liang, X.G.; and Asanuma, H. *Curr. Org. Chem.*, **2009**, *13*, 1065-1084.
- (28) Kashida, H.; Takatsu, T.; Sekiguchi, K.; Asanuma, H. *Chem. Eur. J.* **2010**, *16*, 2479-2486.
- (29) Lindegaard, D.; Madsen, A. S.; Astakhova, I. V.; Malakhov, A. D.; Babu, B. R.; Korshun, V. A.; Wengel, J. *Bioorg. Med. Chem.* **2008**, *16*, 94.
- (30) Liang, X.G.; Nishioka, H.; Mochizuki T.; Asanuma, H. *J. Mater. Chem.*, **2010**, *20*, 575-581.
- (31) Kashida, H.; Asanuma, H. *Phys. Chem. Chem. Phys.*, **2012**, *14*, 7196-7204.
- (32) Liang, X.G.; Asanuma, H.; Kashida, H.; Takasu, A.; Sakamoto, T.; Kawai, G.; Komiyama, M. *J. Am. Chem. Soc.*, **2003**, *125*, 16408-16415.
- (33) Asanuma, H.; Hayashi, H.; Zhao, J.; Liang, X.G.; Yamazawa, A.; Kuramochi, T.; Matsunaga, D.; Aiba, Y.; Kashida, H.; Komiyama, M.; *Chem. Commun.*, **2006**, 5062-5064.
- (34) Asanuma, H.; Akahane, A.; Kondo, N.; Osawa, T.; Kato, T.; Kashida, H. *Chem. Sci.* **2012**, *3*, 3165-3169.
- (35) Sau, S.P.; Hrdlicka, P.J. *J. Org. Chem.* **2012**, *77*, 5-16.

- (36) Fujii, T.; Kashida, H.; Asanuma, H. *Chem. Eur. J.* **2009**, *15*, 10092-10102.
- (37) a) Kubista, M.; Åkerman, B.; Nordén, B. *J. Phys. Chem.* **1988**, *92*, 2352-2356;
b) Lyng, R.; Rodger, A.; Nordén, B. *Biopolymers*, **1992**, *32*, 1201-1214;
c) Pradhan, P.; Jernström, B.; Seidel, A.; Nordén, B.; Gräslund, A. *Biochemistry* **1998**, *37*, 4664-4673.
d) Nakamura, M.; Fukunaga, Y.; Sasa, K.; Ohtoshi, Y.; Kanaori, K.; Hayashi, H.; Nakano, H.; Yamana, K. *Nucleic Acids Res.* **2005**, *33*, 5887-5895.
- (38) Kypr, J.; Kejnovská, I.; Renčiuk, D.; Vorlíčková, M. *Nucleic Acids Res.* **2009**, *37*, 1713–1725.
- (39) Teo, Y. N.; Kool, E. T. *Bioconjugate Chem.* **2009**, *20*, 2371-2380.
- (40) Clegg, R.M.; Murchie, A.I.H.; Zechel, A.; Lilley, D.M.J. *Proc. Natl. Acad. Sci. USA* **1993**, *90*, 2994-2998.
- (41) MacDonald, D.; Herbert, K.; Zhang, X.; Polgruto, T.; Lu, P. *J. Mol. Biol.* **2001**, *306*, 1081-1098.
- (42) Wang C.; Xu, J.; Weiss, R.G. *J. Phys. Chem. B*, **2003**, *107*, 7015-7025.
- (43) Tanizaki Y.; Yoshinaga, T.; Hiratsuka, H. *Spectrochim. Acta. A.* **1978**, *34*, 205-210
- (44) Asanuma, H.; Fujii, T.; Kato, T.; Kashida, H. *J. Photochem. Photobiol. C* **2012**, *13*, 124-135.

4-7 Appendixes

4-7-1 Symbols, abbreviations and their definition.

Symbol	Definition
P	Donor fluorophore, pyrenecarboxylicacid-D-threoninol conjugant.
E	Acceptor fluorophore, perylenecarboxylicacid-D-threoninol conjugant.
<i>n</i>	Number of inserted AT pairs between dyes in bp unit.
na/nb	FRET pair duplex containing both P and E where <i>n</i> indicates the number of inserted AT pairs between dyes.
na/nd	Donor only duplex containing only P where <i>n</i> indicates the number of inserted AT pairs between dyes.
nc/nb	Acceptor only duplex containing only E where <i>n</i> indicates the number of inserted AT pairs between dyes.
Φ_T	FRET efficiency defined by $\Phi_T = 1/(1 + (R/R_0)^6)$
<i>R</i>	Separation distance between donor and acceptor in Å unit.
<i>R₀</i>	Förster radius. The distance where Φ_T equals 0.5. In this paper, the equation was described in Å unit version. $R_0 = 0.2108 [J(\lambda) \kappa^2 n^{-4} \Phi_D]^{1/6}$ Here, note that <i>n</i> in this equation is refractive index, not the number of inserted AT pairs. This value is typically assumed to be 1.4. (For more detail, see reference 10)
<i>J(λ)</i>	Spectral overlap of donor emission and acceptor absorption. $J(\lambda) = \int_0^\infty I_D(\lambda) \cdot \epsilon_A(\lambda) \cdot \lambda^4 d\lambda$ This value can be calculated from spectra data using above equation. For more detail, see reference 9 and 10.
Φ_D	Quantum yield of the donor.
κ^2	Orientation factor defined by $\kappa^2 = (\cos \theta_T - 3 \cos \theta_D \cos \theta_A)^2$ Assign of the angles are as shown in Figure 4-7a.
θ_T	Total angle of transition dipole moment between donor and acceptor.

θ_D	Angles versus distant axis of donor.
θ_A	Angles versus distant axis of acceptor.
α_1	Amplitude of shorter lifetime component (%). The donor decay was assumed with the typical single- or bi-exponential function of $\alpha_1 \exp(-t/\tau_1) + \alpha_2 \exp(-t/\tau_2)$.
α_2	Amplitude of longer lifetime component (%).
τ_1	The shorter fluorescence lifetime (ns)
τ_2	The longer fluorescence lifetime (ns).
χ^2	Chi-squared value obtained from fitting program.
k_p	The rate constant calculated from shorter fluorescence lifetime of donor emission. This value is equal to the reciprocal of τ_1 .
k_E	The rate constant of FRET calculated from increase of fluorescence emission by following step reaction equation; $[P^*] \xrightarrow{k_E} [E^*] \xrightarrow{k_D} [E]$ $(k_E/(k_D - k_E)) (\exp(-k_E t) - \exp(-k_D t))$
k_D	The rate constant of radiative decay of E .
Φ_{T1}	FRET efficiency calculated from experimental data, based upon decrease in donor emission defined by $\Phi_{T1} = 1 - I_{DA,400}/I_D$. Where $I_{DA,400}$ is emission intensity of FRET pair na/nb at 400 nm, and I_D is that of donor-only duplex na/nd at 400 nm.
Φ_{T2}	FRET efficiency calculated from experimental data, based upon increase in acceptor emission defined by $\Phi_{T2} = [A_A/A_D] [I_{DA,530}/I_A - 1]$. Where A_A and A_D are absorbance of acceptor and donor at 345 nm, respectively, $I_{DA,530}$ is emission intensity of FRET pair na/nb at 530 nm, and I_A is that of acceptor only duplex nc/nb at 530 nm.
Φ_{T3}	FRET efficiency calculated from experimental data, based upon donor decay lifetime $\Phi_{T3} = 1 - \tau_{DA}/\tau_D$. Where τ_{DA} is the lifetime of P in na/nb , and τ_D is the lifetime of P in the donor only duplex 11a/11d . The lifetime of P in 11a/11d was 9.07 ns for $n = 1-12$ and 9.61 ns for $n = 13-21$.

4-7-2 Sequence dependence of fluorophores

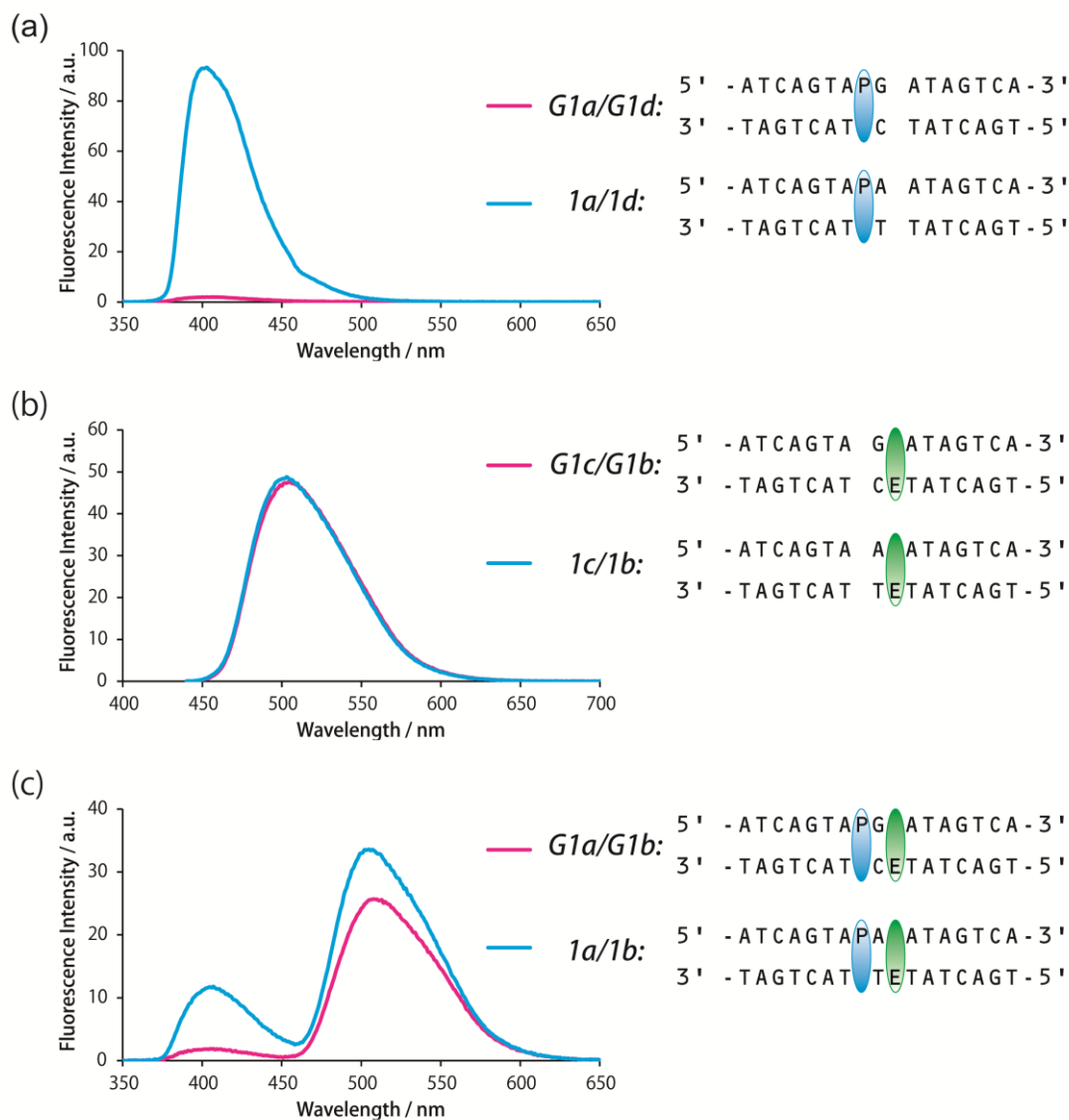


Figure 4-16. Comparison of fluorescence behavior by the effect of neighboring base pair. Solution conditions were as follows: 100 mM NaCl, 10 mM phosphate buffer, pH 7.0, 1.0 μ M each DNA strand. (a) Comparison of fluorescence spectra of donor (**P**). Excitation wavelength was 345 nm. Only donor (**P**) was introduced within DNA duplex. Obviously, fluorescence emission of **P** was significantly quenched neighboring GC pair. (b) Comparison of fluorescence spectra of acceptor (**E**). **E** was directly excited at 428 nm. Only acceptor (**E**) was introduced within DNA duplex. There was no difference between GC pair and AT pair. (c) Comparison of fluorescence behavior of FRET pair duplexes. *G1a/G1b* duplex also exhibited efficient FRET, however, fluorescence intensities of both **P** and **E** were lower than *1a/1b* duplex because quenching by GC pair affected FRET efficiency.

4-7-3 Fluorescence spectra (static) of all FRET pairs

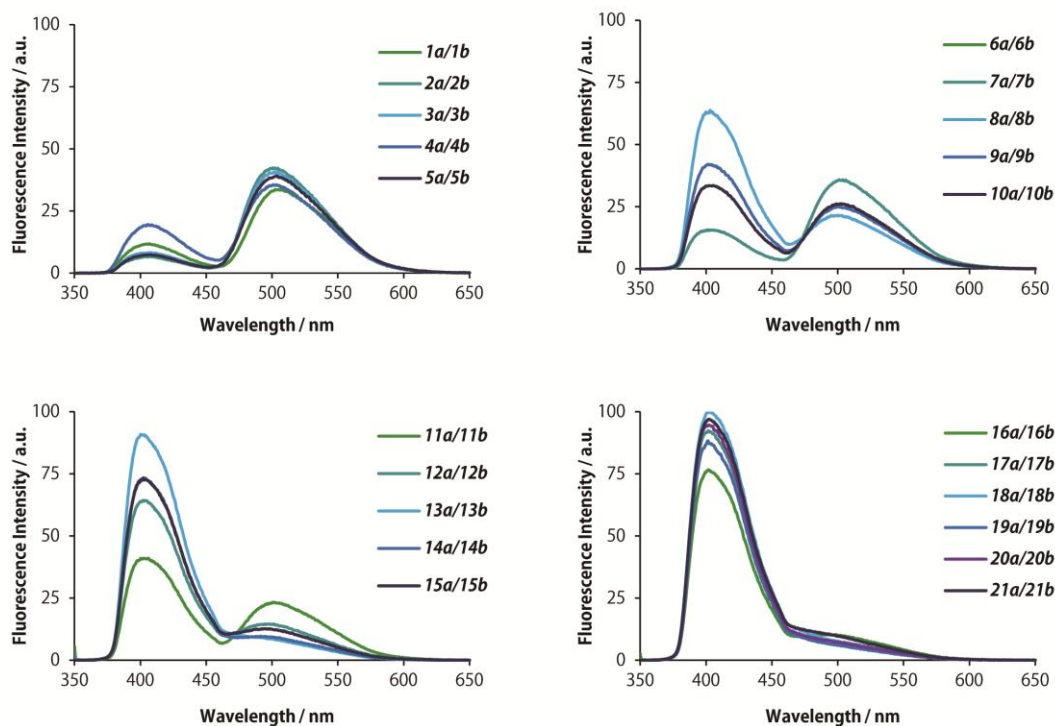


Figure 4-17. Static fluorescence spectra of FRET system containing **P** and **E** ($n = 1-21$) at 20 °C. The excitation wavelength was 345 nm. Solution conditions were as follows: 100 mM NaCl, 10 mM phosphate buffer, pH 7.0, 1.0 μ M each DNA strand.

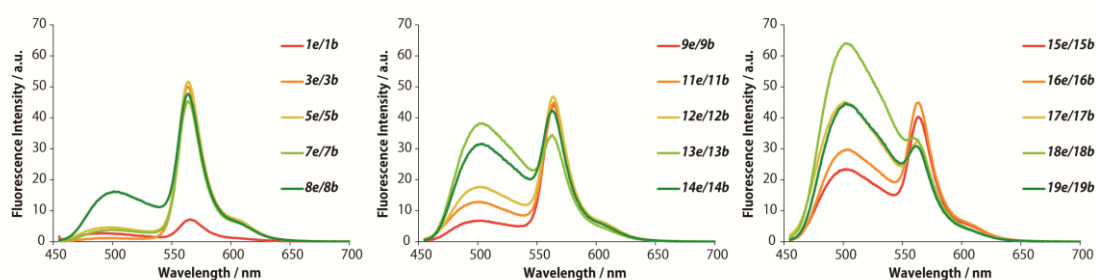
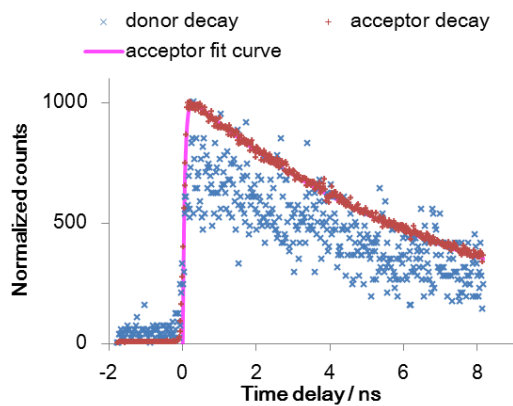


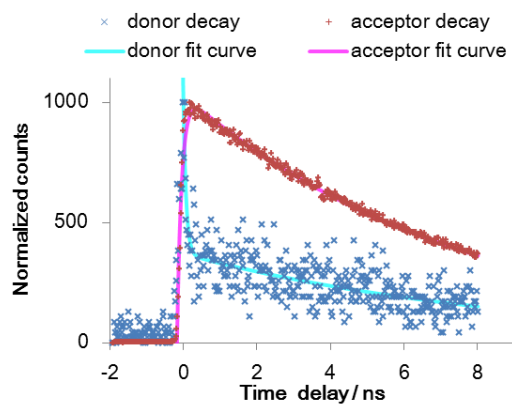
Figure 4-18. Static fluorescence spectra of FRET system containing **E** and **Y** ($n = 1, 3, 5, 7, 8, 9, 11-19$) at 0 °C. The excitation wavelength was 450 nm. Solution conditions were as follows: 100 mM NaCl, 10 mM phosphate buffer, pH 7.0, 1.0 μ M each DNA strand.

4-7-4 Fitting data of time-resolved fluorescence spectroscopy

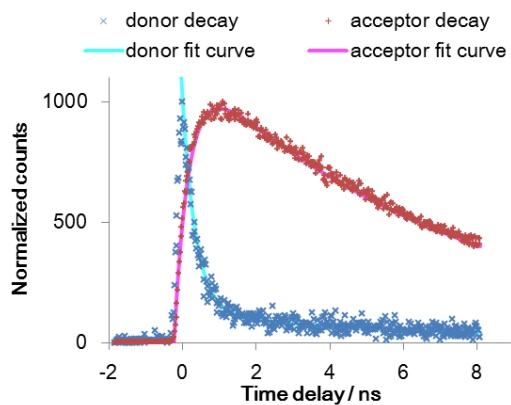
1a/1b



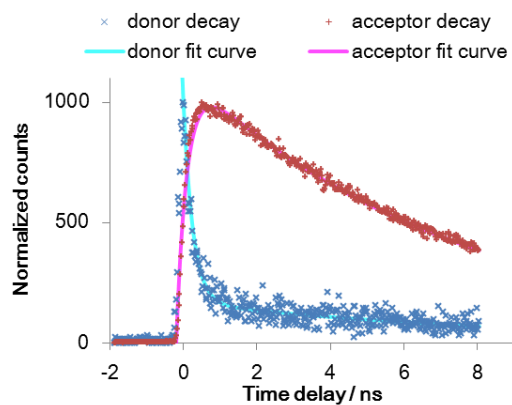
2a/2b



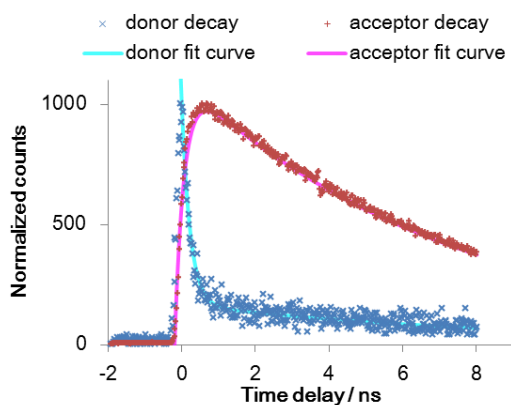
3a/3b



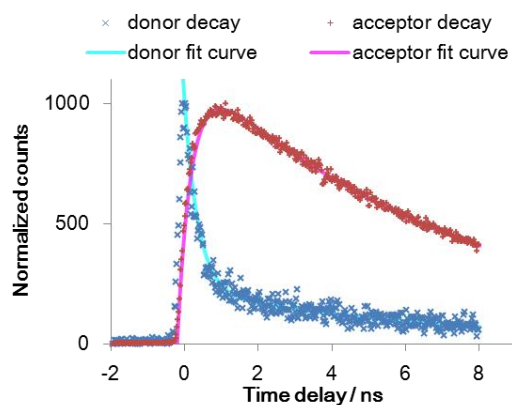
4a/4b



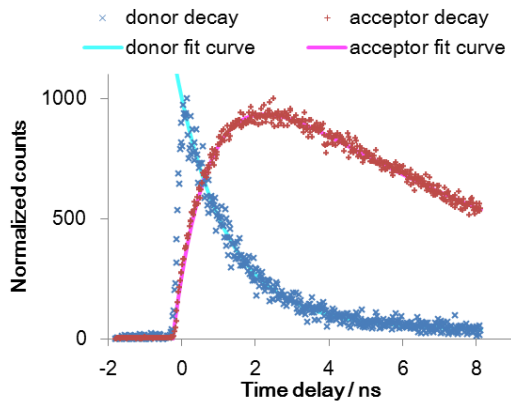
5a/5b



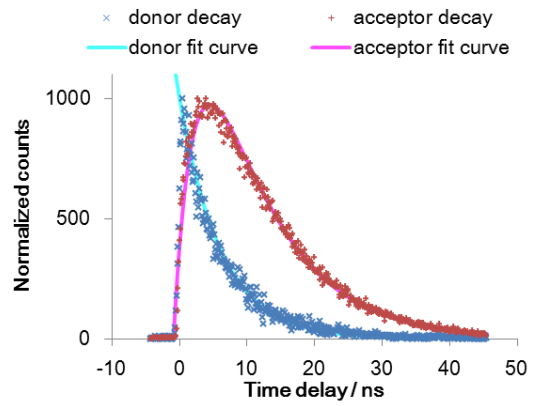
6a/6b



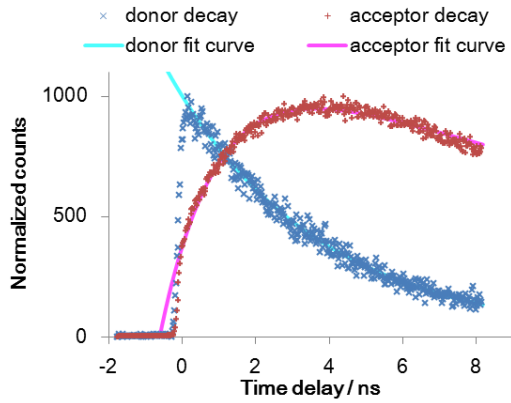
7a/7b



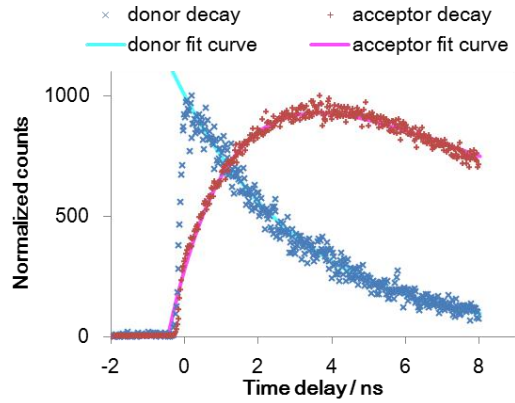
8a/8b



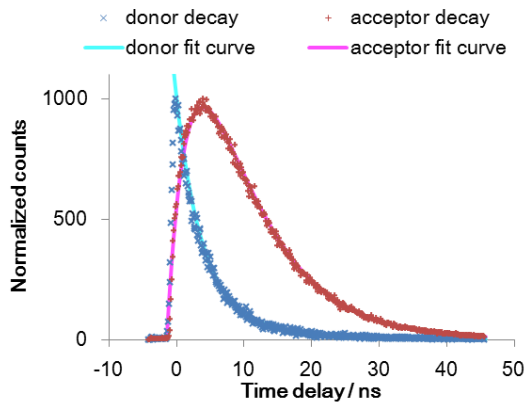
9a/9b



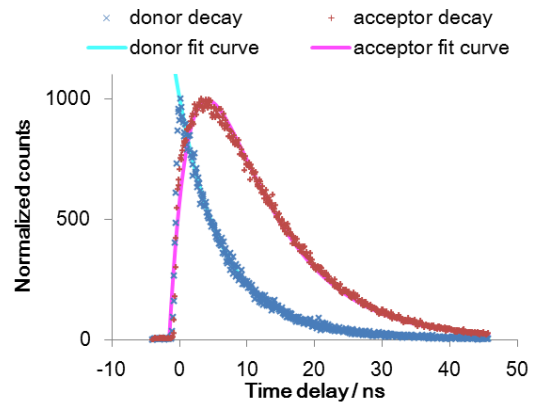
10a/10b



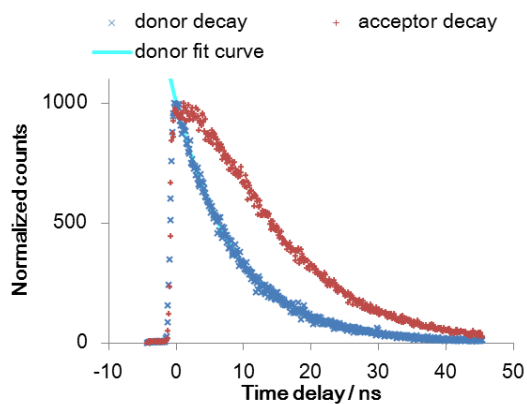
11a/11b



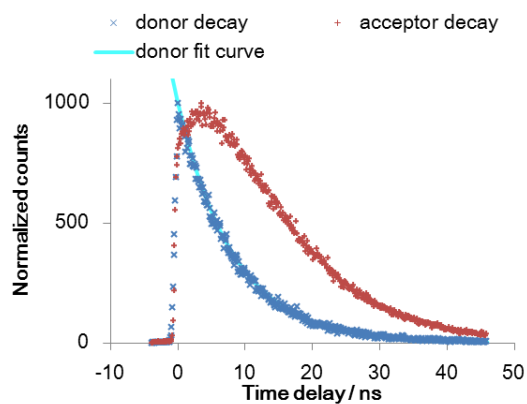
12a/12b



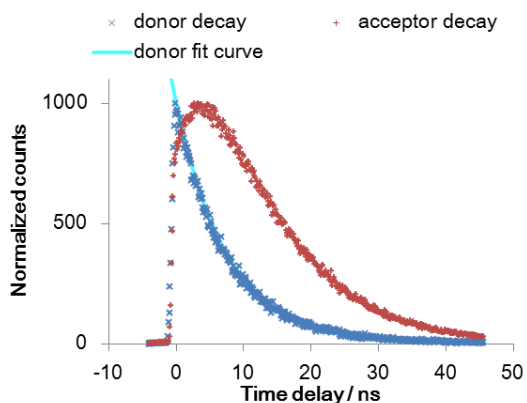
13a/13b



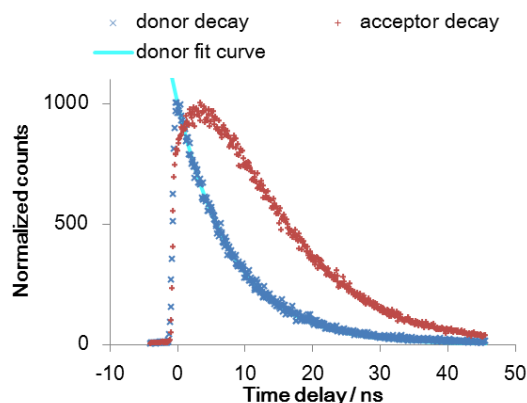
14a/14b



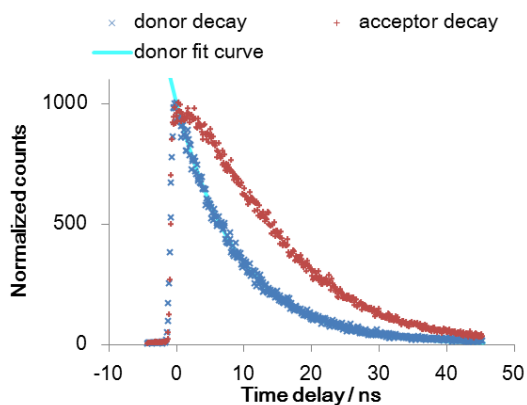
15a/15b



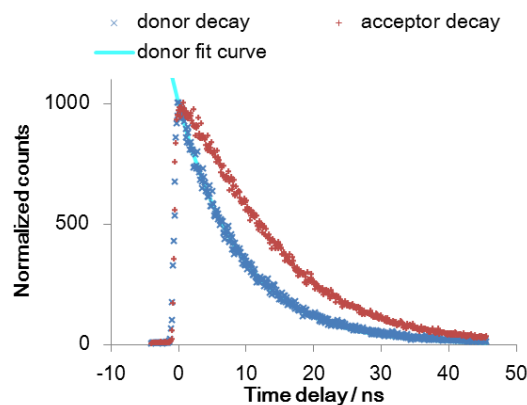
16a/16b



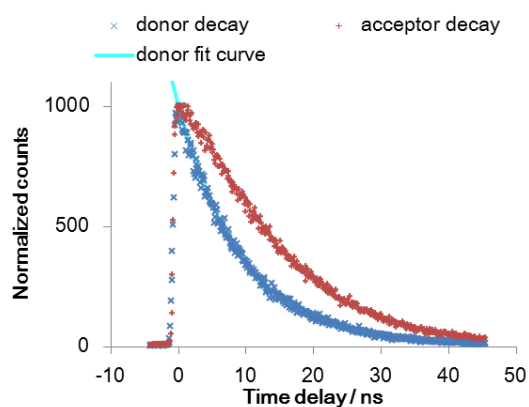
17a/17b



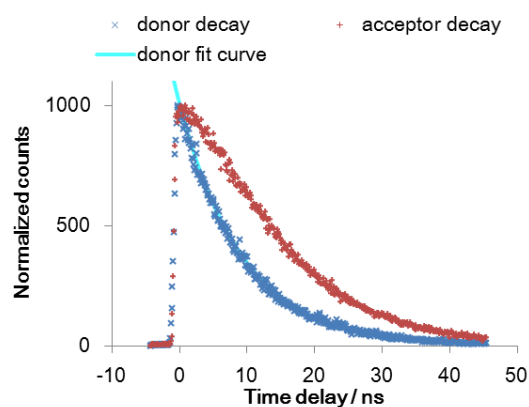
18a/18b



19a/19b



20a/20b



21a/21b

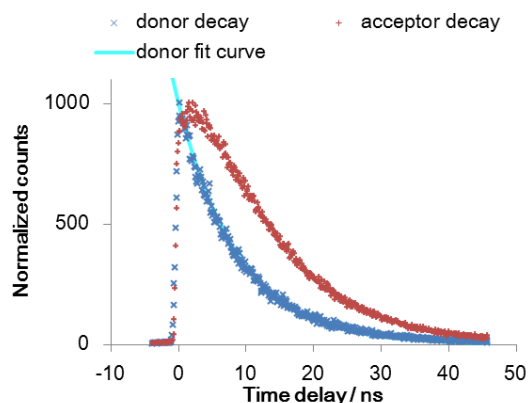


Figure 4-19. Acceptor rise fitting curve and donor decay curves. Blue “x” mark indicates normalized donor decay counts and cyan line is its fitting curve. Red “+” mark indicates normalized acceptor counts. Pink line shows fitting curve of the acceptor rise and decay.

Table 4-3. Fluorescence decay fitting results with fixing longer lifetime.

n	τ_1/ns	α_1	τ_2/ns	α_2	χ^2
1	n.d.	n.d.	n.d.	n.d.	n.d.
2	0.08	1.00	9.07	0.00	1.32
3	0.39	0.90	9.07	0.10	1.37
4	0.26	0.94	9.07	0.06	1.36
5	0.19	0.87	9.07	0.13	1.23
6	0.44	0.82	9.07	0.18	1.32
7	1.35	0.91	9.07	0.09	1.41

Although longer life time was fixed with the fluorescence lifetime of the duplex containing only **P**, the fitting results were consistent with the results in the main text Table 1.

4-7-5 Exciton coupling between dyes located in close proximity

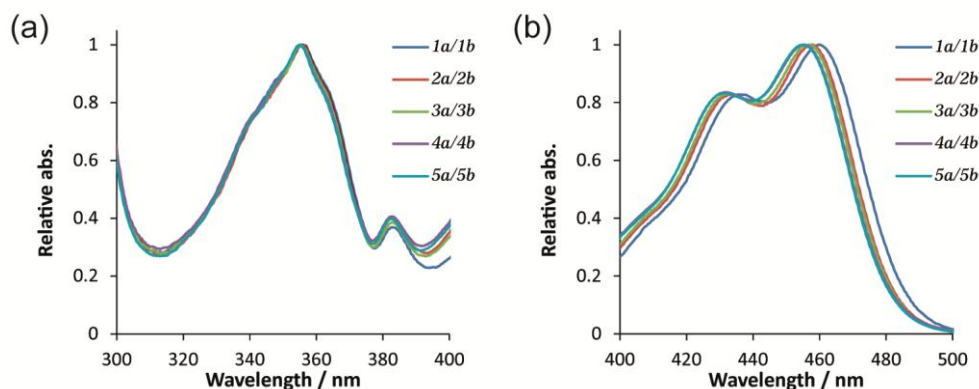


Figure 4-20. Absorption spectra of FRET pairs ($n = 1-5$). Conditions: 100 mM NaCl, 10 mM phosphate buffer, pH 7.0, 5.0 μ M each DNA strands, 20°C. The absorbance around 350 nm is **P** and around 450 nm is **E**. For **1a/1b**, λ_{\max} of dyes were slightly red-shifted by exciton coupling.

4-7-6 T_m analysis of all modified and native DNA duplex

Table 4-4. The results of T_m measurement

n	na / nb FRET pair	na / nd Donor only	nc / nb Acceptor only	nc / nd Native
1	54.6	49.2	51.7	45.7
2	58.2	51.8	53.6	48.7
3	57.3	51.1	53.5	48.8
4	58.0	54.0	55.0	51.6
5	57.9	53.5	55.8	51.3
6	59.3	55.2	57.1	53.3
7	60.9	56.4	58.6	54.0
8	59.5	55.9	58.2	54.5
9	60.9	57.2	58.8	55.5
10	60.0	57.1	59.0	55.9
11	61.9	58.2	59.8	56.4
12	57.0	53.4	59.3	57.0
13	62.7	59.2	60.9	57.3
14	63.2	59.5	60.8	57.7
15	60.6	57.7	60.4	58.0
16	63.2	60.2	61.4	58.5
17	63.0	60.1	61.6	58.7
18	61.1	58.7	60.9	59.4
19	63.5	60.9	62.4	59.5
20	63.7	62.1	62.9	59.9
21	62.7	60.7	62.6	60.2
G1	54.7	49.9	54.2	47.6

Measurement conditions: 100 mM NaCl, 10 mM phosphate buffer, pH 7.0, 5.0 μ M each ODN; 0.5 °C/min.

4-7-7 Multiple incorporation of donors; light-harvesting FRET system

FRET from multiple donors to single acceptor can enhance fluorescence emission intensity of acceptor. Here, as the donor, four or two pyrenes (**P**) were introduced into DNA duplex containing single perylene (**E**) as the acceptor (Table 4-5).

Table 4-5. The sequence of modified ODNs used here containing **P** and **E**.

Name	Sequence	Representation
<i>2a/2b</i>	5' -ATCAGT APAA A TAGTCA -3' 3' -TAGTCA T T ET ATCAGT -5'	
<i>P4a/P4b</i>	5' -ATCAGT APAPA APAPA TAGTCA -3' 3' -TAGTCA T T ET T T ATCAGT -5'	
<i>3P2a/P2b</i>	5' -ATCAGT APAAA AAAPA TAGTCA -3' 3' -TAGTCA T TTT ETTT T ATCAGT -5'	
<i>1P2a/P2b</i>	5' -ATCAGT AAAPA APAAA TAGTCA -3' 3' -TAGTCA TTT ET TTT ATCAGT -5'	

P4a/P4b contains four **P** moieties and their separation distances are 1 and 3 bp, which are sufficiently close within R_0 . **E** was located at the center of the complementary strand. As controls, *3P2a/P2b* and *1P2a/P2b*. *3P2a/P2b* and *1P2a/P2b* contain two **P** moieties in the separation distance of 3 and 1 bp, respectively. Moreover, *2a/2b* FRET pair duplex, which exhibited the highest FRET efficiency, was also prepared to estimate the effect of multiple donors. As shown in Figure 4-21a, *P4a/P4b* possessed intensive fluorescence emission. Its relative intensity at 500 nm belonging to acceptor emission was three times as high as that of *2a/2b*. The FRET efficiency of *P4a/P4b* was as high as 0.98 – 1.0, which was larger than that of *2a/2b*. Hence the FRET efficiency could be improved by introduction of multiple donors. Similarly, *3P2a/P2b* and *1P2a/P2b* also showed enhanced fluorescence intensity of acceptor. Although *3P2a/P2b* exhibited approximately doubled acceptor emission, its FRET efficiency was 0.88, which was slightly smaller than *3a/3b* (0.91-1.0) suggesting that multiple intercalations of dyes would change relative orientation between dyes and the structure of DNA helix. For *1P2a/P2b*, FRET efficiency was approximately 0.97 – 1.0, this value was larger than

that of *1a/1b* FRET pair duplex (0.88). This would be because remained donor emission was slightly quenched by **E** or **P**. UV-Vis spectrum of *1P2a/P2b* showed red-shift of λ_{\max} indicating exciton coupling (Figure 4-12b). Slight red-shift of acceptor emission in fluorescence spectrum also suggested such interactions between dyes. The curve named “Sum” in Figure 4-21a indicated simple summation of fluorescence spectra of *3P2a/P2b* and *1P2a/P2b*. Comparing *P4a/P4b* with Sum, the acceptor emission of *P4a/P4b* was slightly lower than that of Sum, however, the donor emission was as low as that of *2a/2b* or *1P2a/P2b*. Again, fluorescence behavior of *P4a/P4b* did not equal to the Sum. Therefore the energy transfer from multiple donors to single acceptor is not integration of single path. Excited energy would be delocalized among dyes and such interaction between dyes should be considered in multiple donors FRET system.

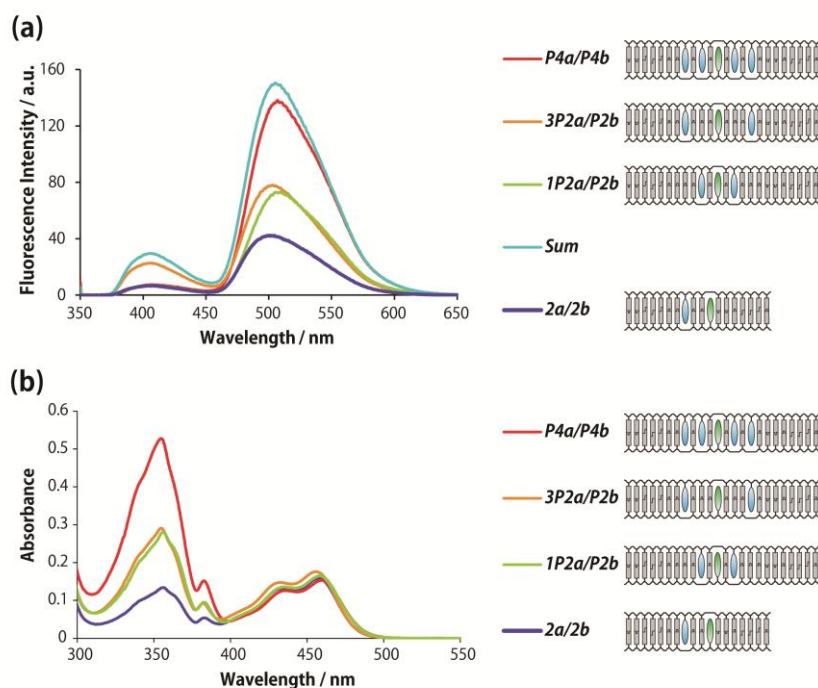
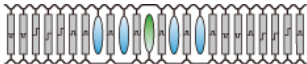
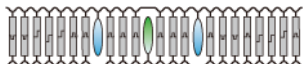
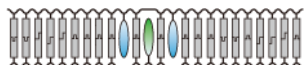


Figure 4-21. Spectroscopic behaviors of multiple donors FRET system. (a) Fluorescence emission spectra of modified DNAs at 20 °C. “Sum” indicated the summation of *3P2a/P2b* + *1P2a/P2b*. The excitation wavelength was 345 nm. Solution conditions were as follows: 100 mM NaCl, 10 mM phosphate buffer, pH 7.0, 1.0 μ M each ODN. Before measurements, samples were heated at 80 °C for 5 min followed by cooling gradually at the rate of 4 °C/min to 20 °C. (b) UV-Vis spectra of modified ODNs. Spectra at 300-500 nm are magnified in the inset. Solution conditions were as follows: 100 mM NaCl, 10 mM phosphate buffer, pH 7.0, 5.0 μ M each ODN.

Table 4-5. The sequence of modified ODNs used here containing **P** and **E**.

Name		Relative Int. at 400 nm ^a	Relative Int. at 500 nm ^b	Φ_{T1} ^c	Φ_{T2} ^d	ϵ_{345} / $M^{-1} cm^{-1}$
<i>2a/2b</i>		1	1	0.95	1.03	2150 (1)
<i>P4a/P4b</i>		1.10	3.09	0.98	1.01	8901 (4.1)
<i>3P2a/P2b</i>		3.51	1.84	0.88	0.87	4451 (2.1)
<i>1P2a/P2b</i>		1.05	1.62	0.97	1.16	4850 (2.3)
SUM	—	4.55	3.46	—	—	9300 (4.3)

a: Emission intensity at 400 nm relative to that of *2a/2b*. *b*: Emission intensity at 500 nm relative to that of *2a/2b*. *c*: FRET efficiency based on donor decrease. *d*: FRET efficiency based on acceptor increase.

For further applications, an advanced linear probe containing multiple donors FRET system was proposed. This design provides 1) quick response by stem less design, 2) large Stoke's shift utilizing FRET, 3) intensive emission of acceptor fluorophore by enlarged extinction coefficient and light-harvesting from multiple donors. This is still just no more than a design, however, it will shed light to the development of a novel highly sensitive fluorescent probe.

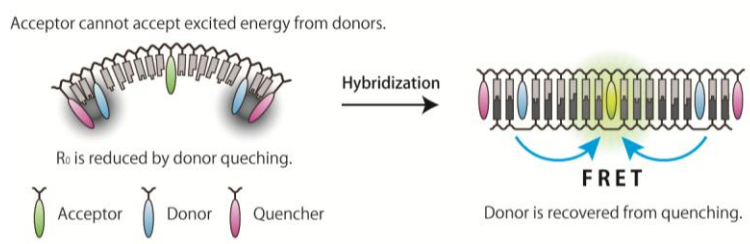


Figure 4-22. An illustration of the design of advanced linear probe utilizing FRET from multiple donors. Before hybridization, donors are quenched and its R_0 is significantly dropped owing to decline of Φ_D . Hence the acceptor cannot accept excited energy from donors and no FRET will be observed. Once the target sequence was hybridized, donors will be separated from quencher and the Φ_D will be recovered, the acceptor can emit fluorescence by energy transfer from donors. Here, in order to suppress background, the acceptor should be carefully selected so as not to be directly excited. Additionally, the separation distance between donor and acceptor in the hybridized state should be within R_0 for efficient energy transfer, whereas in the quenched state, the distance should be far enough over R_0 for avoiding unexpected energy transfer from quenched donors. Furthermore, introduction of the quencher at the end of DNA will provide resistance to enzyme degradation *in vivo*.

4-7-8 Theoretical calculation of Förster radii between various dyes

For future applications utilizing FRET, Förster radii between various fluorophores were briefly summarized here. Förster radius (R_0) can be calculated by using following equations. Note that differences in spectral shape and quantum yields of dyes owing to neighboring nucleobases were disregarded here. Hence theoretical values presented here are only rough estimates.

$$R_0 = 0.2108 [J(\lambda) \kappa^2 n^{-4} \Phi_D]^{1/6} \quad J(\lambda) = \int_0^\infty I_D(\lambda) \cdot \varepsilon_A(\lambda) \cdot \lambda^4 d\lambda$$

κ^2 : Orientation factor (averaged value 2/3 was used here)

n : refractive index, 1.4 was used here.

Φ_D : Quantum yield of donor $J(\lambda)$: Spectrum overlap

$I_D(\lambda)$: Fluorescence emission $\varepsilon_A(\lambda)$: Absorption

Fluorescence emission

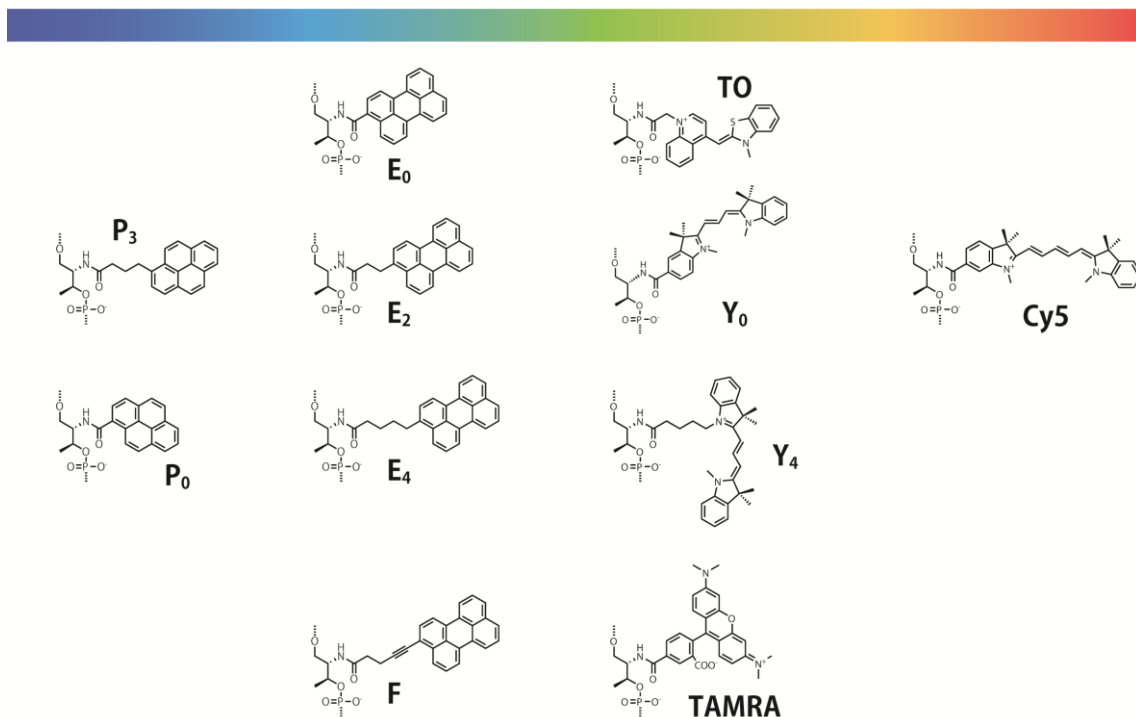


Figure 4-23. The structures and names of fluorophores tethered via D-threosinol scaffold.

Table 4-6. List of .properties of FRET between various fluorophores.

Donor	Excitation / nm	Φ_D	Acceptor	Emission / nm	Stokes' shift / nm	$J(\lambda)$ / $M^{-1} cm^{-1} nm^4$	$R_0(\kappa^2=2/3)$ / \AA
P ₃	350	0.003 ^a	E ₀	500	150	2.31 x 10 ¹⁴	14.8
			E ₂	460	110	2.67 x 10 ¹⁴	15.1
			E ₄	465	115	2.77 x 10 ¹⁴	15.3
			F	475	125	2.59 x 10 ¹⁴	15.1
P ₃ (Shielded) ^f	345	0.19 ^a	E ₀	500	155	2.31 x 10 ¹⁴	29.6
			E ₂	460	115	2.67 x 10 ¹⁴	30.3
			E ₄	465	120	2.77 x 10 ¹⁴	30.5
			F	475	130	2.59 x 10 ¹⁴	30.1
P ₀	355	0.50 ^b	E ₀	500	145	4.50 x 10 ¹⁴	38.8
			E ₂	460	105	4.60 x 10 ¹⁴	39.0
			E ₄	465	110	4.61 x 10 ¹⁴	39.0
			F	475	120	5.40 x 10 ¹⁴	40.0
E ₀	455	0.25 ^b	TO	535	80	8.21 x 10 ¹⁵	56.1
			Y ₀	565	110	5.50 x 10 ¹⁵	52.5
			Y ₄	565	110	4.73 x 10 ¹⁵	51.2
			TAMRA	580	125	2.40 x 10 ¹⁵	45.7
E ₂	450	0.65 ^c	TO	535	85	5.94 x 10 ¹⁵	62.4
			Y ₀	565	115	2.12 x 10 ¹⁵	52.5
			Y ₄	565	115	1.89 x 10 ¹⁵	51.5
			TAMRA	580	130	6.78 x 10 ¹⁴	43.4
E ₄	455	0.57 ^c	TO	535	80	6.06 x 10 ¹⁵	61.2
			Y ₀	565	110	2.20 x 10 ¹⁵	51.7
			Y ₄	565	110	1.96 x 10 ¹⁵	50.7
			TAMRA	580	125	7.05 x 10 ¹⁴	42.8
F	465	0.56 ^c	TO	535	70	8.56 x 10 ¹⁵	64.6
			Y ₀	565	100	3.74 x 10 ¹⁵	56.3
			Y ₄	565	100	3.27 x 10 ¹⁵	55.1
			TAMRA	580	115	1.31 x 10 ¹⁵	47.3
TO	515	0.11 ^d	Cy5	660	145	> 2.42 x 10 ¹⁵ †	> 39.9†
Y ₀	550	0.30 ^e	Cy5	660	110	> 4.47 x 10 ¹⁵ †	> 52.3†
Y ₄	550	0.30 ^e	Cy5	660	110	4.30 x 10 ¹⁵ †	> 51.9†
TAMRA (GC neighbor)	560	0.09 ^a	Cy5	660	100	7.53 x 10 ¹⁵	46.7
TAMRA (Shielded) ^f	555	0.30 ^a	Cy5	660	105	6.06 x 10 ¹⁵	55.0

†: Under estimation due to incomplete emission data.

a: Quenching state by adjacent GC pair. See Chapter 3.

b: See Chapter 4.

c: Quantum yield determined from the quantum yield of perylene in N₂-bubbled cyclohexane (0.78) used as a reference.

d: Nygren, J.; Svanvik, N.; Kubista, M. *Biopolymers*. **1998**, *46*, 39-51.

e: Iqbal, A.; Arslan, S.; Okumus, B.; Wilson, T.J.; Giraud, G.; Norman, D.G.; Ha, T., Lilley, D.M.J. *Proc. Nat. Acad. Soc.* **2008**, *105*, 11176-11181.

f: Dyes are shielded by two H·H pairs.

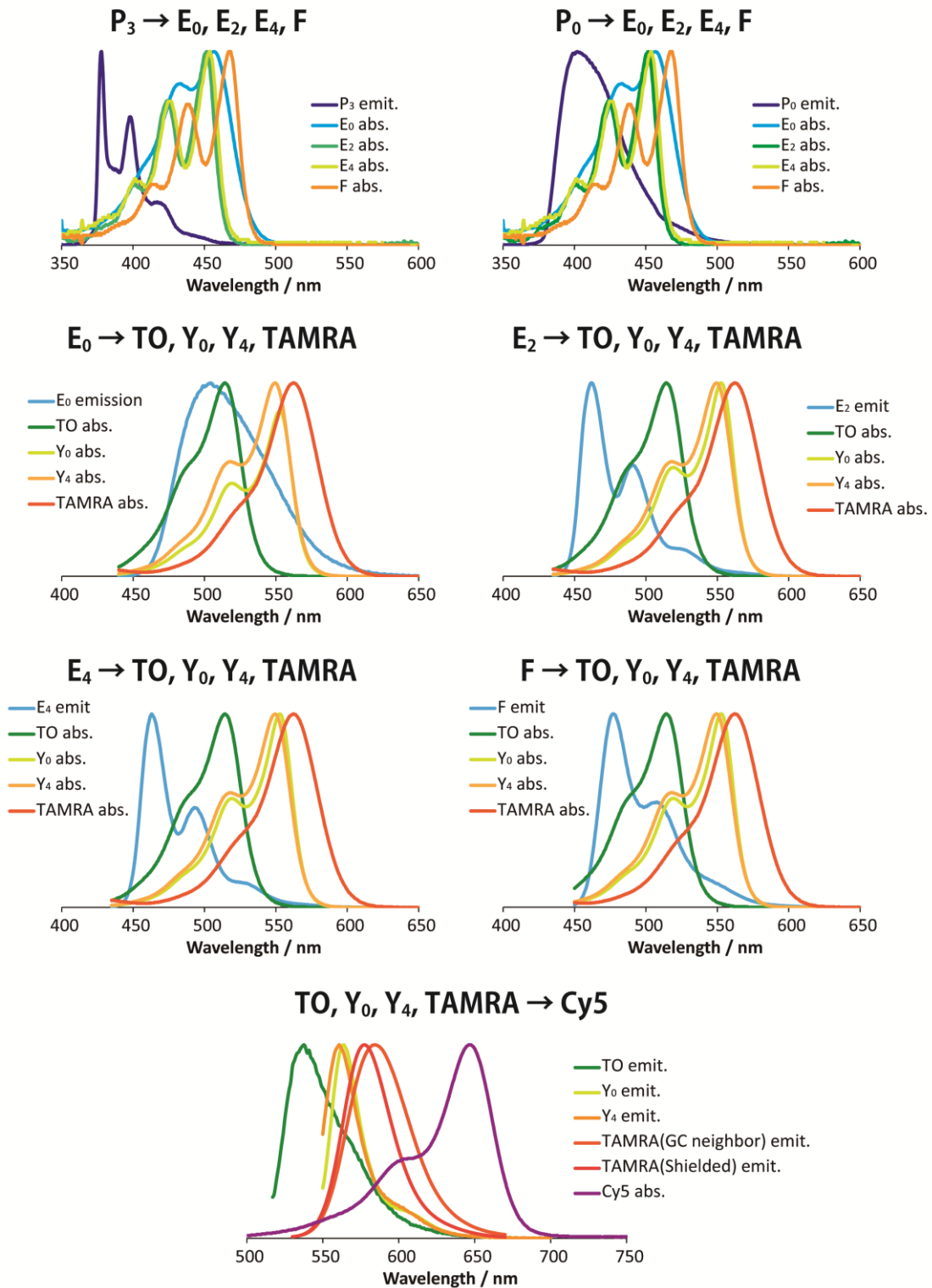


Figure 4-24. Spectral overlap of various fluorophores.

LIST OF PUBLICATIONS

1) Kato, T.; Liang, X. G.; Asanuma, H. "A model of elongation of short DNA sequence by thermophilic DNA polymerase under isothermal conditions." *Biochemistry*, **2012**, *51*, 7846-7853.

2) Kato, T.; Kashida, H.; Kishida, H.; Yada, H.; Okamoto, H.; Asanuma, H.; "Development of a robust model system of FRET using base-surrogates tethering fluorophores for strict control of their position and orientation within DNA duplex." *J. Am. Chem. Soc.*, **2012**, *accepted*. DOI: 10.1021/ja309279w

Other Reference Publications:

*International Symposium

3) Liang, X.G.; Kato T.; Asanuma, H. "Mechanism of DNA elongation during *de novo* DNA synthesis." *Nucleic Acids Symp. Ser.* **2007**, *51*, 351-352.

4) Liang, X.G.; Kato T.; Asanuma, H. "Unexpected efficient *ab initio* DNA synthesis at low temperatures by using thermophilic DNA polymerase." *Nucleic Acids Symp. Ser.* **2008**, *52*, 411-412.

5) Kato, T.; Liang, X. G.; Asanuma, H. "Unexpected non-specific DNA synthesis by thermophilic DNA polymerase." *2010 International Chemical Congress of Pacific Basin Societies (Pacifichem2010)*, **2010**.

6) Kato, T.; Kashida, H.; Kishida, H.; Yada, H.; Okamoto, H.; Asanuma, H. "Development of a robust FRET system within DNA duplex using base-surrogate tethering fluorophores" *The 39th International Symposium on Nucleic Acids Chemistry (ISNAC2012)*, **2012**.

*Journal Articles

- 7) Kashida, H.; Sekiguchi, K.; Higashiyama, N.; Kato, T.; Asanuma, H. "Cyclohexyl "base pairs" stabilize duplexes and intensify pyrene fluorescence by shielding it from natural base pairs." *Org. Biomol. Chem.*, **2011**, *9*, 8313-8320.
- 8) Nishioka, H.; Liang, X. G.; Kato, T.; Asanuma, H. "Photon-fueled DNA nanodevice carrying two different photoswitches." *Angew. Chem. Int. Ed.*, **2012**, *48*, 1760-1762.
- 9) Asanuma, H.; Fujii, T.; Kato, T.; Kashida, H. "Coherent Interactions of Dyes Assembled on DNA" (Review) *J. Photochem. Photobiol. C*, **2012**, *13*, 124-135.
- 10) Asanuma, H.; Akahane, M.; Kondo, N.; Osawa, T.; Kato, T.; Kashida, H. "Quencher-free linear probe with multiple fluorophores on acyclic scaffold" *Chem. Sci.*, **2012**, *3*, 3165-3169.

*Authored Work

- 11) Liang, X.G.; Kato T.; Asanuma, H. "*de novo* DNA Synthesis by DNA Polymerase." *Bacterial DNA, DNA Polymerase and DNA Helicases*, Nova Science Publishers Inc., NY. **2009**

*Patents

- 12) 「DNAの増幅方法」梁興国, 浅沼浩之, 鈴木昌友, 加藤智博 出願人: 国立大学法人名古屋大学, 特許公開: 特開 2011-010591
- 13) 「ターゲットDNAの増幅方法」梁興国, 浅沼浩之, 鈴木昌友, 加藤智博 出願人: 国立大学法人名古屋大学, 特許公開: 特開 2011- -000058

LIST OF PRESENTATIONS

- 1) Liang, X. G.; Kato, T.; Asanuma, H. "Unexpected efficient *ab initio* DNA synthesis at low temperature by using thermophilic DNA polymerase" (Poster) *SNAC2007, 5th International Symposium on Nucleic Acids Chemistry*, The University of Tokyo, **2007 Nov.**
- 2) Kato, T.; Liang, X. G.; Asanuma, H. "超好熱性ポリメラーゼの低温下における高効率 *de novo* DNA 合成" (Poster) *FIBER Forum 2007*, Konan University, **2007 Dec.**
- 3) Liang, X. G.; Kato, T.; Asanuma, H. "DNA ポリメラーゼによる *de novo* DNA 合成のメカニズム解明" (Oral) *日本化学会第 88 春季年会(2008)*, Rikkyo University, **2008 Mar.**
- 4) Kato, T.; Liang, X. G.; Asanuma, H. "DNA ポリマーの *de novo* 合成とそのメカニズム" (Oral) *第 57 回高分子学会年次大会*, Pacifico Yokohama, **2008 May.**
- 5) Liang, X. G.; Kato, T.; Asanuma, H. "Mechanism of DNA elongation during *de novo* DNA synthesis" (Poster) *18th International Roundtable on Nucleoside, Nucleotides and Nucleic Acids (IS3NA)*, Kyoto University, **2008 Sep.**
- 6) Kato, T.; Liang, X. G.; Asanuma, H. "DNA ポリメラーゼによる *de novo* DNA 合成の開始段階のメカニズム解明" (Oral) *日本化学会第 89 春季年会(2009)*, Nihon University, **2009 Mar.**
- 7) Kato, T.; Liang, X. G.; Asanuma, H. "超好熱性 DNA ポリメラーゼによる短鎖 ssDNA の高効率な伸長反応" (Poster) *第 24 回生体機能関連化学シンポジウム, 第 12 回バイオテクノロジー部会シンポジウム*, Kyushu University, **2009 Sep.**
- 8) Kato, T.; Liang, X. G.; Asanuma, H. "好熱性 DNA ポリメラーゼによる鋳型非存在下での短鎖 ssDNA の伸長反応とそのメカニズム" (Oral) *日本化学会第 90 春季年会(2010)*, Kinki University, **2010 Mar.**
- 9) Kato, T.; Liang, X. G.; Asanuma, H. "超好熱性 DNA ポリメラーゼによる *de novo* DNA 合成とその機構解明" (Poster) *第 4 回バイオ関連化学シンポジウム*, Osaka University, **2010 Sep.**

- 10) Kato, T.; Liang, X. G.; Asanuma, H. "Unexpected non-specific DNA synthesis by thermophilic DNA polymerase." (Oral) *2010 International Chemical Congress of Pacific Basin Societies (Pacifichem2010)*, Hawaii, USA, **2010 Dec.**
- 11) Kato, T.; Sekiguchi, K.; Kashida, H.; Asanuma, H. "人工塩基対導入による蛍光色素の高輝度化" (Poster) *日本化学会生体機能関連化学部会第 26 回若手フォーラム*, Tsukuba University, **2011 Sep.**
- 12) Kato, T.; Sekiguchi, K.; Kashida, H.; Asanuma, H. "蛍光色素の高輝度化を目指した新規人工塩基対の開発" (Poster) *第 5 回バイオ関連化学シンポジウム-第 26 回生体機能関連化学シンポジウム、第 14 回バイオテクノロジー部会シンポジウム、第 14 回生命化学研究会シンポジウム、第 8 回ホスト-ゲスト化学シンポジウム*-, Epochal Tsukuba, **2011 Sep.**
- 13) Kato, T.; Kashida, H.; Asanuma, H. "DNA 二重鎖内部における蛍光色素のエネルギー移動に関する研究" (Oral) *日本化学会第 92 春季年会(2012)*, Keio University, **2012 Mar.**
- 14) Kato, T.; Kashida, H.; Kishida, H.; Yada, H.; Okamoto, H.; Asanuma, H. "DNA 二重鎖内部に導入した蛍光色素間の FRET 効率に関する研究" (Poster) *第 6 回バイオ関連化学シンポジウム-第 27 回生体機能関連化学シンポジウム、第 15 回バイオテクノロジー部会シンポジウム、第 15 回生命化学研究会シンポジウム*-, Hokkaido University, **2012 Sep.**
- 15) Kato, T.; Kashida, H.; Kishida, H.; Yada, H.; Okamoto, H.; Asanuma, H. "DNA 二重鎖内部に固定化した蛍光色素間のエネルギー移動に関する研究" (Oral) *光化学討論会 2012*, Tokyo Institute of Technology, **2012 Sep.**
- 16) Kato, T.; Kashida, H.; Kishida, H.; Yada, H.; Okamoto, H.; Asanuma, H. "Development of a robust FRET system within DNA duplex using base-surrogate tethering fluorophores" (Poster) *The 39th International Symposium on Nucleic Acids Chemistry (ISNAC2012)*, Nagoya University, **2012 Nov.**
- 17) Kato, T.; Kashida, H.; Kishida, H.; Yada, H.; Okamoto, H.; Asanuma, H. "DNA 二重鎖内部へ付加的に導入された色素間の FRET に関する研究" (Oral) *日本化学会第 93 春季年会(2013)*, Ritsumeikan University, **2013 Mar.**

LIST OF AWARD

1) **2008 Mar.** 名古屋大学大学院工学研究科物質制御工学専攻修士論文発表会 優秀賞

2) **2012 Sep.** The Excellent Student Award on the Annual Meeting on Photochemistry 2012.

3) **2012 Nov.** Outstanding Poster Presentation Award in 2012 at The 39th International Symposium on Nucleic Acids Chemistry (ISNAC2012).

ACKNOWLEDGMENT

The present article is a thesis for application of doctoral degree at the Department of Molecular Design and Engineering, Graduate School of Engineering, Nagoya University. All the study work was carried out under direction of Professor Hiroyuki Asanuma from April 2007 to March 2013.

I would like to express my deepest gratitude to Prof. Hiroyuki Asanuma and Prof. Xingguo Liang who provided helpful comments and suggestions. I am also indebted to Associate Professor Hiromu Kashida for his advice and valuable discussions. I would also like to thank Prof. Hiroshi Okamoto and Prof. Hideo Kishida whose comments made enormous contribution to my work. I would also especially thank Prof. Xingguo Liang who provided carefully considered feedback and valuable comments.

I would also like to say thanks for co-worker Mr. Koji Sekiguchi, Mr. Masatomo Suzuki, Mr. Kenjiro Kato, Mr. Naofumi Higashiyama, Mr. Yasuaki Okayama and other members of Asanuma Laboratory for their contribution and advice for this study. I would especially thank Mr. Koji Sekiguchi and Mr. Naofumi Higashiyama for providing me their valuable data in Chapter 3.

I am also greatly indebted to “Japan Society for the Promotion of Science Fellows” for their financial support to me.

Finally, I would like to express my gratitude my family for their moral support and warm encouragements.